CHARACTERISATION OF PLD ACTIVITY IN REAL-TIME

MINA-OLGA ALETRARI

A THESIS SUBMITTED IN PARTIAL FULFILMENT OF THE DEGREE
OF DOCTOR OF PHILOSOPHY

SEPTEMBER 2010

DEPARTMENT OF BIOLOGICAL SCIENCES
UNIVERSITY OF WARWICK
COVENTRY
CV4 7AL

Contents

List of Tables

List of Figures

Acknowledgments

I would like to thank laboratory M022 for all their support and encouragement over the course of this PhD. Particular thanks are reserved for Jeanette, a great source of friendship and advice over the last few years, who helped pass many long days in the laboratory.

A number of colleagues provided technical support without which my data would have been less complete. These include Dr Rebecca Stratton, Dr Lorenzo Frigerio, Dr Graham Ladds, Professor Michael Wakelam and Dr Paul Squires. Particular thanks are due to my supervisors, Dr Matthew Hodgkin and, latterly, Professor Chris Dowson for helping guide the direction of this project.

Professor Glenn Prestwich (University of Utah, USA) generously provided the novel fluorescent lipid used throughout this project.

I would like to thank Dr David Metcalfe for many hours proof reading this thesis – any errors remaining are the result of reader fatigue and remain my responsibility alone. Finally, I would like to thank my parents for their patience – hopefully my days as a student are coming to an end.

Declaration

I hereby declare that the work submitted in this thesis is my own under the supervision of Dr Matthew N. Hodgkin in the Department of Biological Sciences, University of Warwick, with the exception of those instances where the contribution of others has been specifically acknowledged. All sources of information have been specifically acknowledged by means of references.

None of the information contained herein has been used in any previous application for a degree.

Summary

PLD catalyses hydrolysis of phosphatidylcholine (PtdCho) to produce phosphatidic acid (PtdOH) and choline. PtdOH is a second messenger responsible for a multitude of cell processes, ranging from cytoskeletal rearrangement to cell proliferation. Antigenic stimulation of RBL-2H3 mast cells and growth factor stimulation of endothelial HeLa cells results in PLD-dependent exocytosis and endocytosis, respectively. A novel fluorescent PtdCho (fPtdCho) was used to label both cell lines and Bligh-Dyer lipid extraction of fPtdCho-labelled RBL-2H3 cells showed the lipid was intact post-labelling. fPtdCho co-localised up to 50% with the lysosomal marker LysoTracker Red in RBL-2H3 cells, and was not secreted in response to antigenic stimulation as recorded using real-time confocal microscopy. Primary alcohol treatment of fPtdCho-labelled RBL-2H3 cells altered fPtdCho-labelling to diffuse from punctate distribution, suggesting PLD-generated PtdOH is responsible for retention of punctate fPtdCho staining. PLD isoforms 1b and 2a were labelled with Cherry (a red fluorescent protein) and transiently expressed in fPtdCho-labelled HeLa cells. Localisation was assessed using FRET by FRAP technology in live cells and showed that substrate and lipase were in close proximity. These findings will facilitate future development of a live real-time *in vivo* PLD assay. Furthermore, localisation of PLD and its activator Rac1 was assessed at rest and in EGF-stimulated HeLa cells in real-time. This showed co-localisation between PLD and Rac1 following stimulation. The fluorescent PtdCho was also used to develop a novel real-time *in vitro* PLD assay, monitoring fPtdCho metabolism at two second intervals. This *in vitro* assay is more sensitive than traditional end-point assays and will help clarify the relative rate of PLD activation in response to small G-protein activators and other co-factors in real-time.

List of Abbreviations

4E-BP1	4E binding protein 1
5-HT	5-hydroxytryptamine
AcChoEase	Acetylcholinesterase
ADP	Adenosine diphosphate
AP	Assembly protein
Arf	Adenosine diphosphate ribosylation factor
Arl	Arf-like
ARNO	Arf nucleotide site opener
ATP	Adenosine triphosphate
BME	Beta-mercaptoethanol
BODIPY	4,4-difluoro-4-bora-3a,4a-diaza-s-indacene
BODIPY-PtdCho	Acyl-chain glycerophosphocholine linked to BODIPY
BSA	Bovine serum albumin
Btk	Bruton's tyrosine kinase
But-1	Butan-1-ol
But-2	Butan-2-ol
cAMP	Cyclic adenosine monophosphate
Ca^{2+}	Calcium
$CaCl_2$	Calcium chloride
CCT	CTP:phosphocholine cytidylyltransferase
CD	Cytochalasin D
CDP-choline	Cytidine diphosphocholine
CDP-DAG	CDP-choline: 1,2-diacylglycerol cholinophosphotransferase
CEM	Calveolin-enriched membrane
CEMM	Caveolin-enriched membrane microdomain
cGMP	Cyclic guanosine monophosphate
CHO	Chinese hamster ovary
CK	Casein-kinase
CR	Conserved regions
CTP	Cytidine 5'-triphosphate
DAG	Diacylglycerol
DIC	Differential inferface contrast
DMEM	Dulbecco's modified eagle medium
DMSO	Dimethylsulfoxide
DNA	Deoxyribonucleic acid
dNTPs	Deoxyribonucleotides
DRB	5,6-dichloro-1-β-$_D$-ribofuranosylbenzimidazole
dsRed	*Discosoma* red fluorescent protein
DTT	Dithiothreitol
EDTA	Ethylenediaminetetraacetic acid
EEA1	Early endosome-associated antigen 1
EFA6	Exchange factor adenosine diphosphate ribosylation factor 6
EGF	Epidermal growth factor

eGFP	Enhanced green fluorescent protein
EGFR	Epidermal growth factor receptor
EGTA	Ethyl glycol tetraacetic acid
ER	Endoplasmic reticulum
ERK	Extracellular signal-regulated kinase
$Fc_{\varepsilon}RI$	Fragment chrystallizable epsilon region one
FCS	Foetal calf serum
FIPI	5-fluro-2-indolyl des-chlorohalopaemide
fPtdCho	Fluorescent phosphatidylcholine
FRAP	Fluorescence recovery after photobleaching
FRET	Förster (or fluorescence) resonance energy transfer
GAP	Guanine triphosphatase activating protein
GDI	GDP dissociation inhibitors
GEF	Guanine nucleotide exchange factor
GFP	Green fluorescent protein
GRP	General receptor for phosphoinositides
GST	Glutathione-S-transferase
GTPase	Guanine triphosphatase
GTPγS	Guanosine 5'-O-(gamma-thio) triphosphate
HA	Haemagglutinin
HBSS	Hank's balanced salt solution
HCl	Hydrochloric acid
HEK-293	Human embryonic kidney 293
HEPES	N-(2-hydroxyethyl)-piperazine-N'-2-thanesulfonic acid
HKD	$HxK(x)_4D(x)_6GSxN$ – where x is any amino acid
HL60	Human promyelocytic leukemic 60
$[^3H]$-$(Pam)_2$PtdCho	Dipalmitoylphosphatidyl [methyl ^3H]-choline
hPLD	Human phospholipase D
HRP	Horse radish peroxidase
Ig	Immunoglobulin
KCl	Potassium chloride
LAS-AF	Leica Application Software-Advanced Fluorescence Lite software
LB	Luria broth
Lat B	Latrunculin B
mAChR	Muscarinic acetycholine receptor
MAPK	Mitogen-activated protein kinase
MBCD	Methyl-beta-cyclodextrin
MDCK	Madin-derby canine kidney
Mg^{2+}	Magnesium
MgCl	Magnesium chloride
mGluR	Metabotropic glutamate receptor
MHC	Major histocomaptibility protein class
MIN6	Mouse insulinoma cells
MOI	Multiplicity of infection
MOP	3-(N-morpholino) propanesulfonic acid
MP	Mastoparan

mPLD	Mouse phospholipase D
mRFP	Monomeric red fluorescent protein
mRNA	Messenger ribonucleic acid
mTOR	Mammalian target of rapamycin
mTORC	Mammalian target of rapamycin complex
NaCl	Sodium chloride
NaPPi	Sodium pyrophosphate
NLS	Nuclear localisation signal
nm	Nanometer
OD	Optical density
ORF	Open reading frame
PAE	Porcrine aortic endothelial
PBS	Phosphate buffered saline
PC	Phaeochromocytoma
PCR	Polymerase chain reaction
PDE	Phosphodiesterase
PDGF	Platelet derived growth factor
Pearson's R	Pearson's correlation coefficient
PEI	Polyethylenimine
PEMT	Phosphatidylethanolamine *N*-mehtyltransferase
PFA	Paraformaldehyde
PH	Pleckstrin homology
PKC	Protein kinase C
PLA_2	Phospholipase A_2
PLC	Phospholipase C
PLD	Phospholipase D
PMA	Phorbol 12-myristate 13-acetate
PMT	Photo multiplier tubes
PtdBut	Phosphatidylbutanol
PtdCho	Phosphatidylcholine
PtdEth	Phosphatidylethanolamine
PtdIns	Phosphatidylinositol
PtdIns 3-kinase	Phosphatidylinositol 3-kinase
PtdIns(3)P	Phosphatidylinositol 3-phosphate
$PtdIns(3,4,5)P_3$	Phosphatidylinositol 3,4,5-trisphosphate
$PtdIns(3,5)P_2$	Phosphatidylinositol 3,5-trisphosphate
PtdIns(4)P	Phosphatidylinositol 4-phosphate
PtdIns(4)P 5-kinase	Phosphatidylinositol 4-phosphate 5-kinase
$PtdIns(4,5)P_2$	Phosphatidylinositol 4,5-bisphosphate
PtdOH	Phosphatidic acid
PtdSer	Phosphatidylserine
PVDF	Polyvinylidene fluoride
PWO	*Pyrococcus woesei*
PX	Phox homology
RBL-2H3	Rat basophilic leukaemia 2H3
rPLD	Rat phospholipase D

RNA	Ribonucleic acid
RNAi	Interference ribonucleic acid
RT	Room temperature
S6k1	S6 kinase 1
SAP	Shrimp alkaline phosphatase
Sf	*Spodeptera frugiperda*
siRNA	Short interfering ribonucleic acid
SNAP	Synaptosome-associate protein
SNARE	Soluble N-ethylmaleimide-sensitive fusion factor attachment protein
SOB	Super optimal broth
SPR	Surface plasmon resonance
Syt	Synaptotagmin
TAPAS-1	Anchoring phosphatidic acid selective-binding domain 1
Taxol	Paclitaxel
TBE	Tris-borate-ethylenediaminetetraacetic acid
Tdp	Tyrosyl-DNA phosphodiesterase
TGN	*trans*-Golgi network
TIRFM	Total internal reflection fluorescent microscopy
TLC	Thin layer chromatography
TNM-FH	Modified Grace's medium
TNT assay	TNT quick coupled transcription/translation system assay
t-SNARE	Target soluble N-ethylmaleimide-sensitive fusion factor attachment protein
UV	Ultraviolet
VAMP	Vesicle associated membrane protein
v-SNARE	Vesicle soluble N-ethylmaleimide-sensitive fusion factor attachment protein
wt	Wildtype

Chapter 1: Introduction

1.1: Phosphatidylcholine

Phosphatidylcholine (PtdCho) is both structurally important as a cylindrical lipid and precursor of key second messengers (Dowhan and Bogdanov, 2002; McDermott *et al*., 2004). It is the substrate of phospholipases A_2, C and D which produce lysophosphatidic acid, diacylglycerol (DAG) or phosphatidic acid (PtdOH) respectively (Larrodera *et al*., 1990; Cai *et al*., 1992; Kinkaid and Wilton, 1995). This thesis focuses predominantly on the hydrolysis of PtdCho to PtdOH and choline by phospholipase D (PLD). PtdCho is composed of glycerol, two fatty acid chains and a phosphate (PtdOH) carrying the choline headgroup (Sprong *et al*., 2001). PtdCho is a cylindrically shaped lipid unlike its precursor phosphatidylethanolamine (PtdEth) and its product, PtdOH (see Fig. 1.1 pathway highlighted in red) which are both cone shaped lipids (Dowhan and Bogdanov, 2002). Cylindrical lipids typically form lipid bilayers as both the head group and hydrophobic domains are of similar diameter (Dowhan and Bogdanov, 2002). Cone shaped lipids such as PtdEth contain a small head group relative to large hydrophobic domains and preferentially form inverted micellar structures. These structures are supported by the head groups sequestering an internal aqueous core and the hydrophobic domains orienting themselves outwards, thus forming a non-bilayer structure (Dowhan and Bogdanov, 2002).

Homeostasis of choline and PtdCho is maintained in mammalain cells primarily through the cytidine diphosphocholine (CDP-choline) pathway shown in Fig. 1.1, highlighted in green (Li and Vance, 2008). The main source of choline in mammalian cells is dietary, and after choline is absorbed, it is phosphorylated by choline kinase to phosphocholine via the CDP-choline pathway. At this stage, choline can also be oxidised by choline oxidase and converted to betaine by betaine aldehyde in certain cells such as hepatocytes (Prichard and Vance, 1981). The CDP-choline pathway converts phosphocholine to CDP-choline by cytidine 5'-triphosphate (CTP):phosphocholine cytidylyltransferase (CCT). This is a rate-limiting step as CCT is active when membrane-bound and inactive in its soluble form

and the concentration of phosphocholine is up to 40-fold higher than that of CDP-choline (Li and Vance, 2008; Vance and Vance, 2008). The 'bottleneck' is attributed to regulation of CCT by reversible movement of the enzyme on and off membranes through its interactions with anionic lipids, such as the nuclear membrane in Chinese hamster ovary (CHO)-K1 cells (Xie *et al*., 2004; Lagace and Ridgway, 2005; Li and Vance, 2008). The CCT site of lipid interaction has been identified as three α-helical repeats which enhances the ability of CCT-binding to membranes deficient in PtdCho and regulates enzyme activity (Lykidis *et al*., 2001; Xie *et al*., 2004; Li and Vance, 2008). Finally, the intrinsic endoplasmic reticulum (ER) membrane lipid CDP-choline is converted to PtdCho by CDP-choline: 1,2-diacylglycerol cholinophosphotransferase (CDP-DAG –Vance and Vance, 2008).

PtdCho is also synthesised by the methylation of phosphatidylethanolamine (PtdEth) by phosphatidylethanolamine *N*-methyltransferase (PEMT) shown in Fig. 1.1 (highlighted in purple) and is most active in the liver (Vance and Ridgway, 1988). PEMT is a 22.3kDa protein primarily localised to the ER, however previous *in vivo* studies have not shown reactivity with ER proteins but instead were linked to mitochondrial-associated membranes (Cui *et al*., 1993). Furthermore, recent studies suggest that both the N- and C-termini of PEMT are localised externally to the ER as the four transmembrane domains of PEMT span the membrane (Shields *et al*., 2003). PtdCho synthesised by the PtdEth pathway is thought to be essential to membrane stability and synthesis when dietary choline is limited thus also limiting PtdCho-synthesis via the CDP-choline pathway (Li and Vance, 2008). Studies utilising CCTα knockdowns reduce CCT activity of the hepatocytes to 15% of that normally expected (Jacobs *et al*., 2004). In CTα-deficient hepatocytes, PEMT activity increased twofold when compared with controls (Jacobs *et al*., 2004). However, increased PEMT activity (facilitating PtdCho-synthesis) did not compensate for decreased PtdCho-synthesis via the CDP-choline pathway in CCTα-deficient hepatocytes (Jacobs *et al*., 2004). PtdCho-choline homeostasis is thought to be crucial for sustained normal liver function (Li and Vane, 2008).

Figure 1.1: The synthesis and metabolism of phosphatidylcholine. The cycle of phosphatidycholine (phospholipase D substrate) and choline (product of phosphatidylcholine hydrolysis) is summarised below (modified from Lagace and Ridgway, 2005; Li and Vance, 2008). The green pathway highlights phosphatidylcholine synthesis by the cytidine diphosphocholine (CDP-choline) pathway beginning with acetylcholine and choline obtained from the diet. The red pathway highlights processes dependent on phospholipase D activity and the purple pathway highlights synthesis of phosphatidylcholine by phosphatidylethanolamine.

Enzyme abbreviations used in the figure are cytidine diphosphoethanolamine (CDP-ethanolamine), and cytidine diphosphocholine-diacylglycerol (CDP-DAG). The numbers labelling the figure below correspond to the following enzymes: **(1, 16)** choline acetyltransferase, **(2)** choline kinase, **(3)** phosphocholine cytidylyltrasnferase, **(4)** CDP-choline: 1,2-diacylglycerol cholinophosphotransferase, **(5)** sphingomycelin synthase, **(6)** sphingomyelinase, **(7)** choline oxidase, **(8)** betaine aldehyde dehydrogenase, **(9)** phosphatidylserine synthase, **(10)** phosphatidylserine decarboxylase, **(11)** phosphatidylethanolamine N-methyltransferase, **(12)** various phospholipd and lysophospholipid activities, **(13)** ethanolamine kinase, **(14)** phosphoethanolamine cytidylyltransferase, **(15)** CDP: ethanolamine = 1,2-diacylglycerol ethanolamine phosphotransferase, **(17)** phospholipase D, **(18)** CDP-choline synthase, **(19)** phosphatidylserine synthase.

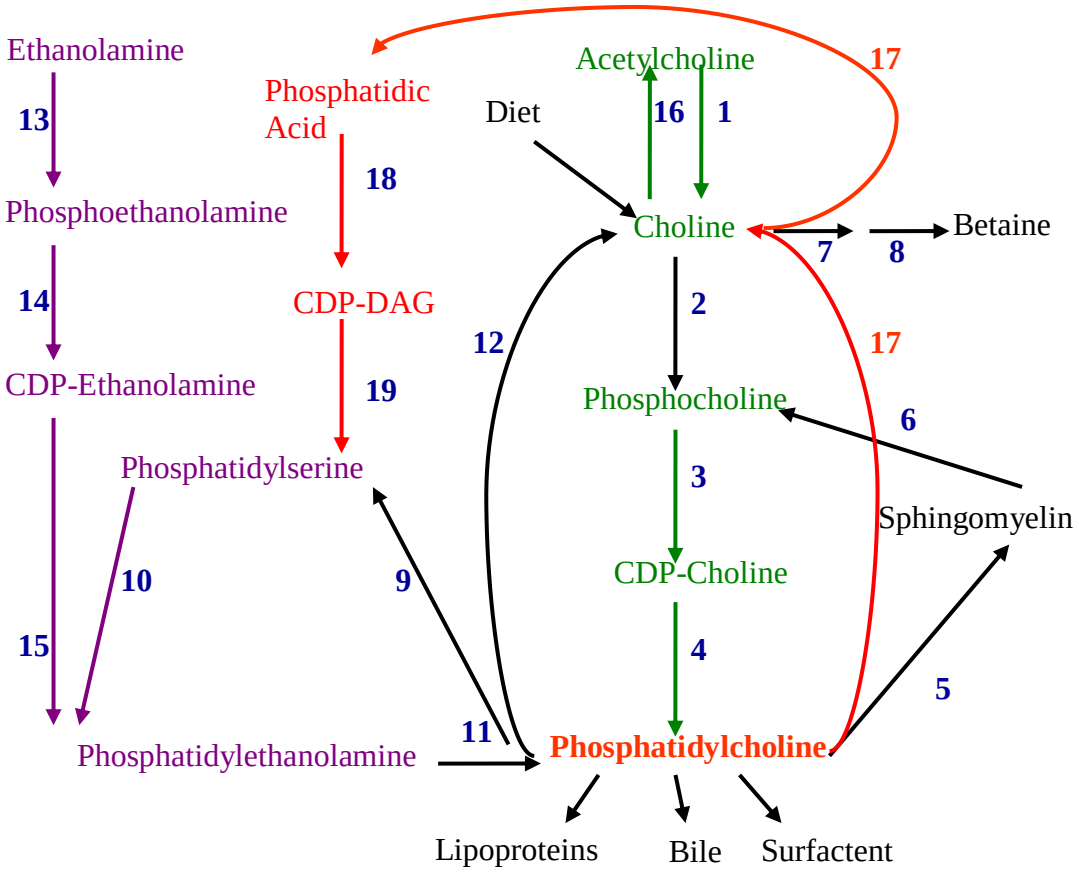

1.2: Phospholipase D structure and localisation

1.2.1: An introduction to the structure of mammalian phospholipase D

Phospholipase D (PLD) is a well characterised lipase involved in a variety of cellular processes ranging from exocytosis to apoptosis. All members of the PLD superfamily contain as least one copy of the conserved catalytic **H**x**K**$(x)_4$**D**$(x)_6$GSxN (HKD) motif (where x is any amino acid – Ponting and Kerr, 1996; Stuckey and Dixon, 1999). The catalytic site of PLD is often constituted by dimerised HKD motifs consisting of conserved histidine, lysine, aspartate and asparagine residues, which are necessary for enzymatic activity (Ponting and Kerr, 1996; Stuckey and Dixon, 1999). The preferential substrate of mammalian PLD is phosphatidylcholine (PtdCho) which PLD hydrolyses to phosphatidic acid (PtdOH) and choline.

Regulatory domains such as the phox homology domain (PX) and the pleckstrin homology domain (PH) are located at the N-terminus of both mammalian PLD1 and PLD2 (Ponting *et al*., 1996; Hodgkin *et al*., 2000; Sciorra *et al*., 2002). These domains mediate the specificity of lipid binding and protein-protein interactions. The PH domain has high substrate specificity for PtdIns(4,5)P_2 and functions together with a polybasic motif to target PtdIns(4,5)P_2-rich membranes (Steed *et al*., 1998; Holbrook *et al*,. 1999; Sciorra *et al*., 1999; Sciorra *et al*., 2002). The polybasic motif has recently been identified and is only conserved in PtdIns(4,5)P_2-dependent PLDs such as mammalian PLD1 and PLD2, and yeast Spo14p (Sciorra *et al*., 1999; Sciorra *et al*., 2002). Although deletion of the polybasic motif does not affect PLD localisation, it does affect lipase activation (Sciorra *et al*., 2002).

Although several regions of PLD are highly conserved between the two isoforms and different species, the PLD1 'loop' region is variable. Between conserved PLD-specific catalytic domains I and II (see Fig. 1.2), PLD1 possesses a 'loop' region. The 'loop' region is highly variable between closely related species (such as human and rat) and PLD1 also undergoes alternative splicing (Hammond *et al*., 1997; Redina and Frohman, 1998; Sung *et al*., 1999a). The loop of PLD1a is 116 amino acid residues whereas alternative splicing results in the removal of 33 amino acids to produce the PLD1b isoform (Hammond *et al*., 1997; Redina & Frohman, 1998; Sung

et al., 1999b). Mammalian PLD2 does not contain this highly variable region and catalytic activity is unaffected by the addition of the 'loop', although PLD2 activity is modestly reduced (Sung *et al*., 1999a). Furthermore, deletion of this region in human PLD1 increased activity by threefold, suggesting it may act as a regulator of PLD1 activity (Sung *et al*., 1999b). This regulatory region is probably responsible for the low basal activity of PLD1 *in vivo* (Sung *et al*., 1999b). The sections following will summarise the characteristics of conserved PLD regions in terms of regulation and activity.

Figure 1.2: A representation of the typical structure of mammalian PLD1 and PLD2. The diagram was modified from McDermott *et al*., 2004. The targets of small G-proteins and PtdIns(4,5)P_2 activators are highlighted on the PLD1 representation. These regions have been characterised by identifying the effects of point mutations/deletions in these regions.

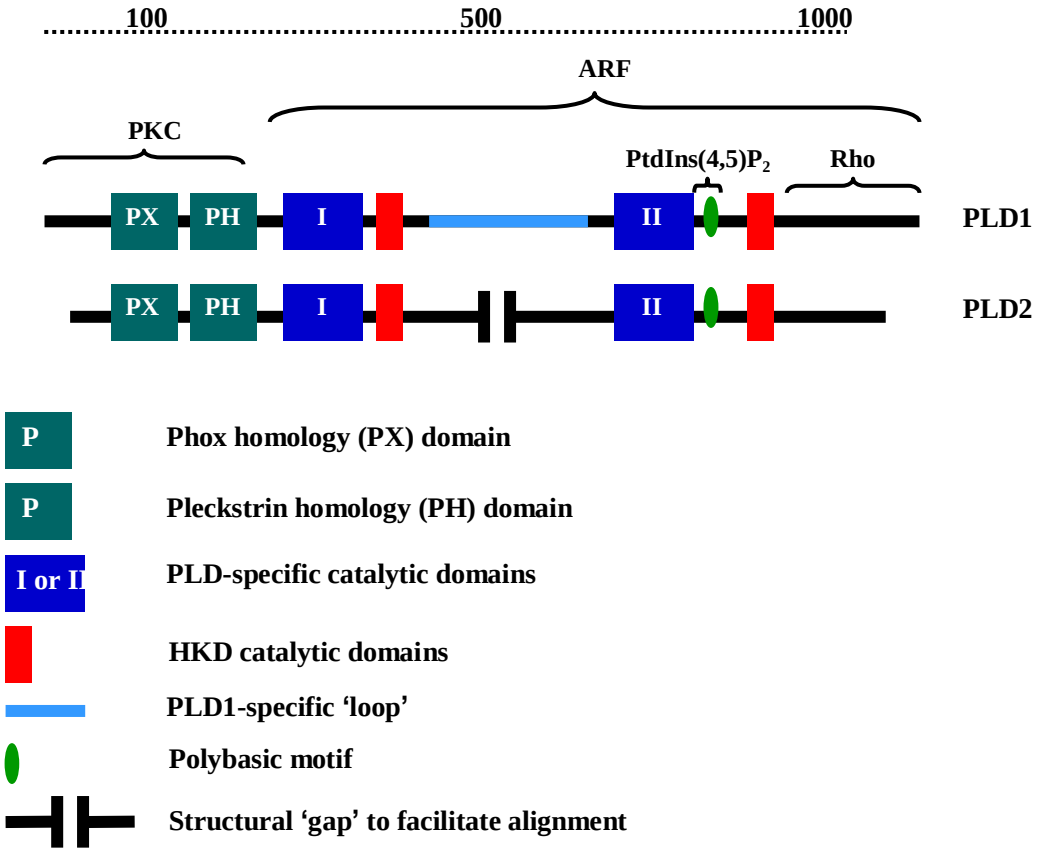

1.2.2: Phox homology domain

The phox homology (PX) domain was first identified at the N-terminus of human, yeast and nematode PLD (Ponting *et al*., 1996; Liscovitch *et al*., 2000; McDermott *et al*., 2004). Although there is a high degree of sequence conservation of N-termini in mammalian PLD1 proteins, there is less homology between mammalian PLD1 and PLD2 (Sung *et al*., 1999a; Sung *et al*., 1999b). The first 100-330 amino acids encode the PX domain (approximately 140 amino acids) and the pleckstrin homology (PH) domain of mammalian PLD (Sung *et al*., 1999b). The role of the PX domain remains unclear, although its removal has no impact on catalytic activity or activation by Arf (Liscovitch *et al*., 2000; Xu *et al*., 2001). Mutagenesis of the PX domain of PLD1 renders the enzyme inactive *in vitro* but increases basal activity *in vivo* and remains responsive to PMA, although to a lesser extent than wildtype PLD (Sung *et al*., 1999b). PX domains have been implicated in protein-protein interactions and lipid binding; specifically phosphatidylinositides (Ponting and Kerr, 1996; Xu *et al*., 2001) including phosphatidylinositol 3,4-bisphosphate (PtdIns(4,5)P_2), PtdIns(3)P, PtdIns(3,5)P_2 and PtdIns(3,4,5)P_3 (Xu *et al*., 2001).

The PX domain of PLD1 specifically binds PtdIns(3,4,5)P_3 *in vitro* but that of PLD2 does not (Lee *et al*., 2005). In addition, mutagenesis of the PX domain results in changed PLD1 localisation in NIH-3T3 cells and is thought to mediate signal transduction via ERK1 and 2 (Lee *et al*., 2005). A modelling study using mammalian PLD1 suggested that the PX domain has two binding pockets (Stahelin *et al*., 2004). The primary binding site is specific to PtdIns(3,4,5)P_3 whilst the secondary binding site has moderate affinity for anionic lipids such as phosphatidic acid (PtdOH) or phosphatidylserine (Stahelin *et al*., 2004). When both binding pockets are occupied, PX membrane affinity is synergistically increased (Stahelin *et al*., 2004). The PX domain of PLD2 acts as a GTPase activating protein (GAP) which can bind directly to the GTPase domain of dynamin (Lee *et al*., 2006). The PX domain itself is thought to have GAP activity and PLD2 with diminished GAP function increases epidermal growth factor (EGF) stimulated endocytosis in HEK-293 cells (Lee *et al*., 2006). These properties implicate the PX domain in signal transduction, membrane affinity, localisation and regulation.

1.2.3: Pleckstrin homology domain

PLC has a known conserved pleckstrin homology domain which binds to PtdIns(4,5)P_2. As PtdIns(4,5)P_2 stimulates PLD activity, studies comparing the sequence of PLC with human PLD (hPLD1a or hPLD1b) or Spo14p (a PtdIns(4,5)P_2-dependent yeast PLD) at first did not identify PH domains (Hammond *et al*., 1995; Hammond *et al*., 1997). However, PH domains were later identified in hPLD1 and hPLD2 isoforms, thus clarifying the role of PtdIns(4,5)P_2 in PLD regulation (Steed *et al*., 1998; Holbrook *et al*., 1999). The sequences of hPLD1 and PLD2 were compared to those of proteins with known PH domains, such as Bruton's tyrosine kinase (Btk) and PLCδ (Hodgkin *et al*., 2000). The interaction between PLD and PtdIns(4,5)P_2 was quantified using surface plasmon resonance (SPR) and monolayers containing PtdEth, PtdCho and activating PtdIns(4,5)P_2 (Hodgkin *et al*., 2000). PH domain residues involved in inositol-phosphate binding were conserved between Btk and PLD1 and PLD2 (Hodgkin *et al*., 2000).

Mutations or the deletion of conserved N-terminal PH domain residues rendered PLD1, PLD2 and Spo14p inactive *in vivo* due to a change in localisation (Sciorra *et al*., 2002). The removal of the N-termini of PLD1 and PLD2 resulted in increased basal activity and responsivity to small G-protein activators (Sung *et al*., 1999a; Sung *et al*., 1999b; Sciorra *et al*., 2002). Deletion of the N-terminus of PLD2 (including the PH domain) resulted in increased catalytic activity and responsiveness to Arf stimulation (Sciorra *et al*., 2002). In addition, a chimera of PLD2 with an insertion of the characteristic 'loop' region of PLD1 decreased basal PLD2 activity, suggesting a regulatory role of basal PLD activity (Sciorra *et al*., 2002). Deletion of the N-termini of human PLD1 (325 residues) and mouse PLD2 (308 residues) did not affect their binding affinity or activation by PtdIns(4,5)P_2 (Sciorra *et al*., 1999). This suggests that the regulation of PtdIns(4,5)P_2 activation of PLD occurs via another PtdIns(4,5)P_2- specific binding domain (Sciorra *et al*., 1999; Sciorra *et al*., 2002). A polybasic motif has been identified in both PLD1 and PLD2 is thought to mediate PtdIns(4,5)P_2 stimulation of PLD. The PH domain is selective for PtdIns(4,5)P_2 but with a lower affinity than the polybasic motif, and the two synergistically function to target PtdIns(4,5)P_2-rich membranes (Sciorra *et al*., 2002). PLD1 localises to the Golgi apparatus and endosomes in COS7 cells and, upon stimulation, migrates to the

plasma membrane and then returns to the endosomes (Du *et al*., 2003). PLD1 (without PX or PH domains) maintains its ability to translocate to the plasma membrane via interactions with its PtdIns(4,5)P_2-specific binding site (Du *et al*., 2003). However, although plasma membrane translocation is not affected, the return of PLD1 to perinuclear endosomes was inefficient without PX and PH domains (Du *et al*., 2003). The specific role of the PH domain in PLD activation and membrane-targeting is complex and has yet to be fully elucidated.

1.2.4: Polybasic motif

The polybasic motif has been identified in PLD which is PtdIns(4,5)P_2-dependent for activity such as mammalian PLD1 and PLD2, and yeast Spo14p. The PH domain is required for PtdIns(4,5)P_2 specificity, however it is thought that the binding affinity and activation of PLD is regulated by the less specific but higher affinity polybasic motif (Sciorra *et al*., 1999; Sciorra *et al*., 2002). The polybasic motif is characterised by a sequence of 21 amino acids rich in charged (i.e. basic) residues which are conserved in combination with aromatic and aliphatic residues, typically comprised of six arginine, lysine or histadine amino acid residues (Sciorra *et al*., 1999; Sciorra *et al*., 2002; McDermott *et al*., 2004). The location of the motif is controversial but has been identified between conserved region II and the second HKD motif, close to the catalytic core (see Fig. 1.2 - Sung *et al*., 1999b; Sciorra *et al*., 2002; Mansfeld and Ulbrich-Hoffmann, 2009). Mutations of the polybasic motif in human PLD2 and yeast Spo14p did not affect their localisation but reduced their responsiveness to PtdIns(4,5)P_2 and were rendered non-functional (Sciorra *et al*., 2002). This supports the theory that the PH domain and polybasic motif function together to target PLD to the appropriate intracellular compartment (using PtdIns(4,5)P_2 specificity and binding), thus ensuring enzyme activity.

1.2.5: PLD catalysis

Members of the PLD superfamily are characterised by the presence of a conserved catalytic **H**x**K**$(x)_4$**D**$(x)_6$GSxN (HKD) motif (where x is any amino acid – Ponting and Kerr, 1996; Stuckey and Dixon, 1999). The HKD motif (otherwise known as conserved regions (CR) II and IV) is comprised of conserved histidine, lysine, aspartate and asparagine residues essential for enzymatic activity (Ponting and Kerr, 1996; Stuckey and Dixon, 1999). The bacterial endonuclease Nuc is a member of the PLD superfamily with only one HKD and four short motifs which are common to all family members (Ponting and Kerr, 1996). However, most members of the PLD superfamily have two HKD motifs and the four short motifs appear in duplicate (i.e. located between domains I and II, and domains III and IV – Ponting and Kerr; McDermott *et al*., 2004). This duplication of conserved regions led to the supposition that PLD is a bi-lobed enzyme which is the product of a gene duplication and fusion event (Ponting and Kerr, 1996). Point mutations of residues in either HKD motif of PLD1 rendered the enzyme inactive (Sung *et al*., 1997; Sung *et al*., 1999a). The basic lysine residue of the HKD motif is thought to aid binding to an acidic substrate and when mutated results in enzyme inactivity (Sung *et al*., 1997; Davies *et al*., 2002; Fedeli *et al*., 2006). Similar mutagenesis experiments on the HKD motifs of PLD2 and yeast Spo14p enzymes corroborated data indicating that both HKD motifs were necessary for catalytic activity (Sung *et al*., 1999a; Sung *et al*., 1999b). Mutation of the lysine residue of the second HKD motif of SPO14 results in enzyme inactivity (*in vitro*) and inhibition of meiosis (Sung *et al*., 1997).

Two models of PLD catalysis were proposed, the first of which suggested that each HKD motif functioned independently, and the other that the HKD motifs dimerise to form a single active site (Ponting and Kerr, 1996). As mutations in one HKD motif resulted in an inactive lipase, it is probable that the active site of PLD is an HKD motif dimer (Sung *et al*., 1997; McDermott *et al*., 2004). In addition, when the C- or N-termini of mammalian PLD1 (isolated from rat brain) were expressed individually in COS7 cells there was no PLD activity (Xie *et al*., 1998). However, when the two were co-expressed in the COS7 cell line wildtype PLD1 activity was restored (Xie *et al*., 1998). The reassociation of N- and C-termini occurred exclusively *in vivo* and was dependent on the conserved HKD motifs (Xie *et al*., 1998; Xie *et al*., 2000).

This further supports the theory that both HKD motifs are needed for PLD catalysed hydrolysis of PtdCho.

The bacterial endonuclease Nuc which has only one HKD motif and one copy of the four short motifs was the first member of the PLD superfamily to be crystalised (Ponting and Kerr, 1996; Stuckey and Dixon, 1999). Nuc was isolated from the pKM101 plasmid of *Salmonella typhimurium* and the crystal structure of this monomer provided information about how HKD motifs form dimers. Two HKD motifs from separated Nuc endonucleases lie parallel on the DNA forming a single active site connected by hydrogen bonds (Stuckey and Dixon, 1999). Resolving the crystal structures of other PLD superfamily members, including the (human) DNA repair enzyme tyrosyl-DNA phosphodiesterase (Tdp1) which also has one HKD motif, reinforced that the catalytic site of PLD superfamily members exists as a dimer of two HKD motifs (Davies *et al*., 2002). Although HKD motifs of mammalian PLDs are also thought to form dimers, it is unclear whether these are homodimeric (between HKD motifs of the same PLD) or heterodimeric (between HKD motifs of separate PLDs). Recent studies proposed that rat PLD (rPLD1 and rPLD2) have the potential to exist as both homodimers and heterodimers (Kam and Exton, 2002).

In vitro experiments using plant PLD (from cabbage) and radio-labelled phosphatidylglycerol (substrate), suggested the presence of a phosphatidyl-enzyme intermediate following hydrolysis or transphosphatidylation (Stanacev and Stuhne-Sekalec, 1970). This catalytic mechanism was dubbed a 'ping-pong' reaction whereby PLD catalysis involves a phosphatidylated enzyme intermediate (Ponting and Kerr, 1996). In the past Nuc has been used to identify the histidine of the HKD motif as a nucleophile in catalysis (Gottlin *et al*., 1998). Crystallisation of the endonuclease further elucidated the role of the histidine residues forming the homodimeric catalytic site of Nuc (Stuckey and Dixon, 1999). The histidine residue from one HKD motif acts as a nucleophile and attacks the phosphate of the phosphodiester bond, thus forming a covalently bonded phosphoenzyme intermediate (see Fig. 1.3 – Stuckey and Dixon, 1999). The histidine residue of the second HKD motif acts as an acid and protonates the leaving group of lipid. The reaction then progresses to form the product (PtdOH) in the presence of water through hydrolysis,

or Ptd-alcohol in the presence of primary alcohol through transphosphatidylation (Stuckey and Dixon, 1999). Experiments using mammalian PLD and more recently PLD from *Streptomyces septatus* TH-2 have been used to further clarify the role of HKD residues in PLD catalysis (Sung *et al*., 1997; Uesugi *et al*., 2005; Uesugi *et al*., 2007). Recent studies have identified the N-terminal HKD motif as the nucleophile in the first part of PLD catalysis, and the effect of specific residues on substrate recognition (Uesugi *et al*., 2005; Uesugi *et al*., 2007).

Figure 1.3: PLD hydrolysis and transphosphatidylation reactions with a PtdCho substrate. The figure summarises hydrolysis and transphosphatidylation of PtdCho by PLD where there is a covalently bonded PLD-PtdOH intermediate. Both hydrolysis and transphosphatidylation reactions involve the nucleophilic attack of the diester phosphate group by either water or a hydroxyl group (i.e. from a primary alcohol), respectively (McDermott *et al*., 2004). The diagram is modified from Uesugi *et al*., 2007 and Uesugi and Hatanaka, 2009 and X represents a polar group.

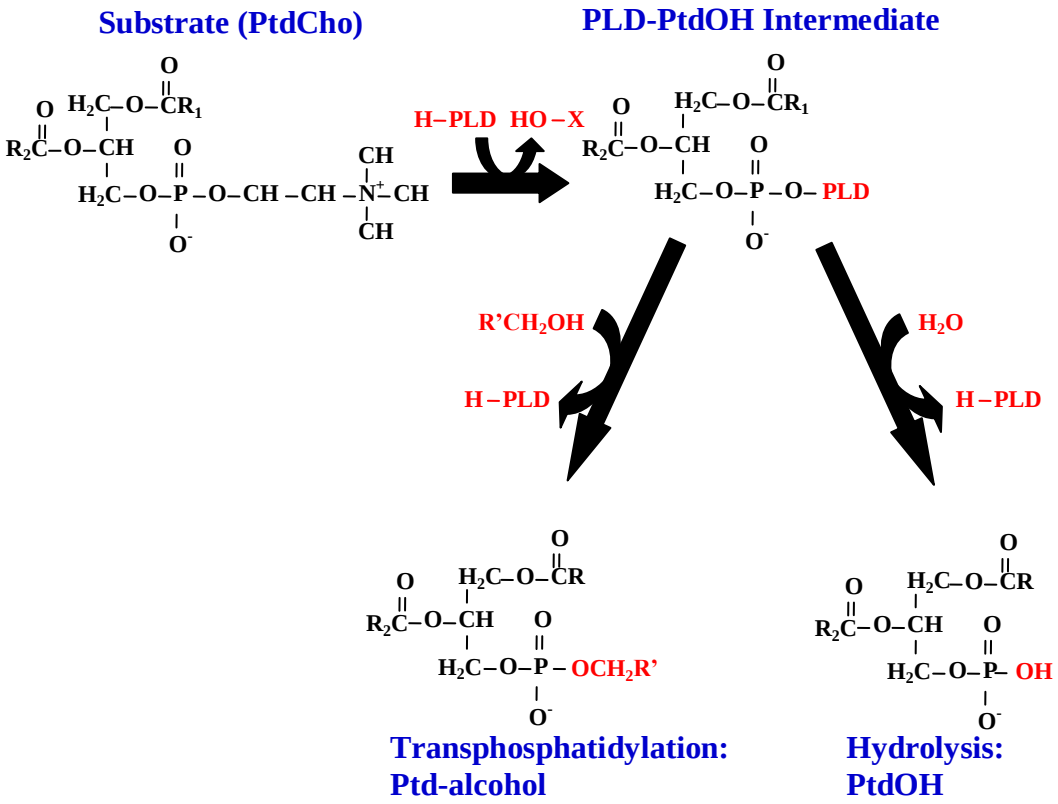

Transphosphatidylation is a transesterification reaction unique to PLD superfamily members. It was first identified in plant PLD (using cabbage PLD – Yang *et al*., 1967) and was developed to quantify PLD activity *in vivo* (Wakelam *et al*., 1995). Transphosphatidylation occurs in the presence of a primary alcohol (usually butan-1-ol) which PLD binds to preferentially (up to 1000-fold preference) over water (Frohman and Morris, 1999). It results in accumulation of the metabolically stable phosphatidylalcohol (Ptd-alcohol) instead of easily degraded PtdOH. The stability of Ptd-alcohol enables *in vivo* PLD activity assays and can also act as a 'functional' inhibitor of PLD activity *in vivo*.

The vaccinia virus protein VP37 has one HKD motif which is required for cell to cell spread of vaccinia virus and is thought to be functionally homologous to mammalian PLD (Sung *et al*., 1997). Although there are many conserved sequences in PLD, they are not all essential for enzymatic activity. The serine residue of the HKD motif forms covalent bonds with PtdOH resulting in a PLD-PtdOH intermediate. The PLD1 lysine-898 residue of the HKD motif substituted with arginine maintained the basic side group but altered orientation and distance from the protein backbone (Sung *et al*., 1997). This mutant was inactive both *in vivo* (expressed in COS7 cells) and *in vitro*, and did not respond to small G-protein activators (PKCα, Rho A or Arf1). Mutating the lysine residue did not impact upon PLD1 localisation and was corroborated using mouse PLD2, which was also inactive when the corresponding lysine residue was substituted with arginine (Sung *et al*., 1999b).

The role of lysine and aspartate residues varies depending on the enzyme substrate. The crystal structure of the Nuc endonuclease implicated both lysine and aspartate residues in binding and neutralising the substrate (Stuckey and Dixon, 1999; McDermott et al., 2004). Later, the crystal structure of *Streptomyces* sp. strain PMF PLD was compared to that of Nuc from *S. typhimurium* (Leiros *et al*., 2000). The three dimensionally reconstructed structures were similar, however the coordinate bond of the histidine residues in the active site varied between the two. Aspartic acid residues were located away from the histidine and active site, which may facilitate deeper penetration of phosphate into the active site (Leiros *et al*., 2000).

The conserved regions of PLD superfamily members have been extensively

investigated using dimerised mammalian PLDs as well as bi-lobed monomer PLDs. Although PX and PH domains are important for PKCα activation, lipid binding and PtdIns(4,5)P_2 specificity, some domains are dispensable in terms of catalytic activity (Sung *et al*., 1997). The least characterised region of PLD is the first conserved domain (CR I) in which some point mutations render the enzyme inactive whereas others hardly affect enzymatic activity. The mutation of leucine-405 to aspartic acid results in PLD inactivity, whilst the substitutions of glycine-412 with alanine or glutamic acid have minimal impact (McDermott *et al*., 2004). The deletion of this region in PLD1 did not affect activity or PtdIns(4,5)P_2 binding (Sung *et al*., 1999b; McDermott *et al*., 2004).

The IYIENQF motif is found in eukaryotic PLDs and has been characterised in the *Torpedo* acetylcholinesterase (ActChoEase) enzyme (Harel *et al*., 1993). The catalytic site of ActChoEase is rich in aromatic residues (such as tryptophan, phenylalanine and tyrosine) and specific for acetylcholine hydrolysis (Harel *et al*., 1993). There are 14 conserved aromatic amino acid residues which contribute to approximately 60% of the total surface area of ActChoEase (Xu *et al*., 2008). The conserved domain III (CR III) of PLD has a sequence enriched with aromatic amino acids which could increase the rate of catalysis (e.g. by interacting with the choline head group of PtdCho) or limit substrate specificity (Frohman *et al*., 1999). This region also encodes a consensus caveolin binding sequence **φ**X**φ**XXXX**φ**, where φ is an aromatic residue (Frohman *et al*., 1999; McDermott *et al*., 2004). The PLD sequence of this motif is Y/FxYxxxF/Y which is thought to target PLD1 to the membrane and PLD2 to caveolae (Okamoto *et al*., 1998; Frohman *et al*., 1999).

The serine reside of a short motif (IGSANIN) conserved in PLD1 located nearest the C-terminus is necessary for correct localisation, catalytic activity and post-translational modification (Manifava *et al*., 1999). Palmitoylation increases protein hydrophobicity and may assist in PLD1-phospholipid interaction (Manifava *et al*., 1999). Modification of the serine-911 residue of PLD1 to alanine resulted in the loss of palmitoylation and changed the expression of PLD1 from punctate perinuclear localisation to cytosolic in COS cells (Manifava *et al*., 1999). This suggests that palmitoylation may not only be dependent on the correct residues but also the catalytic activity of PLD1 (Manifava et al., 1999; McDermott *et al*., 2004).

1.2.6: Expression and subcellular localisation of PLD1 and PLD2

PLD1 and PLD2 are expressed in a variety of tissues and cell lines and both isoforms are commonly co-expressed (although this is not always the case – Meier *et al*., 1999). Expression of PLD in mammalian tissues and cell lines has been analysed primarily using mRNA levels owing to the lack of high affinity antibodies to PLD isoforms (Meier *et al*., 1999). Although mRNA levels have been used as 'markers' for PLD expression, it is unclear how these correspond to protein expression (McDermott *et al*., 2004). The two isoforms are expressed in tissues ranging from heart to brain and have varying expression levels in tissues of the same species, thus implying different functional roles (Meier *et al*., 1999; Millar *et al*., 1999; McDermott *et al*., 2004). The splice variants of the two PLD isoforms are variable in expression levels. PLD1 has two splice variants, PLD1a and PLD1b, where PLD1a has an insertion which does not affect enzymatic activity. Studies assessing expression levels of hPLD1a and hPLD1b found that the shorter splice variant, hPLD1b, was more abundant than hPLD1a in most cell lines (Steed *et al*., 1998). Although *in vitro* assays suggested that PLD1a and PLD1b splice variants had similar properties *in vitro*, studies analysing expression levels of rPLD1a and rPLD1b in a yeast model (*S. pombe*) indicated that the two splice variants responded differently to small G-protein activators (Hammond *et al*., 1997; Katayama *et al*., 1998). There are three splice variants of PLD2; PLD2a, PLD2b and PLD2c which vary in abundance depending on the type of tissue or cell line (Steed *et al*., 1998; Millar *et al*., 1999). PLD2a and PLD2b are expressed in approximately equal amounts and are the most abundant PLD2 isoforms (although PLD2a is slightly more prominent – Steed *et al*., 1998; Millar *et al*., 1999). PLD2c has a 56 base pair insertion which prematurely terminates the polypeptide resulting in truncated protein (Steed *et al*., 1998). PLD2c has the lowest abundance and is expressed at low levels in some tissues, for example brain and skeletal muscle (Steed *et al*., 1998).

The subcellular localisation of PLD1 and PLD2 remains unclear as localisation varies in different cell lines and characterisation is often dependent on the particular molecular markers or antibodies used to probe organelles and assess co-localisation. PLD1a and PLD1b localise to late endosomes and lysosomes of NRK cells but not the Golgi apparatus or the ER (Toda *et al*., 1999). Similarly GFP-PLD1b localised to

the secretory granules and lysosomes of RBL-2H3 cells (but not the Golgi apparatus) and migrated to the plasma membrane upon stimulation (Brown *et al*., 1998). Using U937 promonocytic leukocytes and L1210 lymphocytic leukemia cells, PLD1 was also found to localise to the plasma membrane in unstimulated cells (Kim *et al*., 1999). In the HeLa cell line, PLD1a and PLD1b displayed endosomal localisation but did not localise to the Golgi apparatus, caveolae or clathrin coated vesicles (Hughes and Parker, 2001; reviewed in McDermott *et al*., 2004). Further studies using NIH-3T3 and COS7 cells identified PLD1 localisation in caveolae-enriched microdomains (Kim *et al*., 2000; Xu *et al*., 2000). PLD1 localises to the plasma membrane (co-localising with EGFR) upon EGF stimulation and is also found in caveolin-1 and vesicular structures in the COS7 cell line (Han *et al*., 2002b). GFP-PLD1 co-localised with antibody markers for multivesicular endosomes and late endosomes in HeLa cells (Hiroyama and Exton, 2005b). The same study showed GFP-PLD1 localisation in the trans-Golgi but not the ER, early endosomes or lysosomes of HeLa cells (Hiroyama and Exton, 2005b). In the rat pituitary cell line GH_3, nuclear localisation of PLD1 was enhanced substantially in response to brefeldin A, which resulted in the collapse of the Golgi apparatus (Freyberg *et al*., 2001).

PLD2 is constitutively active when over-expressed in COS7 cells and translocates from the plasma membrane to sub-membranous vesicles upon serum stimulation (Colley *et al*., 1997; Gemeinhardt *et al*., 2009). PLD2 localised with Golgi and ER markers in the COS7 cell line and migrated to the cell edge upon serum stimulation (Divecha *et al*., 2000). PLD2 also localises to the plasma membrane of the RBL-2H3 mast cell line and to the plasma membrane and cytosolic particles in the HeLa epithelial cell line (Cockcroft *et al*., 2001; Hiroyama and Exton, 2005b). GFP-PLD2 did not localise with markers for the ER, Golgi or early endosomes but did co-localise with β-actin in HeLa cells (Lee *et al*., 2001; Hiroyama and Exton, 2005b). PLD2 expression was also found in the cytosol of HeLa cells where PLD2 translocated to membrane ruffles and co-localised with PIP kinase Iα in EGF-stimulated cells (Honda *et al*., 1999). PLD2 localised with endothelial caveolae in primary human endothelial cells and was found in caveolin-enriched membrane microdomains (CEMMS) in NIH 3T3 fibroblasts (Xu *et al*., 2000; Cho *et al*., 2004). In rat NRK cells PLD2 localises to the perinuclear Golgi region and was distributed

throughout the cell in dense cytoplasmic punctiform structures – a fraction of which localised with caveolin-1 and the plasma membrane (Freyberg *et al*., 2002). PLD2 was present in the Golgi apparatus exclusively in the cisternal rims and peri-Golgi vesicles of rat pituitary cells and, in response to brefeldin A, PLD2 translocated to the nucleus (Freyberg *et al*., 2002).

1.3: Phospholipase D activation and regulation (PLD1 and PLD2)

1.3.1: PLD activity in the presence of lipids

The acidic phospholipids which constitute mammalian membranes are phosphatidylcholine (PtdCho), phosphatidylserine (PtdSer), phosphatidic acid (PtdOH) and phosphatidylinositol (PtdIns – Lemmon *et al*., 2008). Inositol lipids are involved in a diverse range of cellular functions including cytoskeletal rearrangement, protein kinase activation, vesicular trafficking and exocytosis (Hinchilffe *et al*., 1998; McDermott *et al*., 2004). The simplest member of this lipid family is PtdIns which makes up approximately 0.5-1.0% of the lipid layer, which faces inside the cell, compared to approximately 25-35% PtdSer (McLaughlin and Murray, 2005; Lemmon *et al*., 2008). PtdIns has a 1,2-diacylglycerol (DAG) backbone and contains five free hydroxyl groups on the inositol ring (McDermott *et al*., 2004; Lemmon *et al*., 2008). PtdIns can be phosphorylated at the 3-, 4-, and/or -5 positions to produce phosphatidyl bis- or tris- phosphates (McDermott *et al*. 2004, Lemmon *et al*., 2008). Several members of the PtdIns lipid family can directly influence PLD activity, although the most potent member is phosphatidylinositol 4,5-bisphosphate (PtdIns(4,5)P_2), which is necessary for both mammalian and yeast PLD activity (DiNitto and Lambright, 2006; Seet *et al*., 2006; Mansfeld and Ulbrich-Hofmann, 2009). Although PtdIns(4,5)P_2 is the most effective PLD activator, PtdIns(3,4,5)P_3 is also effective (Hammond *et al*., 1997). Other PtdIns family members, such as PtdIns, PtdIns(3,4)P_2 and PtdIns(3)P, are either nearly or fully ineffective in respect to PLD stimulation (Liscovitch *et al*., 1994; Hammond *et al*., 1997; Hodgkin *et al*., 2000).

Cellular levels of PtdIns(4,5)P_2 exceed agonist stimulated-levels of PtdIns(3,4,5)P_3, PtdIns(3,4)P_2 or PtdIns(3)P and agonist-stimulated PLD activity has been demonstrated in the absence of measurable PtdIns 3-kinase activity (Cross *et al*., 1996). If PtdIns 3-kinase does regulate PLD, it is unlikely to be direct regulation. PtdIns(3,4,5)P_3, a product of PtdIns 3-kinase action, has been shown to regulate the GTP status of ARF by interacting with the PH domain of the guanine nucleotide exchange factor (GEF) ARNO (Chadrin *et al*., 1996; McDermott *et al*., 2004).

Whilst investigating the effect of a GTPγS-dependent cytosolic factor (later identified as Arf), which stimulated PLD activity in human promyelocytic leukemic (HL60) cells, Ptd(4,5)P_2 was identified as essential for PLD activity and as functioning synergistically in Arf stimulation of PLD (Brown *et al*., 1993). In addition, mammalian PLD isolated from rat brain membrane was potently stimulated by PtdIns(4,5)P_2 *in vitro* (Liscovitch *et al*., 1994). Maximal activity of partially purified PLD is increased tenfold in a PtdIns(4,5)P_2-specific manner, however other more abundant lipids (e.g. PtdSer, PtdOH, PtdIns(4)P or PtdIns) were ineffective in stimulating PLD activity (Liscovitch *et al*., 1994). Similarly, PtdIns(4,5)P_2 potently increased the activity of partially solubilised PLD isolated from human atrial myocardium measured using fluorescent *in vitro* HPLC assays (Kruz *et al*., 2004). Another member of the PtdIns lipid family, PtdIns(3,4,5)P_3, produced from PtdIns(4,5,)P_2 by PtdIns 3-kinase, also stimulated myocardial PLD activity with the same potency as PtdIns(4,5)P_2 but with lower efficiency (Kruz *et al*., 2004). *In vitro* assays using glutathione-S-transferase labelled human PLD1b (GST-hPLD1b) established that both natural polyunsaturated PtdIns(4,5)P_2 and synthetic dipalmitoyl PtdIns(4,5)P_2 were effective GST-hPLD1b activators in the presence of Rac1 (Hodgkin *et al*., 2000). Furthermore, the synthetic PtdIns(3,4)P_2 lipid was also an effective GST-hPLD1b activator (Hodgkin *et al*., 2000). PLD1 bound PtdIns(4,5)P_2 with high specificity and affinity in lipid vesicles (independent of PtdCho content) and was not activated by the PtdIns(4,5)P_2 headgroup (inositol 1,4,5-triphosphate) or the DAG backbone (Hodgkin *et al*., 2000).

The aminoglycoside antibiotic neomycin is a high-affinity ligand of PtdIns(4,5)P_2 and inhibits membrane-bound PLD, although it has no effect on detergent solubilised or partially purified PLD activity (Liscovitch *et al*., 1994; Kurz *et al*., 2004). Neomycin induced inhibition of partially purified rat brain PLD can be reversed by adding PtdIns(4,5)P_2, indicating that neomycin binds endogenous PtdIns(4,5)P_2 (Liscovitch *et al*., 1994). Although PLD2 is not activated by some small G-proteins that induce PLD1 activity, PtdIns(4,5)P_2 is necessary for the activity of both mammalian isoforms (Hammond *et al*., 1995; 1997; Colley *et al*., 1997). Both mammalian and yeast PLD PtdIns(4,5)P_2 binding specificity is attributed to the highly conserved pleckstin homology (PH) and phox homology (PX) domains (Steed *et al*., 1998; Holbrook *et al*., 1999; Seet *et al*., 2006). The PH domain of human

PLD1 has been identified as essential for PtdIns(4,5)P_2 specificity and PLD1 activity and localisation (Hodgkin *et al*., 2000). Two lipid binding pockets have been identified on the PX domain of rat PLD1 which are thought to cause the high level of specificity to PtdIns(4,5)P_2 and other members of the PtdIns lipid family to a lesser extent (Stahelin *et al*., 2004).

In vivo synthesis of PtdIns(4,5)P_2 originates predominantly from PtdIns(4)P, by type I PtdIns 4-P 5-kinases (PtdIns(4)P 5-kinases), such as type Iα PtdIns(4)P 5-kinase in the COS7 cell line (Divecha *et al*., 2000). PtdIns(4)P kinase, purified from bovine brain membranes could be activated by PtdOH by a factor of 20 in micelles containing a combination of PtdIns(4)P and Triton X-100 (Moritz *et al*., 1992). Furthermore, activation of PtdIns(4)P kinase by PtdOH was completely inhibited in the presence of PtdIns(4,5)P_2. Further experiments utilising natural membranes and PtdOH generated by PLD catalysis from purified from rat brain, suggested that PtdOH may be an essential regulator of PtdIns(4)P kinase (Moriz *et al*., 1992).

In COS7 cells, both PLD1 and PLD2 interact with type Iα PtdIns(4)P 5-kinase and *in vivo* PLD2 activity can be regulated solely by expression of this PtdIns(4)P 5-kinase (Divecha *et al*., 2000). Co-expression of PLD2 and type Iα PtdIns(4)P 5-kinase in porcine aortic endothelial (PAE) cells showed that the lipid kinase altered localisation to cytoplasmic punctiform structures thus co-localising with PLD2 (Divecha *et al*., 2000). Transfection of PAE cells using haemagglutinin (HA)-tagged type Iα PtdIns(4)P 5-kinase resulted in plasma membrane localisation and increased activation in response to lyso-PtdOH stimulation (Jones *et al*., 2000). Type Iα PtdIns(4)P 5-kinase activation was notably reduced in cells pre-treated with butan-1-ol, therefore indicating the involvement of PLD as the *in vivo* generator of PtdOH (Jones *et al*., 2000). Arf6 (a PLD1 activator) also co-localises with type Iα PtdIns(4)P 5-kinase in membrane ruffles of agonist-stimulated HeLa cells, and data suggests that this lipid kinase is a downstream effector of Arf6 (Honda *et al*., 1999). Similarly, PLD2 migrates to membrane ruffles suggesting elevated PtdIns(4,5)P_2 (Honda *et al*., 1999). Studies utilising purified lysosomes and Golgi membranes have identified PLD activation as essential for the synthesis of PtdIns(4,5)P_2 (Arneson *et al*., 1999; Siddhanta *et al*., 2000). PtdOH generated by a PLD1-like enzyme, located on the lysosomal surface, potently stimulates type I PtdIns(4)P 5-

kinase and is inhibited by butan-1-ol treatment (Arneson *et al*., 1999). Similarly *in vitro* PtdIns(4,5)P_2 generation by Golgi membranes was halted upon treatment with butan-1-ol (Siddhanta *et al*., 2000). This association between PLD localisation and activity with that of PtdOH activation of type Iα PtdIns(4)P 5-kinase suggests a positive feed-back loop (McDermott *et al*., 2004).

1.3.2: Protein kinase C

The protein kinase C (PKC) superfamily has three subfamilies; the classical isoforms (α, β and γ), the novel isoforms (δ, ε, η, θ and μ) and the atypical isoforms (ζ and λ). The classical PKC isoforms can be stimulated by DAG, Ca^{2+} or phosphatidylserine (PtdSer)-stimulated, whilst novel isoforms are not Ca^{2+} regulated and atypical isoforms are not regulated by Ca^{2+} or DAG (Singer *et al*., 1996; McDermott *et al*., 2004). PLD can be stimulated using Ca^{2+} ionophores (e.g. A23187) and phorbol esters (e.g. PMA) in a variety of tissues and immortalised cell lines which implicates a Ca^{2+}/DAG-sensitive PKC (e.g. classical or novel PKC isoforms – McDermott *et al*., 2004). In addition, prolonged pre-treatment of cells with phorbol esters or PKC inhibitors (e.g. Ro 31-8220) results in the abolishment of agonist-stimulated PLD activity (Min *et al*., 1998b). There are two types of PKC inhibitors, selective inhibitors, such as the benzophenanthridine alkaloid chelerythrine (selective for Ca^{2+} or phospholipid-dependent PKC), and non-selective inhibitors, such as staurosporine (Herbert *et al*., 1990; Bosch *et al*., 1999; Singer *et al*., 1996).

Studies have shown that activation of PLD by PKC isoforms is complex and may occur either through phosphorylation, idependently of phosphorylation or indirectly as discussed below (Singer *et al*., 1996; Brown *et al*., 1998; Min and Exton, 1998; Feng *et al*., 2000). PLD is stimulated by PKCα, PKCβ1 and PKCβ2 but not PKCγ or any other novel or atypical PKC isoforms *in vitro* (Frohman *et al*., 1999). This *in vitro* PLD activation occurred without the addition of phorbol esters, although in the presence of phorbol esters, the potency and efficacy of PKC-mediated PLD activation was augmented (Frohman *et al*., 1999). *In vivo* studies (using either Swiss 3T3 or Rat-6 fibroblasts) have established that PKCα and PKCβ1 enhance agonist-mediated PLD activation using platelet-derived growth factor and endothelin-1 respectively (Pai *et al*., 1991; Eldar *et al*., 1993). Dephosphorylation of PKCα (purified from porcine brain cytosol), using protein phosphatase 1γ or 2A, resulted in a loss of kinase activity but did not affect PKCα activation of PLD, suggesting that PKC-activation of PLD is independent of phosphorylation (Singer *et al*., 1996; McDermott et al., 2004). Furthermore, rat brain PLD1 (rPLD1) expressed in PMA-stimulated Rat-1 fibroblasts indicated that the PKCα binding domain of rPLD was located on the N-terminus and formed a multi-component complex which underwent

serine/threonine phosphorylation (Min and Exton, 1998). Serial deletions of the first 319 N-terminal amino acid residues of purified recombinant PLD1 showed enhanced PLD activity. The most enhanced mutant resulted from deletion of the first 168 amino acid residues, indicating a regulatory domain in this region (Park *et al*., 1998). N-terminal residues 51-115 of recombinant PLD1 were essential for both PMA stimulation and PKCα activation of the phospholipase (Park *et al*., 1998). Further studies support this data showing that deletions of the first 325 N-terminal amino acid residues of PLD1 are required for PKCα-mediated PLD1 activation both *in vivo* and *in vitro,* that PLD1 and PKCα are closely associated and can be co-immunoprecipitated, and that this region functions to inhibit basal PLD activity *in vivo* (Sung *et al*., 1999b). The data may suggest that PKC activation of PLD1 is a result of alleviating an inbuilt inhibition (Park *et al*., 1998; McDermott *et al*., 2004). However, co-expressing PLD1 with dominant negative PKCα (mutated at the ATP-binding site) resulted in a notable inhibition of phosphorylation and PLD1 activation upon EGF stimulation, suggesting a phosphorylation dependent and independent mechanism of PLD1 activation by PKC which has yet to be fully clarified (Frohman *et al*., 1999; Han *et al*., 2002b).

Although PKC association with PLD1 has been extensively studied, PKC regulation of PLD2 has also been reported. PKCδ was co-immunoprecipitated with PLD2 in rat phenochromocytoma PC12 cell extracts *in vivo* and associated with PLD2 in a PMA-dependent manner *in vitro* (Han *et al*., 2002a). Expression of PLD2 in PC12 cells increased PMA and bradykinin-stimulated PLD activity, and upon stimulation PLD2, was phosphorylated (Han *et al*., 2002a). The specific inhibition of PKCδ (using rottlerin) prevented PMA-stimulated PLD2 activity in PC12 cells, suggesting phosphorylation-dependent regulation of PLD2 (Han *et al*., 2002a).

Although PLD is activated by PKC, the mechanism by which the lipase is activated may be indirect. PLD1 is known to translocate to the plasma membrane in response to agonist stimulation, e.g. PMA stimulation of RBL-2H3 cells (Brown *et al*., 1998). PKC (such as PKCβ) is also targeted to the plasma membrane of live cells by two membrane targeting domains known as the C1 and C2 regions (Feng *et al*., 2000). PKC translocation to the plasma membrane may then facilitate PLD interaction with both its substrate PtdCho and PtdIns(4,5)P_2, a lipid activator (Feng *et al*., 2000;

McDermott *et al*., 2004). The activation of PLD1 by PKC in the COS7 cell line resulted from direct PLD1 phosphorylation by PKC which occurred in the caveolin and plasma membrane (Kim *et al*., 2000). Furthermore, PLD2 activation by PKCδ *in vivo* correlated to direct phosphorylation of PLD2 and translocation of PKCδ from the cytosol to the plasma membrane, where PLD2 was primarily localised (Han *et al*., 2002a).

PKCα synergistically stimulates PLD activity in combination with other small G-protein activators such as Arf1, RhoA, Rac1 or Cdc42 (Singer *et al*., 1996; Hodgkin *et al*., 1999). In Rat1 fibroblasts, PKCα binds to rPLD1 and another 220kDa phosphorylated protein in response to phorbol ester stimulation (Min and Exton, 1998). The 220kDa protein can be co-immunoprecipitated with rPLD1, indicating that PKC-mediated serine/threonine phosphorylation of PLD-associated proteins may ultimately result in PLD activation (Min and Exton, 1998). Furthermore, phosphorylation of scaffolding proteins may also facilitate translocation of PLD (Min and Exton, 1998; Exton, 1999). Synergistic activation of PLD by Arf and Rho family members and PKC may be attributed to the phosphorylation of guanine nucleotide exchange factors (GEFs) by PKC (Fleming *et al*., 1997; Exton, 1999). In Swiss 3T3 cells, the Rac1-specific GEF, Tiam1, was selectively threonine phosphorylated in response to a range of stimulators including PMA and lysophosphatidic acid (Fleming *et al*., 1997). Cells exposed to prolonged PMA treatment or treatment with a PKC inhibitor (Ro-31-8220) resulted in a dramatic reduction in the phosphorylation of Tiam1. Furthermore, *in vitro* assays indicated that PKC activity was sufficient for threonine-phosphorylation of Tiam1 (Fleming *et al*., 1997). PKC phosphorylation of Rho family GEFs, such as Tiam1, may activate small G-proteins which are known activators of PLD1 and thus stimulate PLD activity (Fleming *et al*., 1997; Exton, 1999). Treatment of cells using clostridial toxins inhibits PMA stimulation of PLD, further indicating that PKC has an important role in PLD activation (Exton, 1999; McDermott *et al*., 2004).

Although PKC and Arf family members have been found to work together as activators of PLD activity, several studies have suggested that the two proteins do not work synergistically. PMA stimulation of PLD in the HEK cell line was characterised as phosphorylation-dependent and involving PKC independently from

Arf stimulation of PLD (Rümmenapp *et al*., 1997). PKC activated PLD in HEK cell membranes required ATP and treatment with staurosporine (competitive at the ATP-binding site) resulted in a dramatic decrease in PMA stimulation of PLD (Rümmenapp *et al*., 1997).

Rat PLD1 was not activated synergistically by Arf3 and RhoA or by PKCα or PKCβII with these small G-proteins (Min *et al*., 1998a). Synergistic activation of purified recombinant hPLD1b or PLD from detergent-extracted HL60 membranes, using a combinantion of PKCα, Arf1 and Cdc42 has been established (Hodgkin *et al*., 1999). *In vitro* data indicated that both PKCα and PKCβII directly phosphorylated rPLD1 and that this phosphorylation corresponded to the inhibition of the rPLD1 catalytic site. *In vitro* studies suggest that PKC negatively regulates rPLD1 activity by phosphorylation (Min *et al*., 1998a). Furthermore, rPLD1 activation by PKCα and PKCβII, in response to PMA stimulation was ATP-independent (Min *et al*., 1998a). The presence of ATP may act as inhibitory to the activation of purified rPLD1 by PKC (Min *et al*., 1998a; Min and Exton, 1998). The three residues identified in direct phosphorylation of rPLD1 by PKCα *in vitro* were serine 2, threonine 147 and serine 561 (Kim *et al*., 1999). Mutation of any of these key phosphorylated residues resulted in significantly attenuated PLD activity in response to PMA stimulation *in vivo* (Kim *et al*., 1999). Further *in vivo* studies using a triple rPLD1 mutant of these residues resulted in significantly attenuated PLD activation upon PMA stimulation (Kim *et al*., 2000). Furthermore, PLD1 becomes threonine-phosphorylated during PMA treatment of COS cells expressing wildtype PKCα (Kim and Exton, 2003). PKCα lost the ability to bind to the PLD1 active site when the first 10 residues were deleted or residue 10 (phenylalanine) was mutated to alanine or aspartic acid (Kim and Exton, 2003). In addition, time course experiments indicated that PMA stimulation of PLD1 reduced with time as phosphorylation increased. This further supports negative regulation of PLD1 by PKCα, although phosphorylation is a slow process and initial activation of PLD1 was highly correlated with PKCα binding (Kim and Exton, 2003).

Agonist activation of PLD also often results in the stimulation of PtdIns(4,5)P_2 hydrolysis by phospholipase C (PLC – Exton *et al*., 1997). PLC hydrolysis of PtdIns(4,5)P_2 ultimately results in diacylglycerol production and activation of PKC

(Exton *et al*., 1997). An epithelial cell line expressing wildtype or mutant platelet derived growth factor (PDGF) receptor was used to investigate whether PLD activation was dependent upon PLC hydrolysis of PtdIns (Yeo *et al*., 1994). PDGF stimulation of cells expressing wildtype PDGF receptors activated both PLD and PLC, however cells expressing kinase-deficient PDGF receptors did not show this effect (Yeo *et al*., 1994). Stimulation of PLD and PLC was restored using a mutant PDGF receptor able to bind to PLCγ1 and no other signalling molecule (Yeo *et al*., 1994). PLCγ1 activation and corresponding PLD stimulation was probably PKC-dependent as treatment of these cells with PKC-inhibitor R0-31-8220 or pre-treatment with PMA resulted in notably reduced PDGF activation of PLD (Yeo *et al*., 1994). Furthermore, experiments using a fibroblast cell line stably expressing PLCγ1 indicated that PLD activation in response to PDGF stimulation is dependent on PLCγ1 expression (Lee *et al*., 1994). Pre-treatment with tyrosine kinase inhibitors (such as staurosporine or genistein) resulted in dramatically reduced PLD activity and inhibition of PDGF receptor and PLCγ1 tyrosine phosphorylation in PDGF-stimulated cells (Lee *et al*., 1994). Co-expression of PLD1 and PLCγ in HEK-293 cells resulted in increased basal PLD1 activity (Slaaby *et al*., 2000). Although basal PLD2 activity was unaffected by PLCγ, co-expression of PLCγ facilitated insulin stimulated PLD2 activation (Slaaby *et al*., 2000). Furthermore PLD2 was thought to be constitutively associated with PKCα in the HEK-293 cell line (Slaaby *et al*., 2000). Both PLD1 and PLD2 were activated maximally when co-transfected with PKCα in the presence of PLCγ in insulin-stimulated HEK-293 cells (Slaaby *et al*., 2000).

1.3.3: ADP-ribosylation factors

ADP-ribosylation factor (Arf) family members are approximately 21kDa in size and conserved in both structure and function, sharing more than 60% identity in eukaryotes (Boman and Kahn, 1995). The Arf family is divided into Arf and Arf-like (Arl) proteins and are part of the regulatory GTP-binding protein Ras superfamily (Boman and Kahn, 1995). The six ubiquitous mammalian Arf proteins have been divided into three classes and are categorised based on size, amino acid composition, gene structure and phylogenetic analysis (Boman and Kahn, 1995; Moss and Vaughan, 1998). Mammalian Arf1, Arf2 and Arf3 are members of class I, Arf 4 and Arf5 are in class II and Arf6 is alone in class III (Moss and Vaughan, 1998; Donaldson and Honda, 2005). Arf1, Arf3, Arf5 and Arf6 have been implicated in mammalian PLD activation and show only modest differences in potency and efficiency (Brown *et al*., 1993; Massenburg *et al*., 1994; Brown *et al*., 1995; Hiroyama and Exton, 2005a). *In vitro* assays suggest that partially myristolyated recombinant Arf1 resulted in potent PLD activation (from human promyelocytic leukemic (HL60) cell membranes) similar to that of native protein, whereas non-myristoylated Arf1 was a weak PLD activator (Brown *et al*., 1993).

Although Arf stimulates PLD activity directly, other Arf regulatory proteins such as guanine nucleotide exchange factors (GEFs) may have a knock-on effect on Arf stimulation of PLD (Li *et al*., 2003). Arf nucleotide site opener (ARNO)/cytohesin family GEFs are thought to prefer Arf1 as a substrate but may also interact with Arf6 at the plasma membrane of some cell lines (Cohen *et al*., 2007). Transiently expressed ARNO in a rat fibroblast cell line which overexpress human insulin receptors resulted in ARNO translocation to the plasma membrane in response to insulin (Li *et al*., 2003). ARNO is thought to mediate Arf and PLD activation in response to insulin via the insulin receptor (Li *et al*., 2003). Exchange factor for Arf6 (EFA6) is a Sec7 domain-containing Arf GEF, which is Arf6 specific and distinct from the ARNO family of GEFs (Franco *et al*., 1999). EFA6 also has a homologue which contains a Sec7 domain, pleckstrin homology (PH) domain and the same ~150 C-terminal amino acids thought to be responsible for a coil motif (Derrien *et al*., 2002). The EFA6 homologue also interacts with Arf6 both *in vitro* and *in vivo* (in baby hamster kidney cells) and so is a possible candidate for indirect

PLD regulation (Derrien *et al*., 2002). Cytohesin-1 and general receptors for phosphoinositides (GRP1) are also known Arf GEFs both of which contain highly conserved Sec7 and PH domains (Roth, 1999). The PH domains of GRP1 and cytohesin-1 are Arf1 specific, bind to PtdIns(3,4,5)P_3 and may be recruited to membranes by PtdIns 3-kinase activity (Klarund *et al*., 1997; Meacci *et al*., 1997; Roth, 1999).

Inhibitors such as the fungal metabolite brefeldin A have previously been used to characterise the role of Arf by inhibiting GEFs that are responsible for the activation of some Arf family members (Donaldson *et al*., 1992). Brefeldin A treatment of cells results in interference of protein transport from the endoplasmic reticulum (ER) to the Golgi apparatus, resulting in protein acuumulation in the ER (Klausner *et al*., 1992). Brefeldin A treatment of human embryonic kidney (HEK) cells, stably expressing the muscarinic acetylcholine receptor (mAChR) human m3 subtype, resulted in the loss of mAChR-mediated PLD activation (Rümenapp *et al*., 1995). Inhibition of PLD activation was reconstituted in permabilised cells using purified recombinant Arf and was GTPγS-dependent (Rümenapp *et al*., 1995). Arf proteins and their related nucleotide exchange factors regulate the signalling cascade leading from mAChR activation to PLD stimulation in HEK cells (Rümenapp *et al*., 1995). Furthermore, expression of dominant negative Arf1 with preference for the GDP-bound state in HeLa cells resulted in inhibition of ER transport and had a brefeldin A-like phenotype (Dascher and Balch, 1994). Although multiple studies have demonstrated inhibition of PLD stimulation in brefeldin A treated cells other studies have shown treatment with this fungal metabolite has no effect on PLD activity. Short (1 hour) treatment of HL60 cells with brefeldin A did not affect activation of PLD, therefore PLD is unlikely to be regulated by brefeldin A sensitive Arf in HL60 cells (Guillemain and Exton, 1997). However, prolonged (6 hours) treatment of HL60 cells with brefeldin A gradually and completely inhibited activation of PLD by formyl-Met-Leu-Phe and partially inhibited activation by PMA (Guillemain and Exton, 1997). The result of prolonged brefeldin A treatment on HL60 cells may result from the disruption of the Golgi apparatus and inhibition of phospholipase C activity (Guillemain and Exton, 1997). The Arf isoform responsible for PLD activation may be brefeldin insensitive or, alternatively, Arf does not participate in HL60 PLD activation.

HEK cells stably expressing mAChR human m3 subtype were carbachol-stimulated and digitonin permeabilised and Arf activity measured as cytosol to membrane localisation upon fractionation (Rümenapp *et al*., 1995). Carbachol treatment of cells prior to permeabilisation resulted in a ~60% reduction in the release of Arf, therefore indicating an increase in membrane association which is essential for PLD activation (Rümenapp *et al*., 1995; McDermott *et al*., 2004). In addition, Arf and RhoA induced maximal activity of membrane-associated PLD in HL60 cells in the presence of polyphosphorylated inositol lipids (Martin *et al*., 1996). Endogenous Arf and Rho increased their association with membranes in GTPγS-treated HL60 cells, resulting in increased PLD activity (Martin *et al*., 1996). The addition of EDTA resulted in decreased membrane translocation of Arf, increased translocation of Rho and a decrease in stimulated PLD activity (Martin *et al*., 1996). Furthermore, PLD2 and Arf6 co-localise to the plasma membrane of RBL-2H3 cells following antigenic stimulation (Cockcroft *et al*., 2001).

Human PLD1a and PLD1b splice variants are both stimulated by Arf, as is rat PLD1 (Hammond *et al*., 1995; Hammond *et al*.,1997; Park *et al*., 1997). Reports indicate that both PLD1 and PLD2 can be Arf-stimulated, although the magnitude of response varies considerably. Arf1 stimulated activity of hPLD1 expressed in Hi5 insect cells 20-fold compared with a twofold increase of hPLD2 activity (Lopez *et al*., 1998). The PLD1 effector region of Arf1 was identified using substitution and deletion mutants of the small G-protein (Jones *et al*., 1999). The site of interaction between PLD1 and Arf1 was identified as the α2 helix, part of the β2-strand and the N-terminal helix inclusive of the subsequent loop (Jones *et al*., 1999). Furthermore, the first 17 N-terminal amino acids of Arf1 were essential for PLD activity and secretion in HL60 cells (Jones *et al*., 1999). The first 308 N-terminal amino acids of mammalian PLD2 are responsible for both the high basal activity and Arf regulation of PLD2 (Sung *et al*., 1999a). Removal of the first 308 N-terminal amino acids of PLD2 resulted in decreased basal activity *in vivo* and heightened responsiveness to Arf proteins (Sung *et al*., 1999a). Furthemore dominant negative Arf6 inhibited PLD2 and consitutively active Arf6 selectively activated PLD2 in HeLa cells (Hiroyama and Exton, 2005b). Although some studies show that PLD2 is Arf-regulated, PLD2 has historically been characterised as the oleate-dependent PLD

isoform. Two forms of PLD solubilised from rat brain membranes suggested that one form of PLD was Arf1, phosphatidylinositol 4,5-bisphosphate (PtdIns(4,5)P_2) and GTPγS-dependent, whereas the other form was oleate-dependent and unaffected by Arf, PtdIns(4,5)P_2 and GTPγS (Massenburg *et al*., 1994). Subcellular fractionation of RBL-2H3 cells indicates that Arf1-stimulated PLD migrates with markers for secretory granules, whereas oleate-stimulated PLD migrates with plasma membrane markers (Cockcroft *et al*., 2001). This migration pattern is consistent with GFP-PLD1 localisation to secretory granules and GFP-PLD2 localisation to the plasma membrane (Brown *et al*., 1998; Cockcroft *et al*., 2001).

PLD regulation by Arf can be through direct interaction between lipase and small G-protein, or indirect interaction via Arf GEFs or via PtdIns(4)P 5-kinase stimulation (Martin *et al*., 1996). Arf stimulation of PLD increased in the presence of Mg^{2+} ions and ATP in HL60 cells, possibly due to augmented PtdIns(4,5)P_2 levels as a result of increased PtdIns(4)P 5-kinase activity (Martin *et al*., 1996). A GTPγS-dependent protein was identified as the regulator of PtdIns(4)P 5-kinase in the presence of PLD-generated PtdOH (Honda *et al*., 1999). This PtdIns(4) 5-kinase activator was identified as a 21kDa protein which showed sequence homology with both Arf1 and Arf3 (Honda *et al*., 1999). *In vitro* data indicated that Arf1, Arf5 and Arf6 could activate PtdIns(4)P 5-kinase in the presence of PtdOH and GTPγS. Arf6 alone coincides spatially with the kinase *in vivo* and therefore PtdIns(4)P 5-kinase may bind PtdOH directly resulting in a conformational change facilitating the binding of activated Arf (Honda *et al*., 1999).

1.3.4: Rho family GTPases

Rho family GTPases are found in all eukaryotic cell lines and form a distinct subsection of the Ras-related small GTPase superfamily (Aspenström *et al*., 2004; Jaffe and Hall, 2005). Rho family GTPases are encoded by 22 mammalian genes which can be divided into eight groups and include *RhoA*, *Rac1* and *Cdc42*, known phospholipase D (PLD) activators (Powner *et al*., 2002; Walker *et al*., 2002; Aspenström *et al*., 2004; Jaffe and Hall, 2005). Rho family proteins are involved in a range of cellular processes including cytoskeletal rearrangement. Transfection of RhoA in an endothelial cell line resulted in the assembly of actin stress fibres, whereas Cdc42 and Rac1 expression induced formation of thick bundles of actin filaments (Aspenström *et al*., 2004). Rac1 was also involved in the formation of lamellipodia when expressed in the endothelial cell line (Aspenström *et al*., 2004). Rac1 was shown to mediate the rapid accumulation of actin filaments at the plasma membrane, thus producing membrane ruffles, in a growth-factor stimulated fibroblast cell line (Ridley *et al*., 1992).

The role of Rho family GTPases in PLD regulation was first characterised in neutrophil subcellular sections, where GTPγS and phorobl 13-myristate 12-acetate (PMA) stimulated PLD resulted in phosphatidic acid (PtdOH) generation and transphosphatidylation (Olson *et al*., 1991). This suggested that PLD activation required specific protein factors localised in the plasma membrane and, in the presence of inhibitors (e.g. guanosine diphosphate and guanosine monophosphate), failed to stimulate PLD activity (Olson *et al*., 1991). Several studies have since implicated members of the Rho family of GTPases as PLD activators in a range of cell lines and tissues. Activation of PLD has been established in tissues ranging from brain to lung and from the Golgi apparatus of Chinese hamster ovary (CHO) cells to the nuclei of Madin-Darby canine kidney (MDCK) cells (Balboa and Insel, 1995; Ktistakis *et al*., 1996; Provost *et al*., 1996). Examples of PLD activation include activation by Cdc42 and RhoA in the cytosol of human promyelocytic leukemic 60 (HL60) cells (Siddiqi et al., 1995). Another Rho family protein RalA is thought to mediate tyrosine kinase activation of PLD (Jiang *et al*., 1995). Rat tissues including liver, lung, spleen and brain showed an increase in PLD activity in response to RhoA in the presence of GTPγS (Provost *et al*., 1996). Furthermore, *in vitro* PLD assays

utilising purified recombinant protein have identified direct activation of PLD1 by Rac1, Cdc42 and RhoA in the presence of GTPγS (Hodgkin *et al*., 1999).

The yeast-2-hybrid system was used to elucidate RhoA interaction with phospholipase D (Yamazaki *et al*., 1999). Activation of human PLD1 (hPLD1) by RhoA was identified at the C-terminus of the lipase whilst N-terminal hPLD1 did not interact with RhoA (Yamazaki *et al*., 1999). Furthermore, lipid modification of RhoA facilitated more efficient interactions between the lipase C-terminus and activator (Yamazaki *et al*., 1999). Further studies using the yeast split-hybrid system were used to analyse binding and expression of RhoA in the COS7 cells to further elucidate RhoA-mediated hPLD1 activation (Du *et al*., 2000). COS7 cells transiently expressing hPLD1 mutants were harvested and hPLD1 activity assayed *in vitro* in the presence of RhoA and Arf (Du *et al*., 2000). Mutation at residues I870 (I870T) and combined mutations of Q975 and D999 (Q975R and D999V), resulting in near complete loss of RhoA, facilitated hPLD1 activation (Du *et al*., 2000). Studies using phage display of different rat PLD1 (rPLD1) peptides identified the site of GTP-bound RhoA interaction between amino acid residues 873-1024 of the rPLD1 C-terminus (Cai and Exton, 2001). Single mutations in amino acid residues 946-962 resulted in reduced RhoA activation of rPLD1 (Cai and Exton, 2001). Furthermore, double mutations of key residues such as K946A with K962A or V950A resulted in near complete loss of RhoA activation of rPLD1 and PMA stimulation showed no effect (Cai and Exton, 2001).

The switch I domain is a common interaction site of Ras-like G-proteins and is essential for PLD activation (Bae *et al*., 1998). Furthermore, isoprenyl modification of the switch I domain enhances *in vitro* activation of rPLD1 whilst mutation of the conserved residues (e.g. Y84, T37 and F39) eliminated PLD activation (Bae *et al*., 1998). A chimeric protein substituting the N-terminal third of Cdc42 with RhoA increased PLD activation which was attributed to the Q52 residue adjacent to the switch II domain (Bae *et al*., 1998). Furthermore, Cdc42 binding and activation of hPLD1 is inhibited by point mutation Y40C in the Cdc42 switch I domain (Walker and Brown, 2002).

Cdc42 binds directly to PLD1 and consequently activates the lipase in the presence of GTP (Walker *et al*., 2000). Cdc42 binding to PLD1 does not require lipid modification, however geranylgeranylation of Cdc42 at the C-terminus is required for lipase activation (Walker *et al*., 2000). As lipid modification is necessary for Cdc42 activation of hPLD1, this implies that co-localisation of Cdc42, hPLD1 and phosphatidylinositol 4,5-bisphosphate at membranes is crucial for the activation process (Walker and Brown, 2002). Deletion of the 13-amino acid Rho insert region of Cdc42 (residues 120-139) did not diminish PLD1 binding, however modification of the Rho insert region of Cdc42 did inhibit PLD1 activation by Cdc42, as well as activation by Arf and protein kinase C (Walker *et al*., 2000). This suggests that binding and activation of hPLD1 by Cdc42 are distinct, with the switch I domain mediating GTP-dependent PLD1 binding and the insert helix responsible for activation (Walker and Brown, 2002).

Although there is evidence for the direct interaction between Rho family GTPases and PLD activation, this may also result via indirect means (McDermott *et al*., 2004). PLD1 is known to translocate to the plasma membrane in response to stimulation in several cell lines (Brown *et al*., 1998; Powner *et al*., 2002). For example, Rac1 and PLD1 both translocate to the plasma membrane of RBL-2H3 cells in response to antigenic stimulation (Powner *et al*., 2002). In this case, Rac1 association with PLD1 possibly facilitates translocation to the plasma membrane and so PLD1 is located in a region of activation (McDermott *et al*., 2004). This translocation therefore provides an example of the alternative activation mechanisms which Rho family proteins utilise to mediate PLD activation.

1.3.5: PLD inhibitors

Although there are no known inhibitors which act directly on PLD, some proteins indirectly inhibit PLD activity. PLD1 has a low basal activity *in vivo*; however PLD2 is thought to be constitutively active and possibly regulated by cytosolic factors *in vivo* (Colley *et al*., 1997). Preliminary studies identified several cytosolic factors from tissues that inhibited recombinant PLD2 *in vitro* (Colley *et al*., 1997). Bovine brain provided the most abundant inhibitory activity and so an enriched preparation of inhibitors was produced (Colley *et al*., 1997). This preparation had both PLD1 and PLD2 inhibitors, one of which was PLD2-specific (Colley *et al*., 1997). The 18kDa protein was not a GTP-binding protein as it was GTPγS-dependent, remaining stable at 70^{o}C and inhibition could not be overcome by adding phosphatidylinositol 4,5-bisphosphate (PtdIns(4,5)P_2 – Colley *et al*., 1997). Recombinant PLD2 was used in reconstituted assays to identify regulators in cells and tissues (Jenco *et al*., 1998). The *in vitro* PLD2-specific heat stable inhibitory protein isolated from bovine brain was a mixture of α- and β-synucleins (Jenco *et al*., 1998). All three naturally occurring synucleins (α-, β-, and γ-synuclein) are equally effective PLD2 inhibitors as are the A53Y or A30P mutants associated with Parkinson's disease (Ahn *et al*., 2002; Payton *et al*., 2004). *In vitro* inhibition of PLD2 by these protein factors could not be overcome by PtdIns(4,5)P_2 or characteristic PLD1 activators. Synucleins are typically located in the brain and are thought to localise to presynaptic nerve terminals where they have been implicated in synaptic transmission (Jenco *et al*., 1998). Tyrosine phosphorylation of α-synucleins is associated with a regulatory role in PLD inhibition as mutation of tyrosine 125 to phenylalanine results in an increased inhibitory effect *in vivo* (Ahn *et al*., 2002). The phox (PX) and pleckstrin (PH) homology domains of PLD and the amphipathic repeat region and non-Aβ component of α-synuclein are required for binding between the two (Ahn *et al*., 2002). Furthermore, Ca^{2+}-dependent protein kinase phosphorylation has been implicated in reduced synuclein inhibition of PLD2 (Jenco *et al*., 1998).

Another non-PtdIns(4,5)P_2-dependent inhibitor of both oleate- and PtdIns(4,5)P_2-dependent PLD activity is β-actin (Lee *et al*., 2001). β-actin inhibition of PLD2 could be partially overcome by ADP-ribosylation factor 1 (Arf1) *in vitro* (Lee *et al*.,

2001). β-actin is a 43kDa PLD-binding protein isolated from rat brain, which inhibits both PLD isoforms with similar binding and potency in a concentration dependent manner (Lee *et al*., 2001). The region between amino acids 613 and 723 of PLD2 is essential for direct β-actin binding (Lee *et al*., 2001). Co-immunoprecipitation studies using the COS7 cell line showed that both PLD1 and PLD2 co-immunoprecipitated with β-actin (Lee *et al*., 2001). Another cytoskeletal actin-binding protein, α-actinin is a member of the spectrin superfamily and a known inhibitor of myocardial PLD (Park *et al*., 2000; Sjöblom *et al*., 2008). In non-muscle cells α-actinin localises to actin filaments and to local adhesion sites (Sjöblom *et al*., 2008). Myocardial PLD is primarily associated with α-actinin and localises to sarcolemmal membranes (Park *et al*., 2000). Like β-actin, α-actinin binds directly to PLD2 and *in vitro* binding assays have identified the first 185 N-terminal amino acids of murine PLD2 as the site of interaction (Park *et al*., 2000). Furthermore, purified α-actinin inhibition of PLD2 is reversible in the presence of Arf1 (Park *et al*., 2000). Although α-actinin and β-actin interact at different sites, the interaction between α-actinin and PLD2 can be terminated by β-actin (Lee *et al*., 2001). Although α-actinin shares sequence homology with fodrin, another PLD inhibitor, the two proteins function via different mechanisms (Fukami *et al*., 1996; Lukowski *et al*., 1998). While a PtdIns(4,5)P_2 binding site (between residues 168-184) has been identified on α-actinin PLD2, inhibition is thought to proceed via direct interaction between lipase and inhibitor rather than PtdIns(4,5)P_2 sequesteration (Fukami *et al*., 1996; Park *et al*., 2000).

Numerous PLD inhibitors act by hydrolysing or sequestering PtdIns(4,5)P_2 so that this essential cofactor is unavailable to PLD (McDermott *et al*., 2004). Fodrin is an actin-binding protein which is a non-erythroid spectrin and located on the intracellular face of the plasma membrane (Lukowski *et al*., 1996; Lukowski *et al*., 1998). Fodrin contains a PtdIns(4,5)P_2-binding PH domain which is thought to sequester PtdIns(4,5)P_2, rendering it unavailable to PLD, thus inhibiting lipase activity (Lukowski *et al*., 1998). Furthermore, dimeric and tetrameric erythroid spectrin, which are fodrin analogues, also facilitate inhibition of PLD activity (Lukowski *et al*., 1996). Synaptojanin is a 150kDa protein purified from rat brain which is a member of the inositol polyphosphate 5-phosphatase family (Chung *et al*., 1997). Synaptojanin inhibits PLD activated by Arf and PtdIns(4,5)P_2 *in vitro* by

hydolysing both the 4- and 5- phosphates of the compound, thus converting it to phosphatiylinositol (Chung *et al*., 1997). As PtdIns(4,5)P_2 is hydrolysed by synaptojanin, it is unavailable as a cofactor of PLD and so results in *in vitro* PLD inhibition (Chung *et al*., 1997).

Purification from rat brain identified numerous PLD inhibitors including the clathrin assembly protein 3 (AP3), later referred to as AP180 (Lee *et al*., 1997; Lee *et al*., 2000). AP180 is approximately 165kDa and binds both pre-assembled clathrin cages and inositol hexakisphosphate, although this binding does not impact on AP180-mediated PLD inhibition (Lee *et al*., 1997). AP180 binds the PLD co-factor PtdIns(4,5)P_2 with low affinity but this is not the mechanism which facilitates PLD inhibition (Lee *et al*., 1997). *In vitro* binding assays show AP180 is likely to bind directly to PLD, thus causing inhibition. Amino acid residues 290 to 320 of AP180 are essential for both PLD binding and inhibition (Lee *et al*., 1997).

Amphiphysins I and II have been identified as PLD inhibitors isolated from rat brain (Lee *et al*., 2000). Amphiphysin I is a multi-linker protein which interacts with amphiphysin II, PtdIns(4,5)P_2 and PLD at the N-terminus (Wu *et al*., 2009). Amphiphysins I and II form a heterodimer which then associates with the clathirin coat and is thought to interact directly with PLD, inhibiting both PLD1 and PLD2 isoforms (Lee *et al*., 2000). The first 1-373 amino acid residues of amphiphysin I reportedly bind to PLD and inhibit activity (Wu *et al*., 2009). Lee *et al*., (2000) showed that the heterodimer formed was responsible for dynamin recruitment via the two SH3 domains and simultaneously bound the AP2 adapter protein complex. Clathrin coat assembly required several proteins including AP2 (which initiates clathrin assembly) and AP180. The amphiphysin heterodimer also bound synaptojanin to the SH3 domains resulting in competitive binding with dynamin. Furthermore, amphiphysin I, AP180 and synaptojanin are all nerve-terminal proteins which inhibit PLD and are specific to synaptic vesicles.

Ceramide is at the crux of the sphingolipid pathway and is a second messenger mediating a variety of cellular functions including cell proliferation, differentiation and apoptosis (Mebarek *et al*., 2007). Ceramide may be generated as a result of sphingomyelin hydrolysis by various sphingomyelinases or from other processes

resulting in ceramide synthesis (Mebarek *et al*., 2007). Ceramide is thought to mediate a negative feedback loop which limits myogenic differentiation (Mebarek *et al*., 2007). PLD is necessary for myogenesis and, in a rat myoblast cell line (L60), C6-ceramide decreases PLD1 activity and inhibits PLD1-dependent actin fibre generation (Mebarek *et al*., 2007). C6-ceramide also inhibits PLD activation by PMA in HL60 cells but does not prevent the translocation of protein kinase C (PKC) to the plasma membrane (Venable *et al*., 1996). Cell free assays indicate that PLD inhibition by ceramide is facilitated by inhibiting PKC-mediated PLD activation (Venable *et al*., 1996). Although Venable *et al*. (1996) showed that PKC translocation was unaffected by ceramide treatment, other reports show that PKCα, PKCβ, Arf1, Cdc41 and RhoA translocation is inhibited by C2-ceramide (Abousalham *et al*., 1996). C2-ceramide inhibition of PLD activity via PKC may be attributed to intracellular Ca^{2+} levels as C2-ceramide possibly blocks Ca^{2+} influx (Nakamura *et al*., 1996). Indirect inhibition of PLD by C2-ceramide reversibly inhibits mammalian PLD1 and PLD2 (expressed in Sf9 insect cells) *in vitro* activity, by reacting with the catalytic core of the lipases (Singh *et al*., 2001). This inhibition was more evident when PtdIns(4,5)P_2 concentration was rate limiting and assays using micelles indicated that PtdIns(4,5)P_2 and ceramide were competitively binding to PLD (Singh *et al*., 2001). PLD2 was also inhibited by C16-ceramide, although analogues of both C2- and C16-ceramide did not inhibit PLD activity (Singh *et al*., 2001).

Other lipid inhibitors of PLD have been identified in pig colon mucosa. The PLD inhibitor was purified and contained lysophosphatidylserine, phosphatidylinositol and lysophosphatidylinositol (Kawabe *et al*., 1998). Lysophosphatidylserine was identified as the most potent PLD inhibitor and inhibition was not reversible by increasing substrate concentration or PtdIns(4,5)P_2 of the cell free assays (Kawabe *et al*., 1998). Lysophosphatidylserine inhibited the activity of oleate-dependent, Arf-dependent (PLD1a and PLD1b) and PtdIns(4,5)P_2-dependent (PLD 2) activity (Kawabe *et al*., 1998).

More recently, pharmacological PLD inhibitors have been identified (Scott *et al*., 2009; Su *et al*., 2009). Highly potent, isoform-specific PLD inhibitors have been synthesised which have a greater than 100-fold selectivity for the different PLD

isoforms both *in vitro* and *in vivo* (Scott *et al*., 2009; Su *et al*., 2009). The pharmacological inhibitor 5-fluoro-2-indolyl des-chlorohalopaemide (FIPI), for example, is a potent PLD2 inhibitor both *in vitro* and *in vivo* (Su *et al*., 2009). FIPI inhibits a multitude of processes including cytoskeletal reorganisation, cell spreading and chemotaxis (Su *et al*., 2009). These PLD-specific inhibitors will aide future research identifying the roles of PLD *in vivo,* solidifying data previously established using primary alcohols as functional inhibitors.

1.3.6: Post-translational modification

Palmitoylation of human PLD1 is thought to impact upon both enzymatic regulation and its localisation (Manifava *et al*., 1999). The palmitoylation sites of PLD1 were identified as Cys240 and Cys241 within the PH domain, where Cys241 accounted for the majority of the post-translational modification (Sugars *et al*., 1999). Mutating both Cys240 and Cys241 reduced PLD1 enzymatic activity (between 50-80%) *in vivo* although there was no impact upon *in vitro* PLD1 activity (Sugars *et al*., 1999; reviewed in McDermott *et al*., 2004). The localisation of a double Cys240 and Cys241 mutant (substituting cysteine with either serines or alanines), resulted in a change in the localisation of PLD1 from punctate cytoplasmic expression to expression on the plasma membrane of COS cells (Sugars *et al*., 1999; reviewed in Mansfeld and Ulbrich-Hofmann, 2009). Although it was initially thought that only catalytically active PLD1 would be palmitoylated, point mutations of rat PLD1 (rPLD1) disproved this theory (Xie *et al*., 2001). Palmitoylation needs both the association between both N- and C-termini of PLD1 and, more specifically, the first 168 amino acid residues are needed for palmitoylation (but are non-essential for catalytic activity – Xie *et al*., 2001). Removing N-terminal residues of rPLD1 results in a catalytically active mutant as the conserved C-terminal is responsible for catalytic activity but the protein is not palmitoylated (Xie *et al*., 2001). Hierarchy of membrane-targeting signals exists for PLD1 involving lipid modification of the PH domain. In this model, PLD1 binds to membranes via its PH domain with a subsequent or concurrent fatty acylation, stabilising this interaction (Xie *et al*., 2001; Sugars *et al*., 2002; McDermott *et al*., 2004).

1.3.7: Phosphorylation of PLD

Phosphorylation has been reported to act both directly and indirectly on enzyme regulation (McDermott *et al*., 2004). PLD activation has been characterised using various growth factors including epidermal growth factor (EGF) in rat pancreatic acini cells (Rydzewska and Morisset, 1995). Activation of EGFR stimulates PLD activity and can be inhibited by pre-incubating acini cells with staurosporine, a protein kinase C and tyrosine kinase inhibitor (Rydzewska and Morisset, 1995). Pre-incubation of endothelial cells with tyrosine kinase inhibitors (e.g. genistein, erbstatin or herbimycin) resulted in reduced PLD activation by 4-hydroxynonenal, whilst pre-incubation with protein tyrosine phosphatase inhibitors increased 4-hydroxynonenal PLD activation (Natarajan *et al*., 1997). EGF stimulates both PLD1 and PLD2 but the EGF receptor has been shown to constitutively associate only with PLD2, with phosphorylation of the Tyr11 residue of PLD2 following EGFR stimulation (Slaaby *et al*., 1998). However, human EGFR was used in combination with rPLD1 with point mutations of the Tyr11 amino acid residue, therefore it is not clear if these observations are physiologically relevant (McDermott *et al*., 2004). Expression of human PLD1 in HL-60 granulocytes was phosphorylated on tyrosine residues and hPLD1 could be co-immunoprecipitated with a variety of unidentified phosphorylated proteins in the presence of tyrosine phosphatase inhibitors, e.g. peroxides of vanadate (Marcil *et al*., 1997).

PLD was stimulated by H_2O_2 in the presence of vanadate and, in Swiss 3T3 cells, rPLD1 formed a complex with platelet-derived growth factor (PDGF) receptor, PKCα and another 62kDa protein (Min *et al*., 1998b). Treatment of cells with either H_2O_2 or vanadate alone did not stimulate PLD activity or induce tyrosine phosphorylation of members of the rPLD1 immune-complex (Min *et al*., 1998b). Characterisation of rPLD1 in Swiss 3T3 cells suggested that phosphorylation and PLD activity could be inhibited by protein-tyrosine kinase inhibitors (e.g. genestein and herbimycin A), down regulation of PKC through prolonged exposure to PMA and inhibition of PKC using inhibitors, e.g. Ro 31-8220 and calphostin C (Min *et al*., 1998b). In addition, studies using HEK-293 cells expressing the M3 muscarinic receptor identified two pathways by which overexpressed PLD could be stimulated, a PKC- and a Ras/Ral-dependent pathway (Voss *et al*., 1999). PLD activation by

receptor tyrosine kinase agonists with endogenously expressed receptors in HEK cells (such as EGF, PDGF and insulin) were used to investigate PLD activity (Voss *et al*., 1999).

PLD activation in phaeochromocytoma cells (PC12 or PC2) also involves a tyrosine kinase, however it remains unclear whether PLD is phosphorylated directly or whether an intermediate protein is phosphorylated (Mehta *et al*., 2003). Peroxyvanadate was the only agent which caused tyrosine phosphorylation of PLD, although both time-course and concentration-dependent assays indicated that PLD activation was not correlated with peroxyvanadate-mediated phosphorylation (Mehta *et al*., 2003). Human promyelocytic leukemic (HL60) cells treated with peroxyvanadate indicated that PLD1 could be directly phosphorylated, as did experiments using Swiss 3T3 cells (Marcil *et al*., 1997; Min *et al*., 1998b). Furthermore, a yeast split-hybrid system was used to produce PLD1 alleles and the interaction between PLD1 and G protein-coupled receptors was investigated (Du *et al*., 2000). Results showed that direct stimulation of PLD1 (*in vivo*) by RhoA or PKC was essential for significant activation but that PLD1 phosphorylation and localisation was independent of these stimulatory pathways (Du *et al*., 2000). EGF stimulation of HEK-293 cells showed phosphorylation of tyrosine-11 of mouse PLD2 (Slaaby *et al*., 1998). COS7 cells transiently expressing PLD1 stimulated with EGF resulted in both activation and phosphorylation of PLD1 (Han *et al*., 2002b). Point mutations at phosphorylation sites (substituting Ser2, Thr147, and Ser561 with alanine) resulted in reduced PLD1 activity and inhibited phosphorylation of the Thr147 amino acid residue (Han *et al*., 2002b; Farquhar *et al*., 2007). In more recent studies PC12/PC2 cells expressing human PLD2 (which does not have a comparable tyrosine residue) indicated that hPLD2 was still tyrosine phosphorylated indicating that other tyrosine residues can also be phosphorylated (Mehta *et al*., 2003). Although tyrosine phosphorylation has an essential role in PLD2 activation (using a variety of agents) it is thought that this is not due to direct phosphorylation of PLD2 (Mehta *et al*., 2003).

PKCα binding and activation of PLD1 is dependent on the phenylalanine residue at position 663 at the C-terminus of PKCα (Hu and Exton, 2003). Deletion up to or substitution (F663D or F663A) of this residue results in the loss of binding,

activation and threonine phosphorylation of PLD1, indicating that both regulatory and catalytic domains of PKCα are necessary for these functions (Hu and Exton, 2003). PLD1 activation by PMA was notably faster than threonine phosphorylation and, as phosphorylation increased, PLD1 activity decreased over time. Initial PMA-activation of PLD1 is correlated with PKCα binding whilst phosphorylation is associated with PLD1 inactivation (Hu and Exton, 2003).

PLD can be activated by RhoA (in the presence of PtdIns(4,5)P_2) in membranes m3 muscarinic acetycholine receptor (mAChR)-expressing HEK-293 cells and is phosphorylation-dependent (Schmidt *et al*., 1999). The serine/threonine kinase Rho-kinase is stimulated by RhoA and over-expression or constitutive expression of Rho-kinase increases m3 mAChR-mediated PLD stimulation, comparable to that mediated by RhoA over-expression (Schmidt *et al*., 1999). HA-1077, a Rho-kinase inhibitor, inhibits RhoA-induced PLD stimulation in the membranes of intact HEK-293 cells as well as PLD stimulation by the m3 mAChR but not PKC and so is thought to be a regulator of PLD activity (Schmidt *et al*., 1999; McDermott *et al*., 2004). Endogenous serine phosphorylation of PLD1, by a 40kDa casein-kinase 2 (CK2)-like family member utilizing GTP was observed in intact CHO cells and is inhibited by heparin or 5,6-dichloro-1-β-$_D$-ribofuranosylbenzimidazole (DRB – Ganley *et al*., 2001). Co-expression of PLD1 with recombinant CK2α and β subunits in COS7 cells showed that PLD1 is associated with the β subunit. Point mutation of the serine residue (at position 911) with alanine resulted in a catalytically inactive non-phosphorylated PLD1 (Ganley *et al*., 2001). *In vitro* assays of PLD1 activity after serine phosphorylation (by CK2) indicated that PLD1-mediated PtdCho hydrolysis was unaffected (Ganley *et al*., 2001). Serine/threonine phosphorylation of rPLD1 has been implicated in maintaining structural stability of the lipase, although was not essential for catalytic activity (Xie *et al*., 2000). Furthermore, for serine/threonine phosphorylation to take place, association between the N- and C-termini of rPLD1 was required for the modification to occur and it has been suggested that CK2 may be the kinase that achieves this change (Xie *et al*., 2000; Ganley *et al*., 2001). As phosphorylation does not impact upon catalytic activity or the response of rPLD1 to its activators, the role of serine/threonine phosphorylation of PLD1 could be involved in phosphorylation-dependent trafficking events or influence PLD localisation (Xie *et al*., 2000; Ganley *et al*., 2001).

1.4: A summary of selected phosphatidic acid targets

1.4.1: Activation of phosphodiesterase-4 (PDE4) isoforms by phosphatidic acid

Phosphodiesterases (PDEs) are responsible for the hydrolysis of cyclic adenosine monophosphate (cAMP) and cyclic guanosine monophosphate (cGMP), therefore modifying intracellular concentrations of these second messengers (Manganiello, 2002). cAMP is an omnipresent second messenger with multifaceted spatiotemporal regulation and is responsible for many key cellular functions, including transcription regulation (Beavo and Brunton, 2002; Houslay and Adams, 2003). Once cAMP is generated, degradation by cAMP-specific PDEs is the only mode of inactivation (Houslay and Adams, 2003; Huston *et al*., 2006). The PDE superfamily is composed of 11 gene families, which are structurally related but functionally distinct and are strictly regulated (Manganiello, 2002). Multiple PDEs can be derived from a single PDE gene and it is thought that up to 30 different proteins are synthesised in mammalian cells. PDE4 is the enzyme principally responsible for degrading cAMP and the unique N-terminal regions of PDE4 isoforms determine their interactions with particular signalling and scaffolding proteins (Huston *et al*., 2006).

The cAMP-specific PDE4 family members are encoded by four genes (A, B, C and D) producing several isoforms, each characterised by distinct N-terminal regions, some of which respond to phosphatidic acid (PtdOH) activation (Housley and Adams, 2003; Huston *et al*., 2006). Each of the PDE4 variants encodes a minimum of two proteins which are classified as 'long' or 'short' variants (Nemoz *et al*., 1997). 'Long' variants are between 90 and 130kDa (such as PDE4A5, PDE4B1 and PDE4D3) whereas 'short' variants are between 66 and 74kDa (such as PDE4A1, PDE4B2, PDE4D1 and PDE4D2 – Nemoz *et al*., 1997). PtdOH is a known activator of the aforementioned 'long' PDE4 variants, which are thought to be specifically activated by anionic lipids (El Bawab *et al*., 1997; Nemoz *et al*., 1997). However, the 'short' PDE4 variants are unresponsive to PtdOH activation (Nemoz *et al*., 1997).

PDE isoforms are targeted intracellularly by their association with various proteins (Baillie *et al*., 2002). For example, the entirely membrane-associated PDE4A1 isoform has an association with PtdOH through its unique tryptophan anchoring

phosphatidic acid selective-binding domain 1 (TAPAS-1) N-terminal microdomain (Baillie *et al*., 2002; Huston *et al*., 2006). TAPAS-1 is an 11-residue helical domain which has high selectivity for PtdOH-interaction (Baillie *et al*., 2002). This unique microdomain inserts into the lipid bilayer in a calcium-dependent manner, thus controlling PDE4A1 membrane association (Baillie *et al*., 2002; Huston *et al*., 2006).

PtdOH is also a known activator of PDE4D3 and is thought to aide the formation of PDE4D3 dimers (Grange *et al*., 1998). Furthermore, the acidic groups of PtdOH are essential for activation as PDE4D3 was activated by acidic phospholipids but remained unresponsive in the presence of both zwitterionic phospholipids and anionic detergents (Grange *et al*., 1998). These results support earlier data showing PDE4A5 activation by PtdOH but not diacylglycerol (DAG – El Bawab *et al*., 1997). The PtdOH-binding site of PDE4D3 was identified in the N-terminal domain between amino acid residues 31-59, a region rich in basic and hydrophobic residues (Grange *et al*., 2000). Furthermore, deletion of these residues hindered PtdOH-binding and PtdOH activation of PDE4D3 (Grange *et al*., 2000). Depletion of endogenous PtdOH in mouse Leydig tumour cells suggested that cAMP levels were PtdOH-modulated through direct PDE4D3 interaction in an *in vivo* model (Grange *et al*., 2000). Control of cAMP-specific PDE4 isoforms by acidic phospholipids indicates a mechanism by which external stimuli, such as growth factors, hormones or other proteins (e.g. lectin protein concanavalin A) are able to influence cAMP-dependent signal transduction in stimulated cells (El Bawab *et al*., 1997; Nemoz *et al*., 1997).

1.4.2: Activation of the mammalian target of rapamycin by phosphatidic acid

Phosphatidic acid (PtdOH) and choline are the products of phospholipase D (PLD) catalysed hydrolysis of phosphatidylcholine (PtdCho). PtdOH is a second messenger in its own right and has a range of targets, one of which is the mammalian target of rapamycin (mTOR – Fang *et al*., 2003). There are two distinct mTOR complexes known as mTORC1 and mTORC2 (Bai and Jiang, 2010). The rapamycin-sensitive mTORC1 has been extensively studied and is regulated by a range of factors including grwoth factors, mitogens and PtdOH (Bai and Jiang, 2010). PtdOH enhances activity of the cytosolic protein kinase mTOR *in vivo* (Hay and Sonenberg, 2004; Stace and Ktistakis, 2006). Past studies have both identified and cloned mTOR and found that this kinase forms a complex with an intracellular receptor responsible for inhibiting progression of the cell cycle (Brown *et al*., 1994). The drug rapamycin was first isolated from a strain of soil bacteria and forms an inhibitory complex with its intracellular receptor, the FK506-binding protein, FKBP12 (Chen *et al*., 1995; Hay and Sonenberg, 2004). This complex binds to the C-terminus of TOR proteins therefore inhibiting their activity (Chen *et al*., 1995; Hay and Sonenberg, 2004). The mTOR region which binds the intracellular receptor FK506-binding protein also binds PtdOH with a high degree of selectivity (Fang *et al*., 2001; Stace and Ktistakis, 2006). Mammalian cells stimulated with mitogen resulted in the PLD-dependent increase of cellular PtdOH (Fang *et al*., 2001). PtdOH was found to directly bind to the mTOR region targeted by rapamycin and this interaction correlated with an increase in mTOR-activated downstream effectors (Fang *et al*., 2001).

PtdOH generated by both PLD hydrolysis of PtdCho and by diacylglycerol kinase (DAG kinase) phosphorylation of DAG has been implicated in mTOR activation (Fang *et al*., 2003; Ávila-Flores *et al*., 2005; Stace and Ktistakis, 2006). mTOR is known to regulate cell growth and proliferation by targeting ribosomal S6 kinase 1 (S6k1) and eukaryotic translation inhibition factor 4E binding protein 1 (4E-BP1 – Fang *et al*., 2003). PLD1-generated PtdOH was implicated in mTOR regulation as over-expression of wildtype PLD1 in serum-stimulated cells resulted in an increase of S6K1 activity (Fang *et al*., 2003). Furthermore, depletion of endogenous PLD1 using interference RNA (RNAi) resulted in drastic inhibition of both S6K1 and 4E-

BP1 hyper-phosphorylation in mammalian cell lines (Fang *et al*., 2003). PtdOH generated by DAG phosphorylation has also been shown to increase phosphorylation of the downstream mTOR target p70S6 kinase (Ávila-Flores *et al*., 2005). Over-expression of DAG kinase ζ (but not DAG kinase α) in serum-starved HEK-293 cells resulted in the phosphorylation of the mTOR target p70S6 kinase (Ávila-Flores *et al*., 2005). Addition of serum to cells over-expressing DAG kinase ζ resulted in higher p70S6 kinase phosphorylation and resistance to rapamycin treatment (Ávila-Flores *et al*., 2005). The effect of the DAG kinase ζ on the downstream hyper-phosphorylation of p70S6 kinase required the PtdOH binding region of mTOR (Ávila-Flores *et al*., 2005). Depletion of endogenous DAG kinase ζ using small interfering RNA (siRNA) resulted in attenuated phosphorylation of p70S6 kinase in serum-treated cells (Ávila-Flores *et al*., 2005). These findings indicate that PtdOH produced from PLD-indepentent pathways are also effective mediators of mTOR signalling (Ávila-Flores *et al*., 2005; Stace and Ktistakis, 2006). Recent studies have indicated that PLD2-generated PtdOH may activate p70S6 kinase directly (Lehman *et al*., 2007). Over-expression of PLD2 in the COS7 cell line resulted in increased ribosomal p70S6 kinase activity and corresponding downstream phosphorylation events (Lehman *et al*., 2007). Activation of p70S6 kinase was thought to be PLD2-dependent and mTOR-independent as neither rapamycin-inhibition nor silencing the mTOR gene attenuated the increase in p70S6 kinase activity induced by PLD2 (Lehman *et al*., 2007).

Although PtdOH is an established mediator of mTOR signalling, the spatial interaction between PtdOH and mTOR remains unclear (Stace and Ktistakis, 2006). As mTOR often targets proteins involved in translational control by enabling recruitment of ribosomes to messenger RNA (mRNA), this kinase possibly constitutively localises to intracellular membranes (Fang *et al*., 2003; Stace and Ktistakis, 2006). mTOR localised to intracellular membranes would potentially be activated by PLD-generated PtdOH, thus facilitating the phosphorylation of downstream targets (Fang *et al*., 2003; Stace and Ktistakis, 2006). However, other possibilities such as non-membrane associated mTOR activity and mTOR activation by a pre-existing 'pool' of PtdOH cannot yet be discounted (Stace and Ktistakis, 2006).

1.4.3: The effect of phosphatidic acid on the serine/threonine kinase Raf1

The serine/threonine kinase Raf1 is an essential part of the mitogen-activated protein kinase (MAPK) signalling cascade (Rizzo *et al*., 2000). Activation of phospholipase D (PLD) by extracellular signals and consequent phosphatidic acid (PtdOH) generation resulted in activation of the Raf1-MAPK signalling cascade (Rizzo *et al*., 1999). Glutathione S-transferase (GST)-fusion protein of Raf1 containing the cysteine-rich domain (amino acid residues 139-184) bound to liposomes in a phosphatidylserine (PtdSer)-dependent manner. Furthermore, the Raf1 GST-fusion protein encoding residues 1-147, which overlaps with the cysteine-rich domain, was able to bind to GTP-Ras with high affinity. Removal of the last 17 residues, forming a Raf1 GST-fusion protein with residues 1-130 resulted in a notable decrease in GTP-Ras binding (Ghosh *et al*., 1994). Further studies of full-length Raf1 showed that the kinase bound both PtdSer and the PLD product PtdOH, and the C-terminal domain of Raf1 (residues 295-648) bound strongly with PtdOH. Deletion mutants were used to identify the 35 C-terminal residues (amino acids 389-423) as the PtdOH-binding site of Raf1. Inhibition of PtdOH generation using 1% ethanol, in canine kidney cells, resulted in reduced translocation of Raf1 to the plasma membrane. These results identified PtdOH as a key regulator of Raf1 translocation and eventual activation *in vivo* (Ghosh *et al*., 1996). Inhibition of Arf proteins by brefeldin A corresponded to inhibition of PLD-mediated PtdOH generation, Raf1 translocation and activation, and MAPK phosphorylation in response to stimulation (Rizzo *et al*., 1999). Addition of PtdOH to brefeldin A treated cells restored Raf1 translocation, however PtdOH did not activate Raf1 *in vitro* or *in vivo*, suggesting it is responsible for Raf1 membrane association (Rizzo *et al*., 1999). Progressive mutations within the tetrapeptide motif (residues 398-401) of human Raf1 resulted in reduction and eventual elimination of Raf1-PtdOH binding (Ghosh *et al*., 2003). Furthermore, mutation of this region showed that Raf1-PtdOH binding and consequent signalling is essential in the embryological development of zebrafish embryos (Ghosh *et al*., 2003).

Raf1 activation by insulin in Rat1 fibroblasts (overexpressing the human insulin receptor, HIRcB) initiates Raf1 association with intracellular membranes (Rizzo *et al*., 2000). Mutations of Raf1 in the PtdOH-binding domain inhibited Raf1

translocation in response to agonist stimulation, whereas mutation of the Ras-binding domain did not (Rizzo *et al*., 2000; Rizzo and Romero, 2002). Over-expression of the Raf1 mutant preventing translocation in HIRcB cells operated as a dominant negative mutant preventing MAPK phosphorylation, thus inhibiting the MAPK pathway (Rizzo *et al*., 2000). Inhibition of MAPK phosphorylation also occurred in cells expressing a dominant negative Ras mutant but did not inhibit Raf1 translocation in response to stimulation (Rizzo *et al*., 2000). Activated Raf1 is phosphorylated on serine 338 (predominantly due to oncogenic Ras activity) and tyrosine 341 (mainly attributed to Src activity – Mason *et al*., 1999). Maximal Raf1 activity occurs when both sites are phosphorylated. Inhibiting phosphorylation of either site renders Raf1 inactive (Mason *et al*., 1999). Furthermore Raf1 phosphorylation is dependent on the interaction between Raf1 and Ras-GTP (Mason *et al*., 1999). PLD-generated PtdOH therefore regulates agonist-induced Raf1 translocation independent of Ras, but is dependent on Ras for activation and participation in the MAPK cascade (Rizzo *et al*., 2000).

1.5: The role of phospholipase D in endocytosis and exocytosis

1.5.1: Endocytosis

Phospholipase D (PLD) is an important facilitator of multiple trafficking events including vesicle trafficking between the Golgi apparatus and the endoplasmic reticulum, and endocytosis. PLD localisation has been characterised in a variety of different cultured cell lines and tissues where expression has been identified in a range of organelles including the nucleus, lysosomes, secretory granules, endosomes and the Golgi apparatus (Colley *et al*., 1997; Brown *et al*., 1998; Kim *et al*., 1999; Freyberg *et al*., 2002). PLD generated phosphatidic acid (PtdOH) is necessary for the internalisation of receptor-ligand complexes (Antonescu *et al*., 2010). Endocytosis of transmembrane receptors generally progresses via clathrin-coated vesicles, which bud from the plasma membrane and eventually deliver their cargo to endosomes for recycling or degradation (Haucke *et al*., 2005).

Initiation of clathrin-mediated endocytosis commences with the recruitment of the heterotrimeric adaptor protein AP2 to the plasma membrane (Haucke and Camilli, 1999). Several membrane proteins act as docking sites for AP2 including synaptotagmin and PLD1 – PLD-generated PtdOH is negatively charged and thought to contribute to the AP2 docking site (West *et al*., 1997; Haucke and Camilli, 1999; J.S. Lee *et al*., 2009). The PLD co-factor phosphatidylinositol 4,5-bisphosphate (PtdIns(4,5)P_2) also binds and recruits the AP2 complex to sites of endocytosis (Chapman *et al*., 2002). Increased PLD activity augments membrane recruitment of AP2 and is also thought to impact on the association between AP2 and synaptotagmin. In the presence of ATP and the non-hydrolysable GTPγS, PLD stimulates the interaction between AP2 and the docking protein synaptotagmin (West *et al*., 1997; Haucke and Camilli, 1999).

Endocytosis of the EGFR is dependent upon PLD1 activity and the PLD1 regulators protein kinase Cα (PKCα) and RalA (Shen *et al*., 2001). PLD1 activity is thought to be auto-regulated by phosphatidic acid, which binds to the phox homology (PX) domain of PLD1 (J.S. Lee *et al*., 2009). Endocytosis and degradation of EGFR in response to EGF stimulation is accelerated by over-expression of PLD1 or PLD2 and

slowed by over-expression of catalytically inactive PLD1 or PLD2 (Shen *et al*., 2001). PtdOH promotes binding of the μ2 medium chain of the AP2 complex to the pleckstrin homology (PH) domain of PLD1, thus facilitating EGFR endocytosis (J.S. Lee *et al*., 2009). Internalisation of EGFR is halted in response to PLD inhibitors such as the accessory proteins of the brain clathrin coat synaptojanin, AP180 and amphiphysin I and II (Shen *et al*., 2001; Lee *et al*., 2000; Donaldson *et al*., 2009).

Inhibition of DAG kinase resulted in a notable decrease of PtdOH, resulting in decreased epidermal growth factor receptor (EGFR) endocytosis in the epithelial monkey kidney cell line BSC-1 (Antonescu *et al*., 2010). However, contrary to previous findings, Antonescu *et al*., (2010) showed that inhibition of PLD activity (using both siRNA depletion and pharmacological inhibition) led to elevated cellular PtdOH concentration. Consistent with higher PtdOH levels, PLD inhibition promoted EGFR endocytosis and clathrin coated pit dynamics (Antonescu *et al*., 2010). Inhibition of DAG kinase resulted in decreased (over 50%) PtdOH production, corresponding to a reduction in EGFR internalisation in BSC-1 cells (Antonescu *et al*., 2010). This means that the majority of cellular PtdOH is not PLD-generated and that PtdOH may be regulatory rather than essential for EGFR endocytosis (Antonescu *et al*., 2010). PtdOH is not universally essential for clathrin-mediated endocytosis but instead is required for internalisation of a cargo-selective subset of clathrin coated pits (Antonescu *et al*., 2010). PLD2 interacts with dynamin in a GTP-dependent (and EGF-dependent) manner, implicating the lipase in the regulation of dynamin via GTP-GDP cycling (Park *et al*., 2004). PLD functions as a GTPase activating protein (GAP) via its PX domain, thus directly activating dynamin (Park *et al*., 2004). Expression of the PX domain of either PLD1- or PLD2-stimulated EGFR endocytosis suggested that the PX domain itself is a GAP (Lee *et al*., 2006; Donaldson *et al*., 2009). Wildtype PLD (but not mutated PLD defective for GAP function) increased EGFR endocytosis at physiological EGF concentrations *in vitro* (Lee *et al*., 2006). The interaction between dynamin and PLD may be important to EGF-stimulation of PLD. Furthermore, PLD may regulate clathrin-dependent endocytosis independently of PtdOH or DAG production (Donaldson *et al*., 2009).

PtdOH production occurs either via PLD-mediated hydrolysis of phosphatidylcholine (PtdCho) or through diacylglycerol (DAG) kinase activity (Antonescu *et al*., 2010). Both PtdOH and DAG are negatively charged and promote extreme membrane curvature which aids vesicle fission during endocytosis (Snyder and Pierce, 2006). The membrane-bound lipase PLD2 has been found to localise to endosomes and the plasma membrane. PLD2 is essential to the clathrin-mediated endocytosis of several receptors, including μ-opioid and angiotensin II receptors (Koch *et al*., 2004; Du *et al*., 2004). PLD2-generated PtdOH recruits AP2, thus triggering vesicle budding from donor membranes (Liscovitch *et al*., 2000; Kuwahara *et al*., 2008). The PLD2 inhibitor α-synuclein is thought to inhibit endocytosis by negatively regulating PLD2 activity (Kuwahara *et al*., 2008). Mutant α-synuclein (A53T) associated with Parkinson's disease was a more potent inhibitor of PLD2 activity than the wildtype α-synuclein (Kuwahara *et al*., 2008). Defects in synaptic vesicle endocytosis due to α-synuclein over-expression are therefore possibly caused by upregulation of normal α-synuclein function (Kuwahara *et al*., 2008).

Studies also demonstrated that PLD2 was essential for the recycling of transferrin receptor in the epithelial HeLa cell line (Padrón *et al*., 2006). However, inhibition of PLD2 did not result in the inhibition of transferrin receptor endocytosis, supporting more recent data suggesting PLD-generated PtdOH may be regulatory in this process (Padrón *et al*., 2006). Over-expression of the nucleotide exchange factor ADP-ribosylation factor 6 (EFA6) did not reduce internal accumulation of transferrin receptors in cells which were previously siRNA depleted of PLD (Padrón *et al*., 2006). This possibly indicates that PLD2 is essential for constitutive Arf6-mediated recycling of this transferrin receptor (Padrón *et al*., 2006). The data may also suggest that, in the absence of PLD2, transferrin receptors accumulates in recycling endosomes which are unresponsive to EFA6 (Padrón *et al*., 2006). Similarly, PLD1 is essential for B-cell antigen receptor endocytosis in B-cells (Snyder and Pierce, 2006). PLD1 functional inhibition by primary alcohol or depletion via siRNA knockdown stopped trafficking of B-cell antigen receptor to major histocompatibility protein class II (MHC II)-containing compartments of B-cells (Snyder and Pierce, 2006).

PLD2 has also been implicated in constitutive class I metabotropic glutamate receptors (mGluR) 1 and 5 endocytosis which is not well characterised and may occur through a clathrin-independent pathway (Bhattacharya *et al*., 2004). PLD2 is essential for the internalisation of mGluR1 and mGluR5, as siRNA knockdown and butan-1-ol treatment reduced endocytosis (Bhattacharya *et al*., 2004). In addition, PLD2 co-localises with the class I mGluRs in the endocytic vesicles of both neurons and the cultured HEK-293 cell line (Bhattacharya *et al*., 2004).

1.5.2: Exocytosis

Phospholipase D (PLD) has been implicated in regulated exocytosis in numerous cell lines including rat basophilic leukaemia RBL-2H3, monocyte/macrophage HL-60 and neuroendocrine phaeochromocytoma PC12 cell lines (Way *et al*., 2000; Skippen *et al*., 2002; Lynch and Martin, 2007). In RBL-2H3 cells, PLD1 localises to the secretory granules whilst PLD2 localises to the plasma membrane (Brown *et al*., 1998; Cockcroft *et al*., 2001). PLD2 co-localises with ADP-ribosylation factor 6 (Arf6) on the plasma membrane of antigen stimulated RBL-2H3 cells (Cockcroft *et al*., 2001). Small G-proteins were identified as regulators of the secretory pathway using permeabilised rat peritoneal cells (Howell *et al*., 1987). Rat mast cells treated with Ca^{2+} and GTPγS following streptolysin-O permeabilisation resulted in histamine secretion (Howell *et al*., 1987). Several small G-proteins have since been identified in the regulation of exocytosis, including Arf family proteins (Way *et al*., 2000). Arf family proteins cycle between the cytosol (GDP-bound form) and plasma membrane (GTP-bound form) depending on their activation state (Rümenapp *et al*., 1995; Cockcroft *et al*., 2001). Permeabilised RBL-2H3 cells respond to antigenic stimulation in the presence of Ca^{2+} and MgATP; however an increase in the permeabilisation time pre-stimulus resulted in no response to antigen (Cockcroft *et al*., 2001). The response of RBL-2H3 cells to antigen was quantified by monitoring secretion and PLD activation (Cockcroft *et al*., 2001). In cells which underwent extended permeabilisation and did not respond to antigen, the addition of exogenous Arf proteins recovered PLD activation and secretion in response to stimulation (Cockcroft *et al*., 2001).

The HL-60 cell line was established from an acute myeloid leukaemia patient and cultured cells can differentiate into monocyte/macrophage-like cells (Birnie, 1988). This differentiated cell line has since been used extensively in early characterisation of PLD and PtdOH in regulated exocytosis (Stuchfield and Cockcroft, 1993). Arf proteins regulate the generation of phosphatidylinositol (4,5)-bisphosphate ($PtdIns(4,5)P_2$) in HL-60 cells (Skippen *et al*., 2002). Together, Arf proteins and presumably PLD-generated phosphatidic acid (PtdOH) regulate the activity of phosphatidylinositol 4-phosphate 5-kinase (PtdIns(4)P 5-kinase – Cockcroft *et al*., 2001). Both Arf1 and Arf6 isoforms increase $PtdIns(4,5)P_2$ levels when added to

permeabilised cells which are depleted of Arf1 and Arf6 (Skippen *et al*., 2002). Treatment of cells with a sufficiently potent percentage of butan-1-ol to halt exocytosis proved toxic and so mutant Arf was used (Skippen *et al*., 2002). Expression of an Arf1 mutant specifically activating PtdIns(4)P 5-kinase still increased PtdIns(4,5)P_2 levels, albeit with lower efficiency (Skippen *et al*., 2002). Therefore, PLD-mediated phosphatidic acid (PtdOH) synthesis and Arf protein activity directly activate PtdIns(4)P 5-kinase and increase PtdIns(4,5)P_2 content in the plasma membrane of HL-60 cells (Skippen *et al*., 2002). Synaptotagmin I and IV are Ca^{2+}-sensitive receptors and required for dense-core vesicles exocytosis (Lynch and Martin, 2007). Synaptotagmin I binds to PtdIns(4,5)P_2 in the plasma membrane with a high affinity and plasma membrane concentration of the lipid is important to exocytosis (Holz *et al*., 2000; Chapman, 2002). Increased levels of plasma membrane PtdIns(4,5)P_2 in neuroendocrine PC12 cells may facilitate membrane fusion between secretory vesicles and the plasma membrane (McDermott *et al*., 2004).

PtdIns(4)P 5-kinase and PLD1 are activated by all mammalian Arf isoforms (Arf1-Arf6) with similar potency and efficacy (reviewed in McDermott *et al*., 2004). Arf6 has been extensively characterised as, in chromaffin cells, Arf6 translocates from secretory granules to the plasma membrane in response to stimulation (Caumont *et al*., 1998). In the related PC12 cells this observation was supported as overexpressed Arf6 migrated from granule to plasma membrane fractions upon stimulation (Vitale *et al*., 2002). Similarly, a catalytically inactive Arf6 GDP-bound mutant was still translocated from the secretory granules to the plasma membrane upon cell stimulation. This suggests that GDP/GTP cycling is not essential for Arf6 translocation. The guanine nucleotide exchange factor (GEF) ARNO also localises to the plasma membrane and so Arf6 on the plasma membrane may be available for ARNO at the site of exocytosis (Vitale *et al*., 2002).

The key to PLD involvement in both endocytosis (involving membrane fusion) and exocytosis (involving membrane fission) may be its production of PtdOH. Hydrolysis of PtdCho to PtdOH results in negative membrane curvature because of the contribution of the cone shaped PtdOH to membrane topology, potentially facilitating both membrane fusion and fission events.

1.6: Aims

The overarching aim of this project was to use a novel fluorescent PLD substrate (fPtdCho) to analyse PLD-substrate interaction *in vivo* and record real-time PLD activity *in vitro*. The novel lipid is BODIPY-labelled at the choline head group and contains intramolecular quenching groups. PLD-mediated hydrolysis of the lipid *in vitro* results in increased fluorescence, thus allowing monitoring of real-time PLD activity. PLD localisation with its substrate could be monitored *in vivo* using live rather than fixed cells. Historically, *in vitro* PLD assays have been radioactive and produced only one datat point, wheras this project achieved assay conditions to monitor activity in real-time yielding up to 500 data points. Furthermore, PLD-substrate interaction *in vivo* has never before been attempted using live cells. The broad aims and hypotheses of this project are detailed below:

1) *Does fPtdCho stay intact in labelled RBL-2H3 cells?*
    - fPtdCho labelling of RBL-2H3 cells was assessed using live confocal microscopy as the lipid could not be fixed. The Bligh-Dyer lipid extraction protocol was used on fPtdCho-labelled RBL-2H3 cells to confirm that fPtdCho was still intact and not hydrolysed *in vivo*.

2) *Does fPtdCho localise with secretory lysosomes in labelled RBL-2H3 cells? Is fPtdCho-labelling PLD-dependent and, if so, does it respond to antigenic stimulation?*
    - Antigenic stimulation and degranulation of RBL-2H3 cells is PLD-dependent. The hypothesis was that fPtdCho would localise to the secretory lysosomes of RBL-2H3 cells, presumably making the substrate available for PLD-mediated hydrolysis. Several molecular markers including LysoTracker Red were used to stain fPtdCho-labelled RBL-2H3 cells. Live confocal imaging was used to record data and Image J to assess co-localisation.
    - Primary alcohol treatment of fPtdCho-labelled RBL-2H3 cells helped determine whether fPtdCho staining was PLD-dependent. Transphosphatidylation altered fPtdCho staining of cells from punctate to diffuse, as recorded using live confocal microscopy.

- Although staining appeared dependent on PLD-mediated PtdOH generation, real-time antigenic stimulation (recorded using live microscopy) did not change the localisation of fPtdCho staining.

3) *Can fPtdCho be used as a PLD substrate in vitro to analyse lipase activity in real-time? If so, can established assays be modified to yield real-time data?*
   - Purified recombinant glutathione-S-transferase (GST) labelled human PLD1 (hPLD1) was expressed in Sf9 insect cells and used in real-time *in vitro* assays. Conditions were modified from established end-point PLD assays and fPtdCho-hydrolysis monitored fluorimetrically.
   - Basal and G-protein activated PLD activity were recorded at two second intervals by measuring fluorescence increase as fPtdCho was hydrolysed.

4) *Does PLD1b or PLD2a localise with its small G-protein activator Rac1 in HeLa cells? Does the lipase localise with its activator upon stimulation?*
   - PLD1b and PLD2a were labelled with the red fluorescent protein Cherry, expressed in the pcDNA3.1(-) plasmid. HeLa cells were transiently transfected with Cherry-PLD1b or -PLD2a and localisation analysed using fixed and live confocal microscopy.
   - Rac1 was labelled with green fluorescent protein and transiently transfected into HeLa cells. Cherry-PLD and Rac1 co-localisation was assessed in double-transfected cells in resting and agonist-stimulated cells (fixed).

5) *Does fPtdCho co-localise in HeLa cells expressing Cherry-PLD1b? Can this then be developed into an in vivo real-time assay?*
   - fPtdCho-labelled HeLa cells were transfected using Cherry-PLD1b and co-localisation between the two assessed using live FRET by FRAP technology. Data indicated that the two were in close proximity which lays the foundation for developing a live real-time *in vivo* PLD assay.

Chapter 2: Methods

2.1: Materials

All analytical grade reagents used for experimental work were sourced from Sigma-Aldrich (Dorset, UK) or Fischer Scientific (Loughborough, UK). Specialist lipids were supplied by Lipid Products (Surrey, UK) and molecular markers by Invitrogen through Fischer Scientific (Loughborough, UK). Purified recombinant small G-protein activators were sourced from Bioquote Limited (York, UK).

2.2: Tissue culture techniques of mammalian cell lines

2.2.1: Subculturing of mammalian cell lines

Rat basophilic leukemia (RBL-2H3), human embryonic kidney (HEK-293), Swiss 3T3, and HeLa cell lines were cultured using Dulbecco's Modified Eagle Medium (DMEM) containing glutamax (or glutamine) supplemented with 10% foetal calf serum (FCS) (henceforth "complete DMEM"). Monolayers were cultured in 25 cm^2 or 75 cm^2 sterile vented flasks to a density of 70-90%, passaging every 2-3 days.

Confluent RBL-2H3 cells were washed 3 times using complete DMEM and monolayers disrupted using 25 cm cell scrapers. RBL-2H3 cells were further cultured at a 1/10 dilution and discarded before passage 15.

Swiss 3T3, HEK-293 and HeLa cell lines were washed with phosphate buffered saline (PBS) before incubating the flask at 37^oC/5% CO_2 (2 minutes) in 2 ml of trypsin (0.25%) in medium and saline. Flasks were tapped hard to displace the cells 10 ml complete DMEM was added and cells were centrifuged at 800 RPM for 3 minutes. The pellet was resuspended in fresh medium and cultured at a suitable dilution; typically between 1/3 and 1/10.

2.2.2: Freezing and thawing of mammalian cell lines

All mammalian cell lines were cultured to 90% confluency in 75 cm^2 sterile vented flasks and passaged into 1.5 ml cryovials. Cells were passaged as previously described (refer to Section 2.2.1) and centrifuged at 800 RPM for 3 minutes. The medium was removed and the cell pellet resuspended in 1 ml FCS and 10% dimethyl sulfoxide (DMSO) before aliquoting 1 ml/cryovial. Cryovials were frozen -80^oC for up to 24 hours before transfer to liquid nitrogen for long term storage.

Thawing was achieved by transferring cells from liquid nitrogen immediately to 37^oC. They were then transferred to a 75 cm^2 flask with 10 ml of complete DMEM. The medium was replaced 3-4 hours after thawing.

2.3: Transient transfections using plasmid DNA

2.3.1: Culturing cells for transient transfection

All mammalian cell lines were subcultured as previously described (refer to Section 2.2.1) and RBL-2H3, HeLa and Swiss 3T3 cells plated onto 6-well plates with methanol-sterilised circular (22 mm diameter) coverslips 24 hours prior to transfection. Cells were seeded at a 1/10 dilution in a final volume of 2 ml complete DMEM for 24 hours prior to transfection, achieving a final confluency of 40-50%.

Similarly, HEK-293 cells were passaged and cultured in 6-well plates at a dilution of 1/10 on methanol-sterilised poly-D-lysine coated coverslips 24 hours prior to transfection. Poly-D-lysine was used at a concentration of 0.1 mg/ml applied to the cover slips for 10 minutes and washed 3 times with 2 ml filter sterilised PBS before adding 2 ml complete DMEM per well.

2.3.2: Transient transfections using Lipofectamine™ and polyethylenimine

RBL-2H3 cells cultured in 6-well plates were incubated in 1 ml DMEM (no additions) for 2 hours prior to transfection. Polyethylenimine (PEI) was used at a final concentration of 20 µM in 100 µl of N-(2-hydroxyethyl)-piperazine-N'-2-ethanesulfonic acid (HEPES) pH 7.5 and incubated with 6 µg of DNA at room temperature (RT) for 15-20 minutes. Lipofectamine™ (6 µl) was added to each complex and incubated for 15-20 minutes at RT; complexes were then added to RBL-2H3 cells and mixed gently. Transient transfections were initially incubated on a strong magnet (PromoKine) for 15 minutes at 37°C/5% CO_2 and further incubated for 5 hours before 2 ml of complete DMEM halted the transfections. After 48 hours, cells were washed 3 times (5 minutes per wash) with filter sterilised PBS before and after incubation with 4% paraformaldehyde (PFA) for 1 hour at room temperature (RT). Cells were then mounted onto slides using Centifluor™ and sealed with nail varnish.

HeLa cells were transfected using 3 µg of DNA for single transfections and 6 µg for co-transfections. DNA was incubated in 50 µl HEPES, pH 7.5 with 40 µM PEI for

15-30 minutes at RT. 3 µl Lipofectamine™ was then diluted in 50 µl HEPES, pH 7.5 and added to each complex for a further 15-30 minutes at RT. Complete DMEM was replaced with 1 ml DMEM (no additions) immediately before complexes were added and incubated for 6 hours at 37°C/5% CO_2. Transfections were quenched with 2 ml complete DMEM and incubated for a further 24 hours before fixing and mounting onto slides.

2.3.3: Transient transfections using Lipofectamine™ and PLUS™ Reagent

HEK-293 or Swiss 3T3 cells cultured in 6-well plates were incubated in 1 ml DMEM (no additions) for 2 hours prior to transfection. Each transient transfection used either 6 µg DNA for single transfections or 8 µg DNA for co-transfections. 100 µl DMEM (no additions) was added to the DNA before incubation with 6 µl PLUS™ Reagent for 15-20 minutes. 5 µl Lipofectamine™ was added to each complex and incubated for 15-20 minutes and added to the cells before mixing gently.

Transfections using HEK-293 cells were incubated for 4-5 hours at 37°C/5% CO_2 before the transfection media was replaced with 2 ml complete DMEM for a further 48 hours before fixing as previously detailed (refer to Section 2.3.2).

Transient transfections using Swiss 3T3 cells were treated as detailed previously (refer to Section 2.3.1). Cells were incubated on a strong magnet (PromoKine) for 15 minutes at 37°C/5% CO_2 and then for 5 hours before adding 2 ml complete DMEM. Cells were fixed 48 hours later using 4% PFA and mounted using Centifluor™.

2.4: Live confocal microscopy

2.4.1: Maintenance of mammalian cells during live confocal microscopy

RBL-2H3, HEK-293, HeLa and Swiss 3T3 cells were subcultured and seeded in fluorodishes – 35 mm in circumference with a 23 mm glass bottom. All cell lines were cultured at a 1/10 dilution in 2 ml complete DMEM in fluorodishes 24 hours prior to live confocal microscopy.

During live confocal microscopy, cells were washed once and incubated in 1 ml of carbonate supplemented Hank's Balanced Salt Solution (HBSS) buffered with 20 mM HEPES pH 7.4. 1 mM calcium chloride ($CaCl_2$) was added to the HBSS to replicate the physiological environment in which cells undergo antigenic.

2.4.2: Live labelling of cells using the novel fluorescence phosphatidylcholine

RBL-2H3, HEK-293, Swiss 3T3, HeLa and MIN6 cells were labelled using a novel fluorescent version of phosphatidylcholine (PtdCho), synthesised in the laboratory of Professor G. Prestwich (Utah, USA). The novel BODIPY-labelled PtdCho was resuspended in DMSO (100 ng/µl). Cells cultured in fluorodishes for approximately 24 hours were labelled with 1 µg DBPC in 1 ml HBSS + 1 mM calcium (Ca^{2+}). Cells were washed once with 1 ml HBSS + 1 mM Ca^{2+} and labelled with the novel lipid for a minimum of 2 hours at 37^{o}C/5% CO_2. The 1% DMSO content (10 µl) did not have a toxic effect on the cells.

RBL-2H3, Swiss 3T3 and HeLa cells were treated with the novel lipid for up to 24 hours during a live imaging time course. Cells were not labelled under sterile conditions and so each fluorodish was washed twice with complete DMEM + 100 U/ml penicillin and 100 µg/ml streptomycin before incubation in 2 ml at 37^{o}C/5% CO_2 overnight.

SP5 confocal microscopy was used for live imaging of the novel fluorescence lipid. The argon laser was used for live imaging of novel PtdCho-labelled cells excited at 488 nm. Cells were incubated at 37^{o}C for the duration of live experiments.

2.4.3: Live labelling of cells using molecular markers

RBL-2H3, HEK-293, Swiss 3T3, HeLa and MIN6 cells were labelled using the following molecular markers: Hoechst 33342, LysoTracker Red DND-99 (Image-iT LIVE Lysosomal and Nuclear Labelling Kit), MitoTracker Red CMXRos, FM4-64, acridine orange and BODIPY-PC. All cell labelling was performed in fluorodishes with a final volume of 1 ml in HBSS + 1 mM Ca^{2+}.

The nuclear marker Hoechst 33342 was used at a concentration of 2.0 µg/ml in HBSS+ 1 mM Ca^{2+} and incubated at 37^{o}C/5% CO_2 for 15 minutes. Cells were then washed twice with HBSS + 1 mM Ca^{2+} before confocal imaging using the ultra violet (UV) laser.

The lysosomal marker LysoTracker Red DND-99 was used at a concentration of 100 nM. Cells were labelled for 1 minute at RT before washing with HBSS+ 1 mM Ca^{2+}. Finally, cells then imaged using the 594 nm laser on the confocal microscope.

The mitochondrial marker MitoTracker Red CMXRos was used at a concentration of 100 nM. Cells were labelled for 30 minutes at 37^{o}C/5% CO_2 before live imaging using the 594 nm laser.

The membrane marker FM4-64 was used at a concentration of 2.5 µM and imaged immediately using the 488 nm laser of the confocal microscope.

RBL-2H3 and HEK-293 cells were also labelled using acridine orange and BODIPY-PC. Acridine orange was used at concentrations of 3 µM and 6 µM and incubated at 37^{o}C/5% CO_2 for 5 minutes or 2 hours. The acyl-modified glycerophosphocholine BODIPY-PC was used at a concentration of 1 µg/ml and incubated at 37^{o}C/5% CO_2 for 10 minutes or 2 hours, modifying the protocol used by Laulagnier *et al*., 2005. Images were recorded using the argon laser of the confocal microscope at 488 nm.

2.4.4: Live treatments and their effects on the localisation of molecular markers

RBL-2H3 cells were treated with methyl-β-cyclodextrin (MBCD), wortmannin, and cytochalasin D to determine the effects of each on the localisation of either DBPC or LysoTracker Red.

2.4.4.1: Treatment of RBL-2H3 cells with MBCD

RBL-2H3 cells were pre-treated with 10 mM MBCD in 1 ml HBSS for a minimum of 30 minutes and maximum of 2 hours at 37°C/5% CO_2 prior to labelling with the novel PtdCho and real-time live imaging. 1 hour pre-treatment using MBCD at 37°C/5% CO_2 was used to asses the effect on LysoTracker labelling in RBL-2H3 cells prior to live confocal imaging. RBL-2H3 cells were also treated with 10 mM MBCD for up to 1 hour after lipid labelling.

2.4.4.2: Treatment of RBL-2H3 cells with wortmannin

RBL-2H3 cells were pre-treated with 100 nM wortmannin at 37°C/5% CO_2 in 1 ml HBSS for up to 2 hours and labelled for 2 hours with 1 µg novel PtdCho before real-time live imaging. RBL-2H3 cells were also labelled with the novel lipid and then treated with wortmannin (100 nM) for up to 1 hour at 37°C/5% CO_2.

2.4.4.3: Treatment of cells with cytochalasin D

Cytochalasin D (CD) was used at a 1 mM concentration dissolved in DMSO. RBL-2H3 or HeLa cells were labelled with the novel PtdCho for 2 hours and then treated with 1 µM CD for 5 hours and imaged every hour as part of a time course. Similarly RBL-2H3 cells were labelled with novel PtdCho and treated with CD for 2 hours before antigenic or phorbol 12-myristate 13-acetate (PMA) stimulation and imaged using real-time confocal microscopy. HeLa cells were treated with 1 µM CD for 1 hour prior to labelling with fluorescent PtdCho and live confocal imaging. HeLa cells transfected with Cherry-PLD1b were treated with CD for 1 hour 24 hours after transfection and imaged using live confocal microscopy.

2.4.4.4: UV treatment of RBL-2H3 cells

RBL-2H3 cells were labelled with 1 µg of the novel PtdCho for 2 hours at 37°C/5% CO_2 in 1 ml HBSS + 1 mM Ca^{2+} before UV treatment. Cells were exposed to 600

mJoules (mJ) of UV light in a UV Crosslinker (Hoefer Scientific Instruments) prior to live confocal imaging at various time points up to 24 hours.

2.4.5: Live stimulation of RBL-2H3 cells

RBL-2H3 cells were stimulated live on the confocal microscope, incubated in 1 ml HBSS + 1 mM Ca^{2+} and labelled with a molecular marker.

Cells were sensitized overnight using rat anti-DNP IgE (1 μg/ml, LO-DNP-30), washed once using 1 ml HBSS + 1 mM Ca^{2+} and labelled with either LysoTracker Red or the novel PtdCho. They were stimulated using 100 ng/ml DNP-KLH in 1 ml HBSS + 1 mM Ca^{2+} on the stage of the inverted SP5 confocal microscope at 37^{o}C (Farquhar *et al*., 2007).

PMA stimulation was used on RBL-2H3 cells first labelled using either LysoTracker Red or the novel fluorescent lipid. Cells were treated with 100 nM PMA in 1 ml HBSS + 1 mM Ca^{2+} on the heated stage of the SP5 confocal microscope.

RBL-2H3 cells stimulated with the calcium ionophore A23187 were washed once and labelled with either LysoTracker Red or the novel lipid and incubated in 1 ml HBSS + 1 mM Ca^{2+}. 0.1 μM A23187 was the most potent concentration (deduced using β-hexosaminidase assays) used during live real-time RBL-2H3 cell stimulation.

2.4.6: Stimulation of HeLa cells using epidermal growth factor (EGF)

Transfected HeLa cells were treated with 20 μM epidermal growth factor (EGF) for 10 minutes at 37^{o}C/5% CO_2 and then fixed with 4% PFA for 1 hour and washed 3 times with filter sterilised PBS (5 minutes per wash). Similarly, HeLa cells used for live microscopy were washed once with HBSS + 1 mM Ca^{2+} and stimulated with 20 μM EGF at 37^{o}C during real-time confocal imaging. Cells were also treated with 20 μM EGF at 37^{o}C/5% CO_2 for 10 minutes prior to washing with HBSS + 1 mM Ca^{2+} and real-time confocal imaging.

2.5: Fixed labelling of RBL-2H3 cells and immunocytochemistry

2.5.1: Fixed cell images

RBL-2H3 cells were grown on methanol-sterilised coverslips in 6-well plates and labelled with LysoTracker Red. Cells were then fixed using 4% PFA and washed once using filter sterilised PBS. The cells were permeabilized with 0.1% Triton-X-100 for 5 minutes, blocked with 5% donkey serum for 1 hour and washed again with filter sterilised PBS. The cells were incubated overnight at $4^{o}C$ with primary polyclonal rabbit anti-rat histamine unconjugated antibody (1:250) and washed again with filter sterilised PBS for 5 minutes. Finally, the cells were treated with the secondary anti-rabbit Alexa 488 antibody (1:500) for 1 hour at RT. Cells were washed with filter sterilised PBS for 5 minutes and mounted onto slides using Centifluor™.

2.6: Recording activity of stimulated RBL-2H3 cells

2.6.1: Treatment of RBL-2H3 cells in the β-hexosaminidase assay

RBL-2H3 cells were seeded in 12-well plates using a 1/5 dilution of the original culture in a 1 ml final volume of complete DMEM. To eliminate interference from FCS proteins, each well was washed twice using no additions DMEM and once using HBSS + 1 mM Ca^{2+}.

Each well was incubated in 250µl of HBSS + 1 mM Ca^{2+} and stimulated using antigenic stimulation in the context of IgE, PMA or A23187 as described previously (refer to Section 2.4.5). A23187 affects secretion in a concentration dependent manner and RBL-2H3 secretion was measured in response to 10 µM, 1 µM and 0.1 µM A23187 to identify the concentration which induces maximum secretion. All stimulation results were calculated as a percentage relative to cells treated with 0.1% Triton X-100.

Each treatment was performed in triplicate and allowed to incubate for 1 hour at $37^{o}C$/5% CO_2. The reactions were centrifuged at 13,000 RPM for 5 minutes and 20µl transferred to a 96-well plate. An equal volume of the β-hexosaminidase substrate 1 mM nitrophenyl N-acetyl-D-glucosamide (in 0.1 M sodium citrate buffer, pH 4.5) was added for 1 hour (Howl *et al*., 2003). The reaction was terminated using 200 µl 0.1 M sodium carbonate/0.1 M sodium hydrogen carbonate buffer, pH 10.5. The resulting yellow pigment was measured using a colorimeter at 405 nm taking readings in triplicate and averaged.

2.7: Tissue culture techniques of *Spodoptera frugiperda*

2.7.1: Culturing and maintenance of the *Spodoptera frugiperda* insect cell line

The *Spodoptera frugiperda* (Sf9) insect cell line was maintained in TC-100 insect medium with L-glutamine and sodium bicarbonate or modified Grace's medium (TNM-FH) with L-glutamine. The medium was supplemented with 10% FCS, 100 U/ml penicillin and 100 µg/ml streptomycin.

Sf9 cells were cultured in monolayers in either 25 cm^2 or 75 cm^2 sterile vented flasks grown at 27^oC. Monolayers were cultured to approximately 90-100% confluency before subculturing by tapping the flasks hard to displace the cells and gently resuspending. Typically cells were passaged at 1/2, 1/3, or 1/5 dilutions.

During logarithmic growth, Sf9 doubling time is approximately 24 hours and cells at this phase were infected with baculovirus. Cells were seeded at a density of approximately 0.5×10^5 cells/ml and allowed to grow to 1×10^6 cells/ml before infection.

2.7.2: Freezing and thawing of Sf9 cells

Sf9 cells were cultured to approximately 1×10^6 cells/ml in sterile vented flasks before subculturing. Cells were tapped hard to displace the confluent monolayer and centrifuged at 800 RPM for 3 minutes. The medium was then refreshed with 1/10th of the original volume of the culture and the pellet resuspended. An equal volume of 10% DMSO in fresh medium was added before aliquoting 0.5 ml into cryoviles. Cells were frozen slowly at -80^oC and transferred for long term storage to liquid nitrogen.

Cells were transferred from liquid nitrogen and thawed immediately at 37^oC. Cells were then transferred to 25 cm^2 sterile vented flasks with 5 ml complete medium and refreshed 1 hour after thawing.

2.8: Infection and harvesting of Sf9 cells

2.8.1: Infection of Sf9 cells with baculovirus

Sf9 cells were cultured in 4 ml complete TNM-FH media in 25 cm^2 sterile vented flasks to a density of approximately 1×10^6 cells/ml at the time of infection. Cells were infected with the baculovirus at 1×10^8 virions/ml containing either human PLD1 (hPLD1) or hPLD2 to give a multiplicity of infection (MOI) of 5. The baculovirus was provided by Professor M. J. O. Wakelam (Cambridge, UK).

2.8.2: Harvesting infected Sf9 cells and purifying protein using the glutathione-S-transferase (GST) tag

Sf9 cells infected with baculovirus containing GST labelled hPLD1 or hPLD2 were incubated at 27^{o}C for 48 hours. Cells were harvested from 25 cm^2 flasks using cell scrapers and centrifuging at 800 RPM for 3 minutes. Pellets were resuspended in 1 ml of warmed (37^{o}C) PBS and centrifuged at 1600 RPM for a further 3 minutes. The supernatant was discarded and pellet resuspended in 500 µl lysis buffer (10 mM Tris, 130 mM NaCl, 10 mM sodium fluoride, 10 mM sodium pyrophosphate (NaPPi), pH 7.5) with 1% Triton-X-100 and protease inhibitors. The lysate was then sonicated briefly and stood for 30 minutes at 4^{o}C. At each step of the purification process a 20 µl sample was removed and denatured using an equal volume of ×2 NuPAGE Sample Reducing Buffer with 1% 2 M dithiothreitol (DTT) and heated to 75^{o}C.

Glutathione S-transferase (GST)-hPLD1b and GST-hPLD2a proteins were extracted from the lysate using 1 step affinity purification. Approximately 400 µl glutathione sepharose 4B was pulsed at 1000 RPM to give a final bed volume of between 100-300 µl of glutathione sepharose beads. Beads were washed with 1 ml lysis buffer, centrifuged at 1000 RPM for 20 seconds and allowed to stand (although not to dry).

Following the 4^{o}C 30 minute incubation, the lysate was centrifuged for 30 minutes at 4^{o}C at 13,200 RPM. The pellet remaining was resuspended in 500 µl lysis buffer without detergent and the supernatant applied to the sepherose beads and agitated at 4^{o}C for 2-4 hours on a rotator. The glutathione sepharose column and lysate were

centrifuged at 1000 RPM for 60 seconds and the supernatant removed and stored at 4^{o}C. GST beads were washed using lysis buffer without detergent 3 times to remove all traces of detergent from the protein. During each wash the beads were allowed to stand at RT for 5 minutes, and then centrifuged at 1000 RPM for 60 seconds. Protein was eluted using 200 µl of 10 mM glutathione in 50 mM Tris pH7.5 and stored at -80^{o}C. Samples taken at each stage of the purification process were used to analyse the efficiency of protein expression and purification using western blotting.

2.9: Western blotting

2.9.1: SDS-PAGE electrophoresis

Samples collected at each step of GST-hPLD purification described previously (refer to Section 2.8) were denatured using NuPAGE Sample Reducing Buffer and heated to 75^{o}C. To reduce sample viscosity at least 1 freeze thaw cycle was completed. NuPAGE Bis-Tris mini gels were used under reduced conditions; the buffer of the lower chamber contained running buffer and the upper chamber 200 ml running buffer and 500 µl antioxidant. Half the volumes of samples taken from each GST purification step were run (20 µl-30 µl). Rainbow Molecular Weight Markers were used for reference points on each gel. The NuPAGE gels were run for 50 minutes at 200V.

2.9.2: Transferring proteins from NuPAGE gel to PVDF membrane

Proteins separated by NuPAGE gels were transferred onto polyvinylidene fluoride (PVDF) membranes. Whatman 3MN filter paper (8.5 cm x 7.5 cm) was soaked in transfer buffer (12 mM Tris, 96 mM Glycine, 10% Methanol, 5% of 10% SDS solution). The PVDF membrane (8 cm x 7 cm) was then washed in methanol and the excess washed away with distilled water. The PVDF membrane was soaked in transfer buffer and the gel 'sandwiched' with the PVDF membrane and a piece of filter paper on the back of the gel. A second piece of filter paper was placed at the front of the gel. These layers were then put into a cassette with sponges and run at 25 V for 90 minutes. The lower chamber was filled with water and the upper chamber with transfer buffer.

2.9.3: PVDF membrane immunoblotting

PVDF membranes were blocked for 1 hour at RT with 5% marvel in TST buffer (10 mM Tris, 100 mM NaCl, 0.05% Tween 20, pH 7.5 using HCl) with agitation. Membranes were washed briefly with 5 ml TST buffer and incubated with the primary antibody (in 5% marvel) overnight at RT. The membrane was washed 5 times (5 minutes per wash) using 25 ml TST buffer and incubated for 1 hour with the

appropriate horse radish peroxidase (HRP) secondary antibody 1:5000 dilution (in 5% marvel). The membrane was washed 5 times and developed using the EZ-ECL Chemilluminescene Detection Kit for HRP as per the manufacturer's instructions. Kodax BioMax XAR Film 18 cm x 24 cm was used and developed to analyse western blots. Antibodies used for immunoblotting PVDF membranes are listed in Table 2.1.

Table 2.1: Antibodies used to probe GST, hPLD1 and hPLD2 proteins for immunoblotting PVDF membranes. Antibodies used for probing GST and hPLD1 or hPLD2 were incubated at RT overnight at a dilution of 1/1000 in 5% marvel. PVDF membranes were then probed with the appropriate 1/5000 secondary HRP antibody for 1 hour at RT.

Antigen	Supplier	Dilutions	Secondary Antibody
GST	Sigma	1:1000	Anti-Mouse
PLD1	Santa Cruz	1:1000	Anti-Goat
PLD1	Sylvain Bourgoin (Canada)	1:1000	Anti-Rabbit
PLD2	Sylvain Bourgoin (Canada)	1:1000	Anti-Rabbit

2.9.4: PVDF membranes: stripping and re-probing

PVDF membranes were incubated in stripping buffer (62.5 mM Tris, 2% SDS, 100 mM β-mercaptoethanol (BME), pH 6.8 using HCl) for 1 hour at RT with agitation. Membranes were transferred to clean falcon tubes and washed extensively with TST buffer between 60 to 90 minutes. PVDF membranes were blocked using 5% marvel (refer to Section 2.9.3) and re-probed with primary and secondary antibodies.

2.10: Fluorescent *in vitro* PLD assays

2.10.1: Measuring *in vitro* GST-hPLD1 activity

Real-time *in vitro* GST-hPLD1 assays were completed in a final volume of 100 µl at 37^{o}C. Each assay contained 50 µl lipid vesicles (x2 stock), 50 µM guanosine 5'-O-(gamma-thio) triphosphate (GTPγS), 3 mM magnesium (Mg^{2+}), 2 mM Ca^{2+} and 400 mM sodium chloride (NaCl). Vesicles were created using the following: 134 µM L-α-phosphatidylethanolamine (PtdEth), 24 µM phosphatidylinositol-4,5-bisphosphate (PtdIns(4,5)P_2) and 0.5 µg of the novel fluorescent lipid. The lipids were dried under a gentle stream of nitrogen gas before resuspending in 400 µl sonication buffer (125 mM HEPES, 200 mM potassium chloride (KCl), 2.5 mM DTT, 7.5 mM ethyl glycol tetraacetic acid (EGTA) and pH 7.5). Vesicles were vortexed briefly and sonicated for 20 seconds at 5mA. Vesicles were stored at RT and protected from the light; fresh vesicles were created for each set of experiments. Purified recombinant GST-hPLD1 protein preparations were thawed on ice and added to each assay. The fluorescent vesicles were finally added to the assays. Known GST-hPLD1 activators such as PKCα, histadine-tagged Rac1 wildtype (wt), Rac1 (constitutively active) and adenosine diphosphate (ADP) ribosylation factor (Arf1) maintained in buffer following the manufacturer's instructions (substituting 0.1% glycerol for dextran). 2 µg of each activator were added to the assay immediately prior to recording PtdCho hydrolysis (using relative fluorescence emitted). Total assay volume was 100 µl in black-bottomed, 96-well plate. Fluorescence readings were taken every 2 seconds using a fluorimeter (at 37^{o}C) and data recorded concurrently using excitation at 485 nm and fluorescence emission detection at 535 nm.

2.11: Molecular biology techniques

2.11.1: Making and transforming chemically competent cells

Frozen *Escherichia coli* dh5α was resuspended in 1 ml of Luria broth (LB), plated on non-selective LB agar plates and incubated at 37^{o}C overnight. A single colony was used to seed a 10 ml super optimal broth (SOB medium) mini-culture (5 g bacto tryptone, 1.25 g yeast extract**,** 0.5 ml 5 M sodium chloride, 0.625 ml 1 M potassium chloride and 2.5 ml 1 M magnesium chloride) incubated at 37^{o}C/250 RPM overnight.

The mini-culture was used to seed a 200 ml SOB maxi-culture incubated at 37^{o}C until the optical density (OD) at 550 nm was 0.45. All of the following steps were completed at 4^{o}C. Cells were chilled for 30 minutes and centrifuged for 15 minutes at 4000 RPM. The supernatant was discarded and cells resuspended in 66 ml buffer RF1 (100 mM rubidium chloride, 50 mM manganese chloride, 20 mM potassium acetate, 10 mM calcium chloride, 15% glycerol, pH 5.8) and chilled for 1 hour. Cells were then centrifuged and resuspended in 16 ml buffer RF2 (10 mM 3-(N-morpholino) propanesulfonic acid (MOPS), 10 mM rubidium chloride, 75 mM calcium chloride, 15% glycerol, pH 6.8) and chilled for 15 minutes. Chemically competent cells were flash frozen in 200 µl aliquots (using dry ice and ethanol) and stored at -80^{o}C.

To transform chemically competent cells, aliquots were thawed slowly and ligations or plasmid DNA (1:500 of maxi-prep DNA) were added to 100 µl cells. The cells were incubated 15-30 minutes at 4^{o}C and heat shocked at 42^{o}C for 2 minutes, followed by 2 minutes at 4^{o}C. 100 µl of ×2 LB was added and the cells incubated at 37^{o}C for 30 minutes with agitation. The transformed cells were then plated onto selective plates and incubated overnight at 37^{o}C.

2.11.2: Ligations of cDNA into vector plasmids

Standard ligations used T4 ligase followed the manufactures instructions. Final volumes of ligations (10 µl or 20 µl) were dependent on insert concentration using 25-50 ng vector and 50-100 ng insert in a ×5 ligation buffer. Ligations were

incubated for a minimum of 3 hours ('sticky' end ligations) or overnight ('blunt' end ligations).

Shrimp alkaline phosphatase (SAP) or rAPid Alkaline Phosphatase were used in a 2 step ligation where vector DNA was dephosphorylation (following manufacturer's instructions). The vector was dephosphorylated prior to ligation with insert cDNA as detailed previously.

All ligations were transformed using chemically competent cells as described previously (refer to Section 2.11.1) and plated onto selective LB agar plates.

2.11.3: DNA extraction from Miniprep and Maxiprep *E.coli* cultures

Miniprep cultures inoculated using a single colony (picked from LB agar plates) were grown in 10 ml LB with antibiotics (0.1 mg/ml ampicillin or kanomycin) and incubated for 16-18 hours at 37^{o}C/280 RPM. Plasmid Miniprep DNA was extracted using the QIAprep Spin Miniprep Kit protocol following the manufacturer's instructions and eluted using 50 µl autoclaved water.

Miniprep DNA was amplified using Maxiprep cultures with a total volume of 100 ml LB and supplemented with an appropriate antibiotic. Maxiprep cultures were inoculated either with 2 ml Miniprep culture or a single colony and incubated at 37^{o}C/280 RPM for 16-18 hours. Plasmid DNA Purification QIAGEN Plasmid Maxi protocol was used to extract Maxiprep DNA (utilising the QIAGEN Plasmid Maxi Kit). Plasmid DNA was eluted following the manufacturer's instructions and allowed to air dry before resuspension in 250-500 µl autoclaved water (~1-2 µg/µl).

Concentration and purity of Maxiprep DNA was spectrophotometer-determined at 260 nm and 280 nm. Purity was analysed using the A_{260}/A_{280} ratio and concentration deduced using the value for A_{260} multiplied by 50 (the optical density equals to 1 at 260 nm of a 50 µg sample) and multiplying by 100 (to convert to µg/µl).

2.11.4: Polymerase chain reaction mutagenesis and screening

Primers were phosphorylated using T4 kinase incubated with 6µl ×5 Forward Reaction buffer, 1.5µl 2.5 mM adenosine triphosphate (ATP) and 1µl T4 kinase in a final volume of 30µl. The T4 kinase reaction mixture was incubated at 37^{o}C for 15 minutes followed by 10 minute incubation at 65^{o}C. The reaction mixture was allowed to cool before primers were used for polymerase chain reaction (PCR).

PCR reactions used to amplify sequences used a standard master mix containing 150µl betaine/DMSO, 99µl dH_2O, 30µl ×10 buffer with $MgSO_4$, 3µl of template DNA (diluted 1/50 Miniprep DNA), 12 µl mixed primers after kinase treatment and 6µl deoxyribonucleotides (dNTPs) from a 10 mM stock concentration. Each reaction contained 90µl PCR master mix and 0.5µl *Pyrococcus woesei* (PWO) DNA Polymerase to maximise the amount of DNA. Reactions conditions were modified depending on the size of the fragment being amplified and extension time was appropriate to the length of the DNA (typically 1 minute per 1000 base pairs) at 40^{o}C, 50^{o}C and 60^{o}C.

Single colonies were picked from selective plates and resuspended in 100 µl of water. The mastermix of the PCR reaction contained 20 µl PCR buffer (without Mg^{2+}), 10 µl W-1, 6 µl 50 mM Mg^{2+}, 2 µl 10 mM dNTP mix, 2 µl of each primer and 2 µl 5 u/µl Taq polymerase (recombinant) with V_T of 211 µl. 1 µl of the resuspended colonies and 9 µl PCR master mix were used for each PCR orientation reaction. The PCR screening program used was at 50^{o}C with a 1 minute extension time for 30 cycles. PCR screening was used to assess if the ligated fragment was inserted into the correct open reading frame (ORF) of the vector plasmid.

2.11.5: Restriction enzyme digests – analytical and preparative

Analytical restriction enzyme digests were used to identify fragment size and confirm restriction sites of cloned plasmids. Analytical digests using 0.5-1 µl DNA, 1 µl of the appropriate buffer and 0.5 µl restriction enzyme (final volume 10 µl) and incubated at 37^{o}C for 90 minutes. The digests were visualised using ×2 loading buffer (30% glycerol, 0.025% bromophenol blue) by agarose gel electophoresis. All

restriction enzymes were from Invitrogen (except HindIII, Fermentas) and protocols adhered to manufacturers instructions using appropriate buffers and conditions.

Preparative digests using Miniprep or Maxiprep DNA (final volume 30 µl) were incubated at 37^{o}C for 3 hours. Preparative digests were run on agarose gels and the appropriate bands extracted from the gel (refer to Section 2.11.7).

2.11.6: Agarose gel electrophoresis and DNA quantification

DNA was visualised using UV light after agarose gel electrophoresis where DNA was intercalated using ×2 loading buffer containing ethidium bromide. Both analytical and quantitative digests were run on 1-2% agarose gels (1-2 g agarose, 10 ml ×5 Tris-borate-ethylenediaminetetraacedic (EDTA) acid (TBE) buffer, 10 µl of 10 mg/ml stock ethidium bromide to V_T of 100 ml) in running buffer (25 ml ×5 TBE buffer to a V_T of 250 ml). 5 µl of 10% 1Kb DNA ladder was used on analytical gels to determine the size of fragments produced using restriction enzyme digests.

DNA quantification was used to aid ligations 2 µl of purified insert and vector DNA were quantified using agarose gel electrophoresis of the DNA. Insert and vector DNA were compared against 10 µl of 10% 1Kb DNA ladder and quantified.

2.11.7: Purification of preparative DNA

Preparative DNA was purified using gel electrophoresis in which the appropriate band was cut from the gels using UV light and purified using the QIAquick Gel Extraction Kit (following manufacturer's instructions). DNA was eluted from the QIAquick Gel Extraction columns using 50µl autoclaved water and then used for ligations.

2.11.8: Sequencing of plasmid DNA

Plasmid Miniprep DNA was sequenced using the Molecular Biology Service, University of Warwick. 2 µl of miniprep DNA and a 1/20 dilution of the appropriate primer were submitted for sequencing.

Sequencing data was viewed (using ChromasLite) and sequences analysed using LALIGN (comparing the actual sequence with the predicted sequence constructed using GCK). The entire sequence data for the ~3000 base pairs of human PLD1b or PLD2a were combined to make a single ORF and LALIGN was used to demonstrate that the obtained sequence matched the expected sequence (generated *in silico*). The *in silico* sequence is derived from the published sequences associated with the accession numbers for PLD1b (Accession No. Q133393-2) and PLD2a (Accession No. O14939). All the primers used for sequencing (Appendix 1) were designed and sourced from VH Bio Limited.

2.11.9: Cloning of pcDNA3.1(-)-mRFP-PLD1b or -PLD2a

Primers to the N-terminal and C-terminal of mRFP from the dsRedm plasmid (obtained from Dr G. Ladds, Coventry, UK) using the standard PCR protocol (refer to Section 2.11.4) and used to generate a PCR product for the ORF of mRFP with an engineered XbaI site, (using primers move dsRed F (XbaI) to engineer an XbaI site and move dsRed R). The PCR product was purifed (QIAquick Gel Extraction Kit) and both the PCR product and pcDNA3.1(-) were digested using XbaI-XhoI and re-purified. The PCR product was ligated with the linearised pcDNA3.1(-) vector. Ligations were transformed by heat shock into chemically competent *E. coli* and plated onto LB agar plates containing ampicillin (100 µg/ml). Ampicillin resistant colonies were screened for the mRFP ORF using a PCR-based screen with forward and reverse primers from pcDNA3.1(-) called T7 and 1491. Positive clones were Miniprep cultured in 10 ml LB broth with ampicilin overnight and plasmid DNA extracted (QIAprep Spin Miniprep Kit). Positive clones were sequenced (Molecular Biology Service, University of Warwick) using primers T7 and 1491.

PLD1b was cloned by PCR into the EcoRV site of pcDNA3.1(-)-mRFP using T4 kinase treated PLD1b (start) F and PLD1b reverse primers. Similarly, PLD2a was cloned by PCR into the EcoRV site of pcDNA3.1(-)-mRFP using T4 kinase treated PLD2a (start) F and PLD2a reverse primers. The PCRs were performed using the standard protocol (refer to Section 2.11.4) at 40^{o}C, 50^{o}C and 60^{o}C and the products purified using gel electrophoresis (QIAquick Gel Extraction Kit). PLD1b or PLD2a were SAP ligated with pcDNA3.1(-)-mRFP linearised with EcoRV. Ligations were

then transformed by heat shock into chemically competent *E. coli* and plated on to LB agar plates containing ampicillin (100 µg/ml). Ampicillin resistant colonies were screened for the presence of the PLD1b ORF or PLD2a ORF using a PCR-based screen using forward primer from the mRFP ORF (dsRed sequencing) and reverse primers PLD1b XhoI reverse or PLD2a Inside XhoI (reverse). Positive clones were Miniprep cultured overnight in 10 ml LB broth with ampicillin and the plasmid DNA extracted (QIAprep Spin Miniprep Kit).

2.11.10: Cloning of pcDNA3.1(-)-Cherry-PLD1b or -PLD2a

Primers to the N-terminal and C-terminal of Cherry form of GFP (obtained from Dr G. Ladds, Coventry, UK; Shaner *et al*., 2004) were used to generate a PCR product for the ORF of Cherry-GFP. The N-terminal primer inserted an XbaI site directly N-terminal to the ATG of the Cherry ORF using the Cherry forward primer. The PCR product was generated (using Cherry forward and Cherry reverse primers) using the standard protocol PCR protocol (refer to Section 2.11.4). The PCR product was purified by gel electrophoresis and ligated into pcDNA3.1(-) linerarised with XbaI and EcoRV. Ligations were transformed by heat shock into chemically competent *E. coli* which were plated onto LB agar plates containing ampicillin (100 µg/ml). Ampicillin resistant colonies were screened for the presence of the Cherry ORF using a PCR-based screen with primers from either side of the pcDNA3.1 multi-cloning site using T7 and 1491. Positive clones were grown in 10 ml LB broth with ampicillin overnight and plasmid DNA extracted (Qiagen Miniprep Kit) and restricted with XbaI-EcoRV prior to sequencing (Department of Biological Sciences, University of Wariwck sequencing service) and this clone was called pcDNA3.1(-)-Cherry.

PLD1b was cloned by PCR into the EcoRV site of pcDNA3.1-Cherry using primers to the N- and C-terminals of PLD1b (using PLD1b (start) forward and PLD1b reverse primers). The PCR was performed at 40^{o}C, 50^{o}C and 60^{o}C and the product was purified by gel electrophoresis. The purified PCR product was then ligated with pcDNA3.1-Cherry linerarised with EcoRV. Ligations were transformed by heat shock into chemically competent *E. coli* which were plated onto LB agar plates containing ampicillin (100 µg/ml). Ampicillin resistant colonies were screened for

the presence of the PLD1b ORF using a PCR-based screen with the forward primer from Cherry and a reverse primer from PLD1b (PLD1b Xho reverse). Positive clones were grown in 10 ml LB broth with ampicillin overnight, plasmid DNA extracted (Qiagen Miniprep Kit) and subject to diagnostic restriction enzyme digests with XbaI plus EcoRV or KpnI. Positive clones were sequenced (Molecular Biology Service, University of Warwick).

PLD2a was cloned by PCR into the EcoRV site of pcDNA3.1-Cherry using primers to the N- and C-terminals of PLD2a (using PLD2a (start) forward and PLD2a reverse primers). The PCR was performed at 40^{o}C, 50^{o}C and 60^{o}C and the product purified by gel electrophoresis. Purified PCR products were ligated with pcDNA3.1-Cherry linerarised with EcoRV. Ligations were transformed by heat shock into chemically competent *E. coli* and plated onto LB agar plates containing ampicillin (100 μg/ml). Ampicillin resistant colonies were screened for the presence of the PLD2a ORF using a PCR-based screen with the forward primer from Cherry and a reverse primer from PLD2a (PLD2a reverse). Positive clones were grown in 10 ml LB broth with ampicillin overnight and plasmid DNA extracted (Qiagen Miniprep Kit) and sequenced (Molecular Biology Service, University of Warwick). The amino acid sequences, protein sequences and plasmid maps of Cherry-PLD1b and Cherry-PLD2a can be found in Appendices II-IIX.

2.12: The TNT Quick Coupled Transcription/Translation System and phosphorimaging

2.12.1: TNT Quick Coupled Transcription/Translation System

The TNT Quick Coupled Transcription/Translation System assay (TNT assay) was used to ensure stable *in vitro* protein expression of mRFP, PLD1b and PLD2a. The TNT assay was used to confirm *in vitro* (radiolabelling amino acid ^{35}S-methionine) expression of the full-length constructs as *in vivo* transfections were unsuccessful. Radiolabel was incorporated into the protein structure and could be detected using phosphorimaging or x-ray film. A luciferase (61kDa) protein-expressing plasmid was used as a control to confirm the reaction occurred and as a marker of size. TNT proteins were made using 20 µl TNT reticulocyte, 2 µl Miniprep DNA, 10µCi ^{35}S-methionine and nuclease free water (final volume of 25 µl per reaction). Reactions were then incubated at 30^{o}C for 90 minutes. TNT protein mixture (5 µl or 6 µl) was added to 5 µl water and 10 µl of × 2 loading buffer and then incubated at 75^{o}C for 30 minutes. Samples were run on pre-cast NuPAGE Bis-Tris mini gels under reducing conditions (see Section 2.9.1) for 50 minutes, stained, de-stained and dried overnight, previously published in Wright *et al*., 2008 (see Appendix IX).

Coomassie stain was made using 50 ml ethanol, 10 ml glacial acetic acid and 40 ml water with 0.129g of Coomassie Blue. The gel was submerged in the stain, heated for 30 seconds, then cooled with agitation for 15 minutes. The de-staining process occurred in 2 steps: first, the same proportions of ethanol and glacial acetic acid were used as the Coomassie stain but without Coomassie Blue. The second contained 10 ml ethanol, 5 ml glacial acetic acid and 85 ml water. Both de-stains were heated for 30 seconds and allowed to cool with agitation for 15 minutes. The gel was soaked in water for 30 minutes followed by soaking in 10% glycerol for 30 minutes. The gel and cellulose paper were then submerged in ×1 drying solution and dried on a scaffold overnight. Phosphorimaging and the more sensitive x-ray imaging technique were used to analyse the gel and identify molecular weight markers. The control TNT protein luciferase was also used as a molecular weight marker of 61kDa.

Chapter 3: Characterising a fluorescent PLD substrate

3.1 Introduction

Mast cells are involved in initiating the inflammatory response via cross-linking the high affinity immunoglobulin E (IgE) receptors ($Fc_{\varepsilon}RI$) with binding of multivalent antigens initiating degranulation (Toru *et al*., 1996). These granules contain inflammatory mediators such as histamine, serotonin, heparin and proteases. Mast cell stimulation and degranulation has been well characterised in the rat basophilic leukaemia (RBL-2H3) cell line which can be induced by antigenic stimulation in the context of IgE, increasing intracellular Ca^{2+} concentration via a calcium ionophore or activating PKCα with phorbol 12-myristate 13-acetate (PMA).

The localisation of the two predominant mammalian PLD isoforms (PLD1b and PLD2a) varies greatly depending on the cell line. In unstimulated RBL-2H3 cells, transiently expressed GFP-PLDlb localises with markers for secretory granules and lysosomes but, upon antigenic stimulation, translocates to the plasma membrane (Brown *et al*., 1998). Degranulation is dependent upon PLD catalysing the hydrolysis of PtdCho to generate PtdOH and choline (Brown *et al*., 1998).

Phospholipases D have the unique ability to mediate a transphosphatidylation reaction that was first identified in cabbage PLD (Yang *et al*., 1967). Primary alcohols (such as butan-1-ol) inhibit PLD-catalysed PtdOH production by interfering with the transesterification of the lipid substrate (PtdCho) and resulting in preferential production of a phosphtidylalcohol (Ptd-alcohol). Primary alcohols are therefore referred to as PLD (enzyme) inhibitors but they are more accurately described as "functional inhibitors". The mechanism by which butanol is proposed to work necessarily assumes the presence of an enzyme-phosphatidyl group intermediate in the catalytic mechanism. The primary alcohol, acting as a stronger nucleophile than the surrounding water, attacks this intermediate, resulting in, for example, production of phosphatodylbutanol (PtdBut) rather than PtdOH. Ptd-alcohols are more metabolically stable than PtdOH in cells and therefore their accumulation not only diverts PtOH signalling but also can be used to assay PLD

catalysed PtdCho hydrolysis from appropriately labelled cells (Frohman *et al*., 1999). Although transphosphatidylation inhibits degranulation in RBL-2H3 following antigenic stimulation, PLD maintains its ability to translocate to the plasma membrane (Brown *et al*., 1998). This discovery indicates that the product of PtdCho hydrolysis, PtdOH, is a key second messenger and mediator of mast cell degranulation. The role of PtdOH in diverse cell processes including exocytosis, endocytosis and cytoskeletal rearrangement is not yet well understood.

A23187, an antibiotic derived from *Streptomyces chartreusensis*, binds to divalent ions (preferentially to Ca^{2+} ions) and transports them across biological membranes (Reed and Lardy, 1972; Luckasen *et al*., 1974). This increase in intracellular Ca^{2+} ions leads to non-PLD dependent exocytosis of RBL-2H3 cells. The secreory granules of RBL-2H3 cells express synaptotagmin (Syt) proteins which are Ca^{2+} sensitive and initiate plasma membrane and vesicle membrane fusion events.

PLD activity can be measured in a number of ways including the accumulation of Ptd-alcohol or via *in vitro* PtdCho hydrolysis assays. Mast cell degranulation can be measured via beta (β)-hexosaminidase assays (measuring lysosomal secretion). Upon PLD activation, the known lysosome marker β-hexosaminidase is secreted (Farquhar *et al*., 2002) which hydrolyses both N-acetylglucosamine and N-acetylgalactosamine (Watanabe, 1936; Wendeler and Sandhoff, 2009).

Using a novel fluorescent (fPtdCho) synthesised in the laboratory of Prof. Glenn Prestwich enabled the characterisation of fPtdCho in several cell lines. The novel fPtdCho is labelled with BODIPY at the choline head group and when it is intact BODIPY fluorescence is internally quenched by non-fluorescent aromatic groups attached to the acyl-chains (see Fig. 3.1). When the lipid is hydrolysed by PLD to release the BODIPY-labelled choline head group, fluorescence emission increases. However, fluorescence is intramolecularly quenched by the presence of aromatic groups inserted into the fatty acid chain. When the lipid is de-quenched (through hydrolysis by PLA_2, PLC or PLD), fluorescence is expected to increase. The aim was to determine the spatio-temporal activation of PLD (by its multiple regulators) to form a PtdCho-hydrolysing complex *in vivo* in real-time. Although the novel

fPtdCho localised in RBL-2H3 cells in a characteristic manner, RBL-2H3 cells were difficult to genetically modify in a reproducible manner.

PLD localisation in RBL-2H3 has been previously characterised using GFP (Brown *et al*., 1998). However, the BODIPY label of the novel fluorescent lipid was also green and so a different fluorophore was needed to unequivocally visualise both PLD and its substrate *in vivo*. PLD was fluorescently labelled with monomeric RFP (mRFP), a derivative of the original DsRed fluorescent protein from the *Discosoma* genus. DsRed had slow fluorescence maturation (from green to red), and tetramers formed *in vivo* are toxic to cells (Baird *et al*., 2000). DsRed was genetically altered using 33 site-directed amino acid substitutions, resulting in the acceleration of the rate of fluorescence maturation and induced preferential formation of either tandem dimers or true monomers (denoted mRFP1 – Bevis and Glick, 2002; Campbell e*t al*., 2002). Additional modifications to the mRFP fusion tag have improved photostability and quantum yield are found in the clone mCherry, which is tenfold brighter than mRFP and benefited from GFP-type termini (which aided in N- or C-terminal fusion) when expressed in mammalian cells (Shaner *et al*., 2004; Shaner *et al*., 2005; Müller-Taubengerger *et al*., 2006). The mCherry fluorescent tag offers the longest wavelength, highest photostability and fastest maturation when compared to other fluorescent proteins developed from mRFP1, (for example mStrawberry and mOrange – Shaner *et al*., 2004). In addition, mCherry rapidly reaches near-complete maturation, has an increased tolerance to N-terminal fusion and tenfold increase resistance to photobleaching (when compared to mRFP1), which renders mRFP1 obsolete (Shaner *et al*., 2004; Shaner *et al*., 2005).

Figure 3.1: The structure of the novel fluorescent PLD substrate. The novel fPtdCho is labelled with BODIPY attached to the choline head group. Intramolecular aromatic groups are present on the acyl-chains of the lipid so when it is intact BODIPY fluorescence is reduced. Upon PLD hydrolysis, the choline-BODIPY head group is released and fluorescence increases *in vitro*. The lipid was synthesized in the laboratory of Professor G. Prestwich (Utah, USA).

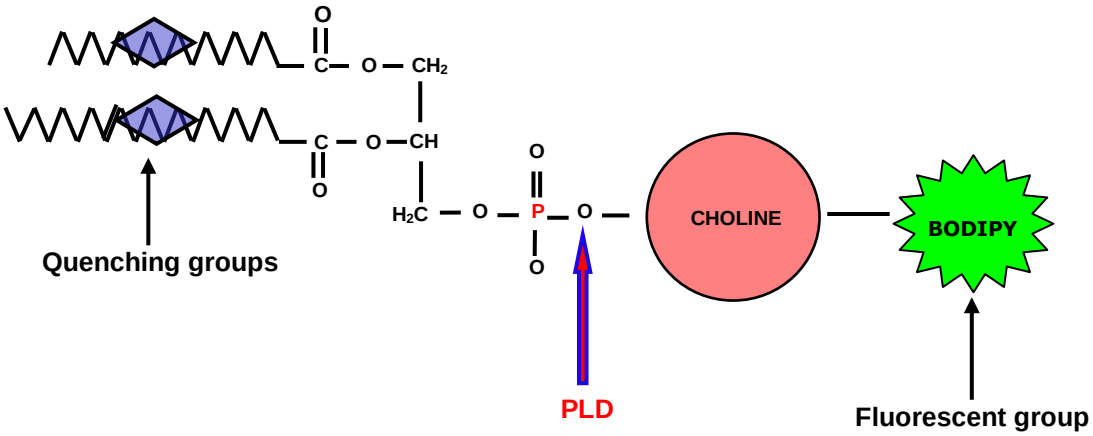

3.2: Characterisation of a novel PLD substrate and other molecular markers in RBL-2H3 cells

3.2.1: Characterisation of a fluorescent PLD substrate in the RBL-2H3 cell line

The fluorescence of the BODIPY group was not fully quenched in the intact fPtdCho lipid and basal fluorescence could still be detected. RBL-2H3 cells were labelled with the 0.5 µg/ml fPtdCho in a salt solution (PBS or HBSS) for 3 hours and the lipids extracted using the Bligh-Dyer method (Bligh and Dyer, 1959). The fluorescence of aqueous and lipid fractions from labelled and unlabelled cells were compared using a fluorimeter. Readings were recorded approximately every second for 60 seconds using an excitation of 488 nm and emission of 530 nm. The fluorescence emissions (see Fig. 3.2a) of the lipid fractions from unlabelled (control) RBL-2H3 cells, were up to 11 times lower than cells labelled with fPtdCho. The fluorescence emissions of lipid fractions from labelled cells were up to five times higher than that of aqueous fractions. In addition, although this change in emitted fluorescence may not seem substantial, chloroform is known to quench fluorescence (Hurtubise, 1975).

RBL-2H3 cells were labelled with 0.5 µg/ml novel fluorescent lipid (in DMSO) for 1-3 hours at 37^{o}C prior to imaging. Although the fPtdCho was expected to stain the plasma membrane, it localised in punctiform structures within the cell cytoplasm (see Fig. 3.2b). Confocal microscopy was used to image the treated cells live at 37^{o}C. The movement of the internalised fluorescent lipid using real-time imaging was recorded over 15 minutes (1 frame/10 seconds) which is condensed into 18 seconds (see Fig. 3.2c for condensed recording). The punctate structures were motile within the RBL-2H3 cells and moved within and between the focal planes. All the cells in dishes treated with the fPtdCho were labelled and displayed characteristic punctiform localisation. fPtdCho labelling of the RBL-2H3 cells was consistently punctate, however the level of fPtdCho uptake was dependent on the cell population and duration of cell exposure to the lipid.

Figure 3.2: Localisation of the novel fluorescent lipid in RBL-2H3 cells.

a) RBL-2H3 cells were grown in 6-well plates in complete DMEM for 24 hours prior to labelling. The cells were washed once with HBSS + 20 mM HEPES and incubated in 1 ml HBSS for 2 hours with 1 µg/ml fPtdCho (in DMSO). Each well was washed with filter sterilised PBS and scraped into a final volume of 700 µl of methanol. 700 µl of chloroform and 630 µl of water (1 chloroform: 1 methanol: 0.9 water) were then also added to the methanol fraction. The mixture was centrifuged (1000 RPM for 2 minutes) and the lipid fluorescence (in chloroform) and aqueous (in methanol/water) fractions was measured (panel **a**). The HBSS cells were labelled in was also measured. Fluorescence was accrued approximately every second for 60 seconds at an excitation of 488 nm and emission of 530 nm in quartz cuvettes. The fluorescence of labelled and unlabelled cell fractions was compared between 2 samples.

b) RBL-2H3 cells used for confocal imaging were grown on glass bottomed fluorodishes for 24 hours. Cells were labelled using 1 µg/ml of fPtdCho for between 60 and 120 minutes prior to real-time confocal imaging. Cells were then washed with filter sterilised PBS + 25 mM HEPES, pH 7.4 and incubated in a final volume of 1 ml. Real-time recording was completed over 15 minutes (1 frame/10 seconds) using the argon laser with an excitation at 488 nm and an emission band width between 500 nm-608 nm. The 488 nm laser power was halved and each time point was scanned twice (and averaged) to reduce photobleaching. A scale calibrated to 25 µm is shown in each panel. The data presented are representative images for 1 experiment of at least 4. Still images of the real-time recording are represented below (panel **b**) whilst the recording is shown in Fig. 3.2**c**.

a

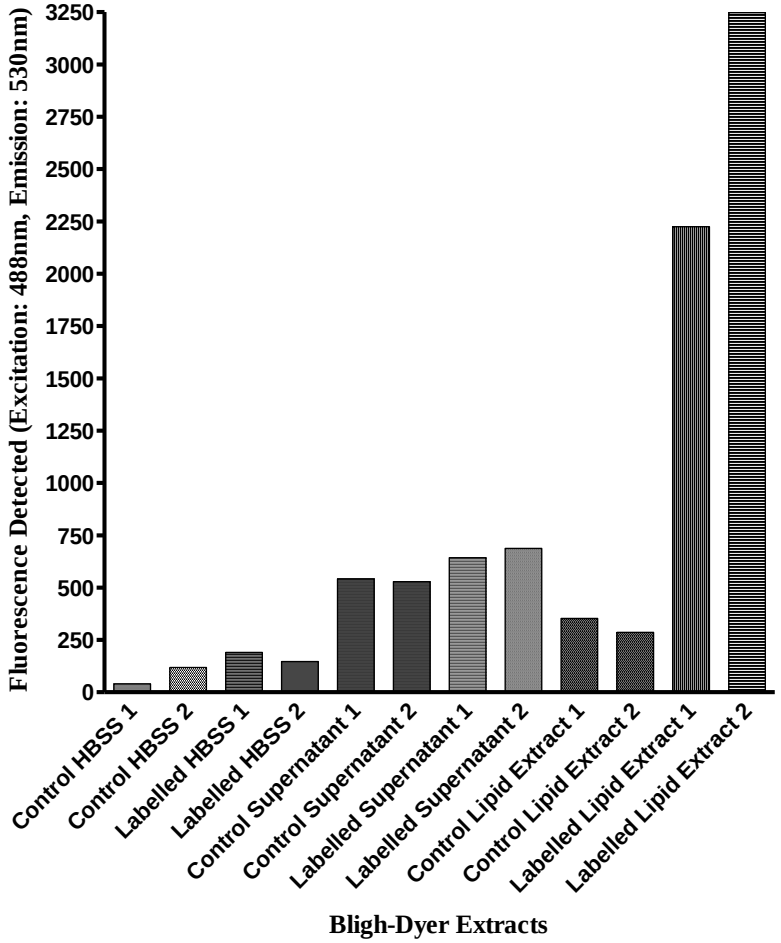
Fluorescence Detected (Excitation: 488nm, Emission: 530nm)
3250
3000
2750
2500
2250
2000
1750
1500
1250
1000
750
500
250
0
Control HBSS 1
Control HBSS 2
Labelled HBSS 1
Labelled HBSS 2
Control Supernatant 1
Control Supernatant 2
Labelled Supernatant 1
Labelled Supernatant 2
Control Lipid Extract 1
Control Lipid Extract 2
Labelled Lipid Extract 1
Labelled Lipid Extract 2
Bligh-Dyer Extracts

b

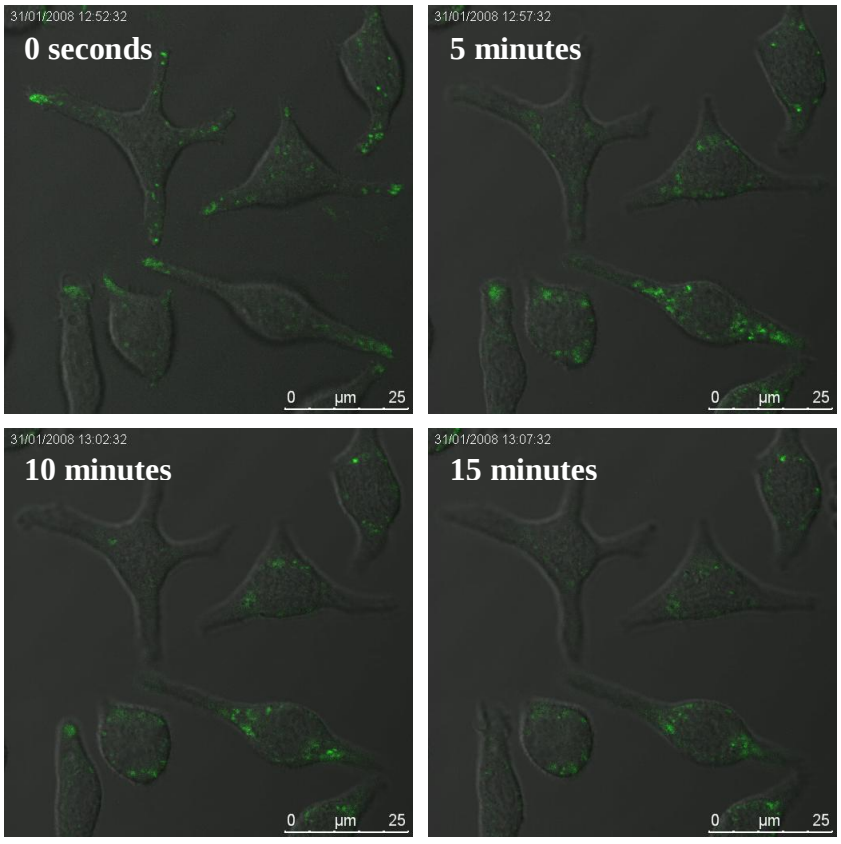
31/01/2008 12:52:32
0 seconds
0 µm 25
31/01/2008 12:57:32
5 minutes
0 µm 25
31/01/2008 13:02:32
10 minutes
0 µm 25
31/01/2008 13:07:32
15 minutes
0 µm 25

The size of the vesicles was analysed using the Leica Application Software (LAS) Advanced Fluorescence (AF) Lite software. Transects were drawn across cells and the fluorescence intensity measured using a stack profile for both DIC and fluorescent channels (see Fig. 3.3). The majority of the vesicles were between 1-2 µm in diameter, although this varied between 0.3 µm and 2.9 µm. The diversity in vesicle size may be due to vesicle movement as vesicles appeared to 'fuse'. The average size of vesicles was calculated using 189 vesicle sizes, and calculated to be 1.38 µm (± 0.04).

The novel fluorescent lipid stably labelled RBL-2H3 cells for up to 24 hours. Although the total fluorescence diminished between 3 and 22 hours, the labelling of punctiform structures in the cell body and processes was maintained (see Fig. 3.4, panels a, b). The lipid was also used to label other cell lines including the Swiss 3T3 fibroblast cell line. Although every cell was labelled with the fPtdCho at 3 hours (see Fig. 3.4, panels c-e), localisation was not as distinctive as in RBL-2H3 cells. Swiss 3T3 cells showed both punctate (see arrows Fig. 3.4, panel e) and diffuse (see circle Fig. 3.4, panel e) labelling. Swiss 3T3 cells were not as effectively labelled as RBL-2H3 cells and after 24 hours the labelling was weakened further.

Figure 3.2: The size of fluorescent PtdCho vesicles in the RBL-2H3 cell line. RBL-2H3 cells were grown on glass bottomed fluorodishes and labelled with 1 µg/ml of the novel fluorescent lipid for 90 minutes and imaged using SP5 confocal microscopy. Using the LAS-AF Lite software sections of the cells were analysed using lines and fluorescence intensity was exported in stack profiles. The size of the line (region of interest) drawn across the cell is represented along the x-axis (µm). The fluorescence intensity across this region of interest excited at 488 nm with an emission bandwidth between 500-608 nm is represented on the y-axis. The fluorescence intensity of the 488 nm channel (■) was compared to the 'control' DIC channel (▲). A representation of 1 region of interest with 2 fluorescence peaks (where each peak was identified as a vesicle) is represented below. Vesicles were analysed across 3 separate experiments using 10 regions of interest each. (n=1, 25 vesicles were identified, n=2, 52 vesicles were identified, n=3, 48 vesicles were identified).

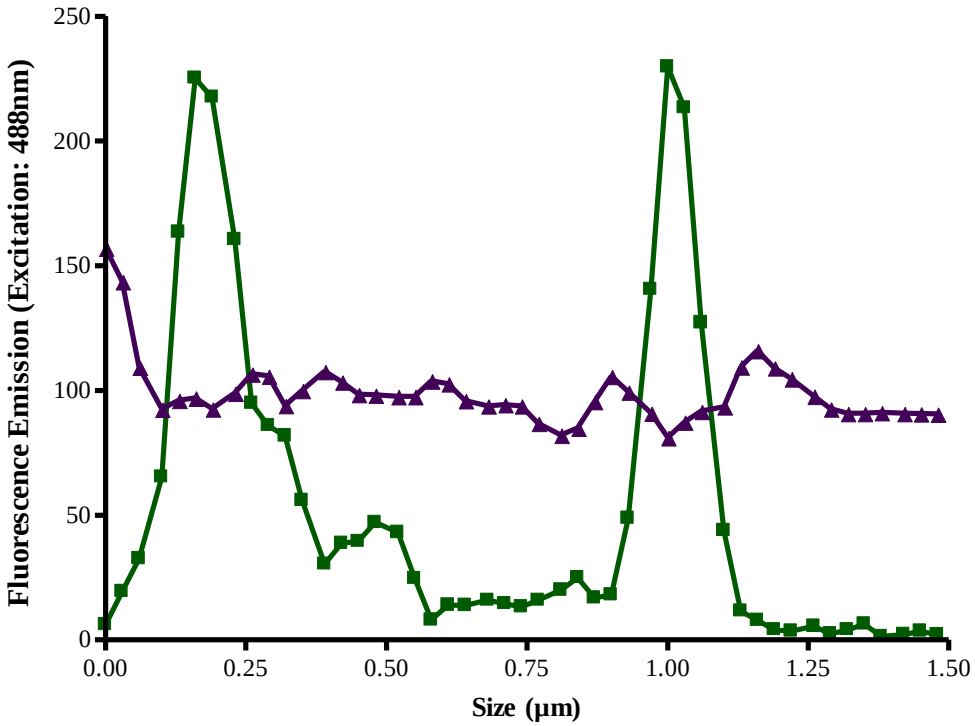

Figure 3.4: The stability of fluorescently labelled RBL-2H3 and Swiss 3T3 cells. RBL-2H3 and Swiss 3T3 cells were grown on glass bottomed fluorodishes for 24 hours prior to labelling. Cells were labelled using 1 µg/ml of fPtdCho for a minimum of 60 minutes prior to confocal imaging. Live cell imaging (at 37^{o}C) excited fluorescence using the 488 nm argon laser with an emission bandwidth between 500 nm-608 nm. RBL-2H3 cells were imaged at various time-points including 3 hours and 22 hours (see panels **a**, **b**). Swiss 3T3 cells were also imaged up to 24 hours (see panels **c-e**). A scale calibrated to 25 µm is shown in each panel. The data presented are representative images for 1 experiment of 5 using RBL-2H3 cells and 1 of 2 using Swiss 3T3 cells.

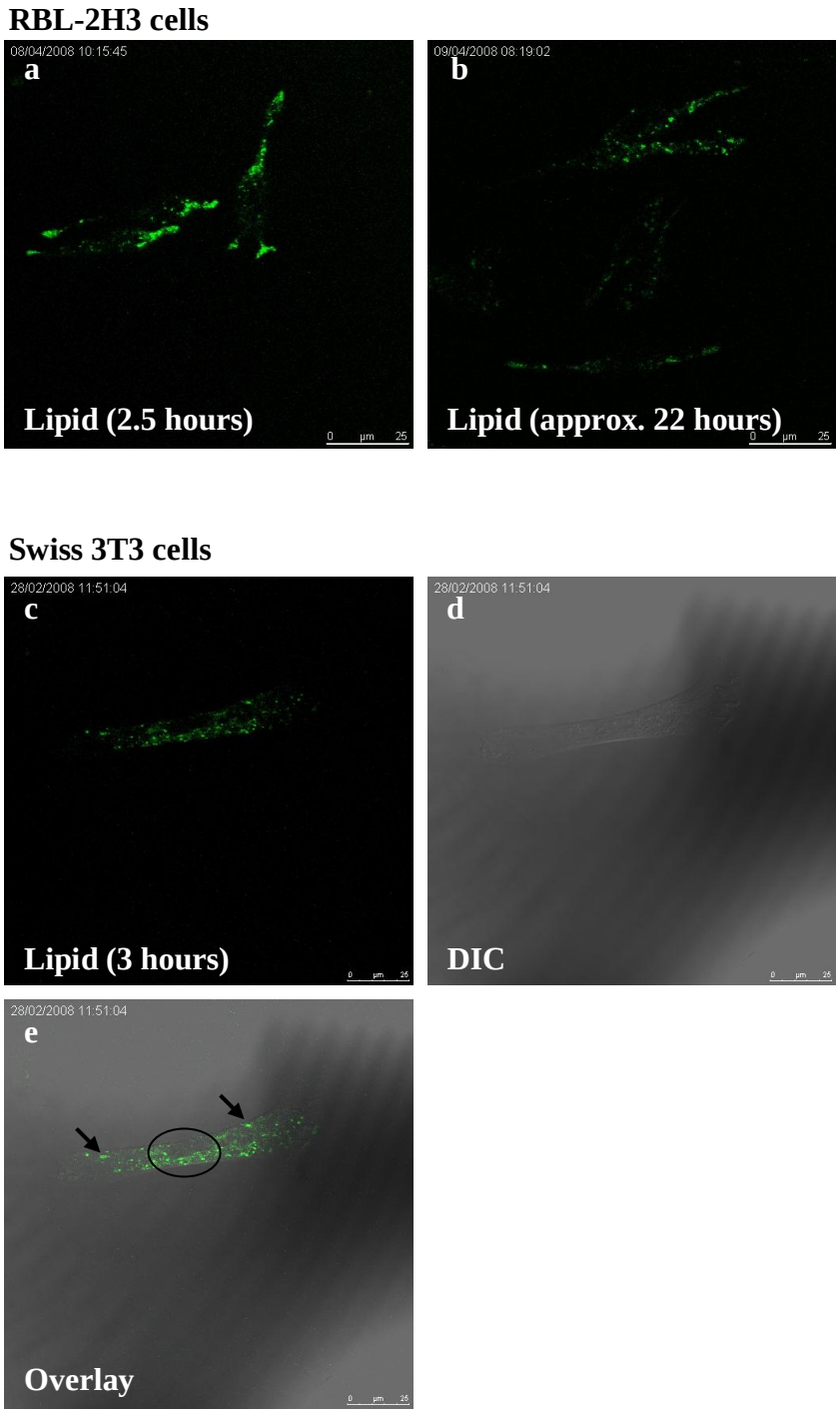

3.2.3: Localisation of a fluorescent PLD substrate with other live molecular markers in RBL-2H3 cells

Although the novel fPtdCho localised to organelles within the cytoplasm, the identity of these organelles was unknown. Fixing the fluorescent lipid using 4% PFA was not possible, as the fluorescence was lost. In addition, the fluorescent lipid would leach out of permeabilised cells and so immunocytochemistry was not possible. Identifying where the fluorescent lipid localises in the RBL-2H3 cells was therefore investigated using live molecular markers.

RBL-2H3 cells were treated first with the fluorescent lipid and then labelled with the membrane marker FM4-64. FM4-64 is an amphiphilic styryl dye comprised of 3 components: hydrophobic tail, body, and dictionic head. These contribute to membrane labelling, the spectral properties of the dye and prevention of dye passage across the membrane, respectively (Betz *et al*., 1996; Fischer-Parton *et al*., 2000). However, the novel lipid (green) did not co-localise with the FM4-64 (red) and localisation did not change over a 15 minute time-course (see Fig. 3.5).

Other molecular markers such as Hoechst 33342 and MitoTracker Red did not co-localise with the novel fPtdCho (see Fig. 3.6). Although the mitochondrial marker MitoTracker Red (see Fig. 3.6, panel b) and the fluorescent lipid (see Fig. 3.6, panel a) labelled punctiform structures within the cell cytoplasm, they did not co-localise. Punctate structures labelled with either fluorescent lipid or MitoTracker Red were distinct from the nucleus (see Fig. 3.6, panel a, c, e).

Figure 3.5: The localisation of the novel fluorescent lipid and the molecular marker FM4-64 in RBL-2H3 cells (time course). RBL-2H3 cells were grown on glass bottomed fluorodishes for 24 hours prior to labelling with 1 µg/ml of the novel fPtdCho, (in HBSS + 20 mM HEPES for a minimum of 60 minutes). Cells were stained with 2.5 µM FM4-64 (in DMSO) washed once with HBSS and imaged at 37^{o}C. Both the BODIPY labelled lipid and the FM4-64 dye were excited at 488 nm using the argon laser. The emission bandwidth of the novel fluorescent lipid was between 491 nm-552 nm whilst the emission bandwidth for FM4-64 was between 604 nm-733 nm. Confocal microscopy was used to record a time-course taking snapshots at 0, 5, 10 and 15 minutes. Although the argon laser was used to excite both channels, controls showed there was no overlap in fluorescence detection between the 2 markers and localisation was distinct (see overlays below). A scale calibrated to 50 µm is shown in each panel. The data presented are representative images for 1 experiment and of at least 2.

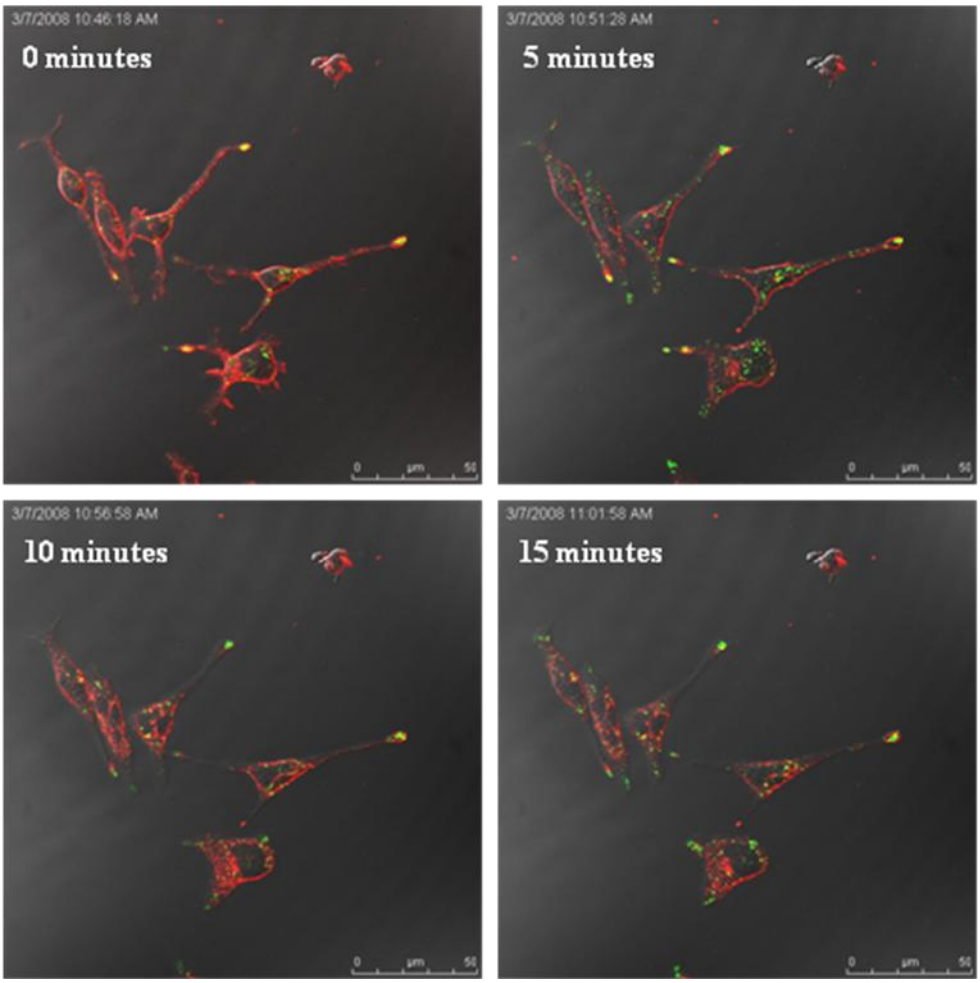

Figure 3.6: The localisation of the novel fluorescent lipid with nuclear and mitochondrial markers in RBL-2H3 cells. RBL-2H3 cells were grown on glass bottomed fluorodishes for 24 hours prior to labelling with the novel lipid. Cells were labelled using 1 µg/ml of fPtdCho in 1 ml HBSS + 20 mM HEPES + 1 mM Ca^{2+} for a minimum of 210 minutes prior to confocal imaging (see panel **a**). Cells were then stained with 100 nM of the mitochondrial marker MitoTracker Red CMXRos (see panel **b**) for 30 minutes at 37°C/5% CO_2 and with the nuclear marker Hoechst 33342 (2.0 µg/ml in HBSS) at 37°C/5% CO_2 for 15 minutes (see panel **c**). Cells were imaged using live SP5 confocal microscopy at 37°C and each channel was scanned sequentially. The fluorescent lipid was excited by the argon laser at 488 nm with an emission bandwidth between 495 nm-582 nm. MitoTracker Red was excited by the DPSS 561 laser at 561 nm with an emission bandwidth between 674 nm-795 nm. Hoechst was excited using the 405 Diode UV laser with an emission bandwidth between 430 nm-480 nm. A scale calibrated to 25 µm is shown in each panel. The data presented are representative images for 1 experiment of 2.

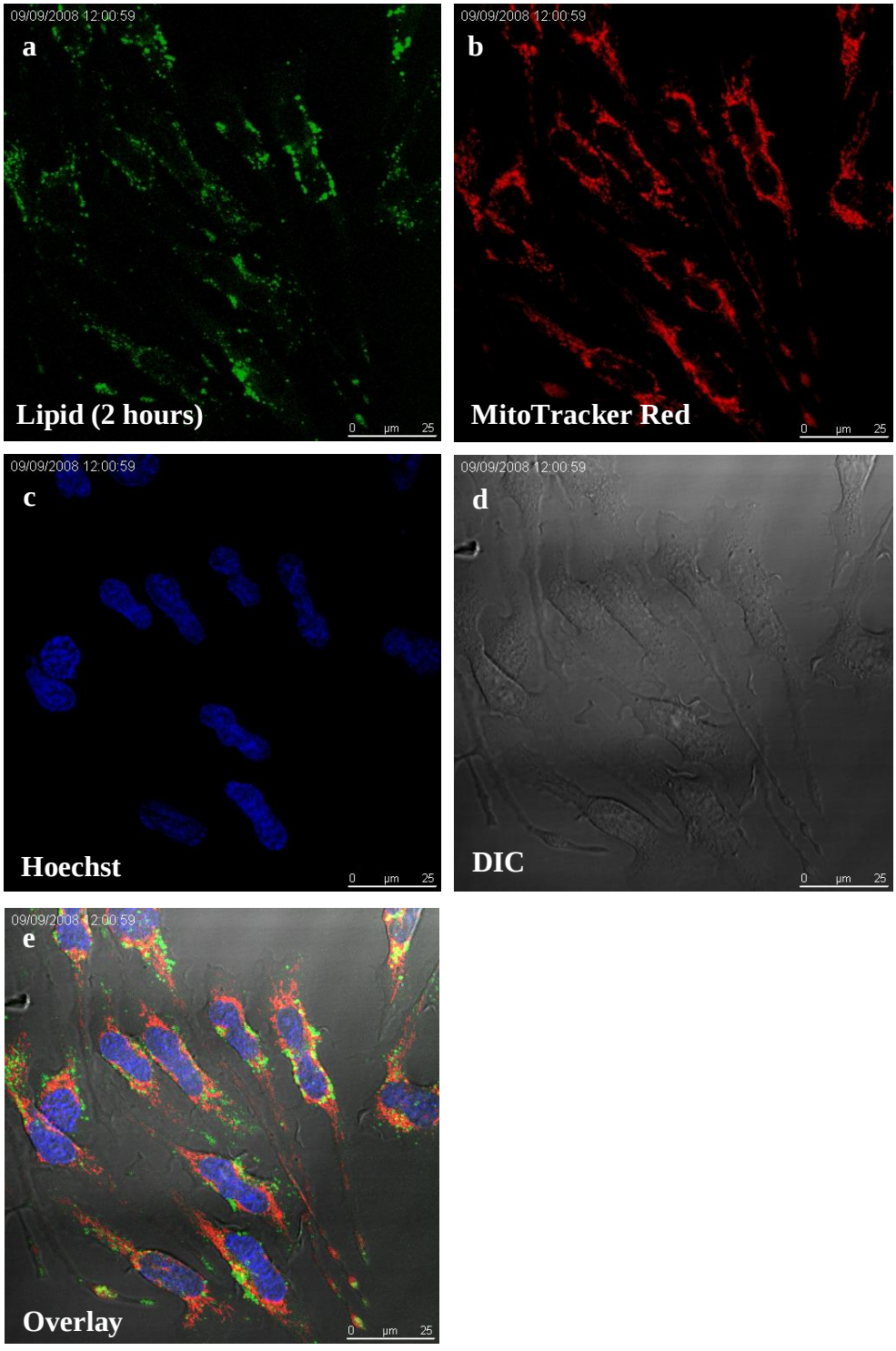
09/09/2008 12:00:59
a
Lipid (2 hours)
0 µm 25
09/09/2008 12:00:59
b
MitoTracker Red
0 µm 25
09/09/2008 12:00:59
c
Hoechst
0 µm 25
09/09/2008 12:00:59
d
DIC
0 µm 25
09/09/2008 12:00:59
e
Overlay
0 µm 25

RBL-2H3 cells labelled with the novel fPtdCho were then treated with 100 nM of the lysosomal marker, LysoTracker Red (see Fig. 3.7, panel a). LysoTracker Red is weakly basic and a known acidotropic molecular probe, which specifically targets and stains acidic compartments in mammalian cells, such as lysosomes (Saito *et al*., 2004). PLD1 localisation varies in different cell lines but it has been suggested that PLD1 may localise in lysosomes (Brown *et al*., 1998; Toda *et al*., 1999). The excitation/emission spectra of the fluorescent lipid and LysoTracker Red were narrowed to minimise cross-channel fluorescence bleed-through. LysoTracker Red was excited at 594 nm with an emission bandwidth between 658 nm-794 nm. The fluorescent lipid was excited at 488 nm and the emission bandwidth was narrowed between 495 nm-533 nm. Background fluorescence was reduced to minimise the influence of unlabelled cells.

Co-localisation between LysoTracker Red and the novel fluorescent lipid in RBL-2H3 cells was analysed using Image J. Imaging data was collected using serial sections (at 1 µm thickness) of each field (see Fig. 3.7, panel b, n=1 and n=2). Individual cells in the field were isolated and the co-localisation between the 2 markers in each section (in the case of n=1 and n=2) was analysed using the Colocalisation Finder plugin. In a third experiment (see Fig. 3.7, panel b, n=3), cells were analysed individually in the focal plane with the most fluorescence. The average Pearson's Correlation Coefficient between the 3 experiments was 0.5, suggesting approximately 50% co-localisation between the 2 markers. Using the unpaired 2-tailed t-test there was no significant difference between the means of these data sets.

Figure 3.7: Analysing co-localisation between the novel fluorescent lipid and LysoTracker Red using Image J. RBL-2H3 cells were grown on glass bottomed fluorodishes for 24 hours prior to labelling with the 0.5 µg/ml novel fPtdCho in 1 ml HBSS + 20 mM HEPES for 90 minutes (see panel **a**, image **a**). Cells were then stained with 100 nM of the lysosomal marker LysoTracker Red (see panel **a**, image **b**) for 1 minute before washing twice with HBSS and imaging live at 37^{o}C. The fluorescent lipid was excited by the argon laser at 488 nm with an emission bandwidth between 495 nm-533 nm using SP5 confocal microscopy. LysoTracker Red was excited by the HeNe 594 laser at 594 nm with an emission bandwidth between 658 nm-794 nm. Serial sections (1 µm thickness) were recorded and cells were analysed individually for co-localisation in each section in experiments n=1 and n=2. A total of 4 fields were analysed in n=1 (25 cells in total) and 3 fields were analysed in n=2 (18 cells in total). Co-localisation in individual cells was analysed in only 1 focal plane in 8 fields of experiment n=3 (50 cells in total). Image J was used to isolate individual cells and calculate the Pearson's R using the Colocalization Finder plugin. An average of all the cells in 3 separate experiments is shown in panel **b**. A scale calibrated to 50 µm is shown in each image (see panel **a**). The data presented are representative images for 1 experiment of 3.

a

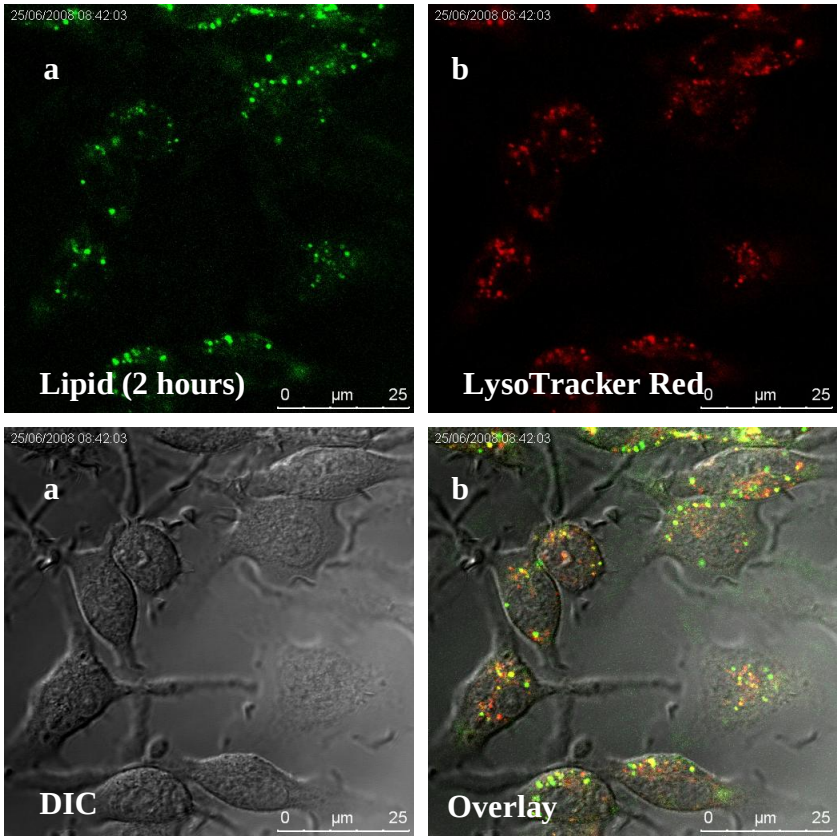
25/06/2008 08:42:03
a
Lipid (2 hours)
0 µm 25
25/06/2008 08:42:03
b
LysoTracker Red
0 µm 25
25/06/2008 08:42:03
a
DIC
0 µm 25
25/06/2008 08:42:03
b
Overlay
0 µm 25

b

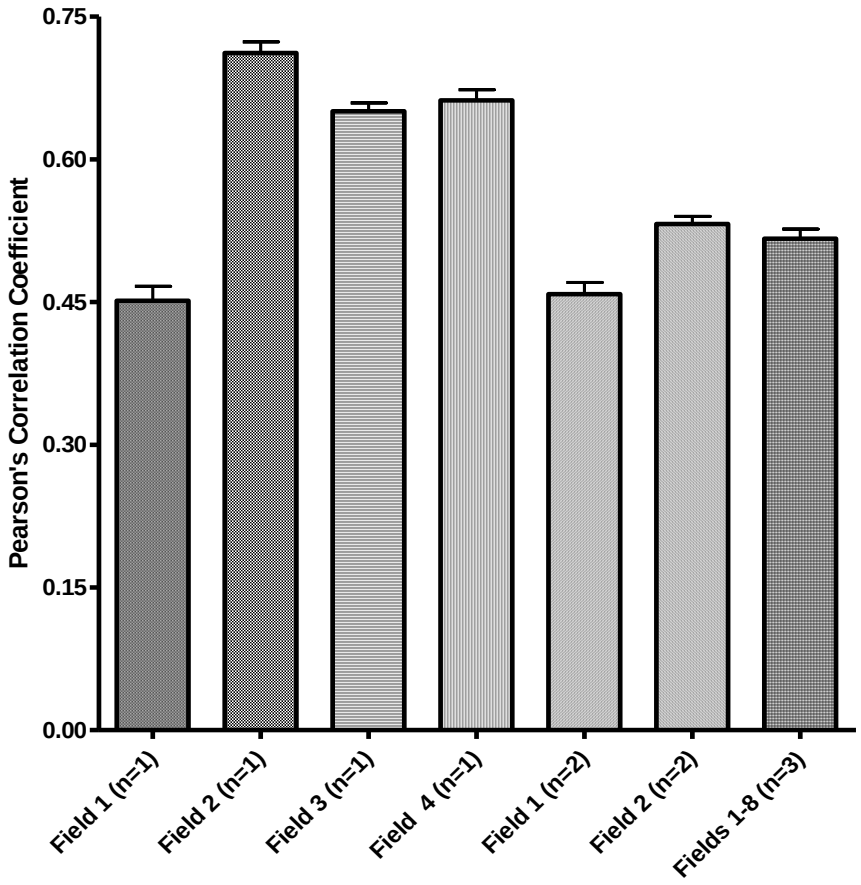
Pearson's Correlation Coefficient
0.75
0.60
0.45
0.30
0.15
0.00
Field 1 (n=1)
Field 2 (n=1)
Field 3 (n=1)
Field 4 (n=1)
Field 1 (n=2)
Field 2 (n=2)
Fields 1-8 (n=3)

3.2.4: Characterisation of LysoTracker Red in the RBL-2H3 cell line

The exocytosis of secretory vesicles from mast cells contributes to the acute and late phase inflammatory response (Baram *et al*., 1999). Lysosomes contain an array of vasoactive amines (e.g. histamine) found in secretory granules and lysosomal enzymes (e.g. β-hexosaminidase), which contribute to the acidic internal environment of lysosomes (Anderson and Orci, 1988). The lysosomal marker LysoTracker Red accumulates in this acidic environment thus labeling the secretory lysosomes of RBL-2H3 cells (Baram *et al*., 1999). The movement and size of LysoTracker Red labelled vesicles in RBL-2H3 cells were compared to that of the novel fluorescent lipid. LysoTracker Red localised in punctiform structures located in the cell body and processes of RBL-2H3 cells (see Fig. 3.8a for snapshots). These punctiform structures moved within the cell body and processes and between focal planes (see Fig. 3.8b for recording). The movement of these vesicles was recorded over a period of 15 minutes using confocal microscopy (1 frame/10 seconds condensed to 18 seconds).

The size of the punctiform structures were typically measured between 1-2 µm in diameter, much like the structures identified when labelling with the novel fPtdCho. The size of the vesicles was analysed using the LAS-AF Lite software as detailed previously (see Section 3.2.1, Fig. 3.3). Vesicle sizes ranged from 0.8 µm to 3.9 µm in diameter when comparing 133 sizes of vesicles in 2 separate experiments, in 4 fields. The average size of vesicles was calculated using 133 vesicle sizes to be 1.7 µm (± 0.05). Using the unpaired 2-tailed t-test there was a significant difference between the mean size of LysoTracker Red and novel fPtdCho labelled vesicles.

Figure 3.8a: The localisation and movement of LysoTracker Red vesicles in the RBL-2H3 cell line. RBL-2H3 cells used for confocal imaging were grown on glass bottomed fluorodishes for 24 hours. Cells were labelled using 100 nM LysoTracker Red DND-99 for 1 minute and washed twice with HBSS prior to live confocal imaging. Real-time recording was completed over 15 minutes (1 frame/10 seconds) using the HeNe 594 laser with an excitation at 594 nm and an emission band width between 668 nm-794 nm. The 594 nm laser power was halved and each time point was scanned twice (and averaged) to reduce photo-bleaching. A scale calibrated to 25 µm is shown in each panel. The data presented are representative images for 1 experiment of at least 2. Still images of the real-time recording are represented in below whilst the recording is shown in Fig. 3.8**b**.

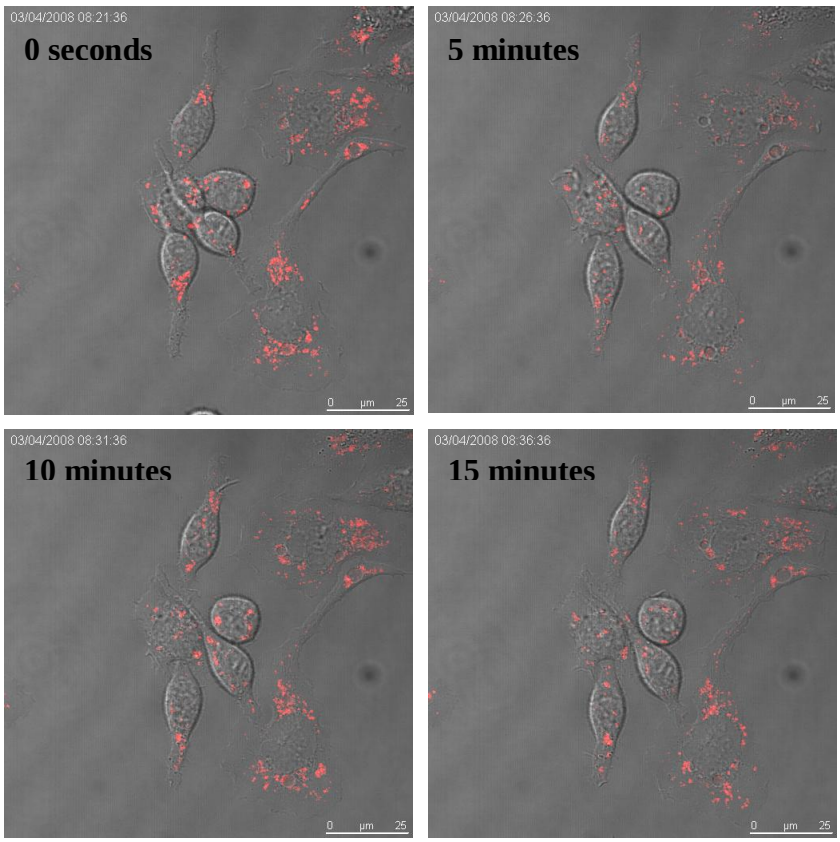

3.2.5: Characterisation of LysoTracker Red in the RBL-2H3 cell line

RBL-2H3 cells treated with 100 nM LysoTracker Red and then fixed with 4 % PFA were permeabilised with Triton-X-100, blocked with donkey serum and probed with a polyclonal rabbit anti-rat histamine antibody overnight. Bound primary antibody was detected with anti-rabbit Alexa-488 antibody (see Fig. 3.9, panel a, images a-d). The excitation and emission spectra of Alexa-488 and LysoTracker Red were narrowed to minimise cross-channel fluorescence bleed-through. LysoTracker Red was excited at 594 nm with an emission bandwidth between 618 nm-753 nm. Alexa-488 was excited at 488 nm the emission bandwidth was narrowed between 495 nm-552 nm. Background fluorescence was reduced to minimise the influence of background pixels on co-localisation analysis.

Image J was used to analyse the co-localisation between LysoTracker Red and the Alexa-488 cross-linked anti-histamine antibody in fixed RBL-2H3 cells. Imaging data was collected using serial sections (at 1 µm thickness) of 3 fields from 2 dishes (see Fig. 3.9, panel b, n=1 to n=3). Image J was used to isolate individual cells in the field and analyse the co-localisation between the 2 markers using the Colocalisation Finder plugin. The average Pearson's R between 3 experiments was 0.48, suggesting approximately 50% co-localisation between LysoTracker Red and the Alexa-488 cross-linked anti-histamine antibody. Using the unpaired 2-tailed t-test there was no significant difference between the means of the 3 data sets.

Figure 3.9: Analysing co-localisation between LysoTracker Red and a histamine antibody using Image J. RBL-2H3 cells were grown on coverslips for 24 hours prior to labelling with 100 nM LysoTracker Red (see panel **a**, image **a**) for 1 minute before fixing for 1 hour using 4% PFA. The cells were washing once with filter sterilised PBS and permeabilised for 5 minutes using 0.1% Triton-X-100. Cells were then incubated in 5% donkey serum (in PBS) before overnight treatment with a polyclonal rabbit anti-rat histamine antibody (1:250 dilution) at 4^{o}C. Cells were washed once with filter sterilised PBS and incubated at room temperature with anti-rabbit Alexa-488 antibody (1:500 dilution – see panel **a**, image **b**). Finally, cells were washed with PBS and mounted. The Alexa-488 antibody was excited by the argon laser at 488 nm with an emission bandwidth between 495 nm-552 nm. LysoTracker Red was excited by the HeNe 594 laser at 594 nm with an emission bandwidth between 618 nm-753 nm. Sequential confocal imaging was used to take serial sections (1 µm thickness) of each field. Individual cells were analysed in each serial section and the co-localisation averaged. Co-localisation analysis was completed using Image J and the Colocalization Finder plugin. A total of 3 separate slides (n=1, n=2 and n=3) were visualised and, on each slide, 3 fields were analysed (29 cells were analysed). An average of all the cells in 3 separate experiments is shown in panel **b**. A scale calibrated to 25 µm is shown in each image (see panel **a**). The data presented are representative images for 1 experiment of 3.

a

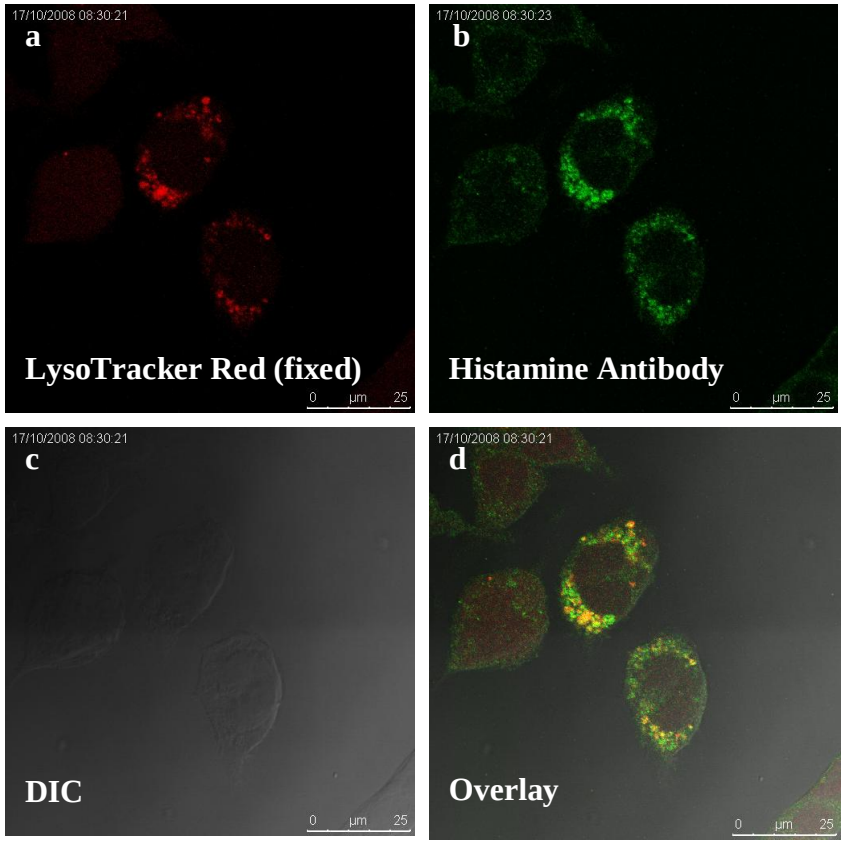
17/10/2008 08:30:21
a
LysoTracker Red (fixed)
0 µm 25
17/10/2008 08:30:23
b
Histamine Antibody
0 µm 25
17/10/2008 08:30:21
c
DIC
0 µm 25
17/10/2008 08:30:21
d
Overlay
0 µm 25

b

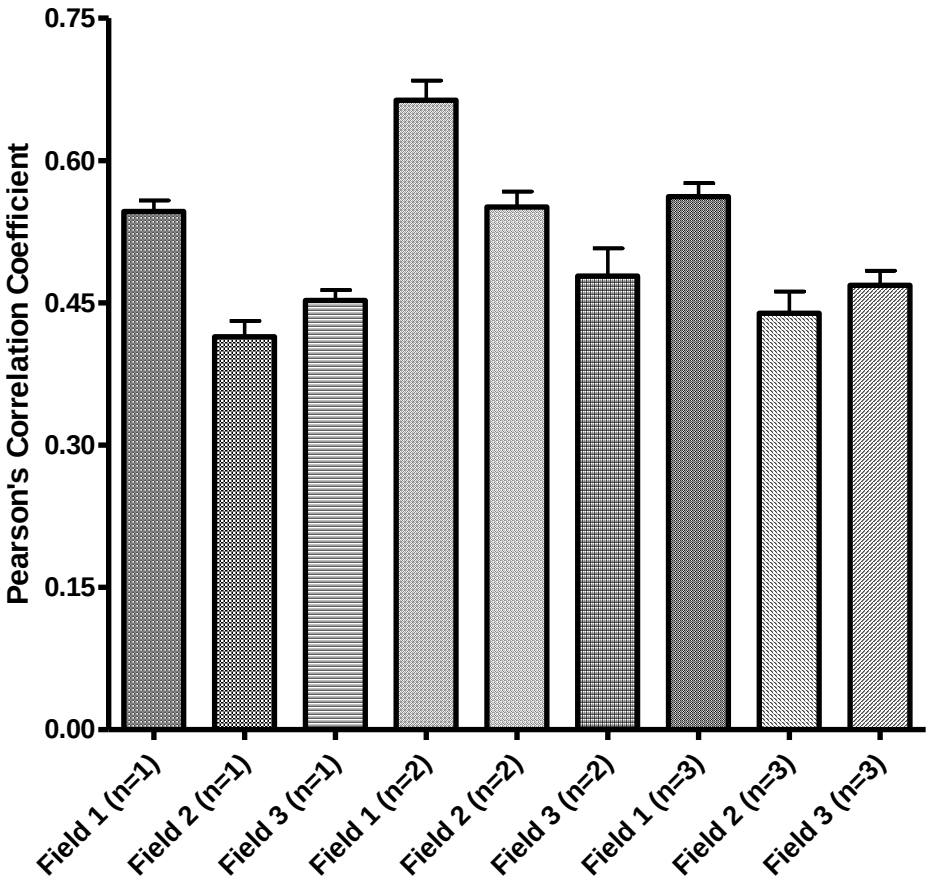
Pearson's Correlation Coefficient
0.75
0.60
0.45
0.30
0.15
0.00
Field 1 (n=1)
Field 2 (n=1)
Field 3 (n=1)
Field 1 (n=2)
Field 2 (n=2)
Field 3 (n=2)
Field 1 (n=3)
Field 2 (n=3)
Field 3 (n=3)

3.2.6: Characterisation of a fluorescent PLD substrate and other molecular markers in the MIN6 cell line

The MIN6 insulinoma cell line is an insulin secreting pancreatic β-cell line (Miyazaki *et al*., 1990; Ishihara *et al*., 1993). The fluorescence of the green fPtdCho was lower in MIN6 cells when compared to RBL-2H3 cell line (see Fig. 3.10, panel a) and was largely diffuse throughout the cytoplasm. The fluorescent lipid did not co-localise with the membrane marker FM4-64 or label the nucleus (see Fig. 3.10, panels b, d). LysoTracker Red treatment of MIN6 cells resulted in predominantly diffuse cytoplasmic staining; however there is also clear localisation in punctiform structures (see Fig. 3.10, panel e) and no labelling of the nucleus (see Fig. 3.10, panels f, h). The localisation of the novel fluorescent lipid and LysoTracker Red are not comparable to that in RBL-2H3 cells. This indicates that the structures which are labelled in RBL-2H3 may be specialised to mast cells and not to secretory cells in general.

Figure 3.10: Localisation of the novel fluorescent lipid and other molecular markers in the MIN6 cell line. MIN6 cells were grown on glass bottomed fluorodishes and labelled with 1 µg/ml of the novel fPtdCho in HBSS + 20 mM HEPES at 37^{o}C/5% CO_2 for 90 minutes (panel **a**). Cells were stained with 2.5 µM FM4-64 (panel **b**) and imaged immediately. MIN6 cells were also labelled with 2.0 µg/ml Hoechst 33342 for 15 minutes at 37^{o}C/5% CO_2 (panel **f**) and then treated with 100 nM LysoTracker Red for 1 minute (see panel **e**). Cells were washed twice with HBSS and data recorded using live sequential confocal microscopy. Both the novel fluorescent lipid and FM4-64 were excited by the argon laser at 488 nm with emission bandwidths between 500 nm-608 nm (green) and between 665 nm-794 nm (red). LysoTracker Red was excited using the HeNe 594 laser at 594 nm with an emission bandwidth between 668 nm-794 nm. Hoechst was excited using the 405 Diode UV laser with an emission bandwidth between 430 nm-480 nm. A scale calibrated to 25 µm is shown in each panel. MIN6 cells were labelled using the novel fluorescent lipid and with LysoTracker Red twice.

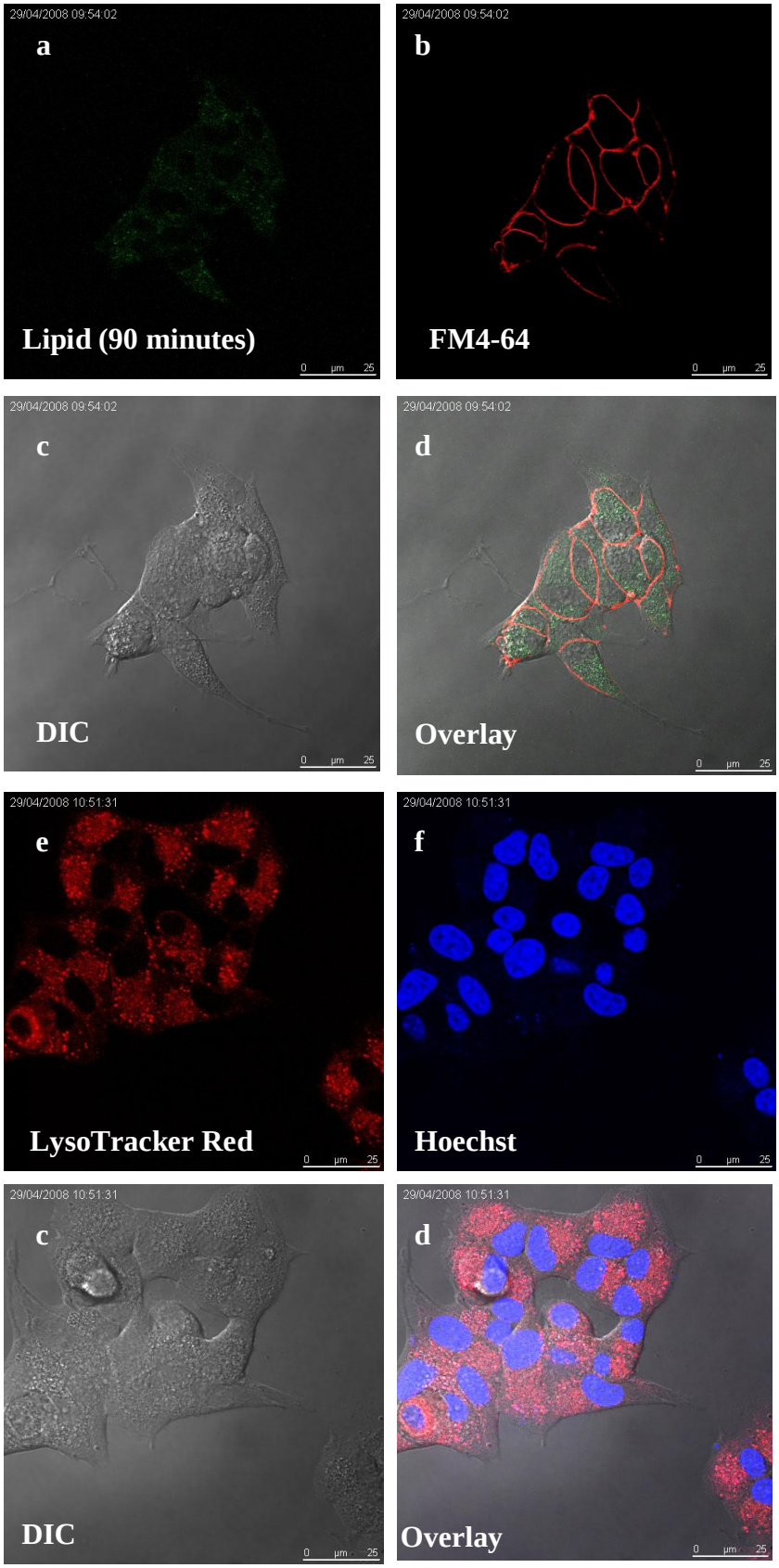
29/04/2008 09:54:02
a
Lipid (90 minutes)
0 µm 25
29/04/2008 09:54:02
b
FM4-64
0 µm 25
29/04/2008 09:54:02
c
DIC
0 µm 25
29/04/2008 09:54:02
d
Overlay
0 µm 25
29/04/2008 10:51:31
e
LysoTracker Red
0 µm 25
29/04/2008 10:51:31
f
Hoechst
0 µm 25
29/04/2008 10:51:31
c
DIC
0 µm 25
29/04/2008 10:51:31
d
Overlay
0 µm 25

3.2.7: Comparing the localisation of the novel fluorescent PtdCho to an acyl-modified BODIPY-PtdCho

The localisation of a commercially available short (acyl)-chain glycerophosphocholine also linked to BODIPY (BODIPY-PtdCho) was analysed in RBL-2H3 and HEK-293 cells. RBL-2H3 cells were stained using 1 µg/ml BODIPY-PtdCho for up to 2 hours. The fluorescence yield of BODIPY-PtdCho was considerably higher than that observed with the novel fluorescent lipid. Labelling RBL-2H3 cells using BODIPY-PtdCho was cytoplasmic, diffuse and non-nuclear. Similar to the novel fPtdCho, BODIPY-PtdCho did not stain the membrane or co-localise with the membrane marker FM4-64 (see Fig. 3.11, panels a-d). As BODIPY-PtdCho does not localise to punctiform structures within the cell, co-localisation between BODIPY-PtdCho and the lysosomal marker LysoTracker Red was not observed (see Fig. 3.11, panels e-h). BODIPY-PtdCho was a useful control for confirming the specific nature of the localisation of the novel fluorescent lipid having the same fluorescent group (attached to the choline).

Characterisation of BODIPY-PtdCho localisation in the epithelial HEK-293 cell line produced similar results to that seen in RBL-2H3 cells. Fluorescent staining was diffuse and cytoplasmic, and did not localise to the plasma membrane or the nucleus (see Fig. 3.12, panels a-d). Although the localisation of the novel fluorescent lipid was also diffuse in HEK-293 cells, the fluorescence yield was notably lower than that of BODIPY-PtdCho.

Figure 3.11: Localisation of BODIPY-PtdCho with FM4-64 and LysoTracker Red in RBL-2H3 cells. RBL-2H3 cells grown on glass bottomed fluorodishes for 24 hours were labelled with 1 µg/ml BODIPY-PtdCho in HBSS + 20 mM HEPES for either 5 minutes (panel **a**) or 120 minutes (panel **e**) at 37^{o}C/5% CO_2. Cells were stained with either 2.5 µM FM4-64 (panel **b**) or 100 nM LysoTracker Red (panel **f**) and imaged at 37^{o}C. BODIPY-PtdCho and FM4-64 were both excited by the argon laser at 488 nm with emission bandwidths between 500 nm-608 nm (green) and between 665 nm-794 nm (red – see panels **a-d**). The emission bandwidth of BODIPY-PtdCho was narrowed (495 nm-571 nm) when imaged with LysoTracker Red. LysoTracker Red was excited with the HeNe 594 laser at 594 nm with an emission bandwidth between 629 nm-764 nm (see panels **e-h**). A scale calibrated to 25 µm is shown in each panel. RBL-2H3 cells exhibited diffuse staining using BODIPY-PtdCho imaged using confocal microscopy in 3 separate experiments.

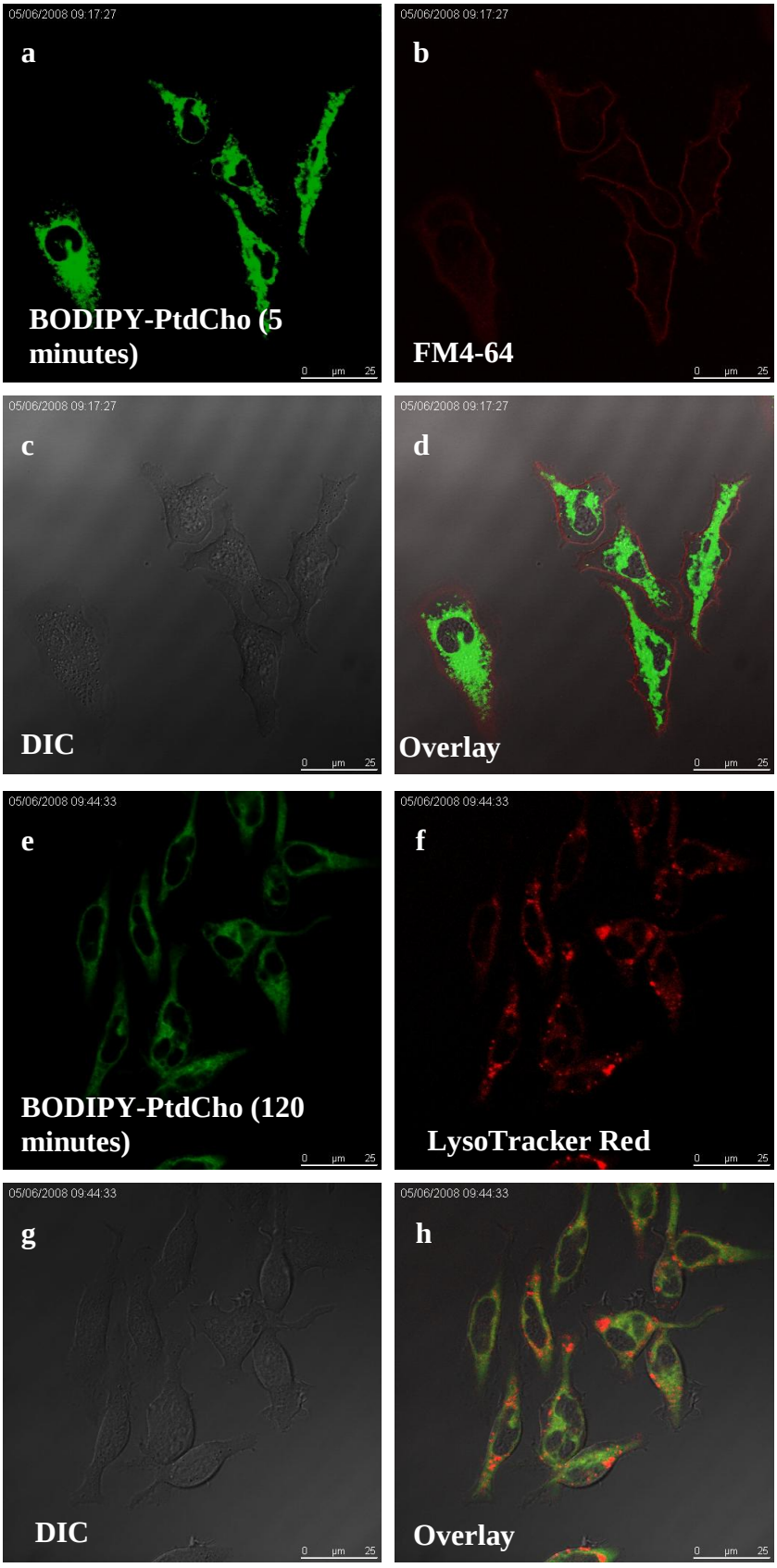
05/06/2008 09:17:27
a
BODIPY-PtdCho (5 minutes)
0 µm 25
05/06/2008 09:17:27
b
FM4-64
0 µm 25
05/06/2008 09:17:27
c
DIC
0 µm 25
05/06/2008 09:17:27
d
Overlay
0 µm 25
05/06/2008 09:44:33
e
BODIPY-PtdCho (120 minutes)
0 µm 25
05/06/2008 09:44:33
f
LysoTracker Red
0 µm 25
05/06/2008 09:44:33
g
DIC
0 µm 25
05/06/2008 09:44:33
h
Overlay
0 µm 25

Figure 3.12: Localisation of BODIPY-PtdCho with FM4-64 in HEK-293 cells. HEK-293 cells were grown on glass bottomed fluorodishes coated in Poly-D-Lysine and labelled with the 1 µg/ml BODIPY-PtdCho in HBSS + 20 mM HEPES at 37°C/5% CO_2 for 120 minutes (panel **a**). Cells were also stained with 2.5 µM FM4-64 (panel **b**) prior to live confocal imaging (at 37°C). BODIPY-PtdCho and FM4-64 were both excited by the argon laser at 488 nm with emission bandwidths between 500 nm-608 nm (green) and between 665 nm-794 nm (red – see panels **a-d**). A scale calibrated to 25 µm is shown in each panel. HEK-293 exhibited diffuse staining using BODIPY-PtdCho in 3 experiments.

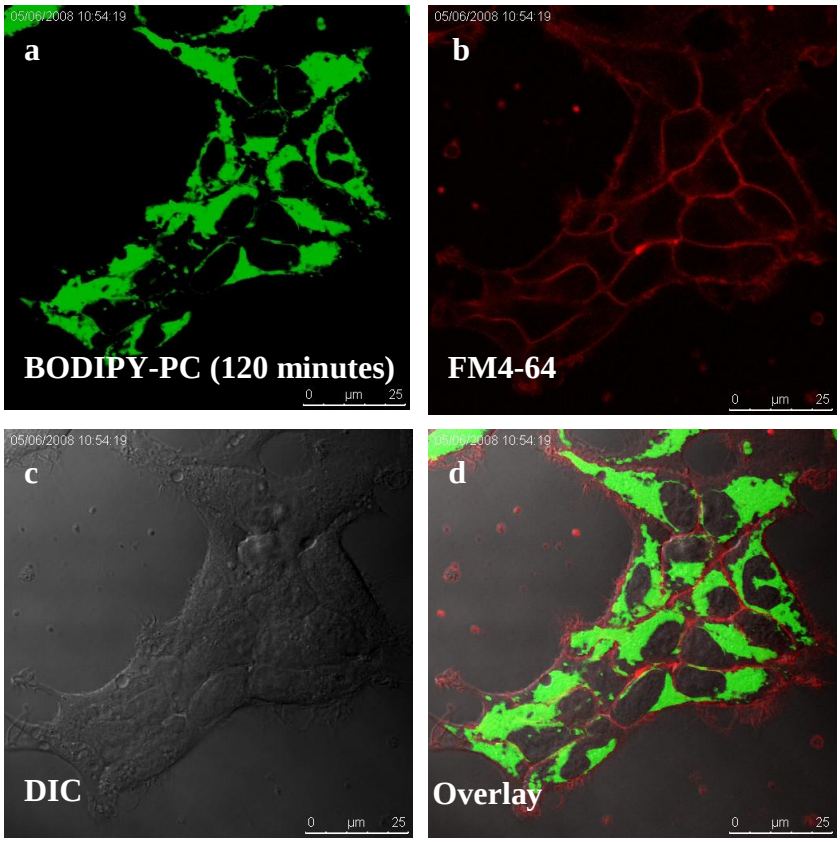

3.2.8: Characterisation of a fluorescent PLD substrate and other molecular markers in the HEK-293 cell line

Although one of the project aims was to create a live *in vivo* PLD assays, RBL-2H3 cells proved difficult to transfect. The HEK-293 epithelial cell line was used as an alternative system as the cells are more easily transfected. The novel fluorescent lipid localised in punctate structures within the cytoplasm but the localisation of the lipid and its fluorescence yield was variable in HEK cells (see Fig. 3.13, panels a, e). In HEK cells, the fluorescent lipid did not localise with the membrane marker FM4-64 (see Fig. 3.13, panels b, d) or with the nuclear marker Hoechst (see Fig. 3.13, panels f, h). LysoTracker Red localised in punctiform structures within the cell and was excluded from the nucleus (data not shown) and largely did not co-localise with fPtdCho (see Fig. 3.14, panels a-d). Whilst the localisation of LysoTracker Red and the novel fluorescent lipid were similar, upon transfection fPtdCho labelling of HEK cells was no longer punctate. Transfection of RBL-2H3 cells was not reproducible and was often accompanied by a high degree of cell death. Whilst HEK-293 cells were readily transfectable, lipid organisation was not as well structured as that of RBL-2H3 cells.

Figure 3.13: Localisation of the novel fluorescent lipid and other molecular markers in the HEK-293 cell line. HEK-293 cells were grown on glass bottomed fluorodishes coated in Poly-D-Lysine and labelled with 1 µg/ml of the novel fPtdCho (in HBSS + 20 mM HEPES) for 120 minutes (panels **a**, **e**). Cells were then stained with 2.5 µM FM4-64 (panel **b**) and imaged immediately. Cells were also labelled with lipid and then with 2.0 µg/ml Hoechst 33342 for 15 minutes at 37^{o}C/5% CO_2 (panel **f**). HEK-293 cells were washed twice with HBSS and data was recorded using live sequential confocal microscopy. Both the novel fluorescent lipid and FM4-64 were excited by the argon laser at 488 nm with emission bandwidths between 491 nm-552 nm (green) and between 583 nm-747 nm (red). Hoechst was excited using the 405 Diode UV laser with an emission bandwidth between 430 nm-480 nm. A scale calibrated to 25 µm is shown in each panel. The data presented are representative images for 1 experiment of at least 2.

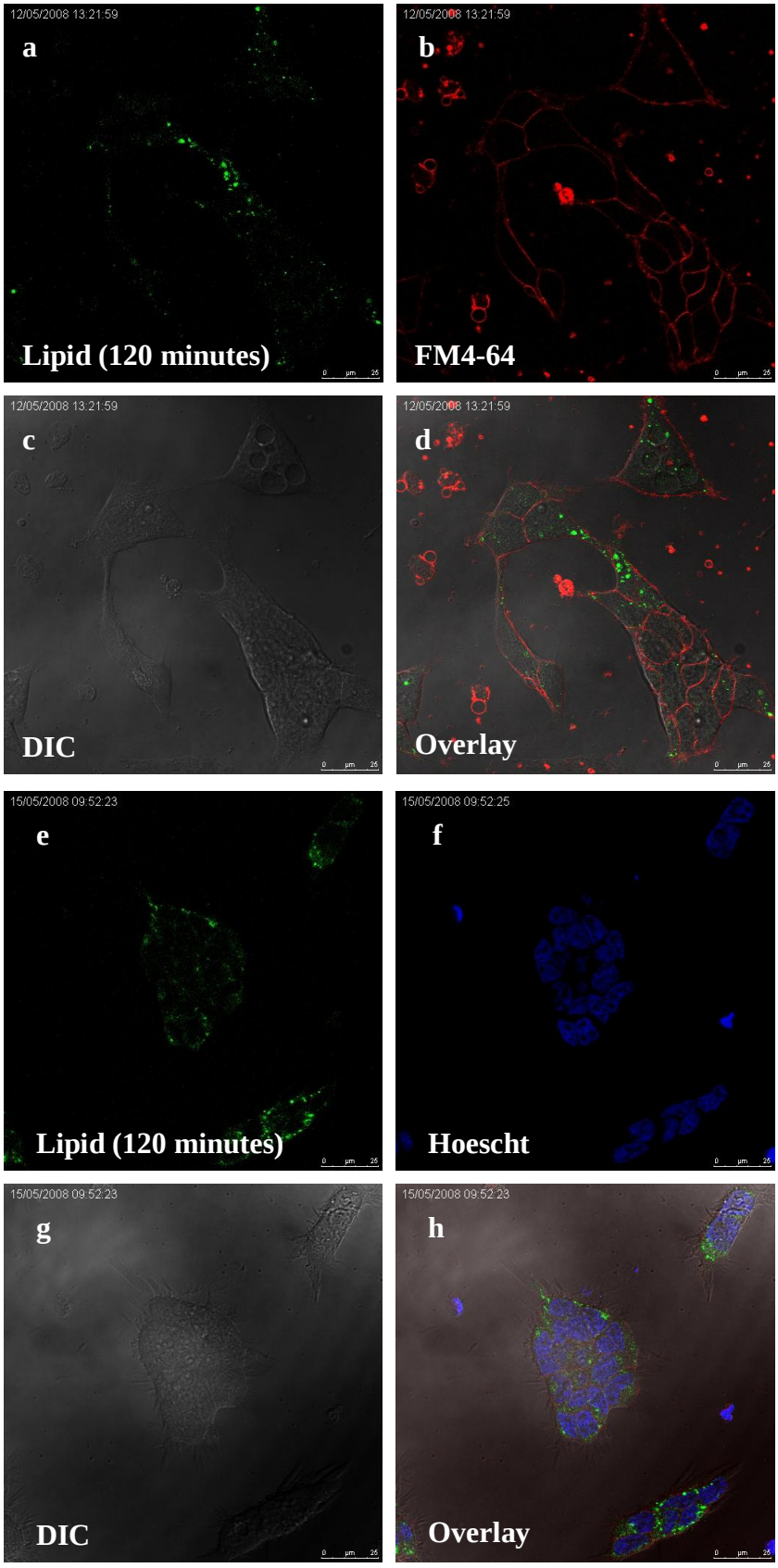
12/05/2008 13:21:59
a
Lipid (120 minutes)
12/05/2008 13:21:59
b
FM4-64
12/05/2008 13:21:59
c
DIC
12/05/2008 13:21:59
d
Overlay
15/05/2008 09:52:23
e
Lipid (120 minutes)
15/05/2008 09:52:25
f
Hoescht
15/05/2008 09:52:23
g
DIC
15/05/2008 09:52:23
h
Overlay

Figure 3.14: Localisation of LysoTracker Red and fPtdCho in the HEK-293 cell line. HEK-293 cells were grown on glass bottomed fluorodishes coated in Poly-D-Lysine prior to labelling. HEK-293 cells were labelled with 1.0 µg/ml of fPtdCho (in HBSS + 20 mM HEPES) for 120 minutes (panel **b**) at 37^{o}C/5% CO_2 and then with 100 nM LysoTracker Red for 1 minute (see panel **a**). HEK-293 cells were washed twice with HBSS and data recorded using live sequential confocal microscopy. LysoTracker Red was excited using the HeNe 594 laser at 594 nm with an emission bandwidth between 658 nm-794 nm. The novel fluorescent lipid was excited by the argon laser at 488 nm with emission bandwidths between 495 nm-552 nm. A scale calibrated to 25 µm is shown in each panel. The data presented are representative images for 1 experiment of at least 2.

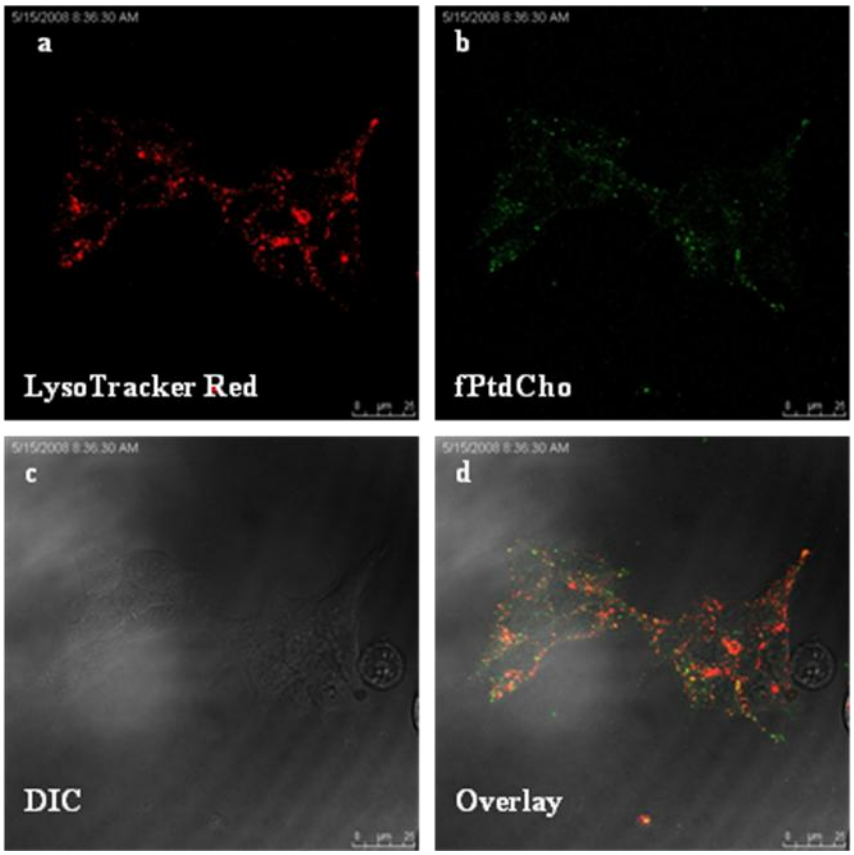

3.3: Stimulation of fluorescently labelled RBL-2H3 cells

3.3.1: Using a secretory lysosomal marker to measure the effectiveness of RBL-2H3 stimulators

The degranulation of RBL-2H3 cells in response to PMA, IgE-antigen and A23187 was quantified using β-hexosaminidase assays (Howl *et al*., 2003). Release of total β-hexosaminidase from RBL-2H3 cells treated with Triton X-100 (0.1%) was scored as 100% and secretion from other treatments was calculated as a percentage of the total (see Fig.3.15). Cells treated with 0.1 μM A23187 released approximately 50% of total β-hexosaminidase with higher concentrations of A23187 – (1 μM and 10 μM) – resulting in approximately 25% and 40% β-hexosaminidase release, respectively. The most potent A23187 concentration was also used in live confocal microscopy experiments (see Section 3.3.4). RBL-2H3 cells stimulated using IgE-antigen secreted approximately 40% of total β-hexosaminidase. Whilst PMA appeared to be an effective mast cell stimulator using confocal microscopy (see Section 3.3.2), the β-hexosaminidase results were not as convincing. β-hexosaminidase secretion of PMA-stimulated RBL-2H3 cells was approximately 15% compared with 12% secretion from control unstimulated cells (the percentage of β-hexosaminidase secreted by control cells is likely due to cell breakage). PMA has an undeniable stimulatory effect on RBL-2H3 cells morphologically as seen by membrane ruffling, blebbing and cell process retraction. However, cells stimulated in this way do not secrete substantial quantities of the lysosome marker β-hexosaminidase.

Figure 3.15: Measuring secretion of RBL-2H3 cells using PMA, A23187 and IgE-antigen using the secretory lysosomal marker β-hexosaminidase. RBL-2H3 cells were grown in 12-well plates to approximately 80-90% confluencey 24 hours prior to the β-hexosaminidase assay. Antigenically stimulated cells were primed overnight using 1 µg/ml anti-DNP IgE (in complete DMEM). Primed RBL-2H3 cells were stimulated using 0.1 µg/ml DNP-BSA for 60 minutes. Cells were stimulated using 0.1 µM A23187, 1 µM A23187, 10 µM A23187, or 100 nM PMA for 60 minutes in 250 µl HBSS + 20 mM HEPES + 1 mM Ca^{2+} at 37°C/5% CO_2. 0.1% Triton X-100 was used to treat cells for 5 minutes before scraping. All treated cells were scraped and centrifuged at 13,000 RPM for 5 minutes. 20 µl of the supernatant combined with 20 µl 1 mM p-nitrophenol-N-acetylglucosamide (in 0.1 M sodium citrate, pH 4.5) in a 96-well plate was incubated at 37°C/5% CO_2 for a further 60 minutes. The reaction was terminated using 200 µl 0.1M sodium carbonate and sodium hydrogen carbonate, pH 10.5. Results were measured continuously using the 405 nm filter on a plate reader. Results recorded were calculated as a percentage of the values recorded for Triton X-100 treated cells. All assays were read in triplicate and repeated at least 4 times. The data presented are the means of these experiments.

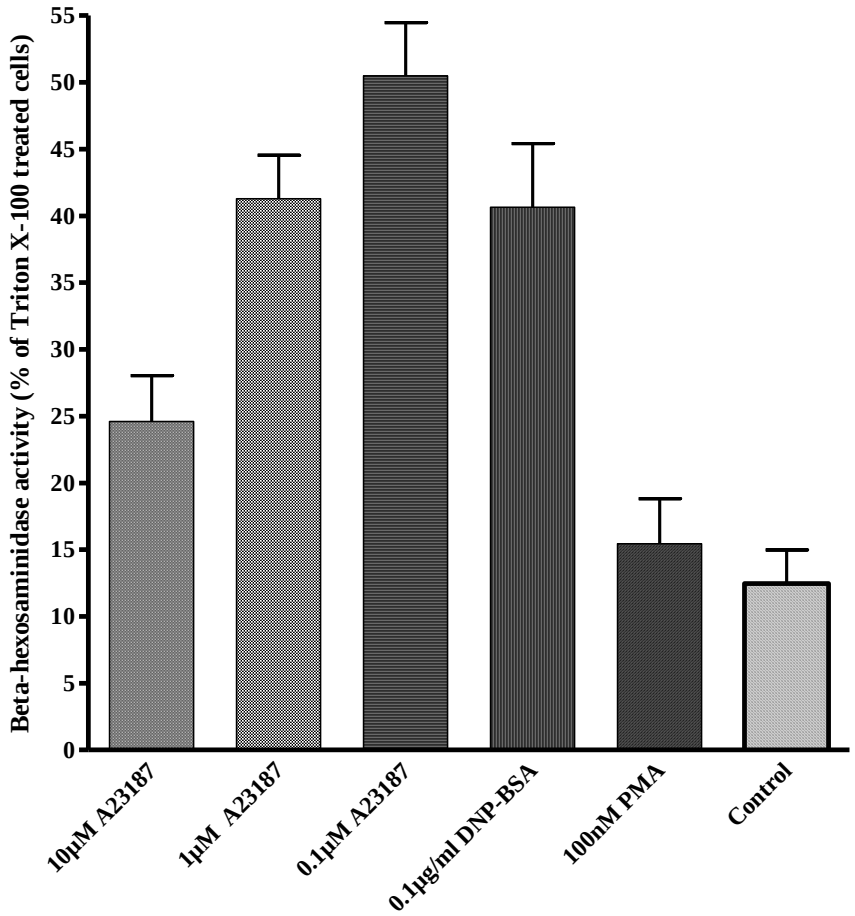

3.3.2: The effect of PMA stimulation on RBL-2H3 cells labelled with novel fluorescent PtdCho or LysoTracker Red

RBL-2H3 cells were labelled with the 0.5 µg of the novel fluorescent lipid for 1 hour and then stimulated using 100 nM PMA. PMA stimulates PKCα activity which in turn stimulates PLD1b and also results in degranulation. PKCα is a known PLD1 activator and the diacylglycerol (DAG) mimetic PMA is used to activate Ca^{2+}-dependent PKCα activation of PLD1 (Takai *et al*., 1979; Castagna *et al*., 1982). Mast cell morphology changes dramatically upon stimulation with PMA as the membrane ruffles and blebs, and the cell processes retract (see Fig. 3.16a for images). Upon PMA stimulation, the cell morphology changes but the novel fluorescent lipid maintains its motility (see Fig. 3.16b for recording). Labelled RBL-2H3 cells were imaged at 37^{o}C using live real-time confocal microscopy. The recording was over 30 minutes (1 frame/20 seconds) and has been condensed to 18 seconds (see Fig. 3.16b for condensed recording), although usually recordings were over 15 minutes. Cells were stimulated 60 seconds after the recording commenced and the cells responded immediately to PMA stimulation.

Real-time recordings of both control and PMA-stimulated RBL-2H3 cells were analysed using the LAS-AF Lite software. Each cell was identified as a discrete 'region' and the fluorescence and DIC data exported. A highly fluorescent area within an individual cell was identified as a 'region of interest' and fluorescence and DIC data from this region were analysed. Mean fluorescence intensity (of either the whole cell or the region of interest) was divided by the DIC and plotted against time. Data were interpreted in this way to account for the movement of the cells between focal planes during the real-time recording. Both non-stimulated control cells (see Fig. 3.17) and PMA-stimulated cells (see Fig. 3.18) appeared to display regular oscillations in fluorescence.

The amount of fPtdCho present in RBL-2H3 cells varied and so the magnitude of oscillations could not be compared between experiments. However, the oscillations were comparable and had a period of approximately 300 seconds. The fluorescence intensity/DIC magnitude of the whole cell compared to the region of interest appears to be closer in control cells (see Fig. 3.17), rather than PMA-stimulated cells (see Fig.

3.18). In addition, small reductions in fluorescence/DIC occur approximately every 100 seconds in PMA-stimulated cells, not seen in controls (see Fig. 3.18). Although it is unclear what these fluorescence oscillations relate to their period appears consistant and may relate to the binding of proteins or other lipids to fPtdCho.

Figure 3.16a: The effect of PMA stimulation on RBL-2H3 cells labelled with novel fluorescent PtdCho. RBL-2H3 cells grown on glass bottomed fluorodishes (for 24 hours) were labelled using 0.5 µg/ml of fPtdCho for 60 minutes prior to real-time confocal imaging. Cells were stimulated using 100 nM PMA approximately 40 seconds after real-time recording commenced. Recording was completed over 30 minutes (1 frame/20 seconds) using the argon laser with an excitation at 488 nm and an emission band width between 500 nm-608 nm. The 488 nm laser power was halved and each time point was scanned twice (and averaged) to reduce photo-bleaching. A scale calibrated to 25 µm is shown in each panel. The data presented are representative images for 1 experiment of 4. Still images are represented below whilst the recording is shown in Fig. 3.16**b**.

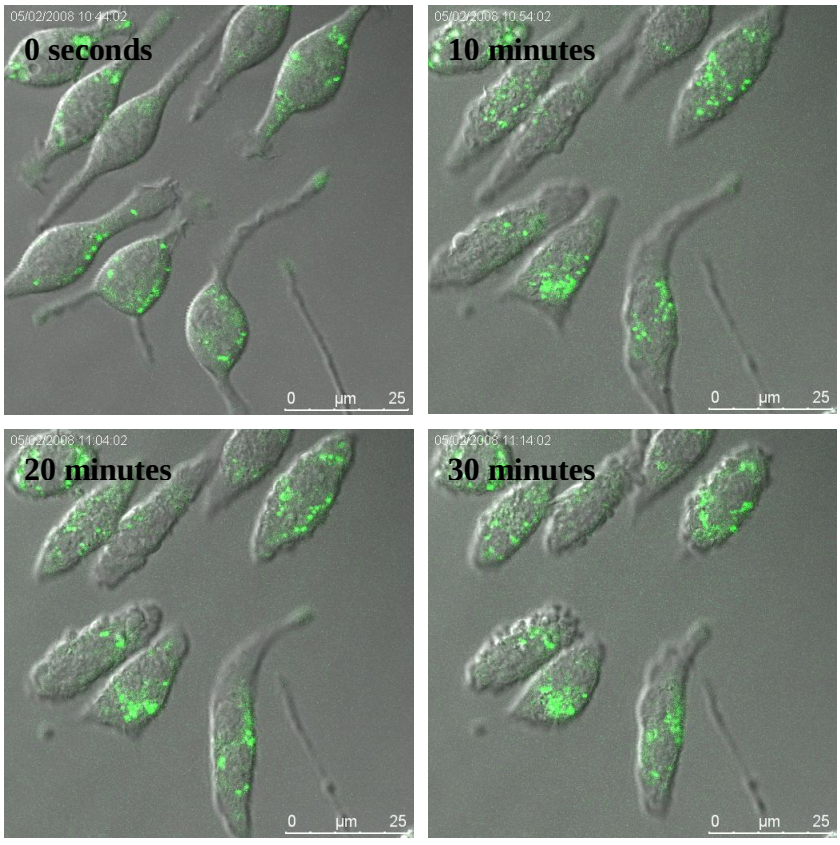

Figure 3.15: Analysis of fluorescence lipid oscillations during real-time recording of resting RBL-2H3 cells. RBL-2H3 cells grown on glass bottomed fluorodishes for 24 hours were labelled using 1 µg/ml of fPtdCho for 90 minutes prior to real-time confocal imaging. Cells were washed with filter sterilised PBS + 25 mM HEPES, pH 7.4 and imaged immediately. Real-time recording was completed over 15 minutes (1 frame/10 seconds) using the argon laser with an excitation at 488 nm and an emission band width between 500 nm-608 nm. The 488 nm laser power was halved and each time point was scanned twice (and averaged) to reduce photo-bleaching. Each cell was identified as a discrete 'region' using the LAS-AF Lite software and mean fluorescence intensity and DIC were exported using the stack profile setting. Within the whole cell the most fluorescence region was identified as a 'region of interest' and fluorescence intensity and DIC data were exported also using the stack profile setting. The mean fluorescence intensity was divided by DIC for the whole cell (■) and the region of interest (▲), and plotted against time (seconds). The data presented here is representative of 1 cell. The experiment was repeated 4 times and 24 cells were analysed in total.

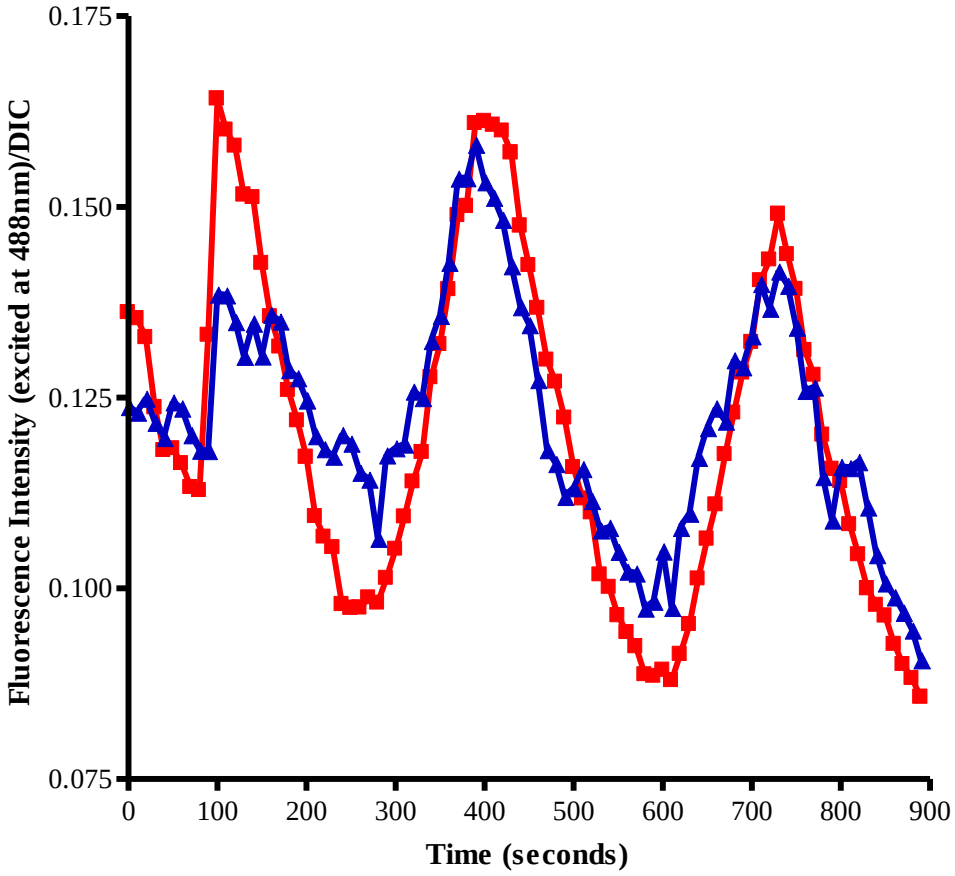

Figure 3.16: Analysis of fluorescence lipid oscillations during real-time recording of PMA stimulated RBL-2H3 cells. RBL-2H3 cells grown on glass bottomed fluorodishes for 24 hours were labelled using 0.5 µg/ml fPtdCho for 60 minutes prior to real-time confocal imaging. Cells were stimulated using 100 nM PMA approximately 40 seconds after real-time recording commenced. Real-time recording was completed over 30 minutes (1 frame/20 seconds) using the argon laser with an excitation at 488 nm and an emission band width between 500 nm-608 nm. The 488 nm laser power was halved and each time point was scanned twice (and averaged) to reduce photo-bleaching. Analyses of the first 900 seconds (15 minutes) of 1 cell are shown below. Each cell was identified as a discrete 'region' using the LAS-AF Lite software and mean fluorescence intensity and DIC were exported using the stack profile setting. Within the whole cell the most fluorescence region was identified as a 'region of interest' and both fluorescence intensity and DIC data were exported. The mean fluorescence intensity was divided by DIC for the whole cell (■) and the region of interest (▲), and plotted against time (seconds). The data is representative of 1 cell. The experiment was repeated 4 times and 39 cells were analysed in total.

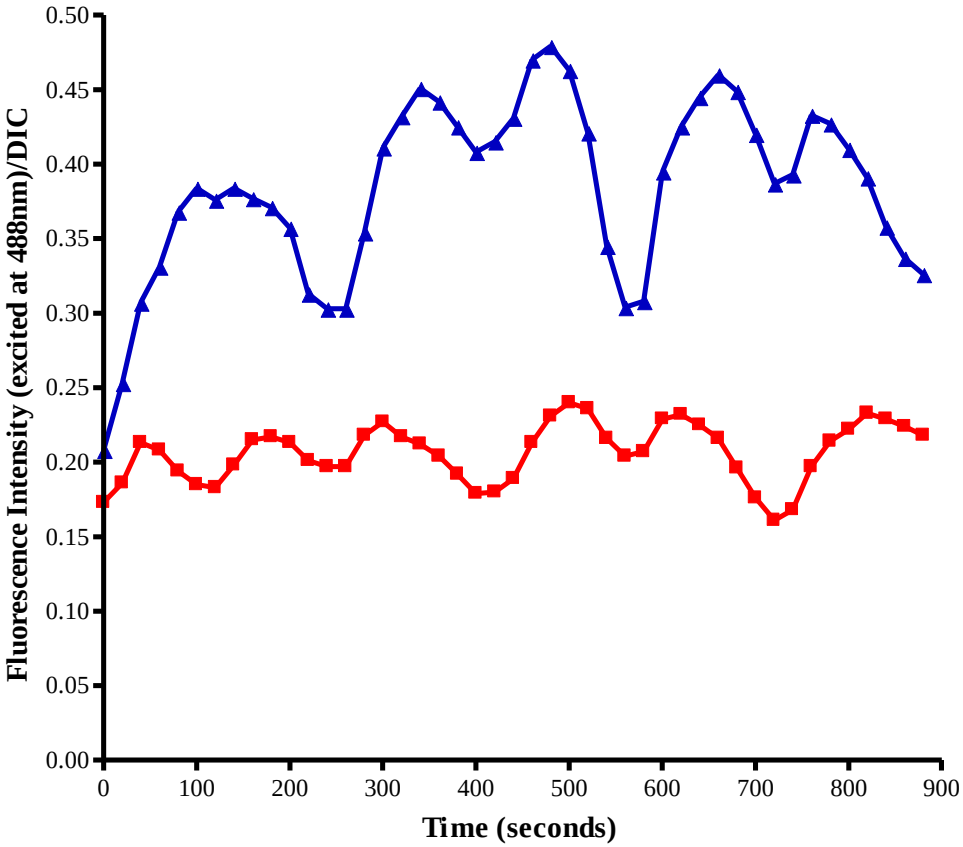

RBL-2H3 cells were labelled with 100 nM LysoTracker Red for 1 minute and stimulated using 100 nM PMA. Although PMA stimulated degranulation and altered cell morphology, LysoTracker Red labelling did not change (see Fig. 3.19a). LysoTracker Red localised to RBL-2H3 lysosomes with punctate staining localised to both cell body and processes. LysoTracker Red is an acidotropic molecular marker targeting acidic compartments such as the secretory lysosomes in RBL-2H3 cells (Kaur and Cutler, 2002; Satio *et al*., 2004). Similar to RBL-2H3 cells labelled with fPtdCho, LysoTracker Red maintained punctate localisation even after PMA-induced degranulation. RBL-2H3 cells labelled with LysoTracker Red responding to PMA (at 37^{o}C) was recorded over 15 minutes (1frame/10 seconds) and condensed to 18 seconds (see Fig. 3.19b for condensed recording) where PMA was added after approximately 100 seconds. LysoTracker also maintained its motility during mast cell degranulation. LysoTracker Red labelled RBL-2H3 cells were also treated with a calcium ionophore (A23187) and IgE/antigen to stimulate degranulation and serve as degranulation controls.

Figure 3.19a: The effect of PMA stimulation on RBL-2H3 cells labelled with LysoTracker Red. RBL-2H3 cells grown on glass bottomed fluorodishes for 24 hours were labelled using 100 nM LysoTracker Red for 1 minute (and washed twice with HBSS + 20 mM HEPES) prior to real-time confocal imaging. Cells were stimulated using 100 nM PMA approximately 100 seconds after recording commenced. Real-time recording was completed over 15 minutes (1 frame/10 seconds) using the HeNe 594 laser with an excitation at 594 nm and an emission band width between 668 nm-794 nm. The 594 nm laser power was halved and each time point was scanned twice (and averaged) to reduce photo-bleaching. A scale calibrated to 25 µm is shown in each panel. The data presented are representative images for 1 experiment of 3. Still images are represented below whilst the recording is shown in Fig. 3.19**b**.

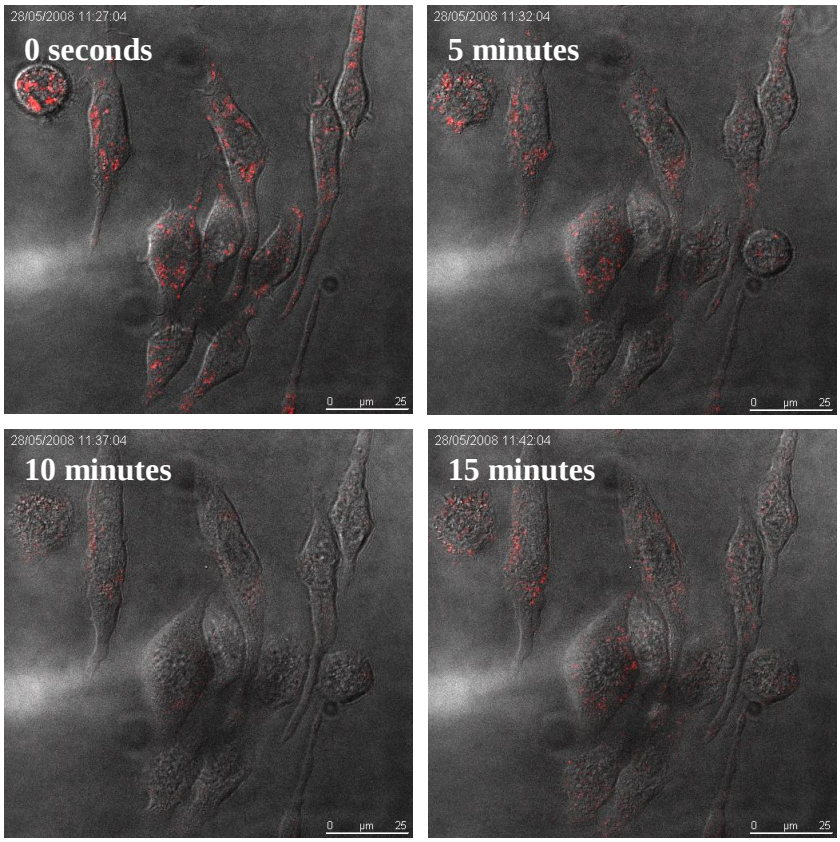

3.3.3: The effect of IgE/antigen stimulation on RBL-2H3 cells labelled with novel fluorescent PtdCho or LysoTracker Red

RBL-2H3 cells were treated with antigen in the context of IgE to simulate the environmental stimuli which promote degranulation *in vivo*. RBL-2H3 cells were sensitised with 1 µg/ml anti-DNP IgE overnight (in complete DMEM), labelled with 0.5 µg/ml lipid (for up to 120 minutes) and stimulated with DNP-BSA either for 2 minutes prior to imaging (Farquhar *et al*., 2007), or stimulated during the real-time recording. Cells stimulated prior to imaging were already responding to the stimulation when recording began and showed ruffling of the membranes (see Fig. 3.20a for images). The effect of IgE stimulation in the context of antigen was recorded over 15 minutes (1 frame/10 seconds, condensed to 18 seconds – see Fig. 3.20b for recording). The power of the 488 nm laser was halved and each frame accumulated twice and averaged to reduce photo-bleaching. The novel fluorescent lipid maintained its punctiform localisation and was not released during degranulation induced (see Fig. 3.20a for images).

RBL-2H3 cells, labelled with the novel fluorescent lipid, were stimulated with 0.1 µg/ml DNP-BSA 3 times every 5 minutes during a real-time recording. This protocol did not impact upon the localisation or retention of the fPtdCho. Similarly, RBL-2H3 cells labelled with the novel fluorescent lipid and stimulated using 0.5 µg/ml DNP-BSA still maintained the lipid in punctate vesicles.

Figure 3.20a: The effect of IgE/antigen stimulation on RBL-2H3 cells labelled with novel fluorescent PtdCho. RBL-2H3 cells grown on glass bottomed fluorodishes for ~8 hours were primed with 1 µg/ml anti-DNP IgE overnight (in complete DMEM). Cells were labelled with 1 µg/ml fPtdCho (120 minutes) and stimulated with 0.1 µg/ml DNP-BSA for 2 minutes (and washed twice with HBSS) prior to confocal imaging. Real-time recording was completed over 15 minutes (1 frame/10 seconds) using the argon laser with an excitation at 488 nm and an emission bandwidth between 500 nm-608 nm. The 488 nm laser power was halved and each time point scanned twice (and averaged) to reduce photo-bleaching. A scale calibrated to 25 µm is shown in each panel. The data presented are representative images for 1 experiment of 2. Still images of are represented below whilst recording is shown in Fig. 3.20**b**.

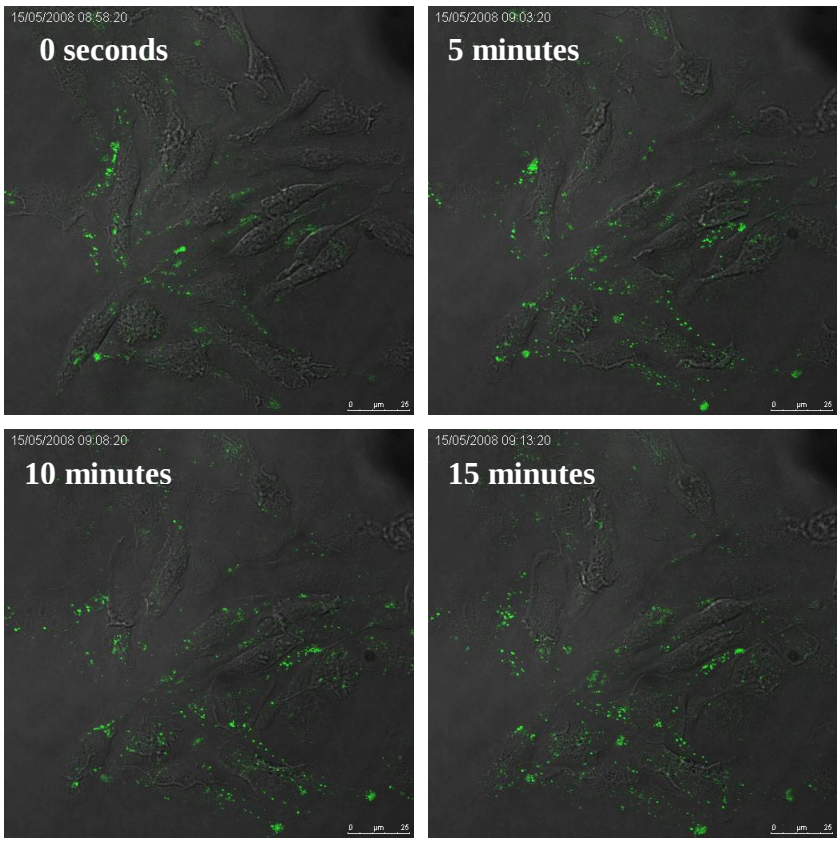

Real-time recordings of IgE/antigen stimulated RBL-2H3 cells labelled with the novel fPtdCho were analysed using the LAS-AF Lite software. The analysis was the same as that used on PMA-stimulated cells (see Section 3.3.2). Data is represented as mean fluorescence intensity divided by DIC versus time (over 900 seconds). Antigenic stimulation produces oscillations in fluorescence approximately every 200-300 seconds (see Fig. 3.21). DNP-BSA was added in frame 5 (after 50 seconds) from the start of the recording. These oscillations are consistent with those noted previously in control and PMA stimulated RBL-2H3 cells (see Fig. 3.17 and Fig. 3.18).

'Dips' in fluorescence between oscillating peaks were detected in PMA-stimulated cells (see Fig. 3.18) and are also evident in degranulation induced by antigenic stimulation (see Fig. 3.21). This may suggest that the oscillations occur in response to PLD-dependent mast cell degranulation. Antigenic stimulation of RBL-2H3 was repeated in 4 separate experiments and, although oscillations were present in 31 of 37 cells analysed, the oscillatory pattern was not as consistent as in PMA-stimulated cells. The variability in results could be attributed to the degree of movement associated using different types of stimulation (or the response of individual cells) during real-time recordings.

RBL-2H3 cells were sensitised with 1 µg/ml anti-DNP IgE overnight (in complete DMEM) and labelled with 100 nM LysoTracker Red. RBL-2H3 cells were stimulated during the real-time recordings with 0.1 µg/ml DNP-BSA in a final volume of 1 ml HBSS + Ca^{2+}. The effect of IgE stimulation in the context of antigen was recorded over 15 minutes (1 frame/10 seconds) and condensed to 18 seconds (see Fig. 3.22b for recording). The power of the 594 nm laser was halved and each image was an accumulation of 2 frames and averaged to reduce photo-bleaching. Although these precautions were taken, LysoTracker Red fluorescence appeared to reduce in response to antigenic stimulation (see Fig. 3.22a for snapshots). Although the fluorescence yield was reduced, the lysosomal marker maintained its intracellular punctiform localisation upon degranulation (Fig. 3.22a for snapshots).

Analysis of the real-time recording using the LAS-AF Lite software indicated that there were fluorescence oscillations of LysoTracker Red in RBL-2H3 cells

responding to antigenic stimulation. Although these oscillations were identified, they were not as consistent as control or PMA stimulated cells labelled with LysoTracker Red (data not shown).

Figure 3.21: Analysis of fluorescence lipid oscillations during real-time recording of RBL-2H3 cells stimulated with IgE (in the context of antigen). RBL-2H3 cells grown on glass bottomed fluorodishes for 8 hours were primed with 1 µg/ml anti-DNP IgE overnight (in complete DMEM). Cells were stimulated with 0.1 µg/ml DNP-BSA for either for 2 minutes (using HBSS – n=2) or during the real-time recording (using HBSS + Ca^{2+} – n=2). Real-time recording was completed over 15 minutes (1 frame/10 seconds) using the argon laser with an excitation at 488 nm and an emission band width between 500 nm-608 nm. The 488 nm laser power was halved and each time point was scanned twice (and averaged) to reduce photo-bleaching. Each cell was identified as a discrete 'region' using the LAS-AF Lite software and mean fluorescence intensity and DIC were exported using the stack profile setting. Within the whole cell the most fluorescence region was identified as a 'region of interest' and both fluorescence intensity and DIC data also were exported. The mean fluorescence intensity was divided by DIC for the whole cell (■) and the region of interest (▲), and was plotted against time (seconds). The data presented is representative of 1 cell stimulated (in HBSS + 1 mM Ca^{2+}) from 1 experiment. The experiment was repeated 4 times and 37 cells were analysed of which 31 showed fluorescence oscillations.

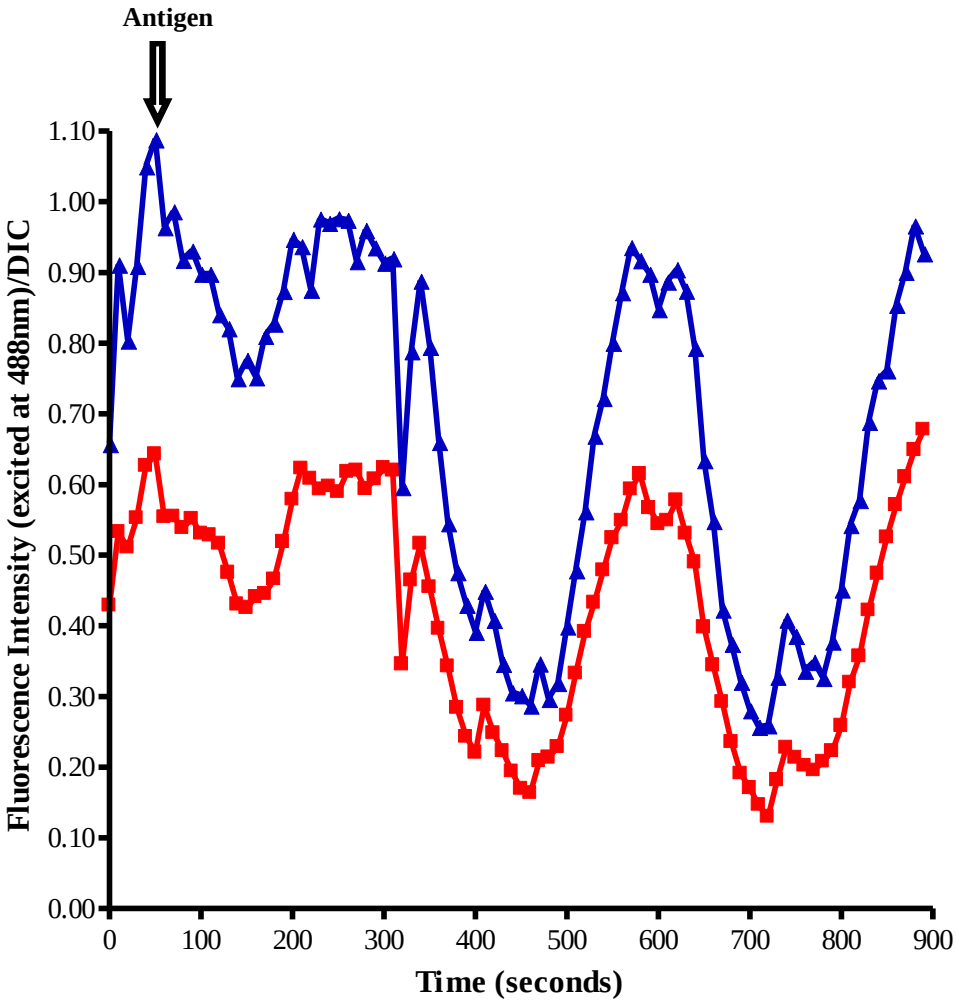

Figure 3.22a: The effect of IgE/antigen stimulation on RBL-2H3 cells labelled with LysoTracker Red. RBL-2H3 cells grown on glass bottomed fluorodishes for ~8 hours were primed with 1 µg/ml anti-DNP IgE overnight (in complete DMEM). Cells were labelled with 100 nM LysoTracker Red for 1 minute and washed twice using HBSS + 1 mM Ca^{2+}. Real-time recording was completed over 15 minutes (1 frame/10 seconds) using the HeNe 594 laser with an excitation at 594 nm and an emission bandwidth between 668 nm-794 nm. The 594 nm laser power was halved and each time point was scanned twice (and averaged) to reduce photo-bleaching. 0.1 µg/ml DNP-BSA was added to the cells approximately 50 seconds (frame 5) after the start of the recording. A scale calibrated to 25 µm is shown in each panel. The data presented are representative images for 1 experiment of 4. Still images are represented below whilst the recording is shown in Fig. 3.22**b**.

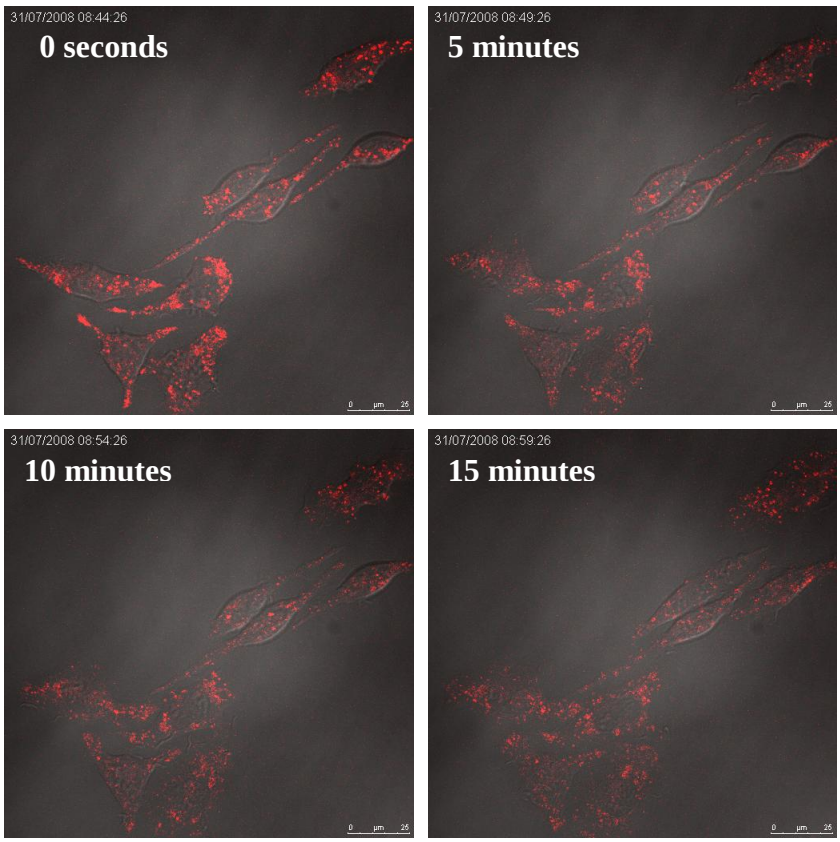

3.3.4: Stimulation of RBL-2H3 cells labelled with LysoTracker Red or the novel fluorescent PtdCho using a calcium ionophore (A23187)

The calcium ionophore A23187 increases intracellular calcium and results in mast cell degranulation. A23187-stimulation of RBL-2H3 cells results in membrane blebbing and ruffling, with cell processes typically extended from either side of the cell body either severed or broadened and then retracted (see Fig. 3.23 and 3.24). RBL-2H3 cells were labelled with 100 nM of the lysosomal marker LysoTracker Red and stimulated with 0.1 µM of the calcium ionophore A23187 (see Fig. 3.23a for images). Real-time imaging of LysoTracker Red labelled cells stimulated with A23187 was recorded over 15 minutes (1 frame/10 seconds) and condensed to 18 seconds (see Fig. 3.23b for recording). A23187 was added to the cells after approximately 50 seconds. LysoTracker Red localised to the expected punctiform structures within the cell body and processes, but the marker disappeared upon A23187 stimulation (see Fig. 3.23a for images). LysoTracker Red was not retained in RBL-2H3 cells 2 to 3 minutes after A23187 stimulation. As LysoTracker Red is an acidotropic molecular marker, perhaps A23187 altered the vesicular pH and LysoTracker Red no longer labelled them. Alternatively, A23187 altered the vesicle membrane, causing release of vesicular contents.

RBL-2H3 cells labelled with 1 µg/ml novel fluorescent lipid (for 180 minutes) in HBSS + 20 mM HEPES + 1 mM Ca^{2+} and real-time imaging of A23187-stimulation of mast cells was recorded over 15 minutes (1 frame/10 seconds condensed to 18 seconds – see Fig. 3.24b for recording). 0.1 µM A23187 was added to the RBL-2H3 cells after approximately 50 seconds (frame 5). The novel fluorescent lipid maintained its characteristic punctiform localisation and was unaffected by A23187 treatment (see Fig. 3.24a for snapshots).

Figure 3.23a: The effect of A23187 stimulation on RBL-2H3 cells labelled with LysoTracker Red. RBL-2H3 cells grown on glass bottomed fluorodishes for 24 hours were labelled with 100 nM LysoTracker Red for 1 minute (and washed twice using HBSS + 20 mM HEPES + 1 mM Ca^{2+}) prior to imaging. Real-time confocal recording was completed over 15 minutes (1 frame/10 seconds) using the HeNe 594 laser with an excitation at 594 nm and an emission bandwidth between 668 nm-794 nm. The 594 nm laser power was halved and each time point was scanned twice (and averaged) to reduce photo-bleaching. 0.1 µM A23187 (in DMSO) was added to the cells approximately 50 seconds (frame 5) after the start of the real-time recording. A scale calibrated to 25 µm is shown in each panel. The data presented are representative images for 1 experiment of 3. Still images are represented below whilst the full length film has been condensed to 18 seconds and is shown in Fig. 3.23**b**.

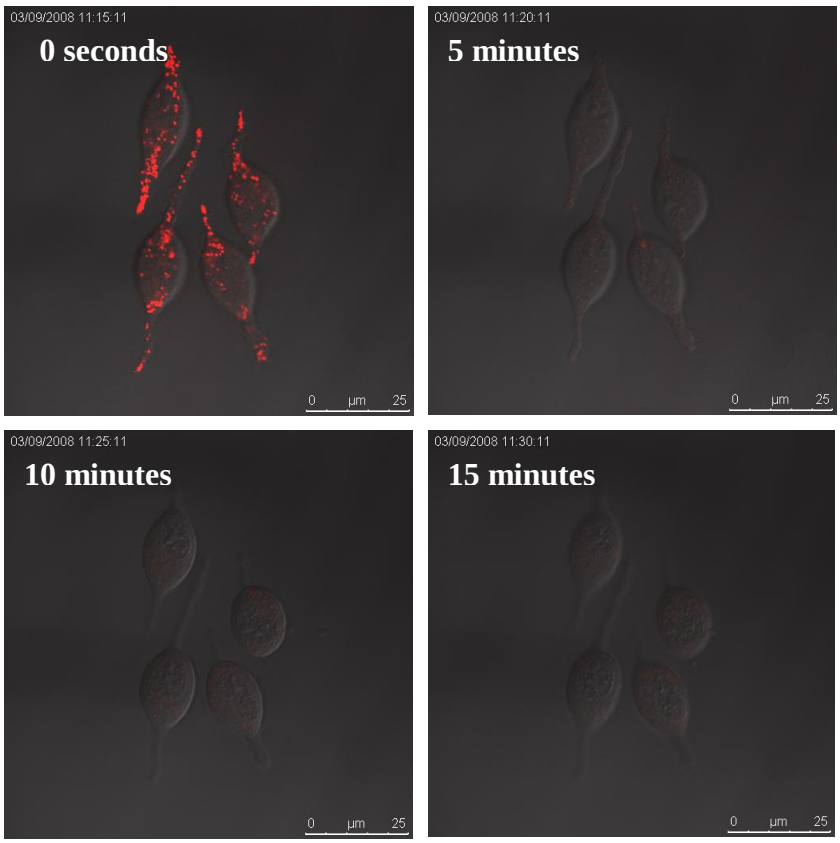

Figure 3.24a: The effect of A23187 stimulation on RBL-2H3 cells labelled with novel fluorescent PtdCho. RBL-2H3 cells grown on glass bottomed fluorodishes for 24 hours were labelled with used 1 µg/ml of the novel lipid for 180 minutes (in HBSS + 20 mM HEPES + 1 mM Ca^{2+}) prior to imaging. Real-time recording was completed over 15 minutes (1 frame/10 seconds) using the argon laser with an excitation at 488 nm and an emission bandwidth between 500 nm-608 nm. The 488 nm laser power was halved and each time point was scanned twice (and averaged) to reduce photo-bleaching. 0.1 µM A23187 (in DMSO) was added to the RBL-2H3 cells during the real-time recording after approximately 50 seconds (frame 5). A scale calibrated to 25 µm is shown in each panel. The data presented are representative images for 1 experiment of 4. Still images are represented below whilst the full length film has been condensed to 18 seconds and is shown in Fig. 3.24**b**.

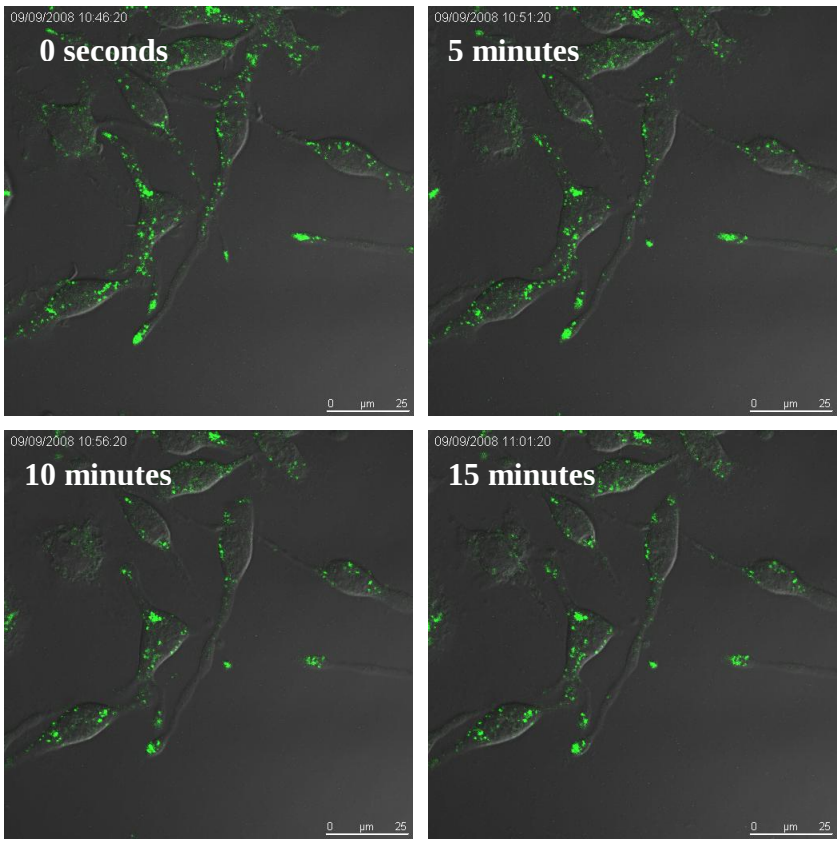

3.4: Identifying the localisation of the novel PtdCho in RBL-2H3 cells in response to a range of inhibitors

3.4.1: The effect of wortmannin on RBL-2H3 cells labelled with novel fluorescent PtdCho or LysoTracker Red

Wortmannin is a fungal metabolite and functions largely as a selective phosphatidylinositol 3-kinase (PtdIns 3-kinase) inhibitor, but also inhibits PLD, PLA_2 and PLC (Cross *et al*., 1995; Nakamura *et al*., 1997). Wortmannin was treated as an indirect PLD inhibitor here and treatment of RBL-2H3 cells with this fungal metabolite could identify if fPtdCho-labelling was PLD-dependent. RBL-2H3 cells treated with 100 nM wortmannin caused broadening of the cell processes and membrane ruffling. RBL-2H3 cells first treated with 100 nM wortmannin for 30 minutes and then labelled with 100 nM LysoTracker Red were unaffected by the wortmannin pre-treatment (n=4 – see Fig. 3.25, panels a-c). Although wortmannin treatment resulted in morphological changes, LysoTracker Red maintained its punctiform localisation.

RBL-2H3 cells were also treated with 100 nM wortmannin for 2 hours and then labelled with 0.5 µg/ml of the novel fPtdCho (in HBSS + 20 mM HEPES). Wortmannin pre-treatment of the cells did not affect the labelling or punctiform localisation of the novel fluorescent lipid (n=2 –see Fig. 3.25, panels d-f). Treatment of RBL-2H3 cells with 100 nM, 500 nM or 1 µM wortmannin did not impact on the punctiform localisation of the novel fPtdCho (data not shown). Furthermore, RBL-2H3 cells labelled first with 0.5 µg/ml novel fPtdCho and then treated with 100 nM wortmannin for 30 minutes (in complete media) retained the punctiform localisation (n=2). Preliminary data suggests that cells labelled first with lipid and then treated with wortmannin maintained their ability to respond to PMA stimulation.

Figure 3.25: The effect of wortmannin on RBL-2H3 cells labelled with novel fluorescent PtdCho or LysoTracker Red. RBL-2H3 cells grown on glass bottomed fluorodishes for 24 hours were treated with 100 nM wortmannin for 30 minutes (in complete media) and labelled with 100 nM LysoTracker Red for 1 minute (and washed twice with HBSS + 20 mM HEPES). The cells were then imaged using live confocal microscopy using the HeNe 594 laser with excitation at 594 nm and an emission bandwidth between 668 nm-794 nm (panels **a-c**). Similarly, cells were treated with 100 nM wortmannin for 2 hours (in complete media) and labelled with 0.5 µg/ml of the novel fluorescent lipid for 2 hours (in HBSS + 20 mM HEPES) prior to live confocal imaging. The argon laser was used with an excitation at 488 nm and an emission bandwidth between 500 nm-608 nm to detect the green lipid (panels **d-f**). A scale calibrated to 25 µm is shown in each panel. The data presented are representative images for 1 experiment of 4 experiments (LysoTracker Red labelling) and 1 of 2 experiments (fPtdCho labelling).

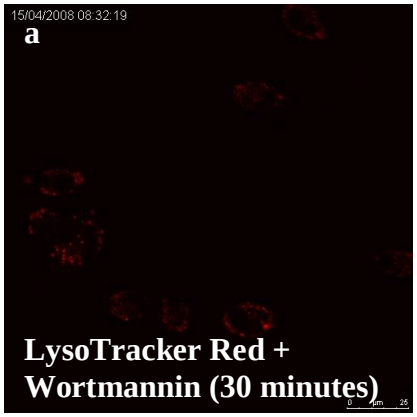
15/04/2008 08:32:19
a
LysoTracker Red +
Wortmannin (30 minutes)

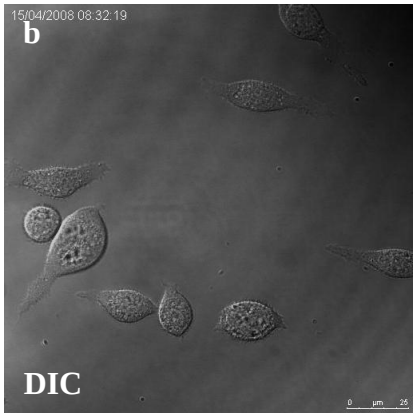
15/04/2008 08:32:19
b
DIC

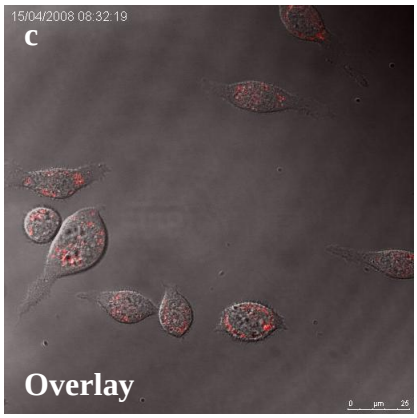
15/04/2008 08:32:19
c
Overlay

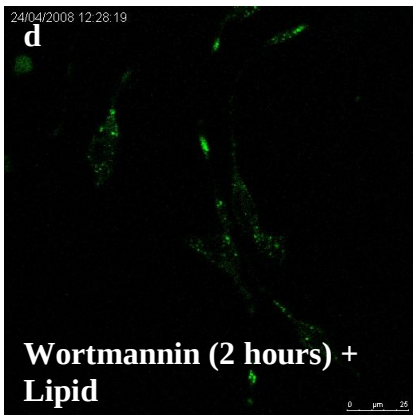
24/04/2008 12:28:19
d
Wortmannin (2 hours) +
Lipid

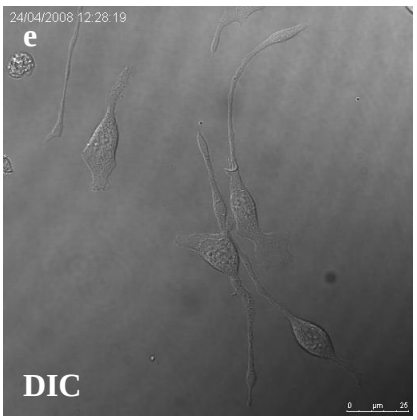
24/04/2008 12:28:19
e
DIC

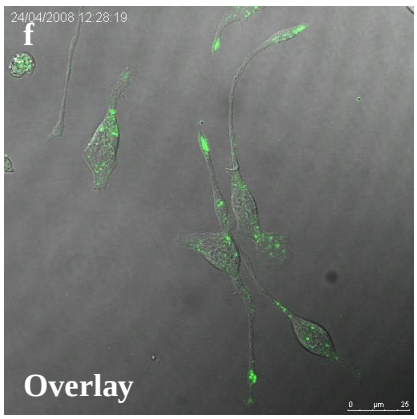
24/04/2008 12:28:19
f
Overlay

3.4.2: The effect of methyl-β-cyclodextrin on RBL-2H3 cells labelled with novel fluorescent PtdCho or LysoTracker Red

Methyl-β-cyclodextrin (MBCD) is a depleting agent used to remove cholesterol from lipid rafts and the plasma membrane and therefore to assess the role of cholesterol-rich membrane sub-domains (such as caveolae, detergent-resistant membranes and lipid rafts) in signalling (Hiroyama and Exton, 2005b). Treatment of HeLa cells with MBCD suggestsed that PLD localisation in membranes is not reliant upon cholesterol (Hiroyama and Exton, 2005b). RBL-2H3 cells were treated with 10 mM MBCD for 30 minutes and labelled with 100 nM LysoTracker Red. LysoTracker Red preserved its characteristic punctiform localisation and motility (see Fig. 3.26, panels a-c). There appeared to be no impact on LysoTracker Red labelling in MBCD pre-treated RBL-2H3 cells. RBL-2H3 cells were first labelled with 0.5 µg/ml novel fluorescent lipid (for 120 minutes) and then treated with 10 mM MBCD (for 60 minutes), however the punctate localisation of fPtdCho was unaffected by this treatment (see Fig. 3.26, panels d-f). Similarly, movement of the punctate vesicles was unaffected by cholesterol depletion. RBL-2H3 cells were treated first with MBCD (30, 60 and 120 minutes) and then labelled with 0.5 µg/ml fPtdCho, but MBCD pre-treatment did not inhibit the fPtdCho-labelling or localisation in RBL-2H3 cells.

Figure 3.26: The effect of MBCD on RBL-2H3 cells labelled with novel fluorescent PtdCho or LysoTracker Red. RBL-2H3 cells grown on glass bottomed fluorodishes for 24 hours prior were treated with 10 mM MBCD for 30 minutes and labelled with 100 nM LysoTracker Red for 1 minute, (then washed twice in HBSS + 20 mM HEPES). Cells were imaged using live confocal microscopy using the HeNe 594 laser excited at 594 nm with an emission bandwidth between 668 nm-794 nm (panels **a-c**). Similarly, cells were first labelled with 0.5 µg/ml fPtdCho for 120 minutes and then treated with MBCD for 60 minutes. The cells were then imaged live using the argon laser with an excitation at 488 nm and an emission bandwidth between 500 nm-608 nm to detect the green lipid (panels **d-f**). A scale calibrated to 25 µm is shown in each panel. The data presented are representative images for 1 of 4 experiments (LysoTracker Red labelling) and 1 of 2 experiments (fPtdCho labelling).

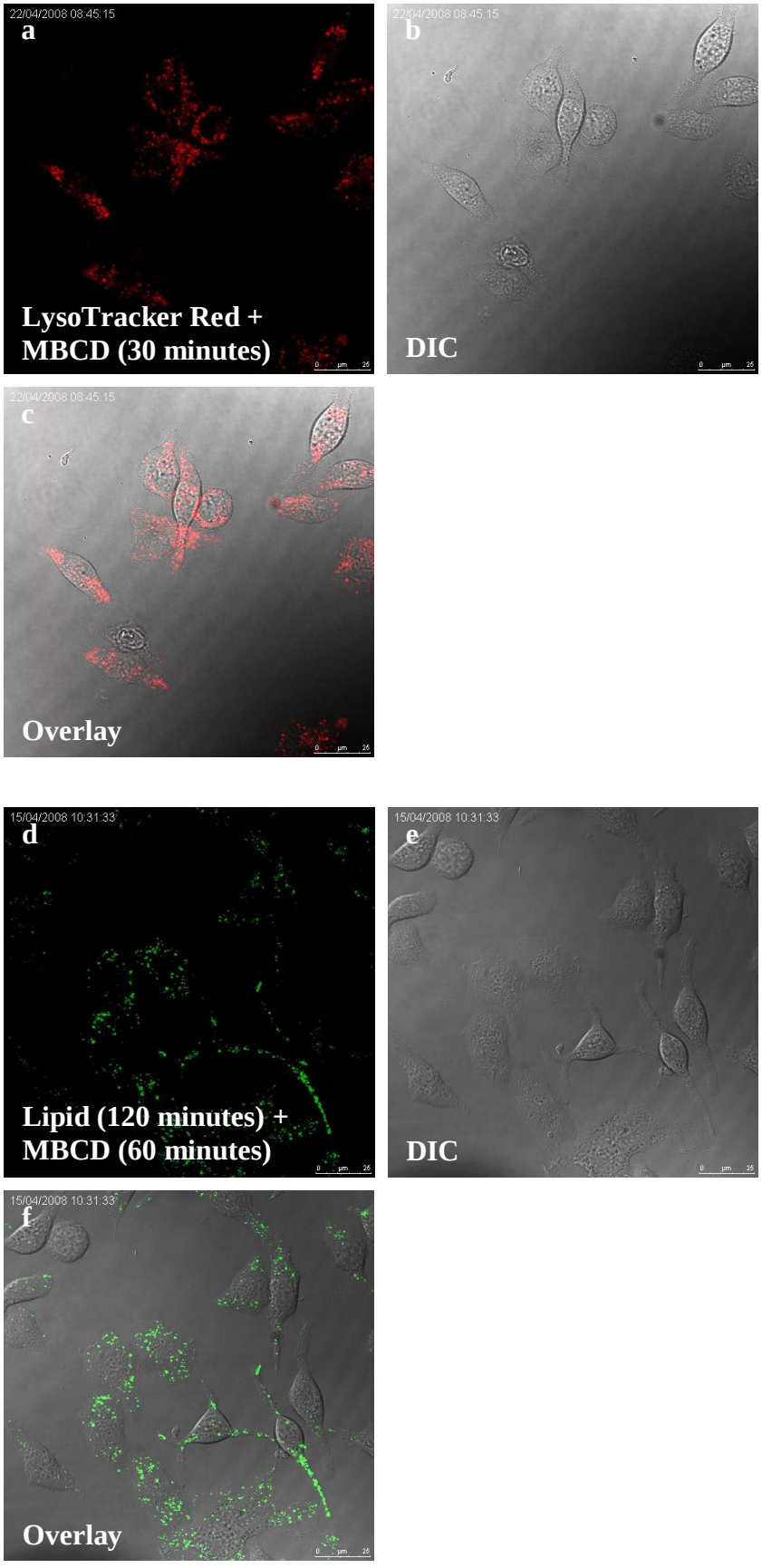
22/04/2008 08:45:15
a
LysoTracker Red +
MBCD (30 minutes)
22/04/2008 08:45:15
b
DIC
22/04/2008 08:45:15
c
Overlay
15/04/2008 10:31:33
d
Lipid (120 minutes) +
MBCD (60 minutes)
15/04/2008 10:31:33
e
DIC
15/04/2008 10:31:33
f
Overlay

3.4.3: The effect of paclitaxel on RBL-2H3 cells labelled with novel fluorescent PtdCho or LysoTracker Red

Paclitaxel promotes assembly and stabilisation of microtubules and is used as a treatment for certain tumours (Gupta, Jr. *et al*., 2003). RBL-2H3 cells treated with 100 µM paclitaxel (also known as taxol) for 18.5 hours in complete media were labelled with either LysoTracker Red or the novel fluorescent lipid. Paclitaxel treatment is typically between 12 and 24 hours so 18.5 hours was used to enable labelling and imaging of the cells. Although paclitaxel induced a change in the morphology of the RBL-2H3 cells, labelling of the cells was unaffected. RBL-2H3 cells showed membrane ruffling and broadening or truncating of processes upon treatment with paclitaxel, similar to the effect of PMA or A23187 treatment (see Fig. 3.27a and Fig. 3.28a for snapshots). RBL-2H3 cells were also pre-treated with 100 µM paclitaxel for 18.5 hours and then labelled with 100 nM LysoTracker Red (see Fig. 3.27a for snapshots). LysoTracker Red labelling was unaffected by paclitaxel pre-treatment of RBL-2H3 cells and was maintained in punctiform localisation and retained motility. Real-time confocal imaging over 15 minutes (1frame/10 seconds condensed to 18 seconds). The real-time recording determined that the movement of lysosomes was not inhibited by paclitaxel treatment (see Fig. 3.27b for recording). 0.5 µg/ml of the novel fluorescent lipid was used to label the cells for 3 hours prior to real-time confocal imaging. Although cell morphology was affected by paclitaxel, the novel lipid maintained punctate localisation within the cell body and processes (see Fig. 3.28a for snapshots). The fPtdCho also maintained motility recorded using real-time microscopy over 15 minutes (1frame/10 seconds condensed to 18 seconds – see Fig. 3.28b for recording).

Figure 3.27a: The effect of paclitaxel treatment on the localisation and movement of LysoTracker Red in RBL-2H3 cells. RBL-2H3 cells grown on glass bottomed fluorodishes for 8 hours were treated with 100 µM paclitaxel (in DMSO) for 18.5 hours prior to labelling. RBL-2H3 cells were labelled with 100 nM LysoTracker Red for 1 minute and washed twice in HBSS + 20 mM HEPES + 1 mM Ca^{2+}. Control cells were treated with paclitaxel and vehicle (DMSO) and imaged in the same manner. Real-time recording was completed over 15 minutes (1 frame/10 seconds) using the HeNe 594 laser with an excitation at 594 nm and an emission bandwidth between 668 nm-794 nm. The 594 nm laser power was halved and each time point was scanned twice (and averaged) to reduce photo-bleaching. A scale calibrated to 25 µm is shown in each panel. The data presented are representative images for 1 experiment of 2. Still images are represented below whilst the full length film has been condensed to 18 seconds and is shown in Fig. 3.27**b**.

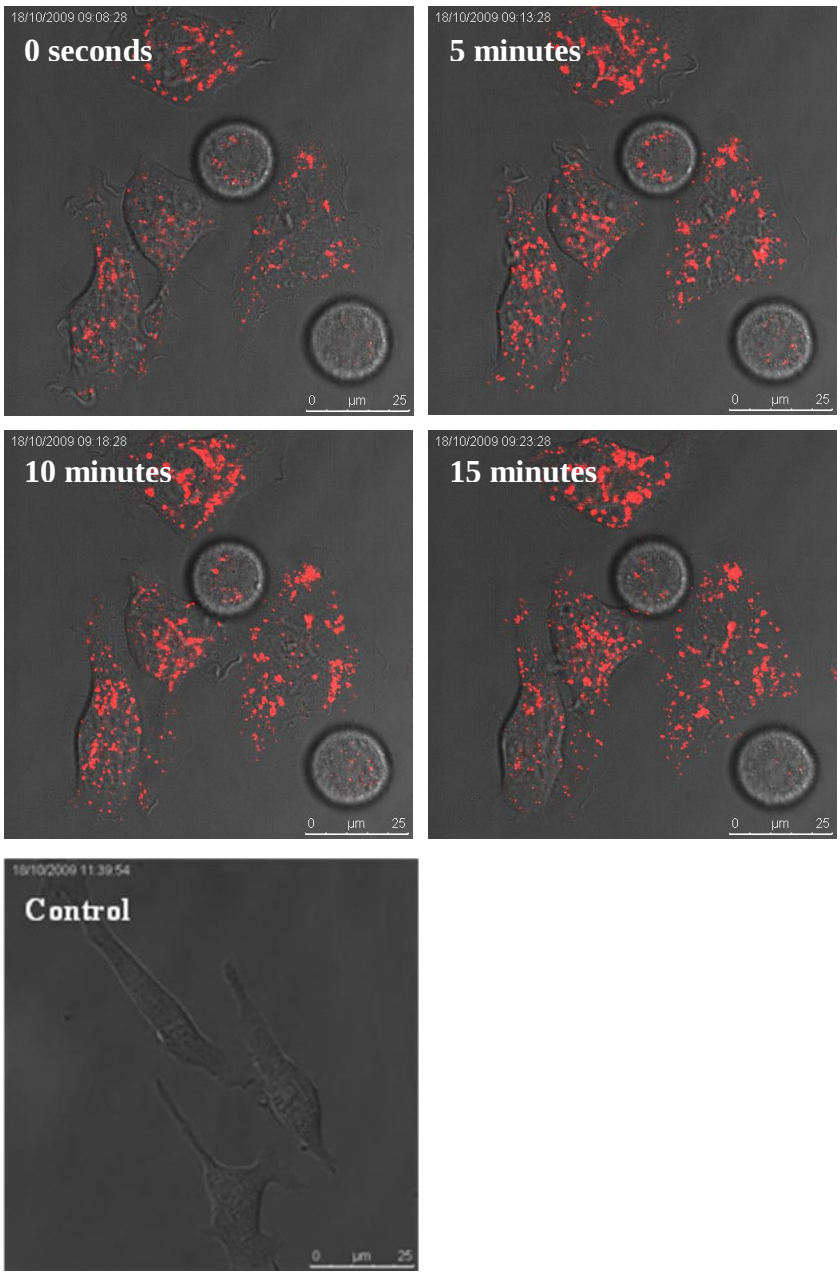

Figure 3.28a: The effect of paclitaxel treatment on the localisation and movement of the novel fluorescent lipid in RBL-2H3 cells. RBL-2H3 cells grown on glass bottomed fluorodishes for 8 hours were treated with 100 µM paclitaxel (in DMSO) for 18.5 hours prior to labelling with 0.5 µg/ml novel fPtdCho for 3 hours in HBSS + 20 mM HEPES + 1 mM Ca^{2+}. Real-time recording was completed over 15 minutes (1 frame/10 seconds) using the argon laser with an excitation at 488 nm and an emission bandwidth between 500 nm-608 nm. The 488 nm laser power was halved and each time point was scanned twice (and averaged) to reduce photo-bleaching. A scale calibrated to 25 µm is shown in each panel. The data presented are representative images for 1 experiment of 2. Still images are presented below whilst the full length film has been condensed to 18 seconds and is shown in Fig. 3.28**b**.

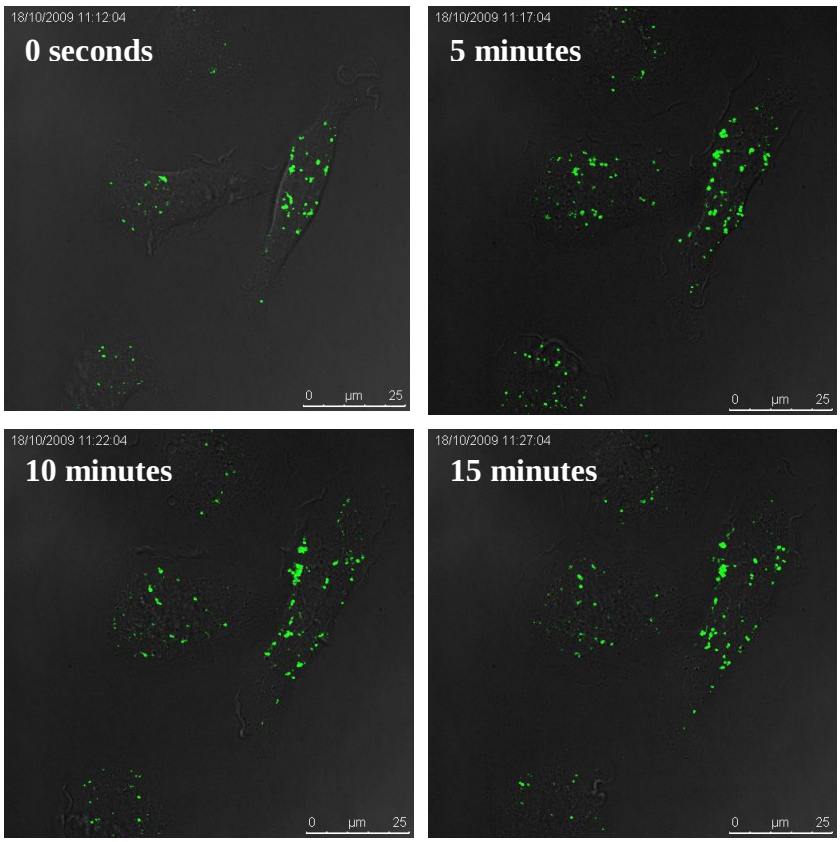

RBL-2H3 cells were also treated with nocodazole which is a more potent microtubule inhibitor then paclitaxel. Cells were treated with 5 µM nocodazole for 1 hour prior to labelling with 0.5 µg/ml fPtdCho for 2 hours. RBL-2H3 cells lost their cell processes and appeared rounded (see Fig. 3.29a for snapshots). Cell rounding precedes cell death; however fPtdCho maintained its punctate localisation within the cell body. Movement of the novel fluorescent lipid was monitored using real-time confocal imaging over 15 minutes (1 frame/10 seconds condensed to 18 seconds – see Fig. 3.29b for recording). Lipid labelling and movement was unaffected by nocodazole pre-treatment. Neither nocodazole nor paclitaxel treatment of RBL-2H3 cells inhibited the movement of the novel lipid and so movement of the punctiform vesicles may not be linked to microtubules.

Figure 3.29a: The effect of nocodazole treatment on the localisation and movement of the novel fluorescent lipid in RBL-2H3 cells. RBL-2H3 cells were grown on glass bottomed fluorodishes overnight prior to nocodazole treatment. 5 µM nocodazole (in DMSO) was used to treat the cells for 60 minutes prior to labelling with 0.5 µg/ml novel fPtdCho for 120 minutes in HBSS + 20 mM HEPES + 1 mM Ca^{2+}. Real-time recording was completed over 15 minutes (1 frame/10 seconds) using the argon laser with an excitation at 488 nm and an emission bandwidth between 500 nm-608 nm. The 488 nm laser power was halved and each time point was scanned twice (and averaged) to reduce photo-bleaching. A scale calibrated to 25 µm is shown in each panel. The data presented are representative images for 1 experiment of 2. Still images are presented below whilst the full length film has been condensed to 18 seconds and is shown in Fig. 3.29**b**.

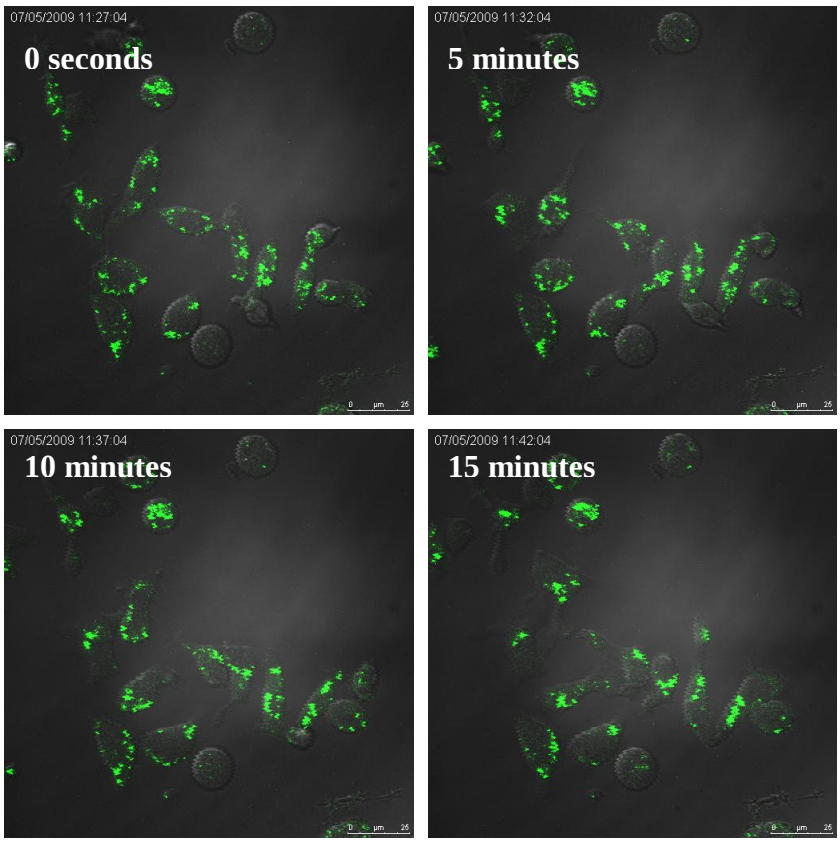

3.4.4: The effect of cytochalasin D on RBL-2H3 cells labelled with novel fluorescent PtdCho or LysoTracker Red

Cytochalasin D (CD) is an inhibitor of cytoskeletal change and acts by capping actin filaments to stabilise the cytoskeleton (Wakatsuki *et al*., 2000). RBL-2H3 cells were labelled with 1 µg/ml novel fPtdCho for 2 hours and treated with 1 µM CD for 5 hours. The effects of CD on cell morphology were monitored every hour (see Fig. 3.30, panels a-f) and compared to the labelling of control cells (see Fig. 3.30, panels g, h). RBL-2H3 cells remained labelled in HBSS + 20 mM HEPES + 1 mM Ca^{2+} for up to 7 hours (see Fig. 3.30, panel h). The novel fPtdCho localised in punctiform structures and did not concentrate in any area within RBL-2H3 cells (see Fig. 3.30, panel a) prior to CD treatment. However, in cells treated with CD, the novel lipid accumulated at the tips and the bases of cell processes within 1 hour (see arrows, Fig. 3.30, panel b). Treatment of cells with CD for 3 hours altered cell morphology producing rounded cell bodies with multiple short processes (see Fig. 3.30, panels d-f). This data suggests that the movement of fPtdCho-labelled vesicles is influenced by the state of the actin cytoskeletal and upon inhibition with CD their movement is impaired. Vesicle size was not significantly different from control cells (compared using the 2-tailed Student's t-test) and CD treatment of cells did not inhibit the movement of the fPtdCho.

Figure 3.30: The effect of cytochalasin D on the localisation and movement of the novel fluorescent lipid in RBL-2H3 cells. RBL-2H3 cells were grown on glass bottomed fluorodishes overnight prior to labelling with 1 µg/ml novel fPtdCho, (for 2 hours in HBSS + 20 mM HEPES + 1 mM Ca^{2+}) and imaged live using confocal microscopy (panel **a**). Cells were then treated with 1 µM CD and imaged at 1 hour time points up to 5 hours (panels **b-f**). Control cells were labelled with the fPtdCho and imaged alongside CD treated cells for up to 7 hours (panels **g**, **h**). Live imaging was completed using the argon laser with an excitation at 488 nm and an emission bandwidth between 500 nm-608 nm. A scale calibrated to 25 µm is shown in each panel. The data presented are representative images for 1 experiment of 2.

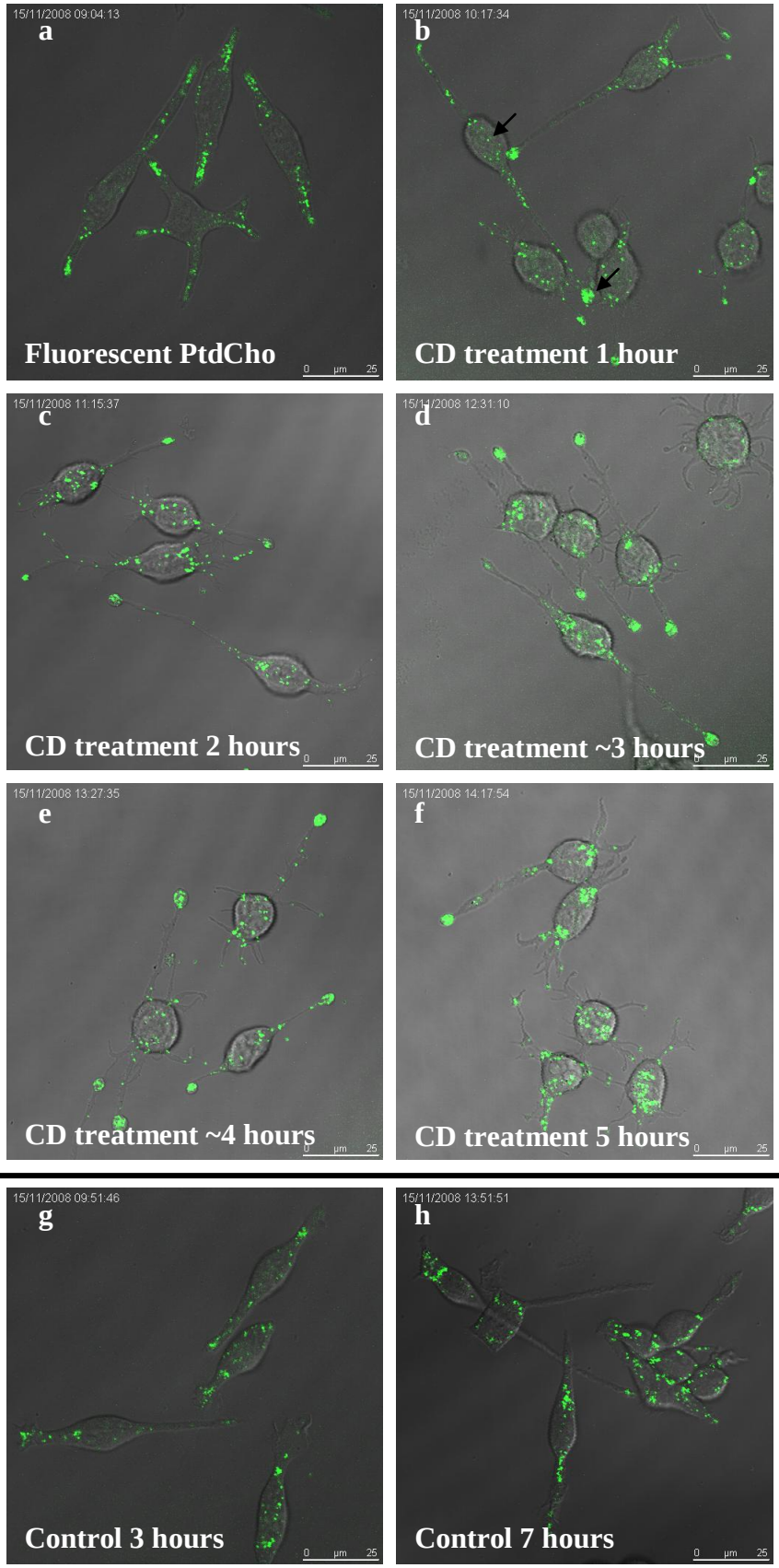
15/11/2008 09:04:13
a
Fluorescent PtdCho
15/11/2008 10:17:34
b
CD treatment 1 hour
15/11/2008 11:15:37
c
CD treatment 2 hours
15/11/2008 12:31:10
d
CD treatment ~3 hours
15/11/2008 13:27:35
e
CD treatment ~4 hours
15/11/2008 14:17:54
f
CD treatment 5 hours
15/11/2008 09:51:46
g
Control 3 hours
15/11/2008 13:51:51
h
Control 7 hours

RBL-2H3 cells labelled with fPtdCho and then treated with CD for 3 hours exhibited a change in lipid localisation that was assessed using live confocal microscopy in which series sections (0.2 µm thickness) were taken from the bottom to the top of cell. These sections were averaged and used to reconstruct the cell using the 3D function of the Leica software. The rotating 3D reconstructions were converted to movies and can be seen in Fig. 3.31a-c. RBL-2H3 cells labelled with the novel fluorescent lipid but not treated with CD (see Fig. 3.31a for 3D reconstruction) showed that the punctiform localisation of fPtdCho was dispersed across the cell body and processes. RBL-2H3 cells labelled with fPtdCho and treated with 1 µM CD for 1 hour (see Fig. 3.31b for 3D reconstruction) showed that lipid concentrated at the base of each cell process (within the cell body). Similarly, cells treated with 1 µM CD for 3 hours (see Fig. 3.31c for 3D reconstruction) showed concentration of the lipid within the cell body and at the tips of the cell processes.

RBL-2H3 cells were also labelled with the lysosomal marker LysoTracker Red and treated with 1 µM CD. The localisation of LysoTracker Red was punctate and spread across the cell body and processes (see Fig. 3.32, panel a). Cells were then treated with CD and imaged after 1 and 3 hours (see Fig. 3.32, panels b, c), and LysoTracker Red was seen to concentrate at the tips of the cell processes within 1 hour (see Fig. 3.32, panel b). LysoTracker Red localisation did not alter between 1 and 3 hours after CD treatment. The localisation and accumulation of LysoTracker Red was similar to that seen using the novel fPtdCho (see Fig. 3.30 and Fig. 3.31). The effect of LysoTracker Red and fPtdCho labelling on CD treated RBL-2H3 cells was comparative as no co-labelling experiments were undertaken.

Figure 3.31: The effect of cytochalasin D on the localisation and movement of fPtdCho in RBL-2H3 cells reconstructed in 3D. RBL-2H3 cells were grown on glass bottomed fluorodishes overnight prior to labelling with 1 µg/ml novel fPtdCho for 2 hours (in HBSS + 20 mM HEPES + 1 mM Ca^{2+}). Live confocal microscopy was used to record data prior to CD treatment (Fig. 3.30**a**). Cells were treated with 1 µM CD and imaged at 1 hour (Fig. 3.30**b**) and 3 hours (Fig. 3.30**c**) points. Serial sections were taken (0.2 µm thickness) from the top to the bottom of the cells. These were averaged and visualised in 3D using the 3D Projection function of the Leica software. Brief movies of the rotating cells can be seen in Fig. 3.30**a-c**. Fluorescence was excited using the argon laser (excitation at 488 nm) and an emission bandwidth between 500 nm-608 nm. A scale calibrated to 10 µm is shown in each movie. The data presented are reconstructions for 1 experiment of 2.

Figure 3.32: The effect of cytochalasin D on the localisation and movement of the LysoTracker Red in RBL-2H3 cells. RBL-2H3 cells were grown on glass bottomed fluorodishes overnight and labelled with 100 nM LysoTracker Red for 1 minute in HBSS + 20 mM HEPES + 1 mM Ca^{2+} and then washed twice. Cells were imaged prior to treatment with CD (panel **a**). Cells were then treated with 1 µM CD and imaged 1 hour and 3 hours after CD treatment (panels **b**, **c**). Live imaging was completed using the HeNe 594 laser with an excitation at 594 nm and an emission bandwidth between 668 nm-794 nm. A scale calibrated to 25 µm is shown in each panel. The data presented are representative images for 1 experiment of 2.

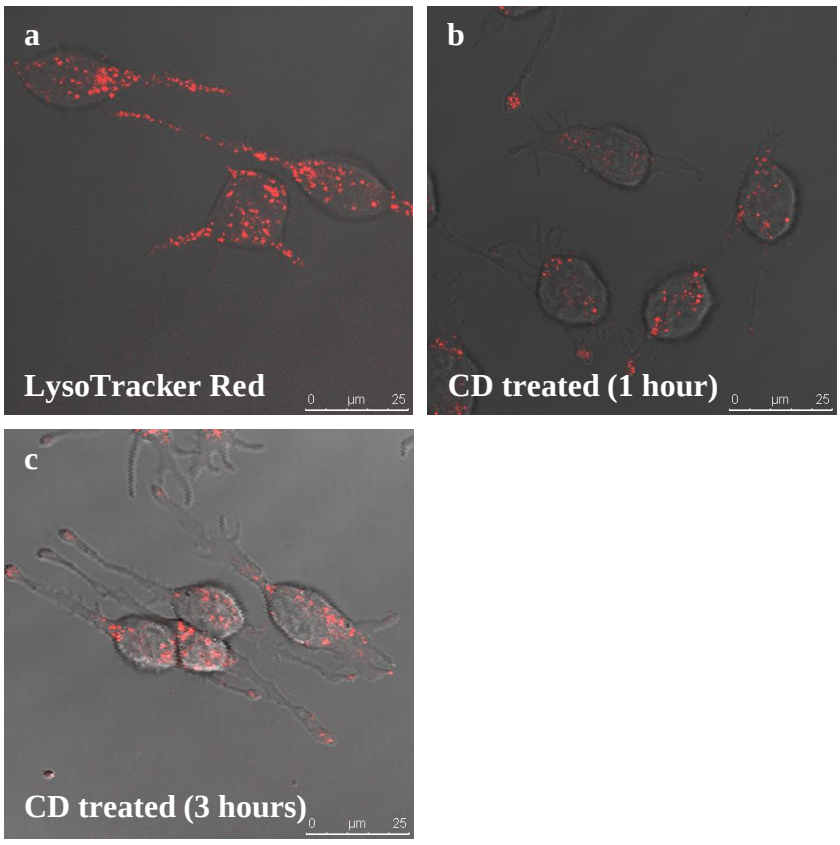

3.4.5: The effect of cytochalasin D on antigenic stimulation of RBL-2H3 cells labelled with novel fluorescent PtdCho

Cytochalasin D is a 'priming' agent for IgE-antigen stimulation of RBL-2H3 cells, although the mechanism is unknown. However, CD may prevent the re-distribution of $Fc_{\varepsilon}RI$ receptors upon antigenic stimulation which would result in the initiation of a signalling cascade. This cascade includes the tyrosine kinase Syk which can activate PtdIns 3-kinase phosphorylation of PtdIns(4,5)P_2 to PtdIns(3,4,5)P_3 and thus activate PLD (Rivera and Olivera, 2008).

RBL-2H3 cells were sensitisated with 1 µg/ml anti-DNP IgE overnight (in complete DMEM) and labelled with 1 µg/ml of the fPtdCho for 2 hours prior to treatment with 1 µM CD for 2 hours. The effect of CD treatment could be seen by the aggregation of fPtdCho to the tips of the cell processes (see Fig. 3.33a for snapshots). RBL-2H3 cells were stimulated during the real-time recordings with 0.1 µg/m DNP-BSA in a final volume of 1 ml HBSS + Ca^{2+} and the effect of CD on antigenically stimulated cells was recorded over 15 minutes (1 frame/10 seconds condensed to 18 seconds – see Fig. 3.33b for recording). The 488 nm laser power was halved and, each frame accumulated twice and averaged to reduce photo-bleaching. The novel fluorescent lipid maintained its punctiform localisation, was not expelled upon degranulation and did not change upon antigenic stimulation (see Fig. 3.33a for snapshots). Similarly, PMA-stimulated RBL-2H3 cells pre-treated with CD were able to respond and fluorescent lipid localisation was unaffected (data not shown).

Figure 3.33a: The effect of CD on IgE/antigen stimulated RBL-2H3 cells labelled with novel fluorescent PtdCho. RBL-2H3 cells grown on glass bottomed fluorodishes for 8 hours were primed with 1 µg/ml anti-DNP IgE overnight (in complete DMEM). Cells were labelled with 1 µg/ml fPtdCho (2 hours) and treated with 1 µM CD for 2 hours in HBSS + 20 mM HEPES + 1 mM Ca^{2+}. Real-time recording was completed over 15 minutes (1 frame/10 seconds) using the argon laser with an excitation at 488 nm and an emission bandwidth between 500 nm-608 nm. The 488 nm laser power was halved and each time point was scanned twice (and averaged) to reduce photo-bleaching. RBL-2H3 cells were stimulated with 0.1 µg/ml DNP-BSA after approximately 50 seconds (frame 5). A scale calibrated to 25 µm is shown in each panel. The data presented are representative images for 1 experiment of 2. Still images are presented below whilst the recording is shown in Fig. 3.33**b**.

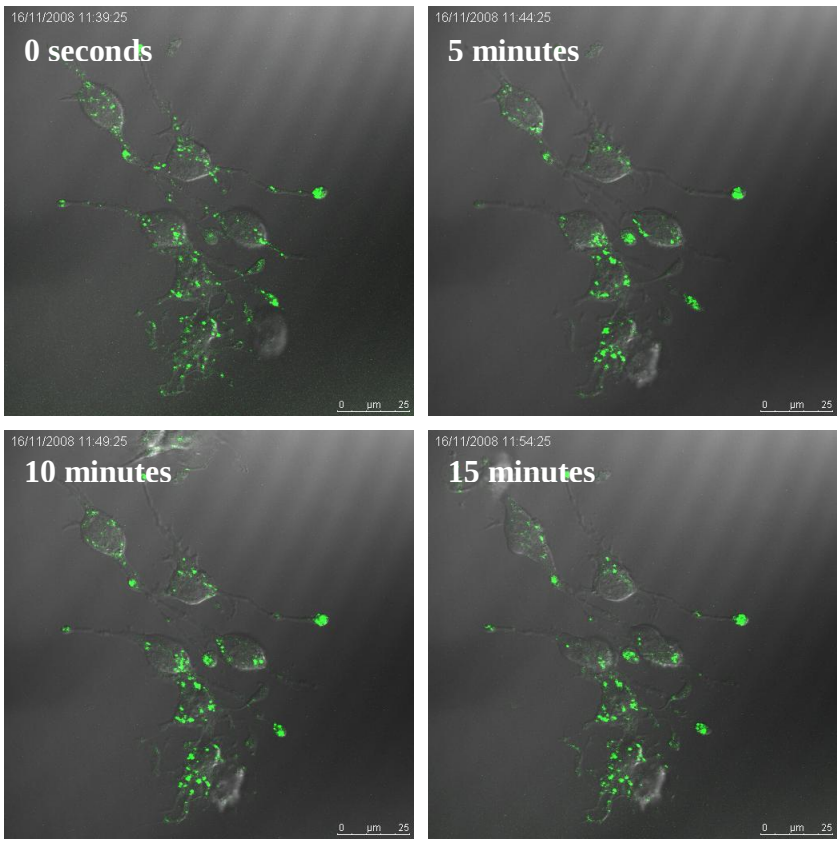

3.4.6: The effect of latrunculin B on RBL-2H3 cells labelled with novel fluorescent PtdCho or LysoTracker Red

Latrunculin B (Lat B) inhibits actin polymerisation in a different manner to cytochalasin D. Latrunculin B binds G-actin which is released from the actin filaments (Lat B binds G-actin 1:1) and stops its re-incorporation into a fibre (Pendleton and Koffer, 2001). RBL-2H3 cells labelled with either LysoTracker Red or the novel fPtdCho were then treated with Lat B. Latrunculin B affected cell morphology, resulting in blebbing of the cell bodies and the production of multiple processes. LysoTracker Red localisation was punctate and distributed in the cell body and processes of RBL-2H3 cells as expected (see Fig. 3.34a, panel a). RBL-2H3 cells were treated with 5 µM Lat B for 1 hour and imaged using live confocal microscopy. LysoTracker Red labelling was reduced and the marker accumulated at the tips of the processes (see Fig. 3.34a, panel b), similar to the effect of CD treatment of RBL-2H3 cells.

RBL-2H3 cells were also labelled with the novel fPtdCho and treated with 1 µM Lat B. After 1 hour the cell bodies appeared more rounded (when compared with controls) and the processes were notably thinner (see Fig. 3.34a, panels c, d). The fluorescent lipid aggregated to the tips of the cell processes, similar to the effect of CD treatment on fluorescent lipid localisation. After 3 hours the cells generated numerous processes and the fluorescent lipid was still aggregated to the tips of these processes (see Fig. 3.38a, panel e). The change in fluorescent lipid localisation upon Lat B treatment was assessed by reconstructing the cells in 3 dimensions. Cells were imaged using live confocal microscopy in which serial sections (0.2 µm thickness) were taken from the bottom to the top of cell. Sections were then averaged and used to reconstruct the cell using the 3D function of the Leica software (seen in Fig. 3.34b). RBL-2H3 cells labelled with the novel fluorescent lipid and treated with 1 µM Lat B for 1 hour (data not shown) and 3 hours (see Fig. 3.34b for 3D reconstruction) showed that the lipid maintained its punctiform localisation and accumulated to the tips of the cell processes.

Figure 3.34a: The effect of latrunculin B on the localisation and movement of the novel fluorescent lipid of LysoTracker Red in RBL-2H3 cells. RBL-2H3 cells grown on glass bottomed fluorodishes overnight were labelled with 1 µg/ml novel fPtdCho for 2 hours in HBSS + 20 mM HEPES + 1 mM Ca^{2+} or 100 nM LysoTracker Red for 1 minute. Cells labelled with LysoTracker Red were washed twice and then imaged using live confocal microscopy (panel **a**). The cells were treated with 5 µM Lat B and imaged after 1 hour (panel **b**); media was replaced and then imaged again at 3 hours (data not shown). Live imaging was completed using the HeNe 594 laser with an excitation at 594 nm and an emission bandwidth between 668 nm-794 nm. Cells labelled with the novel lipid for 2 hours were imaged prior to Lat B treatment (panel **c**). Cells were then treated with 1 µM Lat B and imaged after 1 hour (panel d) and 3 hours (panel **e**). Fluorescent PtdCho labelled cells were imaged using the argon laser (excitation at 488 nm) and an emission bandwidth between 500 nm-608 nm. A scale calibrated to 25 µm is shown in each panel (**a-e**). Fluorescent lipid labelled cells were scanned using serial sections (0.2 µm in thickness) from the top to the bottom of the cells. The serial sections were averaged and visualised in 3D using the 3D Projection function of the Leica Software. Movies of the rotating cells can be seen of cells treated with 1 µM Lat B for 3 hours (Fig. 3.34**b**). A scale calibrated to 10 µm is shown in each movie. The data presented are representative images/movies from 1 experiment of 2.

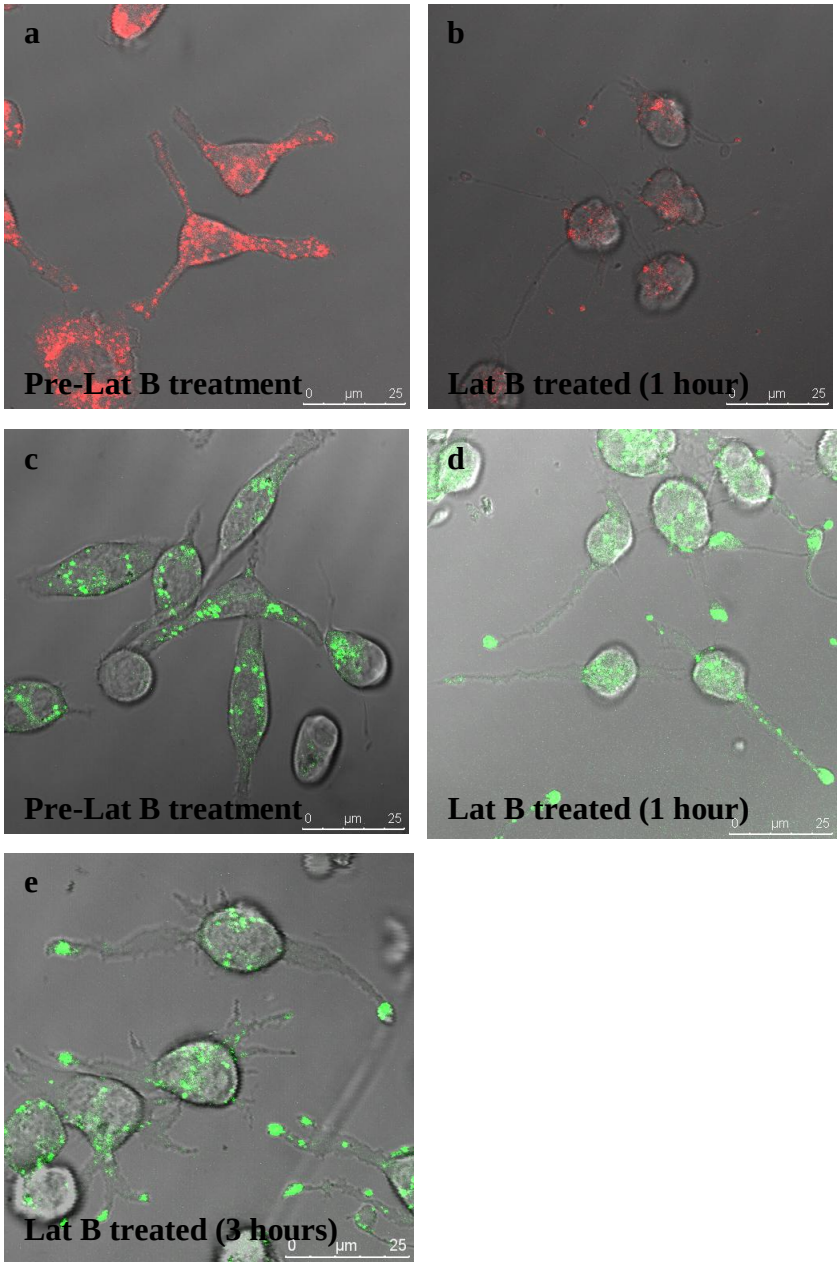
a
Pre-Lat B treatment
0 µm 25
b
Lat B treated (1 hour)
0 µm 25
c
Pre-Lat B treatment
0 µm 25
d
Lat B treated (1 hour)
0 µm 25
e
Lat B treated (3 hours)
0 µm 25

3.4.7: Using a secretory lysosomal marker to measure the effectiveness of RBL-2H3 stimulators in the presence of cytoskeletal inhibitors

The effect of the cytoskeletal inhibitors cytochalasin D (CD) and latrunculin B (Lat B) were investigated using the β-hexosaminidase assay, as described previously (Section 3.3.1). Cells were first treated with either cytochalasin D or latrunculin B for 1 hour and then stimulated using 100 nM PMA, 0.1 µM A23187 and 0.1 µg/ml DNP-BSA (cells stimulated using antigenic stimulation were primed overnight using 1 µg/ml anti-DNP IgE). The effect of Lat B and CD treatment on the percentage β-hexosaminidase secretion was compared against control cells but the treatments showed no effect on secretion (see Fig. 3.35). Similarly, RBL-2H3 cells did not respond to PMA stimulation and treatment of the cells with Lat B and CD had no impact on the percentage β-hexosaminidase secretion. Although CD is thought to amplify the response of mast cells to antigenic stimulation, there was no significant difference between antigenically stimulated control and CD treated cells (compared using the 2-tailed Student's t-test). Similarly, Lat B treated cells which were stimulated with IgE-antigen consistently showed a higher percentage of β-hexosaminidase secretion but this was also not significantly different from control cells. There was no impact of Lat B and CD treatment on cells stimulated with the calcium ionophore A23187, both treatments (and control stimulation) resulted in an average 40-45% β-hexosaminidase secretion.

Figure 3.35: The effect of Lat B and CD on RBL-2H3 mast cell secretion in response to PMA, A23187 and IgE-antigen using the secretory lysosomal marker β-hexosaminidase. RBL-2H3 cells were grown in 12-well plates to ~80-90% confluencey 24 hours prior to the β-hexosaminidase assay. Cells stimulated with IgE-antigen were primed overnight using 1 µg/ml anti-DNP IgE (in complete DMEM). Cells were treated with either 1 µM Lat B or 1 µM CD for 1 hour prior to stimulation. Cells were stimulated using 0.1 µM A23187 or 100 nM PMA for 60 minutes in 250 µl HBSS + 20 mM HEPES + 1 mM Ca^{2+} at 37°C/5% CO_2. Primed RBL-2H3 cells were stimulated using 0.1 µg/ml DNP-BSA for 60 minutes. 0.1% Triton X-100 was used to treat cells for 5 minutes before scraping. All treated cells were scraped and centrifuged at 13,000 RPM for 5 minutes. 20 µl of the supernatant was combined with 20 µl 1 mM p-nitrophenol-N-acetylglucosamide (in 0.1 M sodium citrate, pH 4.5) in a 96-well plate and incubated at 37°C/5% CO_2 for a further 60 minutes. The reaction was terminated using 200 µl 0.1 M sodium carbonate and sodium hydrogen carbonate, pH 10.5. Results were measured continuously using the 405 nm filter on a plate reader and calculated as a percentage of the values recorded for Triton X-100 treated cells. All assays were read in triplicate and repeated 3 times. The data presented are the means of these experiments.

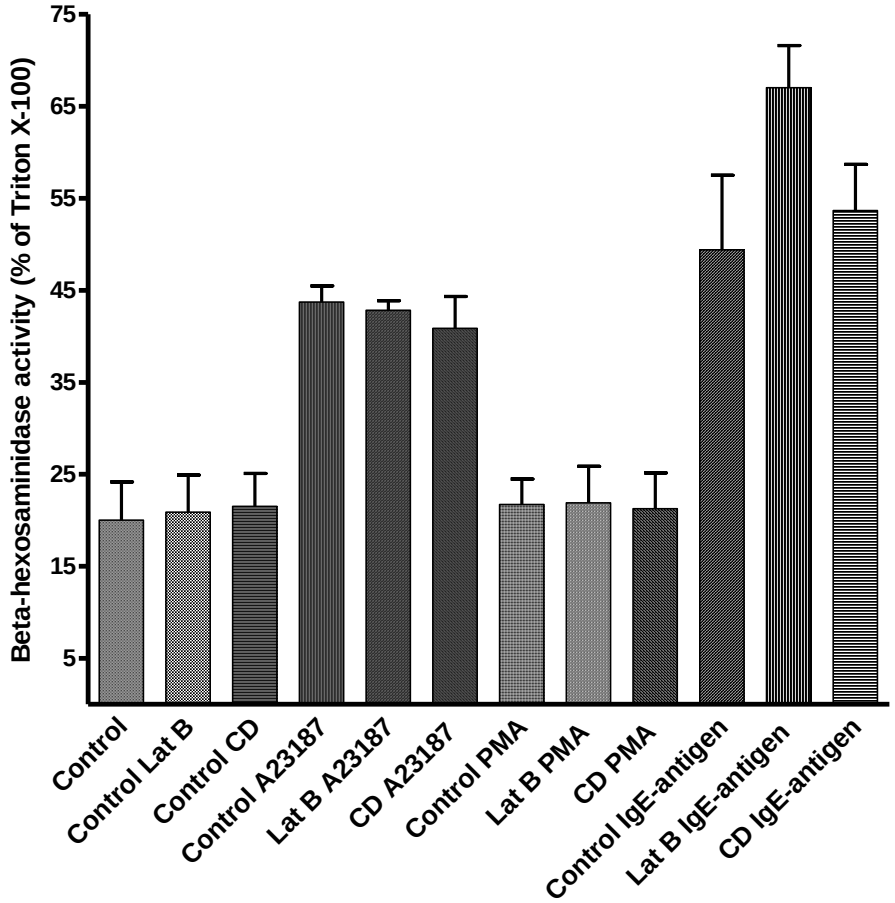

3.4.8: The effect of UV treatment on RBL-2H3 cells labelled with novel fluorescent PtdCho

Treatment of most cell types with UV-light will initiate apoptosis (Teraki *et al*., 1999; Klums and Schwarz, 2000). Apoptosis is programmed cell death and is essential to a number of processes including ensuring normal cell turnover to facillitating the correct development and function of the immune system (Elmore, 2007). RBL-2H3 cells were labelled with 1 µg/ml of the novel fluorescent lipid for 120 minutes (see Fig. 3.36, panel a) before UV treatment. After 10 minutes UV irradiation, the RBL-2H3 cells maintained the punctate localisation of the novel fPtdCho (see Fig. 3.36, panel b). Cells were incubated in complete media with Pen/Strep between time points (e.g. between 5 hours 30 minutes and 22 hours). Although cells were removed from the labelling media, the green lipid was consistently present intracellularly (see Fig. 3.36, panels c, d). The effects of apoptosis, including shrinking of the cells and membrane ruffling were seen approximately 6 hours after UV irradiation of RBL-2H3 cells. RBL-2H3 cells retain their contents, including inflammatory mediators, such as histamine, during apoptosis. The localisation of fPtdCho changed from punctate to diffuse (see Fig. 3.36, panel c) and was maintained for up to 22 hours (see Fig. 3.36, panel d).

Figure 3.36: The effect of UV irradiation on the localisation and movement of the novel fluorescent lipid in RBL-2H3 cells. RBL-2H3 cells grown on glass bottomed fluorodishes overnight were labelled with 1 µg/ml novel fPtdCho for 120 minutes in HBSS + 20 mM HEPES + 1 mM Ca^{2+} prior UV-irradiation. The cells were first labelled and then imaged using live confocal microscopy (panel **a**). Cells were UV irradiated using a UV cross-linker and exposed to 600 mJ UV rays and imaged at 10 minutes (panel **b**), 5 hours 30 minutes (panel **c**) and 22 hours (panel **d**) after UV irradiation. At 10 minutes the cells were maintained in the labelling HBSS + 20 mM HEPES + 1 mM Ca^{2+} solution, however between the subsequent time points, cells were transferred into complete media with antibiotics. Live imaging was completed using the argon laser with an excitation at 488 nm and an emission bandwidth between 500 nm-608 nm. A scale calibrated to 25 µm is shown in each panel. The data presented are representative images for 1 experiment of 2.

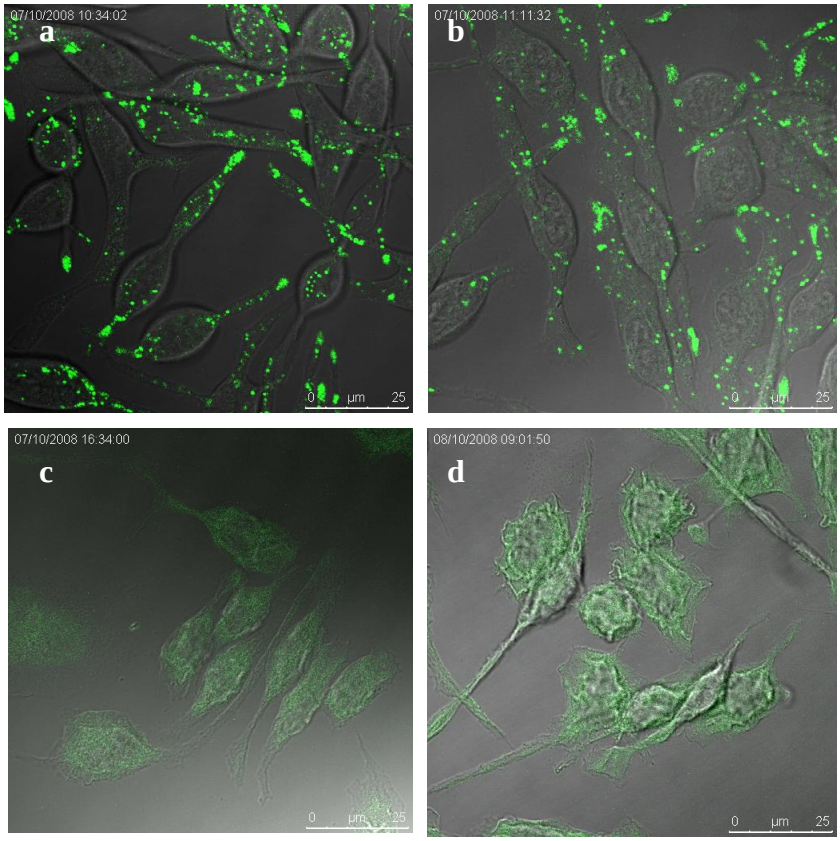

3.4.9: The effect of butanol on RBL-2H3 cells labelled with novel fluorescent PtdCho

Primary alcohols inhibit PLD catalysed PtdOH production by interfering with the transesterification of the substrate lipid and resulting in preferential production of a Ptd-alcohol and consequent functional inhibition of PLD. RBL-2H3 cells were labelled using the novel fluorescent lipid and treated with 0.3% butanol (either butan-1-ol or butan-2-ol). Cells labelled with fPtdCho exhibited the expected punctate localisation prior to treatment with butan-1-ol (see Fig. 3.37, panel a). However, upon treatment with 0.3% butan-1-ol for 15 minutes, the fluorescent lipid staining appeared diffuse and excluded the nucleus (see Fig. 3.37, panel b). Cells labelled with the fPtdCho were also treated with 0.3% butan-2-ol which acted as a control. The fluorescent lipid maintained its punctiform localisation after cells were treated with butan-2-ol with no change in the distribution of the lipid (see Fig. 3.37, panels c, d). RBL-2H3 cells labelled with fPtdCho and treated with either butan-1-ol or butan-2-ol were also stimulated with IgE-antigen (see Fig. 3.38a, panels a, b). Cells which were treated with butan-1-ol did not respond to antigenic stimulation as no membrane ruffling or truncating of cell processes was evident over the 15 minute real-time recording (condensed to 18 seconds – see Fig. 3.38b for recording). Antigenically stimulated butan-2-ol treated cells exhibited ruffling of the cell membrane and processes, indicating that the cells were responding over the 15 minutes of real-time recording (condensed to 18 seconds – see Fig. 3.38c for recording).

Figure 3.37: The effect of butanol treatment on RBL-2H3 cells labelled with fluorescent PtdCho. RBL-2H3 cells grown on glass bottomed fluorodishes overnight were labelled with novel fPtdCho in HBSS + 20 mM HEPES + 1 mM Ca^{2+}prior to butanol treatment. Cells were first labelled and then imaged using live confocal microscopy (panel **a**, **c**). Cells were treated with 0.3% butan-1-ol (panel **b**) or butan-2-ol (panel **d**) for 15 minutes at 37^{o}C/5% CO_2. Live imaging was completed using the argon laser with an excitation at 488 nm and emission bandwidth between 500 nm-608 nm. A scale calibrated to 25 µm is shown in each panel. The data presented are representative images for 1 experiment of 3.

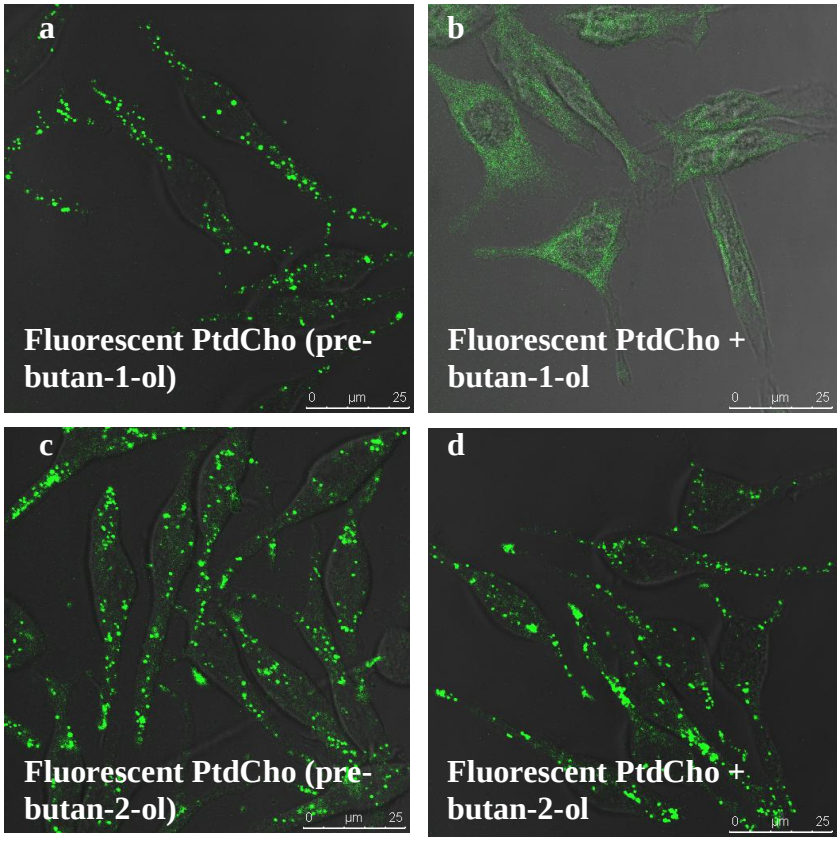

Figure 3.38a: The effect of butanol treatment on RBL-2H3 cells labelled with fluorescent PtdCho and stimulated in the context of IgE/antigen. RBL-2H3 cells were primed overnight with 1 µg/ml anti-DNP IgE (in complete DMEM). Cells were then labelled with the novel fPtdCho in HBSS + 20 mM HEPES + 1 mM Ca^{2+} and treated with 0.3% butan-1-ol (panel **a**) or butan-2-ol (panel **b**) for 15 minutes at 37^{o}C/5% CO_2 and stimulated using 0.1 µg/ml DNP-BSA (added during the real-time recording). Real-time recording was completed over 15 minutes (1 frame/10 seconds) using the argon laser with an excitation at 488 nm and an emission bandwidth between 500 nm-608 nm. The 488 nm laser power was halved and each time point was scanned twice (and averaged) to reduce photo-bleaching. A scale calibrated to 25 µm is shown in each panel. The data presented are representative images for 1 experiment of 2. Still images are represented below whilst the recordings are shown in Fig. 3.38**b** (butan-1-ol) and Fig. 3.38**c** (butan-2-ol).

a

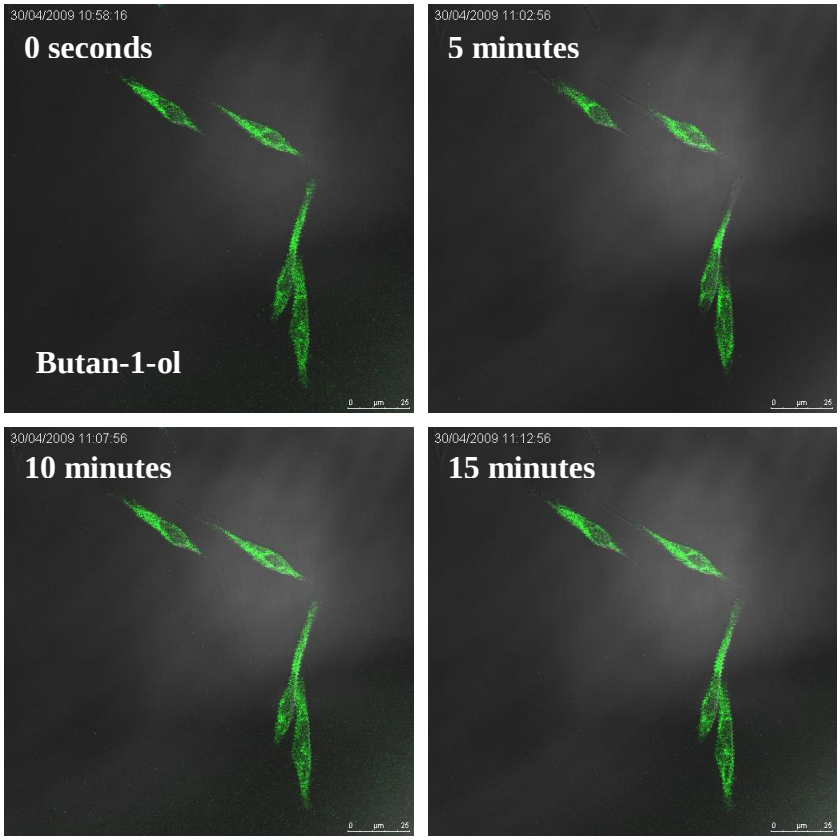
30/04/2009 10:58:16
0 seconds
Butan-1-ol
30/04/2009 11:02:56
5 minutes
30/04/2009 11:07:56
10 minutes
30/04/2009 11:12:56
15 minutes

b

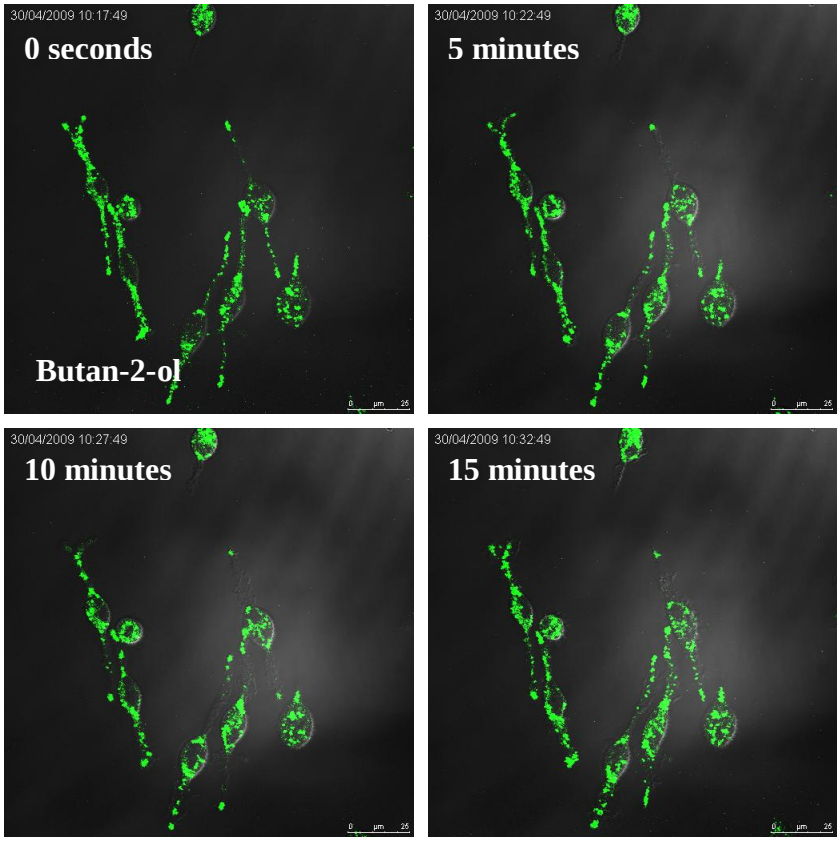
30/04/2009 10:17:49
0 seconds
Butan-2-ol
30/04/2009 10:22:49
5 minutes
30/04/2009 10:27:49
10 minutes
30/04/2009 10:32:49
15 minutes

3.4.10: Using a secretory lysosomal marker to measure the effectiveness of RBL-2H3 stimulators in UV-irradiated or alcohol treated cells

The effects of butanol and UV irradiation on secretion were characterised using the β-hexosaminidase assay as described previously (Section 3.3.1). Cells were first treated with 0.3% butan-1-ol or butan-2-ol for 15 minutes at 37^{o}C/5% CO_2 or UV-irradiated (600 mJ). Treated cells were then stimulated using 100 nM PMA or 0.1 µg/ml DNP-BSA and cells stimulated using antigenic stimulation were primed overnight using 1 µg/ml anti-DNP IgE. Neither butanol treatment nor UV irradiation significantly affected the percentage β-hexosaminidase secretion compared to untreated cells (see Fig. 3.39). RBL-2H3 cells were unresponsive to PMA stimulation and neither butanol nor UV irradiation affected the percentage of β-hexosaminidase secreted. Antigenic stimulation of RBL-2H3 cells treated with butan-1-ol or butan-2-ol were not significantly different from control IgE stimulation (analysed using the 2-tailed Student's t-test). Antigenic stimulation of UV irradiated cells was significantly different from control cells (analysed as previously described). UV irradiated cells treated with Triton X-100 expelled ~35% β-hexosaminidase when compared to control cells treated with 0.1% Triton X-100.

Figure 3.39: The effect of UV irradiation and butanol on RBL-2H3 mast cell section in response to PMA, A23187 and IgE-antigen using the secretory lysosomal marker β-hexosaminidase. RBL-2H3 cells were grown on 12-well plates to approximately 80-90% confluencey 24 hours prior to the β-hexosaminidase assay. Cells stimulated with IgE-antigen were primed overnight using 1 µg/ml anti-DNP IgE (in complete DMEM). Cells were treated with either 0.3% butan-1-ol (But-1) or butan-2-ol (But-2) for 15 minutes at 37°C/5% CO_2. Cells were UV-irradiated using a UV crosslinker for 600 mJ. RBL-2H3 cells were stimulated using 100 nM PMA for 60 minutes in 250 µl HBSS + 20 mM HEPES + 1 mM Ca^{2+} at 37°C/5% CO_2. Primed RBL-2H3 cells were stimulated using 0.1 µg/ml DNP-BSA for 60 minutes. 0.1% Triton X-100 was used to treat cells for 5 minutes before scraping. UV irradiated cells were also treated with Triton X-100 (UV Triton X-100). All treated cells were scraped and centrifuged at 13,000 RPM for 5 minutes. 20 µl of the supernatant was combined with 20 µl 1 mM p-nitrophenol-N-acetylglucosamide (in 0.1 M sodium citrate, pH 4.5) in a 96-well plate and incubated at 37°C/5% CO_2 for a further 60 minutes. The reaction was terminated using 200 µl 0.1 M sodium carbonate and sodium hydrogen carbonate, pH 10.5. Results were measured continuously using the 405 nm filter on a plate reader and calculated as a percentage of the values recorded for Triton X-100 treated cells. All assays were read in triplicate and repeated at least 3 times. The data presented are the means of these experiments.

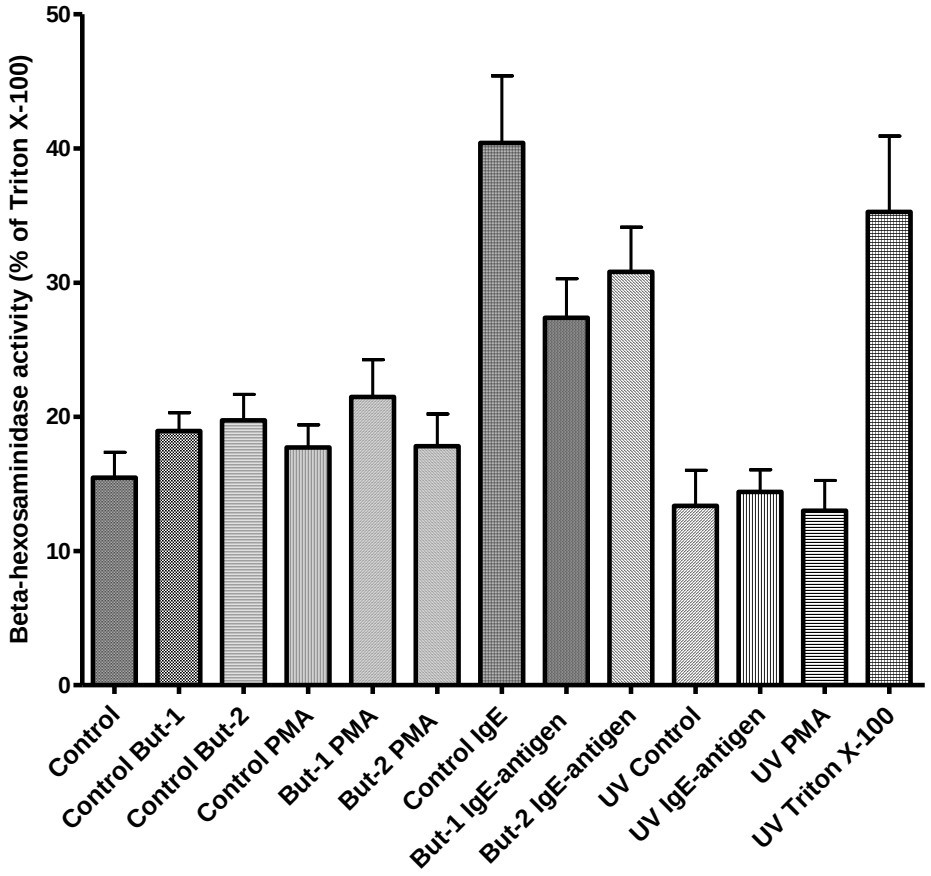

3.5 Discussion

3.5.1: Characterising the localisation and stability of the novel fluorescent lipid

The novel fluorescent form of phosphatidylcholine (fPtdCho) was used to label RBL-2H3 mast cells and consistently localised in punctiform structures within the cell body and processes. These punctate structures were approximately 1 µm in diameter and could be stably labelled for up to 24 hours (the longest time-point taken). Although the novel lipid could potentially be hydrolysed by a number of phospholipases *in vivo* (including PLA_2, PLC and PLD), the punctiform structures imaged using confocal microscopy were most likely of the intact lipid confirmed using the Bligh-Dyer lipid extraction method (see Fig. 3.2). The characteristic punctate localisation of the fPtdCho in RBL-2H3 cells was not consistent between fibroblast, epithelial and insulin-secreting cell lines. RBL-2H3 cells labelled with the novel fluorescent lipid showed no co-localisation between the lipid and plasma membrane, mitochondrial or nuclear markers. Similarly, the localisation of an acyl-modified BODIPY-labelled PtdCho was distinct to that of the novel fPtdCho. Although the same fluorescent group (BODIPY) was used on both forms of phosphatidylcholines, the hydrophobic groups attached to the novel lipid may have influenced its localisation *in vivo*. In fact, fully hydrophilic fluorogenic PtdCho analogues have been synthesised to integrate into the lipid bilayer easily and act as substrates for various lipases including PLD (Rose and Prestwich, 2006).

Although PLD1 expression varies between cell lines, it has been shown to localise to lysosomes and, in unstimulated RBL-2H3 cells, GFP-PLD1 localises with lysosomal and secretory granule markers (Brown *et al*., 1998; Toda *et al*., 1999). Most cells of haematopoietic lineage, including mast cells, have modified the function of their lysosomes to store newly synthesised secretory proteins rather than degrade unwanted protein (reviewed in Blott and Griffiths, 2002). Secretory lysosomes not only remain acidic and retain proteins used for degradation, they also possess the facility to undergo regulated exocytosis (reviewed in Blott and Griffiths, 2002; Griffiths, 1996). The lysosomal marker, LysoTracker Red is an acidotropic molecular probe and specifically targets acidic compartments such as the secretory lysosomes in RBL-2H3 cells (Kaur and Cutler, 2002; Satio *et al*., 2004). The novel

fPtdCho showed approximately 50% localisation with the lysosomal marker in RBL-2H3 cells. This co-localisation suggests that there are two 'pools' of secretory vesicles in RBL-2H3 cells, one of which is populated with the PLD substrate PtdCho and another which is not. As the lysosomal marker labels all acidic compartments within the cell, it is possible that the fPtdCho accumulates only in the vesicles which are dependent on PLD activity (confirmed using butan-1-ol). In support of this hypothesis, LysoTracker Red-labelled lysosomes in PFA-fixed samples co-localised up to 50% with a histamine antibody. Histamine is a marker of secretory lysosomes in mast cells as it is released as part of the inflammatory response (Griffiths *et al*., 1996). Studies characterising the effect of mastoparan analogues suggest that there are two pools of secretory vesicles and that there are differences in the molecular regulation of β-hexosaminidase and 5-hydroxytryptamine (5-HT) exocytosis (Farquhar *et al*., 2002). In addition, PLD activation was correlated with release of β-hexosaminidase but not 5-HT, indicating further that there may be one pool of vesicles which is PLD-dependent and another which acts independently (Farquhar *et al*., 2002).

3.5.2: The effect of UV irradiation on RBL-2H3 cells labelled with fluorescent PtdCho or LysoTracker Red

UV irradiation of RBL-2H3 cells initiates apoptosis, and this type of cell death is characterised by membrane blebbing, cell shrinkage, mitochondrial and nuclear disruption, phosphatidylserine exposure, fragmentation of DNA and finally ordered fragmentation into membrane-enclosed bodies (Degtereve *et al*., 2003; Assunção Guimarães and Linden, 2004; Wright *et al*., 2008). PLD1 contains a caspase 3 cleavage site, which could play a role in regulating the apoptotic program (Wright *et al*., 2008). The expression of a caspase 3 resistant PLD1b in HEK-293 cells reduced PtdCho hydrolysis (initiated by UV irradiation), suggesting that PLD may be a target for caspase mediated destruction, or become deregulated when cleaved by caspase 3 during apoptosis (Wright *et al*., 2008). The organelles labelled by the novel fPtdCho in RBL-2H3 cells were probably degraded and the cellular contents not expelled, indicating regulated apoptosis. As a result, lipid localisation became diffuse and labelled the cytoplasm but did not disappear from the cells altogether. This suggests that deregulation of PLD1 also had an impact on the rate of fPtdCho hydrolysis and,

consequently, PtdOH production. As labelled RBL-2H3 cells were initiated into apoptosis with UV treatment, which caused the fPtdCho-labelled vesicles to disappear, this suggests that they are a target for the apoptotic program. As apoptosis is cell death without inflammation and release of inflammatory mediators, this is consistent with the structures being inflammatory vesicles. Reduction of fluorescence of the novel fPtdCho could also be attributed to photobleaching of the BODIPY tag as a result of UV irradiation, although punctate labelling was maintained immediately after UV treatment and only became diffuse after approximately 5 hours. Further experiments using other apoptotic initiations such as TNF-α or TNF-β would eliminate the risk of photobleaching the substrate and may further support the hypothesis (Teraki *et al*., 1999).

3.5.3: The effect of antigenic stimulation on RBL-2H3 cells labelled with fluorescent PtdCho or LysoTracker Red

Antigenic stimulation of mast cells requires cross-linking of the high affinity IgE receptor FcεRI (Toru *et al*., 1996). Antigen stimulation of RBL-2H3 cells resulted in secretion of ~40% of total β-hexosaminidase. The fPtdCho which is thought to localise to secretory granules was not secreted upon antigenic stimulation. The lysosomal marker LysoTracker Red retained punctate localisation upon antigenic stimulation, although the fluorescence yield was reduced. In RBL-2H3 cells, eGFP-PLD1b co-localises with secretory granule and lysosomal markers (Brown *et al*., 1998) and the fPtdCho PLD substrate possibly localises to the same structures.

PLD has been identified as a key regulator of RBL-2H3 exocytosis and the inhibition of PtdOH production by PLD results in a notable reduction in β-hexosaminidase secretion in RBL-2H3 cells (Brown *et al*., 1998). However, RBL-2H3 cells treated with butan-1-ol exhibited little difference in β-hexosaminidase secretion when compared to controls and butan-2-ol treated cells. Although β-hexosaminidase secretion was unaffected, the characteristic punctate localisation of fPtdCho was lost once treated with butan-1-ol. The novel fPtdCho maintains its punctate localisation in butan-2-ol treated cells. This suggests that the membrane fusion events and signalling cascades facilitated by PtdOH are necessary in the maintenance of punctate lipid labelling. PtdOH produced in a PLD-dependent manner may

contribute either structurally to membrane integrity or downstream as it is also a known second messenger. Antigenic PLD stimulation required sustained PtdOH production during membrane ruffling and this implicates PLD activity in the localisation of the novel fPtdCho (O'Luanaigh *et al*., 2002). Butan-1-ol treated cells labelled with fPtdCho did not appear to respond to antigenic stimulation by membrane ruffling and truncating of cell processes, although β-hexosaminidase assay data were inconclusive. The lack of response to antigenic stimulation (characterised by membrane ruffling) in RBL-2H3 cells treated with butan-1-ol has been documented elsewhere and is reversible (O'Luanaigh *et al*., 2002). In addition, membrane ruffling was shown to be independent to exocytosis of secretory granules, therefore supporting the confocal data presented here (O'Luanaigh *et al*., 2002).

3.5.4: The effect of PMA stimulation on RBL-2H3 cells labelled with novel fluorescent lipid or LysoTracker Red

RBL-2H3 cells labelled with either LysoTracker Red or the novel fPtdCho were stimulated using PMA to activate PKC (most notably the Ca^{2+}-dependent PKCα), a known PLD1 activator (Takai *et al*., 1979; Castagna *et al*., 1982). Although mast cells degranulate upon stimulation with PMA, they do not secrete β-hexosaminidase which supports the suggestion that there are two pools of secretory vesicles in RBL-2H3 cells (Brown *et al*., 1998; Farquhar *et al*., 2002). These results were confirmed as PMA stimulated cells secreted only ~3% more than control (i.e. unstimulated) cells. There was a notable change in the cell morphology upon PMA stimulation, although both the novel fPtdCho and LysoTracker Red retained their punctiform localisation.

3.5.5: The effect of a calcium ionophore (A23187) on RBL-2H3 cells labelled with novel fluorescent lipid or LysoTracker Red

The calcium ionophore A23187 increases intracellular calcium, so resulting in mast cell degranulation. Mast cells express the calcium and phospholipid-binding synaptotogamins (Syt) II, III and V on their secretory vesicles (Baram *et al*., 1999; reviewed in Stinchcombe and Griffiths, 2001). Mast cell excoytosis is mediated by membrane fusion events controlled by soluble N-ethylmaleimide-sensitive fusion

factor attachment proteins (SNAREs) which are regulated by Syt and Rab proteins (reviewed in Schimmöller *et al*., 1998). SNAREs vary between different organelles but their function is to bring together vesicle SNAREs (v-SNAREs) which interact with target membranes (t-SNAREs) or vesicle associated membrane proteins (VAMPs – Puri and Roche, 2008). Mast cells express syntaxins 2, 3 and 4, VAMPs 2, 7 and 8, and synaptosome-associate protein (SNAP)-23 (Hibi *et al*., 2000; Paumet *et al*., 2000; Puri and Roche, 2008). VAMP-2 is not involved in exocytosis whilst VAMP-8 has recently been identified as a key regulatory protein of secretory granule exocytosis (Arora *et al*., 1994; Puri and Roche, 2008). The increase in intracellular Ca^{2+} concentration associated with A23187 treatment of RBL-2H3 cells did not impact upon localisation of the novel fPtdCho. However, the acidotropic marker LysoTracker Red leached out from degranulating RBL-2H3 cells within 5 minutes of A23187 treatment. The impact on the lysosomal marker could be attributed to a pH change within the lysosomes as their acidic content would have been expelled more aggressively than in antigen-IgE- or PMA-stimulated cells, which resulted in degranulation through a PLD-dependent pathway. LysoTracker Red and the novel fPtdCho may also be labelling different parts of the secretory vesicle. As the novel lipid is retained and LysoTracker Red is not, the lysosomal marker is likely to be within the vesicle whilst the novel lipid is more likely to localise to the vesicular membrane.

3.5.6: The impact of a wortmannin or MBCD on LysoTracker Red or fluorescent PtdCho labelled RBL-2H3 cells

Phosphatidylinositol 4,5-bisphosphate (PtdIns(4,5)P_2) is a lipid activator of PLD both *in vivo* and *in vitro* (Hodgkin *et al*., 1999). The pleckstrin homology (PH) domain of PLD uses lipids such as PtdIns(4,5)P_2 to anchor the lipase to membranes *in viv*o or to vesicles containing PtdIns(4,5)P_2 *in vitro* (Hodgkin *et al*., 2000; Höer *et al*., 2000). PtdIns(4,5)P_2 is phosphorylated to phosphatidylinositol 3,4,5-triphosphate (PtdIns(3,4,5)P_3) which has also been found to increase the activity of myocardial PLD in human atrial tissue, but with lower efficiency than PtdIns(4,5)P_2 (Kruz *et al*., 2004). Both PLD1 and PLD2 respond to PtdIns(4,5)P_2 stimulation (Frohman *et al*., 1999; Kruz *et al*., 2004). The fungal metabolite wortmannin has been found to inhibit PLC and PLD activity in neutrophils, possibly by acting as a

phosphatidylinositol 3-kinase (PtdIns 3-kinase) inhibitor (Reinhold et al., 1990; Bonser *et al*., 1991; Cross *et al*., 1995; Cross *et al*., 1997). PtdIns 3-kinase activity is receptor initiated and phosphorylates PtdIns(4,5)P_2 to PtdIns(3,4,5)P_3 (Reinhold et al., 1990; Bonser *et al*., 1991; Cross *et al*., 1995; Cross *et al*., 1997). Treatment of RBL-2H3 cells with wortmannin did not affect the punctate localisation of the novel fPtdCho or the lysosomal marker LysoTracker Red. Wortmannin is used as a PLD inhibitor and is known to inhibit several other lipases (including PLC and PLA_2) at concentrations higher than that needed for PtdIns(4,5)P_2 inhibition (Cross *et al*., 1995). The fluorescent PLD substrate was unaffected by wortmannin treatment but additional information could be gathered if PLD was stimulated by PMA or IgE after wortmannin treatment and analysing fluorescence oscillations.

Methyl-β-cyclodextrin (MBCD) removes cholesterol from the plasma membrane (Hiroyama and Exton, 2005b) and, in HeLa cells, the localisation of PLD was unaffected by cholesterol depletion (Hiroyama and Exton, 2005b). MBCD treatment of RBL-2H3 cells labelled with the fPtdCho or LysoTracker Red did not change the localisation of either marker. This suggests that, like PLD, its substrate localises to the secretory lysosomes independent of the cholesterol content of the plasma membrane.

3.5.7: The effect of microtubule or cytoskeletal dynamics on RBL-2H3 cells labelled with novel fluorescent lipid or LysoTracker Red

Microtubules are arranged in polymerised tubulin heterodimers (composed of α- and β-tubulin) and play an important role in many cellular processes, including intracellular transport of vesicles (Gupta Jr. *et al*., 2003; Jordan and Wilson, 2004). Paclitaxel is an anti-tumour agent that promotes assembly and stabilisation of microtubules (Gupta Jr., *et al*., 2003; Jordan and Wilson, 2004). Nocodazole treatment of HeLa cells results in microtubule depolymerisation, redistribution of tubulin and contractile morphology (Chang *et al*., 2008). There appeared to be no change in movement or localisation of punctate structures labelled with LysoTracker Red or fPtdCho in RBL-2H3 cells. This suggests that the localisation and movement of these structures is independent of the microtubule network.

RBL-2H3 cells were labelled and treated with two inhibitors which can influence the organisation and stability of the actin cytoskeleton. Cytochalasin D (CD) is an inhibitor of actin polymerisation and is thought to 'prime' RBL-2H3 cells to antigenic stimulation (Oka *et al*., 2002). CD treated RBL-2H3 cells sensitised with IgE exhibited an increase in actin assembly, degranulation and intracellular Ca^{2+} (Oka *et al*., 2002). However, our results showed no impact on β-hexosaminidase secretion in RBL-2H3 cells treated with CD and antigenic stimulation. Despite CD having no effect on β-hexosaminidase secretion of RBL-2H3 cells, both fPtdCho and LysoTracker Red changed localisation. Both fluorescent markers were localised to the tips of the cell processes although their movement was not inhibited. CD has been found to cause irregular areas of *de novo* F-actin aggregation, whilst depolymerising pre-existing actin in a human breast cancer cell line (Mortensen and Larsson, 2003). One possibility is that the inhibition of actin polymerisation did not inhibit the movement of the labelled vesicles but did cause the concentration of LysoTracker Red or novel fPtdCho to the bases and the tips of the cell processes. These areas may be points at which actin polymerisation activity was at its greatest. Treating RBL-2H3 cells with CD and then staining with rhodamine-phalloidin could show whether these points of fPtdCho and LysoTracker Red 'pooling' correlated with actin formation.

Latrunculin B (Lat B) is a macrolide toxin (from Red Sea sponge) that destabilises actin filaments. Latrunculin binds to G-actin released from the actin filaments at a 1:1 ratio and prevents its re-incorporation into a fibre (Pendleton and Koffer, 2001). In contrast to CD, Lat B depletes F-actin over a period of time, dependent upon the rate of filament turn-over (Ayscough *et al*., 1997; Pendleton and Koffer, 2001; Mortensen and Larsson, 2003). The movement of fPtdCho in RBL-2H3 cells was not inhibited upon treatment with Lat B. However, the novel fPtdCho accumulated to specific points within the RBL-2H3 cells, which were visually similar to those seen after CD treatment. The similarity in the effect of the two inhibitors indicates that, although the movement of the fPtdCho was not inhibited, the fusion events between vesicle and plasma membrane or other vesicles may be regulated by the actin cytoskeleton. Dependending on the conditions, mast cells pre-treated with 40 µg/ml Lat B and stimulated using the compound 40/80 showed a decrease between ~20-30% in β-hexosaminidase secretion (Pendleton and Koffer, 2001). RBL-2H3

cells treated with Lat B and stimulated with antigen-IgE or A23187 showed no difference in β-hexosaminidase secretion. The discrepancy between our results and published data may be due to the difference in cell type and treatment conditions associated with mast cell stimulation. Evanescent-field fluorescence microscopy was used to assess the movement of secretory vesicles along fluorescently labelled actin fibres in neuroendocrine PC-12 cells (Lang *et al*., 2000). Although some secretory veiscles were mobile (along F-actin bundles) others appeared 'docked' or restrained by the actin cytoskeleton (Lang *et al*., 2000; Burgoyne and Morgon, 2003). In addition, PC-12 cells treated with Lat B showed diminished vesicle movement (Lang *et al*., 2000; Burgoyne and Morgan, 2003). This is consistent with the accumulation of vesicles labelled with fPtdCho observed at the bases and the tips of cell processes of RBL-2H3 cells treated with Lat B or CD. Further characterisation of membrane fusion (in excotytosis) and vesicular movement along the actin cytoskeleton in chromaffin cells – using total internal reflection fluorescent microscopy (TIRFM) – suggests that the disruption of actin dynamins does not significantly impact upon granule motion (Allersma *et al*., 2006; Burchfield *et al*., 2010).

Our data indicate that the actin cytoskeleton is integral to the trafficking of fPtdCho labelled vesicles in RBL-2H3 cells. Treatment with inhibitors does not appear to affect the movement of the fPtdCho-labelled structures, however this project was unable to measure the rate and distance over which these vesicles move. Quantifying the speed and distance of fPtdCho-labelled structures in non-treated RBL-2H3 cells would enable an analysis of inhibitor-treated cells and the effect on labelled vesicles. The movement and accumulation of the fluorescently labelled vesicles suggests that there may be two populations of vesicles which move using different mechanisms and so are not inhibited by identical treatments. Furthermore, developing a live actin label which is either Cherry- or eGFP-labelled would facilitate real-time analysis of fPtdCho- or LysoTracker Red-labelled vesicles in RBL-2H3 cells, and the effect of cytoskeletal inhibitors on their movement.

Chapter 4: Establishing a novel fluorescent *in vitro* PLD assay

4.1: Introduction

Members of the phospholipase D (PLD) superfamily hydrolyse the phosphodiester bond of glycerophospholipids to release a free (unphosphorylated) head group and phosphatidic acid (PtdOH). Mammalian PLD preferentially hydrolyses PtdCho – generating PtdOH and a choline – and predominantly exists in two isoforms, PLD1b and PLD2a, the expression levels of which vary markedly between cell lines (Meier *et al*., 1999).

Members of the PLD superfamily are found in a wide variety of organisms including bacteria, plants and mammals, and are characterised by the presence of a conserved **H**x**K**$(x)_4$**D**$(x)_6$GSx**N** (HKD) motif (where x is any amino acid – Ponting and Kerr, 1996; Stuckey and Dixon, 1999). The HKD motif consists of conserved histidine, lysine, aspartate, and asparagine residues that are essential for the enzyme activity of PLD (Ponting and Kerr, 1996; Stuckey and Dixon, 1999). The lysine residue in the HKD motif is thought to aid substrate-binding of PLD and, when mutated, renders the lipase inactive (Sung *et al*., 1997; Davies *et al*., 2002; Fedeli *et al*., 2006). The first crystal structure of a PLD superfamily member was of the bacterial endonuclease Nuc – isolated from the pKM101 plasmid of *Salmonella typhimurium*. The crystal structure of Nuc provided structural information as to how two HKD motifs from separate Nuc endonucleaes lie in parallel to form a single active site joined by hydrogen bonds (Stuckey and Dixon, 1999). Mammalian PLD has two HKD motifs which are thought to form an interactive catalytic site analogous to that characterised in Nuc which is either homodimeric (between HKD motifs of the same PLD) or heterdimeric (between HKD motifs of separate PLDs - Kam and Exton, 2002).

PLD1 and 2 have up to 50% sequence conservation between the regions that contribute to their regulation and substrate specificity (Sung *et al*., 1999b). Sequence comparison between human PLD1 and 2 with Bruton's tyrosine kinase (Btk) – an

enzyme known to contain a pleckstrin homology (PH) domain – identified a conserved PH domain. The inositol-phosphate binding site in the PH domain of Btk was characterised as involving residues Lys228, Ser230 and Arg253. The PLD PH domain was phosphatidylinositol 4,5-bisphosphate (PtdIns(4,5)P_2) binding-specific (Hodgkin *et al*., 2000). Deletion of the PH domain renders PLD inactive whilst point mutations within the conserved PH domain inhibits PLD activity and prevents normal localisation (Hodgkin *et al*., 2000).

A *phox* (PX) domain in the N-terminal region of PLD is also conserved in human and nematode PLDs (Liscovitch *et al*., 2000). N-terminal deletions up to 325 amino acid residues do not greatly affect basal PLD activity (Sung *et al*., 1999b) and the PX domain may have a role in regulation rather than catalytic activity (Liscovitch *et al*., 2000). *In vivo* deletion of the PX domain of PLD1 increases basal activity of the lipase whilst retaining PKCα responsivity. However, *in vitro* PLD1 is rendered inactive and non-responsive to Arf, Rho and PKCα when the PX domain is deleted (Sung *et al*., 1999b). The PX domain of PLD1 has a high affinity for 3-phosphorylated inositides which increases enzymatic activity (Lee *et al*., 2005). The PX domain of PLD2 is implicated in the activation of PKCζ through direct interaction with its kinase region and independent of lipase activity (Kim *et al*., 2005).

Although PLD1 and 2 contain highly conserved regulatory regions and PLD1 splice variants (PLD1a and PLD1b) have 99.9% homology, they may undertake different intracellular functions (Katayama *et al*., 1998). PLD1 has been characterised extensively in the context of activators which stimulate PLD1 both *in vivo* and *in vitro*. The splice variant related to the current project – PLD1b – is activated in the presence of PtdIns(4,5)P_2, ADP-ribosylation factor (Arf1 or Arf6), protein kinase Cα (PKCα), and members of the Rho superfamily (Hammond *et al*., 1995; Hammond *et al*., 1998; Katayama *et al*., 1998). *In vitro* PLD1 assays using radio-labelled phosphatidylcholine (PtdCho) in the presence of cofactors shows synergistic stimulation of enzyme activity (Hammond *et al*., 1997). PLD2 is unresponsive to small G-protein activation and there is conflicting evidence of PLD2 activation by sodium oleate *in vitro* (Katayama *et al*., 1998; Massenburg *et al*., 1994).

In the past, most *in vitro* PLD assays monitored enzyme activity using tritiated PtdCho and produced a single data point that reflected the particular conditions used in the assay. PLD would be incubated with a small proportion of dipalmitoylphosphatidyl [methyl ^{3}H]-choline ([^{3}H]-$(Pam)_2$PtdCho) substrate in a complex with native PtdCho (isolated from lecithin egg yolk) and PLD hydrolysis would produce water-soluble choline (Kupferberg *et al*., 1981; Wang and Wang, 2001). The vesicles used to assess PLD-activity *in vitro* differed depending on the source of protein (e.g. plant or mammalian PLD) and the PLD isoform. Vesicles would typically contain phosphatidylethanolamine, phosphatidylinositol 4,5-bisphosphate and PtdCho of which the radiolabelled PtdCho would make up a very small proportion (Brown *et al*., 1993; Massenburg *et al*., 1994; Kim *et al*., 1999; Wang and Wang, 2001). Assays for PLD2 frequently included either sodium oleate or oleic acid dependending on the assay (Chalifa *et al*., 1990; Messenburg *et al*., 1994; Kim *et al*., 1999; Wang and Wang, 2001). The incorporation of sodium oleate meant that there was detergent (activity) present in the assay so that lipid vesicles formed readily. Typically the reactions were incubated at 37^{o}C and terminated using a chloroform/methanol solvent mixture or trichloroacetic acid and bovine serum albumin (BSA – Brown *et al*., 1993; Kim *et al*., 1999; Farquhar *et al*., 2007). The phases were then separated and the aqueous phase containing [^{3}H]-choline quantified by liquid scintillation counting/spectroscopy (Brown *et al*., 1993; Kim *et al*., 1999; Hodgkin *et al*., 1999; Farquhar *et al*., 2007). Although thin layer chromatography (TLC) was also used to analyse and quantify *in vitro* assay results, liquid scintillation counting was more common (Chalifa *et al*., 1990). In addition, new methods of *in vitro* analysis were developed including ^{31}P NMR, ^{1}H NMR and fluorescent TLC (where BODIPY-PtdCho was incorporated into vesicles – Ella *et al*., 1994; Yang and Roberts, 2003).

Fluorogenic analogues of PtdCho have been synthesised and phospholipases C and D were used to evaluate their application as lipase substrates (Rose and Prestwich, 2006). The amphiphilic PtdCho analogues were synthesised to allow integration into cells via the lipid bilayer and so facilitate lipase assays *in vivo* (Rose and Prestwich, 2006). A novel fluorescent PtdCho (fPtdCho) substrate was used to further develop the fluorescent TLC assays, first used to characterise PLA_2 activity (Feng *et al*., 2002). The novel fPtdCho is labelled with BODIPY at the choline head group and,

whilst intact, BODIPY fluorescence is internally quenched by non-fluorescent aromatic groups attached to the acyl-chains (Fig. 3.1). When the lipid is hydrolysed by PLD to release the BODIPY-labelled choline head group, fluorescence emission increases. Fluorescent *in vitro* assays were developed using previously established assay conditions (Hodgkin *et al*., 1999; Farquhar *et al*., 2007). In this project, collection of consecutive data points from these fluorescent assays permitted the recording of PLD activity in real-time. The opportunity to monitor the effect of small G-protein activators on PLD1b activity in real-time could help characterise their interactions and ultimately the rate at which they stimulate lipase activity. The previously established radiolabelled PLD assays were not sensitive enough to monitor the effects of assay components, such as magnesium (Mg^{2+}) and calcium (Ca^{2+}) in the absence of activators. As data was collected concurrently, the effect of Mg^{2+} and/or Ca^{2+} ions on PLD activity could be monitored in real-time by measuring fluorescence emission over time.

The novel fluorescent version of the *in vitro* PLD assay provides an opportunity to characterise further PLD catalysed hydrolysis and its interaction with activators in real-time. The product of a single assay is now up to 500 data points, thus yielding significantly more kinetic information resulting from altered assay conditions. Eventually this fluorescent *in vitro* assay could also be used to assess the stoichiometry between small G-proteins and PLD activity by using PLD as an effector.

4.2: Activation of GST-hPLD1 using small G-protein or protein kinase activators

A newly developed real-time assay utilised the unique properties of a fluorescent PtdCho (fPtdCho) substrate to characterise GST-hPLD1b activity. Although the novel fluorescent lipid intramolecularly quenches the BODIPY labelled choline, this process is not 100% efficient. The vesicles used in this real-time assay incorporated the fPtdCho and therefore had a basal level of fluorescence, which was recorded for each experiment. Background fluorescence (measured with all assay components except the fluorescent vesicles and protein) was also recorded for each experiment. As the lipid was hydrolyzed by GST-hPLD1, fluorescence in the assay increased (as the BODIPY labelled head group was no longer internally quenched), therefore indicating GST-hPLD1 enzyme activity.

Real-time *in vitro* assays were completed in a final volume of 100 µl at 37^{o}C. The core components of each assay consisted of 50 µl lipid vesicles, 50 µM GTPγS and 400 mM NaCl. Vesicles constituted 100 µg L-α-phosphatidylethanolamine (PtdEth), 50 µg phosphatidylinositol-4,5-bisphosphate (PtdIns(4,5)P_2) and 0.5 µg of the fluorescent lipid. Lipids were combined and dried under a stream of nitrogen gas before resuspending in 400 µl sonication buffer (refer to Section 2.10.1). Known GST-hPLD1 activators such as PKCα, Rac1 and Arf1 were used to determine the activity and responsiveness of purified recombinant GST-hPLD1 protein preparations. 2 µg of each activator was added to the assay immediately prior to recording fPtdCho hydrolysis by using relative fluorescence emitted. The most effective stimulation of GST-hPLD1 was achieved using a combination of wildtype Arf1 and Rac1 (Hodgkin *et al*., 1999). Fluorescence readings were taken at 2 second intervals using a fluorimeter, and data were recorded concurrently using excitation at 485 nm and fluorescence emission detection at 535 nm. Established tritiated assay conditions were adjusted to accommodate the changed fluorescent assay but used similar concentrations of magnesium (Mg^{2+} – 3 mM), calcium (Ca^{2+}– 2 mM) and the non-hydrolysable GTP analogue (GTPγs – 50 µM).

In the absence of protein activators, basal GST-hPLD1 activity was low with only a small increase in emitted fluorescence over 60 minutes compared to that of the

fluorescence vesicles alone. Combined activation of GST-hPLD1 by wildtype Arf1 and Rac1 proved to be the most effective and reproducible *in vitro* activation of the protein. The combined activation of GST-hPLD1 by wildtype Arf1 and Rac1 and GTPγS resulted in an increase in emitted fluorescence of approximately 15,000 fluorescence units compared to unactivated GST-hPLD1 (see Fig. 4.1). The activated GST-hPLD1 protein showed a marked increase in fluorescence emission (i.e. activity) approximately 10 minutes after the assay was commenced. This lag period was consistently present in assays utilising GST-hPLD1 activators. The lag time was attributed to the time taken for assay contents to form a activation complex and the time taken for components to reach 37^{o}C. The results were recorded concurrently so that basal activity and activation response times of GST-hPLD1 could be directly compared.

Although activation was robust, the magnitude of response was dependent on the protein preparation used. Small scale infections of Sf9 cells with GST-hPLD1-expressing baculovirus produced numerous protein preparations which were then used in *in vitro* assays. In each experiment, a lag time of between 10-20 minutes (dependent on GST-hPLD1 concentration) was present before changes in fluorescence were detected.

Figure 4.1: The effect of wildtype Arf1 and Rac1 on GST-hPLD1 activity using a fluorescent PtdCho substrate. Assays included 50 µl of extruded fPtdCho containing vesicles, 50 µM GTPγS, 400 mM NaCl, 3 mM Mg^{2+}, 2 mM Ca^{2+} and 2 µg of each activator – Arf1 and Rac1 (wt). All assay components (except vesicles) including activators and 10 µl GST-hPLD1 protein were added to each well and kept on ice. Immediately before the assay was commenced, vesicles were added to begin the assay. Fluorescence emissions were recorded using a fluorimeter (at 37 ^{o}C) for 60 minutes. The hydrolysis of fPtdCho was detected using an excitation aperture at 485nm and an emission filter of 535 nm. Fluorescence emissions were accrued at 2 second intervals and recorded concurrently. The change in fluorescence due to GST-hPLD1 (▼) was compared to vesicles incubated without lipase (▲). Background fluorescence was monitored in a well containing water (■). The response of GST-hPLD1 protein to its wildtype Arf1 and Rac1 small G-protein activators (●) was compared to basal GST-hPLD1b activity (▼). This real-time *in vitro* assay was repeated at least twice to ensure results were robust.

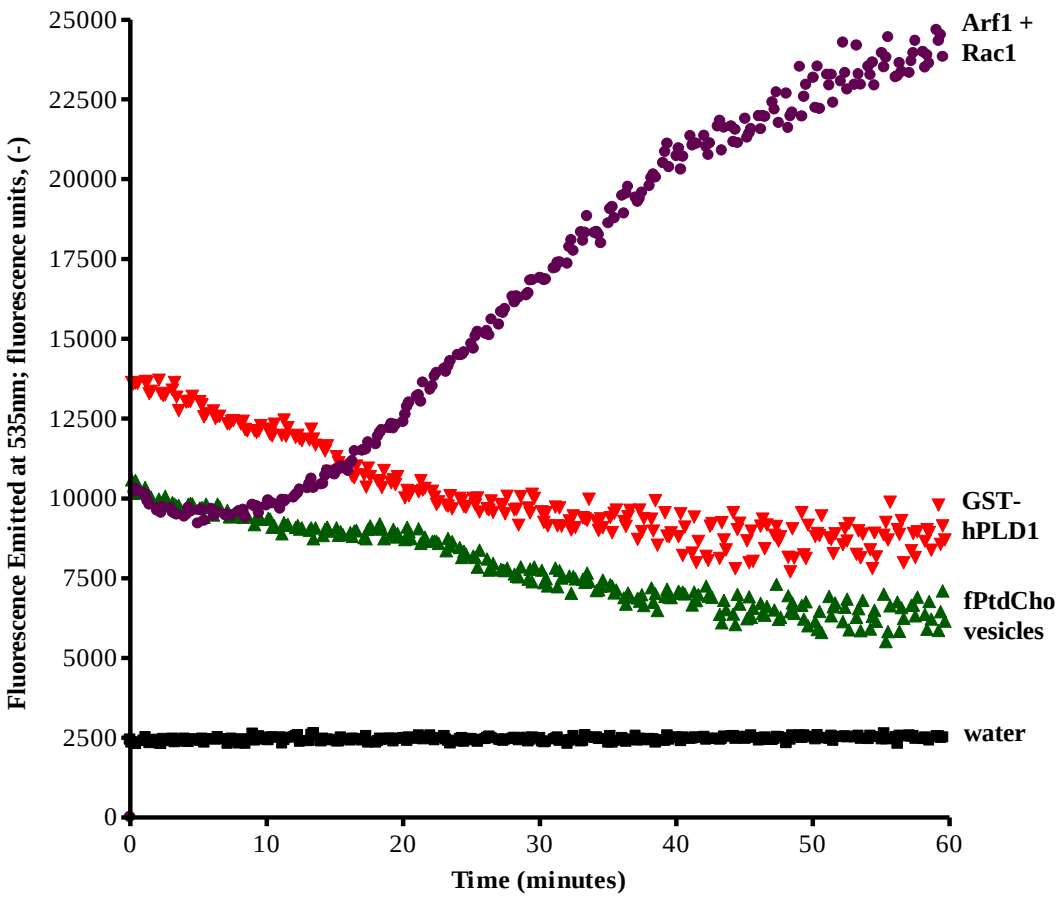

The activity of GST-hPLD1 was assessed in relative emitted fluorescence compared to the fluorescence of vesicles (containing the fPtdCho) alone. The lipid had some residual basal fluorescence which remained consistent throughout all the experiments (see Fig. 4.2). The blank (i.e. water) which controlled for background fluorescence also remained consistent throughout the experiment (data not shown). GST-hPLD1 activity increased dramatically as wildtype Arf1 and Rac1 activated the lipase (see Figs. 4.1 and 4.2). However, the magnitude of activation of GST-hPLD1 by each small G-protein individually using this fluorescent *in vitro* assay was unknown. Tritiated assays using lysates from the HL60 cell line indicated that Arf1 enhanced GST-hPLD1 activity more effectively than Rac1 (Hodgkin *et al*., 1999). In this fluorescent assay, wildtype Arf1 increased GST-hPLD1 activity more than wildtype Rac1 (see Fig. 4.2). The fluorescence emitted was lower for GST-hPLD1 activated by individual small G-proteins, so indicated that wildtype Arf1 and Rac1 synergistically activate GST-hPLD1 (Hammond *et al*., 1995).

The presence of a lag time between the start of the assay and activation of GST-hPLD1 by small G-proteins was a consistent feature. The lag time of GST-hPLD1 activated by single activators (either wildtype Arf1 or Rac1) was approximately 10 minutes (see Fig. 4.2). After the lag time, emitted fluorescence increased linearly so indicating that GST-hPLD1 had been activated. The activation of GST-hPLD1 by the combined small G-proteins reduced the lag time to approximately 5 minutes.

Figure 4.2: Real-time *in vitro* activation of GST-hPLD1 by wildtype Arf1 or Rac1. Assays contained 50 µM GTPγS, 400 mM NaCl, 3 mM Mg^{2+}, 2 mM Ca^{2+} and 2 µg of each (or both) activators – Arf1 or Rac1. All assay components (except 50 µl fluorescent vesicles) including activators and 15 µl GST-hPLD1 protein were added to each well and kept on ice. Immediately before the assay began, vesicles were added to initiate the assay. Fluorescence emissions were recorded using a fluorimeter (at 37°C) for 60 minutes. The hydrolysis of fPtdCho was detected using an excitation aperture at 485 nm and an emission filter of 535 nm. Fluorescence emissions were accrued at 2 second intervals and recorded concurrently. The change in fluorescence due to GST-hPLD1 (▼) was compared to vesicles incubated without lipase (▲). Background fluorescence (water) was monitored but the data is not shown. The response of GST-hPLD1 protein to its wildtype Arf1 and Rac1 small G-protein activators (●) was compared to basal GST-hPLD1 activity (▼). Fluorescence emissions of reactions where GST-hPLD1 protein was activated by Arf1 (●) or Rac1 (▲) were also compared to basal GST-hPLD1 activity (▼). This real-time *in vitro* assay was repeated to ensure the result was reproducible.

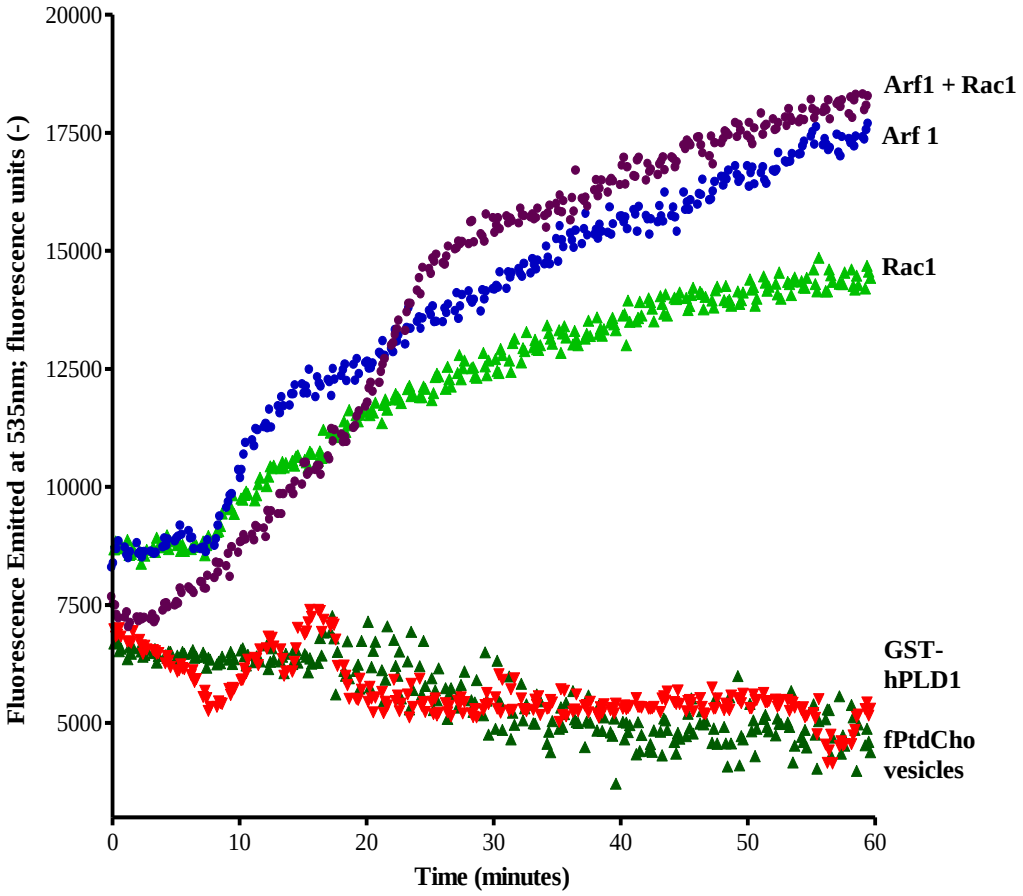

GST-hPLD1 has three main protein activators, i.e. Arf, Rho and protein kinase Cα (PKCα). Previous studies using tritiated *in vitro* assays established that the combined effect of Arf1, Cdc42 and PKCα produced maximal GST-hPLD1 activity (Hodgkin *et al*., 1999). PKCα activation of GST-hPLD1 should have produced similar levels of emitted fluorescence to Arf1 activation of GST-hPLD1. However in this *in vitro* assay system, GST-hPLD1 could not be activated by PKCα (see Fig. 4.3). Activation of PKCα using 100 nM PMA also had no impact on GST-hPLD1 activity. Basal GST-hPLD1 activity steadily increased in the first 60 minutes of the assay and, between 60 and 120 minutes, the activity of activated PKCα, PKCα + 100 nM PMA and basal GST-hPLD1 were similar. Activation of GST-hPLD1 protein using the wildtype small G-protein activators Arf1 and Rac1 were compared to the response resulting from PKCα activation. Arf1 increased GST-hPLD1 activity and the combined activation of GST-hPLD1 by wildtype Arf1 and Rac1 showed a further increase in emitted fluorescence (see Fig. 4.3). The response to small G-protein activators meant that the protein preparation was active but unresponsive to PKCα under these *in vitro* conditions.

Figure 4.3: Comparing GST-hPLD1 activation by small G-proteins and PKCα. Assays were constituted with 50 µM GTPγS, 400 mM NaCl, 3 mM Mg^{2+}, 2 mM Ca^{2+}, and 2 µg of small G-protein activators (wildtype Arf1 or Rac1) or 1 µg PKCα. All assay components (except 50 µl fluorescent vesicles) including activators and 20 µl GST-hPLD1 protein were added to each well and kept on ice. Immediately before the assay commenced, vesicles were added to begin the assay. Fluorescence emissions were recorded using a fluorimeter (at 37°C) for 120 minutes. The hydrolysis of fPtdCho was detected using an excitation aperture at 485 nm and an emission filter of 535 nm. Fluorescence emissions were accrued (approx.) every 2 seconds and recorded concurrently. The change in fluorescence due to GST-hPLD1 (▼) was compared to vesicles incubated without lipase (▲). Background fluorescence (water) was monitored but the data is not shown. Fluorescence emission produced by GST-hPLD1 activation with PKCα (▼) or PKCα + 100 nM PMA (■) was compared to basal GST-hPLD1 activity (▼). Fluorescence emission increase due to GST-hPLD1 activation by wildtype Arf1 and Rac1 (●) or Arf1 alone (●) were used to assess if the protein preparation was active. This real-time *in vitro* assay was repeated twice.

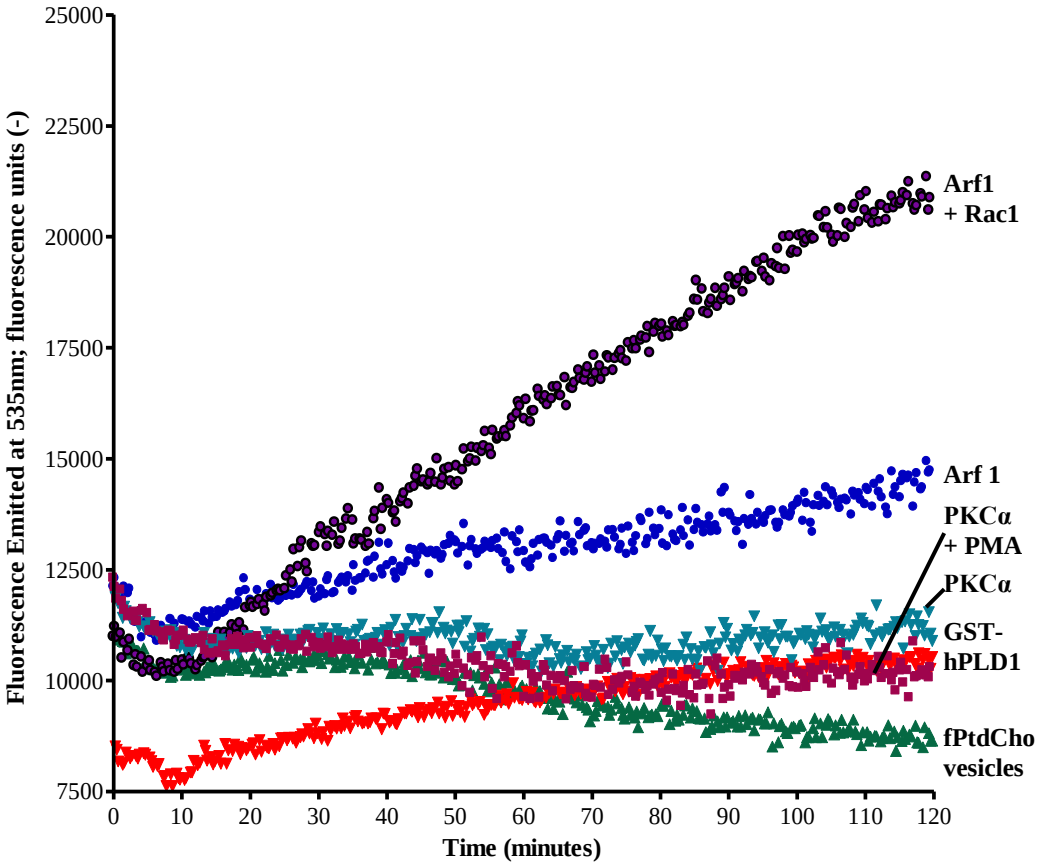

4.3: Assessing the dependence of GST-hPLD1 activity on Mg^{2+} and Ca^{2+}

The conditions originally described for analysing PLD activity *in vitro* were modifications of those used in PLC and PLA_2 assays (Smrcka *et al*., 1991; Murthy and Makhlouf, 1998). As the conditions were designed for the Ca^{2+}-dependent PLA_2 enzyme (Murthy and Makhlouf, 1998), Ca^{2+} was included in the assay. The response of mammalian PLDs to Ca^{2+} concentration has yet to be elucidated, although PLD isolated from porcine lung microsomes showed stimulation by (but not dependence upon) Ca^{2+} and Mg^{2+} (Okamura and Yamashita, 1994; McDermott *et al*., 2004). Standard assay conditions for the fluorescent *in vitro* PLD assay included a combination of 3 mM Mg^{2+} and 2 mM Ca^{2+} ions. The tritated assay was not sensitive enough to detect subtle changes in PLD activity dependent on ion concentrations.

The effects of various concentrations of either Mg^{2+} or Ca^{2+} on GST-hPLD1 activity were assessed in real-time using the novel fPtdCho (see Fig. 4.4). The stimulation effects of these divalent ions were assessed without small G-protein activators. Sufficient GST-hPLD1 was used in each assay to ensure that fluorescence rose consistently throughout the assay compared to the fluorescence of vesicles alone. Neither 3 mM nor 5 mM Mg^{2+} enhanced *in vitro* GST-hPLD1 activity; fluorescence reflected lower GST-hPLD1 activity compared with that in the presence of both 3 mM Mg^{2+} and 2 mM Ca^{2+} ions. These ions are important in small G-protein activation of GST-hPLD1 although, when small G-proteins are not used, Mg^{2+} ions alone had little impact on GST-hPLD1 activity (see Fig. 4.4).

The addition of 2 mM Ca^{2+} caused a noticeable increase in fluorescence emission, so indicating that GST-hPLD1 activity was enhanced in the presence of Ca^{2+} ions. These results are further supported by the effects of 5 mM Ca^{2+} on GST-hPLD1 activity as this concentration further enhanced GST-hPLD1 activity (see Fig. 4.4). The combined effect of 3 mM Mg^{2+} and 2 mM Ca^{2+} resulted in an increased basal GST-hPLD1 activity similar to that seen using 5 mM Ca^{2+} alone. As the results show a clear increase in GST-hPLD1 activity in the presence of Ca^{2+} ions, increasing Ca^{2+} concentration may further optimize GST-hPLD1 *in vitro* activation.

Figure 4.4: The effects of Ca^{2+} and Mg^{2+} on basal GST-hPLD1 activity *in vitro*. Assays were constituted with 50 µM GTPγS, 400 mM NaCl, 50 µl fluorescent vesicles, 20 µl GST-hPLD1b, Mg^{2+} and Ca^{2+}. All assay components (except the vesicles) including the GST-hPLD1 protein were added to each well and kept on ice. Immediately before the assay commenced, vesicles were added to begin the assay. Fluorescence emissions were recorded using a fluorimeter (at 37°C) for 120 minutes. The hydrolysis of fPtdCho was detected using an excitation aperture at 485 nm and an emission filter of 535 nm. Fluorescence emissions were accrued (approx.) every 2 seconds and recorded concurrently. The change in fluorescence due to GST-hPLD1 in the presence of 3 mM Mg^{2+} and 2 mM Ca^{2+} (▼) was compared to vesicles incubated without lipase (▲). Background fluorescence (water) was monitored but the data is not shown. Fluorescence emissions produced by GST-hPLD1 in the presence of 3 mM Mg^{2+} (■), or 5 mM Mg^{2+} (▼) were compared to that of GST-hPLD1 activity in the presence of combined ions (▼) or Ca^{2+} alone. Fluorescence emissions resulting from GST-hPLD1 activity in the presence of 2 mM Ca^{2+} (■) or 5 mM Ca^{2+} (▼) were also compared with the activity induced by a combination of Mg^{2+} and Ca^{2+} (▼) or Mg^{2+} alone. This real-time *in vitro* assay was repeated twice.

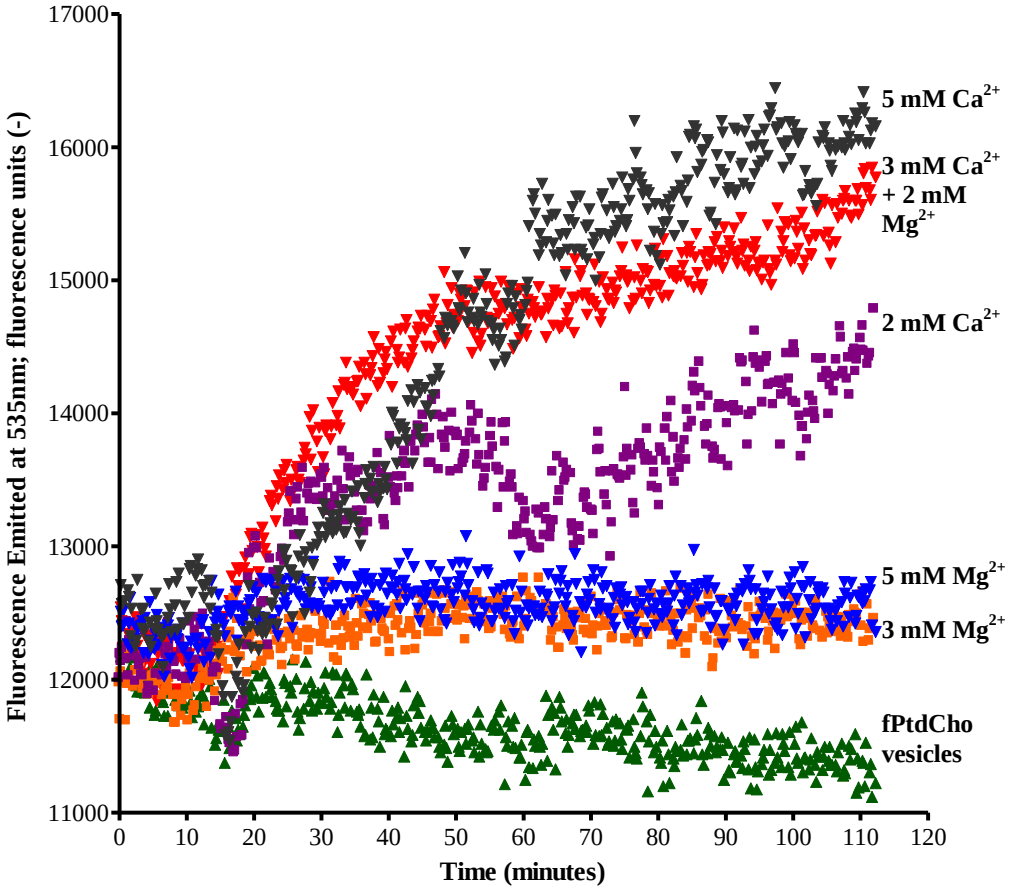

4.4: Effects of GTPγS concentration on small molecular weight G-protein activated GST-hPLD1 *in vitro*

Although GTP is needed for the activity of small G-proteins, the concentration at which GTPγS becomes effective has not been monitored in real-time *in vitro*. The effect of GTPγS on small G-protein activation of GST-hPLD1 was determined using the fluorescent *in vitro* assay and varying GTPγS concentration between 1 µM and 50 µM. The standard fluorescent GST-hPLD1 assay included 50 µM GTPγS which enabled lipase activation by small G-proteins. GST-hPLD1 was activated by either Arf1 (see Fig. 4.5) or Rac1 (see Fig. 4.6) using 50 µM, 10 µM or 1 µM GTPγS. Combined GST-hPLD1 activation by wildtype Arf1 and Rac1 using 50 µM GTPγS emitted the highest level of fluorescence, establishing that the protein was active and responding to small G-protein activators (see Fig. 4.5). GST-hPLD1 activation by Arf1 was monitored in real-time over a period of 120 minutes. Arf1 activation of GST-hPLD1 in the presence of 50 µM GTPγS was no more effective than 1 µM GTPγS. The same lag time was present in all activated protein preparations in the first 10-20 minutes of the *in vitro* assay. Data was recorded concurrently so that each reaction could be compared. The fluorescence of vesicles alone did not fluctuate throughout the assay. There was a slight increase in fluorescence of non-activated GST-hPLD1, demonstrating basal lipase activity and providing a control for Arf1 activated protein.

Similarly, Rac1 activation of GST-hPLD1 in the presence of 50 µM GTPγS was comparable to activation using 1 µM GTPγS (see Fig. 4.6). GST-hPLD1 activity stimulated by Rac1 was enhanced most effectively using 1 µM GTPγS. GST-hPLD1 activation by Rac1 showed no difference using 10 µM or 50 µM GTPγS. The emitted fluorescence of vesicles alone remained below 10,000 fluorescence units throughout the *in vitro* assay.

As different protein preparations were used, the results produced using Arf1 or Rac1 activation of GST-hPLD1 with varying GTPγS concentrations were not directly comparable. However, there was a similar trend between the experiments, so indicating that 1 µM GTPγS was as successful in aiding G-protein activation of the lipase as 50 µM GTPγS.

Figure 4.5: The effects of GTPγS concentration on Arf1 activated GST-hPLD1 *in vitro*. Assays were constituted with 400 mM NaCl, 50 µl fluorescent vesicles, 20 µl GST-hPLD1b, Mg^{2+}, and Ca^{2+} and varying concentrations of GTPγS (between 1 µM-50 µM). All assay components (except the vesicles) including the GST-hPLD1 protein were added to each well and kept on ice. Immediately before the assay commenced, vesicles were added to begin the assay. Fluorescence emissions were recorded using a fluorimeter (at 37°C) for 120 minutes. The hydrolysis of fPtdCho was detected using an excitation aperture at 485 nm and an emission filter of 535 nm. Fluorescence emissions were accrued at 2 second intervals and recorded concurrently. The change in fluorescence due to GST-hPLD1 (▼) was compared to vesicles alone with no lipase (▲). GST-hPLD1 activated by wildtype Arf1 and Rac1 in combination with 50 µM GTPγS (●) was compared to Arf1 activation GST-hPLD1. Arf1 activation of GST-hPLD1 was completed using 50 µM (●), 10 µM (■) and 1 µM GTPγS (▲). Background fluorescence emission was also measured but data is not shown. Readings were collected concurrently in real-time and the *in vitro* assay was repeated twice.

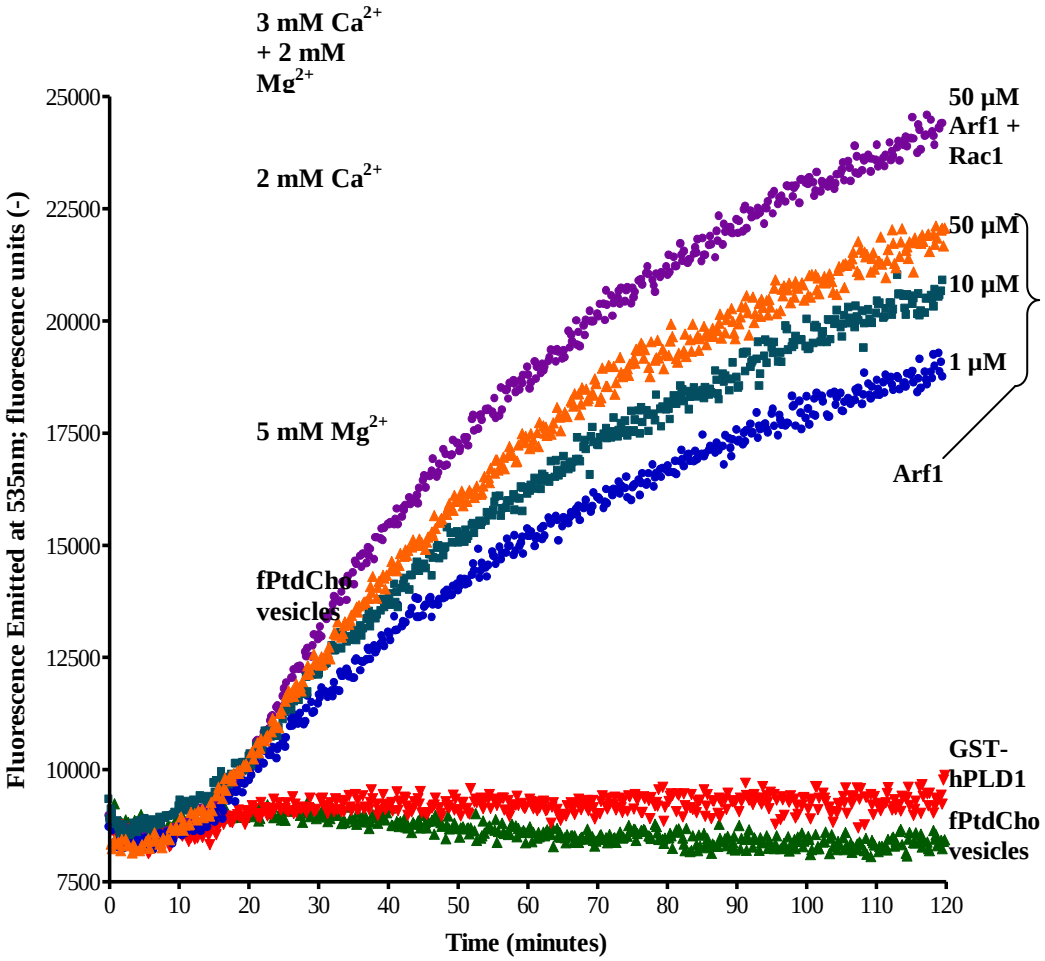

Figure 4.6: The effects of GTPγS concentration on Rac1 (wt) activated GST-hPLD1 *in vitro*. Assays were constituted with 400 mM NaCl, 50 µl fluorescent vesicles, 20 µl GST-hPLD1b, Mg^{2+}, and Ca^{2+} and varying concentrations of GTPγS (between 1 µM-50 µM). All assay components (except the vesicles) including the GST-hPLD1 protein were added to each well and kept on ice. Immediately before the assay commenced, vesicles were added to begin the assay. Fluorescence emissions were recorded using a fluorimeter (at 37°C) for 120 minutes. The hydrolysis of fPtdCho was detected using an excitation aperture at 485 nm and an emission filter of 535 nm. Fluorescence emissions were accrued (approx.) every 2 seconds and recorded concurrently. The change in fluorescence due to GST-hPLD1 (data not shown) was compared to vesicles alone with no lipase (▲). Rac1 activation of GST-hPLD1 was completed using 50 µM (●), 10 µM (■) and 1 µM GTPγS (▲). Background fluorescence emission was also measured (data not shown). Recording of fluorescence emission was concurrent and measured in real-time. This *in vitro* assay was repeated twice.

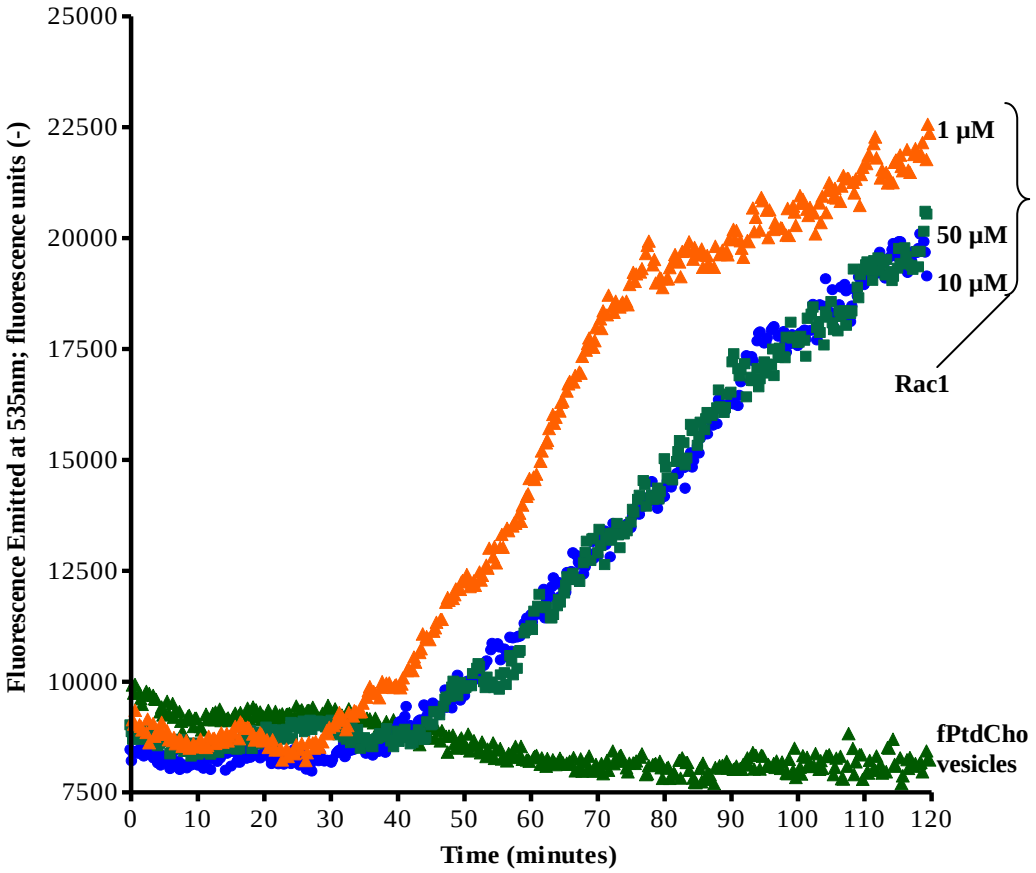

4.5: Stimulation of GST-hPLD1 by wildtype and constitutively active Rac1 *in vitro*

Activation of purified recombinant GST-hPLD1 using wildtype Arf1 or Rac1 has been detailed in previous sections (see Fig. 4.1 and 4.2). Although activation of GST-hPLD1 by Arf1 was consistent and produced comparable results between different experiments and protein preparations, Rac1 activation was more variable.

In some instances, neither wildtype Rac1 nor Rac1 (Q61L) protein could activate GST-hPLD1 even over 120 minutes of incubation. However, in the presence of Arf1 both wildtype Rac1 and Rac1 (Q61L) further enhanced PLD activity. These results suggest a possible hierarchy for activation of PLD by small G-proteins that is accentuated by using small amounts of GST-hPLD1 and a sensitive assay. GST-hPLD1 activated by wildtype Arf1 and Rac1 produced comparable fluorescence emission to Arf1 and Rac1 (Q61L) activation (see Fig. 4.8). The fluorescence emissions were highest in combined activation of GST-hPLD1, although Arf1 alone also activated the lipase. There was a lag time of between 10 and 20 minutes, similar to previous fluorescence *in vitro* experiments.

Due to experimental constraints associated with small scale protein expression and purification, further experiments comparing the two Rac1 proteins were not possible. Experiments would have attempted to identify the degree of dependence (if any) on GTPγS by Rac1 (Q61L) and assess its similarity to wildtype Rac1 activation of GST-hPLD1 alone. Further analysis of activation of GST-hPLD1 by Rac1 (Q61L) *in vitro* may indicate its *in vivo* role and ultimate effect on PLD1b localization (see Chapter 5).

Figure 4.8: Activation of GST-hPLD1 by wildtype Rac1 and its constitutively active mutant Rac1 (Q61L). Assays contained 50 µM GTPγS, 400 mM NaCl, 3 mM Mg^{2+}, 2 mM Ca^{2+} and 2 µg of each (or both) activator – Arf1, Rac1 wildtype or Rac1 constitutively active. All assay components (except 50 µl fluorescent vesicles) including activators and 20 µl GST-hPLD1 protein were added to each well and kept on ice. Immediately before the assay was started vesicles were added. Fluorescence emissions were recorded using a fluorimeter (at 37°C) for 120 minutes. The hydrolysis of fPtdCho was detected using an excitation aperture at 485 nm and an emission aperture of 535 nm. Fluorescence emissions were accrued (approx.) every 2 seconds and recorded concurrently. The change in fluorescence due to GST-hPLD1 (▼) was compared to vesicles incubated without lipase (▲). Background fluorescence (water) was also monitored (data not shown). Activation of GST-hPLD1 by wildtype Arf1 and Rac1 (●) was compared to activation by wildtype Arf1 and Rac (Q61L – ●). GST-hPLD1 was also activation by Arf1 (●), wildtype Rac1 (▲) or Rac1 (Q61L – ▲) alone. Assays were repeated (n=2) comparing different protein preparations to ensure the reproducibility and reliability of these results.

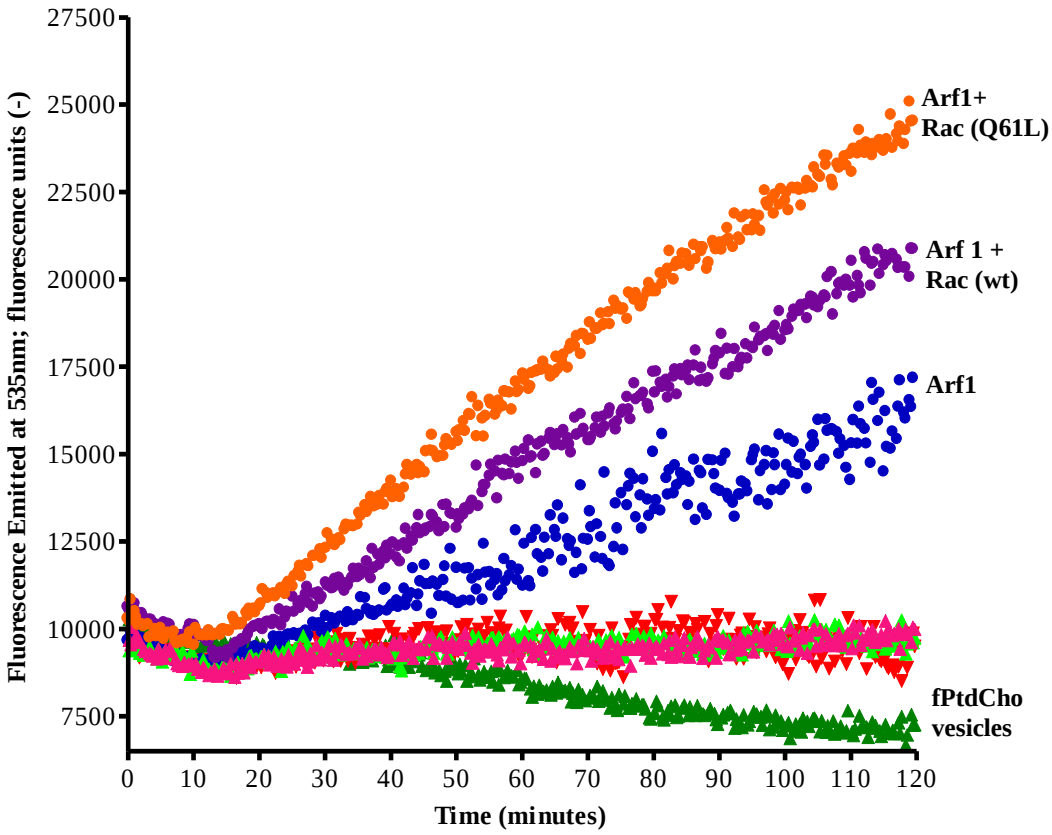

4.6: Discussion

4.6.1: Activation of GST-hPLD1 by Arf1 and Rac1

The novel fPtdCho enabled characterisation of *in vitro* GST-hPLD1 activity in real-time. These real-time assays generated a more comprehensive picture of GST-hPLD1 activity in response to its activators than the previously established assay (Hodgkin *et al*., 1999; Farquhar *et al*., 2007). [^{3}H]-PtdCho assays contributed to our understanding about the interaction of PLD1 with known activators such as Arf1 (a Rho-family member) and PKCα (Ohguchi *et al*. 1997; Hodgkin *et al*., 1999). Although the fPtdCho assay has potential to provide new insight into PLD1 kinetics, it must be optimized and experimental constraints overcome to progress further. Generating sufficient quantities of GST-hPLD1 from Sf9 cells was a key restraint on the *in vitro* experiments as large scale expression and harvesting of protein was not possible. This led to some variation in the level of activity of different GST-hPLD1 purified recombinant protein preparations.

In vitro data suggest that Arf1 and Rac1 activate GST-hPLD1 (activity) synergistically. Similar results using an N-terminally truncated PLD1 protein have proposed Arf1 as a catalytic activator and Rac1 as a binding activator (IUPAC-IUBM, 1982; Henage *et al*., 2006). Catalytic activators such as Arf1 increase the PLD1 catalytic potential dependent on Arf1 concentration. Binding activators such as Rac1 allostericaly regulate PLD1 catalysis by promoting binding activation (Henage *et al*., 2006). The synergistic increase of Arf1 and Rac1 was 200% higher than expected if this combined activation was simply a sum of the effect of each separately (Henage *et al*., 2006). This corresponded to fluorescent *in vitro* data presented here which showed an increase in emitted fluorescence in the presence of two small G-protein activators. Arf1 was found to increase PLD1 catalysis of the radiolabelled substrate when compared to the effect of Rac1 or Cdc42 (Hammond *et al*., 1995; Hammond *et al*., 1997; Hodgkin *et al*., 1999; Powner *et al*., 2002; Henage *et al*., 2006). Our real-time data corroborate these results, which show Arf1 consistently increases fluorescence emission (reflecting GST-hPLD1 activity) at a higher rate than Rac1. Additional experiments activating GST-hPLD1 first with Rac1 (wt), then with Arf1, would provide a further indication of the impact of this

Rho-family member compared against co-operative activation. Similarly, activating GST-hPLD1 with Arf1 and then Rac1 (wt) would also provide a measure of how much Rac1 (wt) contributes to the activation of GST-hPLD1 in this type of co-operative activation.

A comparison of GST-hPLD1 activation using either wildtype Rac1 or constitutively active Rac1 (Q61L) co-operatively with Arf1 did not show a difference in lipase activation. The consistency of GST-hPLD1 activation by Rac1 (wt) or Rac1 (Q61L) with no enhancement using Arf1 would enable further analysis of their individual effects on GST-hPLD activity. For example, removal of GTPγS may halt activation by Rac1 (wt) but not Rac1 (Q61L). Parallel experiments characterising *in vivo* localisation in HeLa cells transiently expressing Rac1 (Q61L) and PLD1b showed substantial changes in morphology and PLD1b localization (see Chapter 5).

4.6.2: Activation of GST-hPLD1 by PKCα

Radioactive *in vitro* assays indicated that the most potent stimulation of GST-hPLD1 occurs in a combined reaction containing Arf1, a Rho-family member and PKCα in the absence of ATP or PMA (Hammond *et al*., 1995; Hammond *et al*., 1997; Hodgkin *et al*., 1999; Henage *et al*., 2006). PKCα maintained some of its ability to activate an N-terminally truncated PLD1, even though the PKCα binding regions in the N-terminus and PH domains were deleted (Henage *et al*., 2006). These results suggest that PKCα also interacts with the C-terminus of PLD1, although both C- and N-termini are needed for maximal PLD1 activation (Henage *et al*., 2006). Although Arf1 and PKCα worked synergistically to activate PLD1, Rac1 and PKCα did not show the same magnitude of reaction (Henage *et al*., 2006). The fluorescent assay did not provide further insight into synergistic activation of GST-hPLD1 by PKCα and small G-proteins as the lipase appeared unresponsive to PKCα in this assay.

The lack of response may be attributed to the way the fluorescent substrate was synthesised. Previously, assays used a relatively small proportion of $[^3H](Pam)_2$PtdCho in conjunction with a large proportion of native PtdCho (egg lecithin – Kupferberg *et al*., 1981). The fluorescent lipid was constructed synthetically which may prove incompatible with PKCα. It is possible that egg

lecithin isolated PtdCho could have been co-purified with small amounts of DAG. Similarly, lecithin PtdCho may contain the correct fatty acid arrangement for PKCα interaction *in vitro*, whilst the synthesis of the novel lipid may have altered this structure.

4.6.3: The effect of Ca^{2+} and Mg^{2+} ions on GST-hPLD1 activity

Examining PLD activity in real-time enabled the optimization of *in vitro* assay conditions, originally based on radioactive assays (Hodgkin *et al*., 1999; Farquhar *et al*., 2007). Although calcium mobilization is necessary for PLD1 activation *in vivo* (Bae *et al*., 2000), its role in *in vitro* assays has not been fully characterized. Increasing the concentration of Ca^{2+} ions *in vitro* resulted in enhanced basal PLD1 activity. GST-hPLD1 modestly increased emitted fluorescence in response to 2 mM Ca^{2+} *in vitro*. However, a further increase to 5 mM Ca^{2+} ion concentration resulted in a notably increased GST-hPLD1 protein activity. This may indicate that Ca^{2+} concentration influences PLD1 activators such as PKCα as well as the phospholipase itself, much like PLA_2 (Lister *et al*., 1989).

Although some plant PLDs can be stimulated by Ca^{2+} (in the 20-100 nM range) the response of mammalian PLDs to Ca^{2+} has not yet been fully elucidated (Wang *et al*., 2002). PLD isoforms isolated from fungal, bacterial, yeast and mammalian sources are all activated by divalent metal ions (Chalifa *et al*., 1990; Mayr *et al*., 1996; Madesh and Balasubramanian, 1997; Hong *et al*., 2003). Ca^{2+} ions bind to lipids including PtdIns(4,5)P_2 and PtdOH, both of which are closely associated with PLD (Faraudo and Travesset, 2007). PLD binding to PtdCho-containing vesicles is Ca^{2+}-dependent, although *in vitro* PtdOH may have an inhibitory effect on PLD, raising the possibility that Ca^{2+} also relieves product inhibition (Yang and Roberts, 2003).

Whilst GST-hPLD1 basal activity was enhanced when exposed to Ca^{2+} ions, Mg^{2+} ions did not have the same effect. Mg^{2+} concentrations of either 3 mM or 5 mM alone did not increase basal PLD1 activity. However, a combination of 3 mM Mg^{2+} and 2 mM Ca^{2+} resulted in a similar activation response as 5 mM Ca^{2+} alone. Previous studies identified Mg^{2+} as an activator of neutral PLD (isolated from rat brain) at a concentration of 2 mM (Chalifa *et al*., 1990). The combined exposure of

PLD to Ca^{2+} (aiding vesicle binding) and Mg^{2+} at a final concentration of 5 mM, possibly constituted the optimal concentration of divalent ions for PLD catalysed hydrolysis.

4.6.4: The effect of GTPγS concentration on small G-protein activated PLD

Although Mg^{2+} ions alone do not appear to increase basal PLD1 activity, G-protein activators such as Arf1 need Mg^{2+} ions to adopt their 'active' conformation via a coordination of the γ-phosphate group of GTPγS with the Mg^{2+} ions and amide group (Thr^{48}) of Arf1 (Goldberg 1998; Kremer *et al*., 2004). The Thr^{48} residue of Arf1 is responsible for the binding of Mg^{2+} ions (for stabilization) and adopting the correct conformation for effector recognition (Goldberg 1998; Kremer *et al*., 2004). As these molecular details are highly conserved between small G-proteins, activation of PLD1 by Rac1 (wt) or Rac1 (Q61L) will also employ similar binding properties between the Mg^{2+} ions and GTPγS.

GTPγS can be used for GST-hPLD1 protein activation *in vitro*, although its role has not been fully characterised. Small G-proteins cycle between an inactive GDP-bound and an active GTP-bound conformation. This cycle, effectively a molecular switch, is regulated by guanine nucleotide exchange factors (GEFs) and GTPase-activating proteins (GAPs). *In vivo*, GEFs release the bound GDP which is then substituted for GTP and GAPs supply a vital catalytic group which is required for GTP hydrolysis (Bos *et al*., 2007). *In vitro*, small G-proteins bound to GTPγS are in the 'active' state and are able to activate PLD1. However, as there is no cycling between the GTP (active) and GDP (inactive) conformations, 50 µM GTPγS is probably in vast excess. GST-hPLD1 activation by either Arf1 or Rac1 in the presence of 50 µM GTPγS was no more effective than using 1 µM GTPγS. There may be some inhibition by GTPγS as reducing its concentration led to slight increases in GST-hPLD1 activation by small G-proteins. Future experiments could attempt to replace the non-hydrolysable GTPγS with GTP, although a higher concentration would be necessary to counter GTP hydrolysis. GTP experiments would help identify whether the small G-proteins function as amplifiers of GST-hPLD1 activity and would perhaps simulate *in vivo* conditions more faithfully.

4.6.5: Comparing the novel fluorescent assay with more established PLD assays

Although the fluorescent PLD1 assay produced real-time results and measured reactions concurrently, the assay volume was double that of radioactive assays. The larger volume was necessary to accommodate the wells of 96-well plates used for the fluorescent assays. As a result of this volume increase, more reagents and protein were needed complete each assay. In addition, due to the small volume of radioactive assays (typically 50 µl), a more concentrated GST-hPLD1 protein preparation was required. Our protein yield was low and so it would not have been possible to complete these fluorescent assays under radioactive conditions. Vesicles contained substantially more fPtdCho than [^{3}H]-(Pam)$_2$PtdCho and this may have caused a change in vesicle structure, therefore affecting hydrolysis. The radioactive *in vitro* assay has proven invaluable in the characterisation of GST-hPLD1 and its activators (Henage *et al*., 2006). The majority of PtdCho in radioactive assays is derived from egg lecithin and so may have the natural fatty-acid structure necessary to accommodate all GST-hPLD1 activators. These include PKCα which did not activate GST-hPLD1 in assays using the synthetic fluorescent PtdCho. However, using an alternative substrate not isolated from lecithin produced a more sensitive assay which could be further optimised by future work.

Fluorescent *in vitro* assays measured the emitted fluorescence in real-time and so the effect of Arf1 or Rac1 on GST-hPLD1 activity could be followed in real-time. The rate of GST-hPLD1 could be directly compared between simultaneous assays. Varying assay conditions could be monitored to assess the rate of GST-hPLD1 activity over a period of time rather than producing only a single data point. Trends in GST-hPLD1 activation using the fluorescent *in vitro* assay could be facilitate the gathering of more information about how small G-protein activators affect lipase activity. The fluorescent *in vitro* assay was also more sensitive than the previously established radioactive assay. Fluorescent assays could be used to characterise subtle changes in assay conditions and track the hydrolysis of fluorescent PtdCho by GST-hPLD1 in real-time. As well as analysing the effect of small G-proteins on GST-hPLD1 activity the effect of divalent cations (Mg^{2+} or Ca^{2+} ions) could also be assessed in real-time. As radiochemical assays were analysed using liquid scintillation counting (Hodgkin *et al*., 1999) the small affect of Ca^{2+} ions on GST-

hPLD1 activity would not have been as apparent. Radioactive assay data could be directly compared to parallel experiments as liquid scintillation counts related directly to the amount of [^{3}H]-choline produced by a known concentration of GST-hPLD1. Although there was less variability in radioactive assays, the procedure to assess lipase activity was time consuming whilst fluorescent assay experiments were completed quickly.

The original fluorescent PLD assay used fPtdCho as a PLD1 substrate and the products of this reaction were analysed using solvent extraction followed by thin layer chromatography and visualised using a long-wave UV lamp (Ella *et al*., 1994). The development of quenched fPtdCho enabled real-time assaying of PLA_2 (Feng *et al*., 2002). The PLA_2 fluorescent assay uses a similar synthetic substrate to monitor PLA_2 and was further developed to analyse PLD1 kinetics. The novel fluorescent PLD1 assay provides an opportunity to analyze further the stoichiometry between PLD and its small G-protein activators, perhaps eventually using PLD as an effector protein. The use of previously established data (e.g. from radioactive assays) could help develop this real-time assay, thus providing more information about the kinetics displayed by GST-hPLD1, both at rest and upon stimulation with known activators.

Chapter 5: The effects of small molecular weight G-proteins on phospholipase D in HeLa cells

5.1: Introduction

Although the localisation and stimulation of PLD in the RBL-2H3 cell line is well characterised, reproducible genetic modification of these cells did not prove possible. Transient transfections with the eGFP- and Cherry-labelled PLD constructs resulted in efficiencies below 10% and high levels of toxicity in the RBL-2H3 cell line. To overcome the limitations of the RBL-2H3 cell line, the HeLa cell line was chosen as an alternative *in vivo* system. The HeLa cell line is an immortalised human epithelial lineage derived from a cervical malignancy, in which epidermal growth factor (EGF) stimulates PLD1-dependent PtdCho hydrolysis, endocytosis and degradation of the EGF receptors (EGFR) (Shen *et al*., 2001; J.S. Lee e*t al*., 2009), cell migration (Kim *et al*., 2006) and mitogenesis (Fukami and Takenawa, 1992). Although PLD regulates different processes in RBL-2H3 and HeLa cell lines, both have PLD-dependent pathways which can be manipulated experimentally. Furthermore, HeLa cells grow reliably and are readily transfectable.

The EGFR is structurally divided into an extracellular EGF binding domain, a single hydrophobic transmembrane anchor sequence (23 amino acids) and a cytoplasmic signalling domain (Ullrich *et al*., 1984). Early studies characterised the cytoplasmic domain of EGFR as containing an EGF-regulated tyrosine kinase, homologous to a number of oncogene products, thus suggesting a role in regulating cell proliferation (Ushiro and Cohen, 1980; Carpenter and Cohen, 1990). The necessity of a functional PKC for EGF stimulated accumulation has not yet been elucidated. Initial studies suggest that functional PKC is necessary for at least part of EGF stimulation accumulation of PtdCho and DAG (in certain cell lines) which seemingly occur via separate pathways (Cook and Wakelam, 1992). Whilst PtdCho hydrolysis takes place via a PLD-catalysed pathway, DAG accumulation does not (Cook and Wakelam, 1992). Furthermore, EGF activation of EGFR results in elevated levels of PtdOH, a second messenger associated with a number of cellular processes including cell proliferation (English *et al*., 1996), endocytosis (Shen *et al*., 2001), exocytosis (Way *et al*., 2000) and cytoskeletal rearrangement (Ha and Exton, 1993). EGF

stimulation of human embryonic kidney 293 (HEK-293) cells showed that PLD2 interacts with EGFR and is tyrosine-phosphorylated following EGFR activation (Slaaby *et al*., 1998)**.** The kinase activity of EGFR is crucial for PLD2 tyrosine phosphorylation (on tyrosine-11), however as only basal PLD2 activity is affected by mutations of tyrosine-11, this suggests tyrosine phosphorylation is important for interactions between PLD2 and SH2-containing proteins (Slaaby *et al*., 1998; Ahn *et al*., 2003). EGF stimulation induced an interaction between the oncogene c-Src and PLD1 or PLD2 in epithelial cells that was synergistic and amplified cellular proliferation (Ahn *et al*., 2003). In the A431 epithelial cell line, EGF-stimulated PLD activity has been linked to the activation of extracellular signal-regulated kinase (ERK – Shen *et al*., 2001). It is suggested that the interaction between Src and PLD results in tyrosine phosphorylation of both PLD isofoms and that PLD in turn activates c-Src and ultimately ERK activation and cell proliferation (Ahn *et al*., 2003).

Previous studies in HEK-293 cells showed that PLD1 did not form a physiological complex with EGFR (Slaaby *et al*., 1998). Although in COS7 cells transiently expressing PLD1, EGF induced activation of PLD1 and phosphorylation of the PLD1 threonine-147 residue (Han *et al*., 2002b). After EGF stimulation, phosphorylated PLD1 localised to the plasma membrane, co-localised with EGFR and caveolin-1 and was also found in vesicular structures (Han *et al*., 2002b) possibly lysosomes or endosomes (Toda *et al*., 1999; Hughes and Parker, 2001). The localisation of PLD1 to calveolin-enriched membrane (CEM) via palmitoylation is important for both activation and phosphorylation of PLD1 in response to EGF stimulation (Han *et al*., 2002b).

HeLa cells are readily transfected and so facilitated analysis of localisation between PLD1 and known activators such as members of the Rho family of GTPases. The ultimate aim was to observe where and when PLD comes together with its multiple activators and effectors to form a PtdCho hydrolysing complex in response to extracellular stimuli. Key objectives were to demonstrate interaction between PLD1b or PLD2a and known small G-protein activators *in vivo*. The use of specific G-protein mutants could reveal details of the activation of PLD1b via GTP hydrolysis. Rac1 mutants included dominant negative Rac1 in which threonine (T)

was mutated to asparagine (N) (denoted Rac1-T17N) and constitutively active Rac1 where glutamine (Q) was point mutated to leucine (L) (denoted Rac1-Q61L). This provided the foundations for further investigation into Rac1 and its relationship with PLD both pre- and post-EGF stimulation.

The novel fluorescent PtdCho (fPtdCho) characterised in RBL-2H3 cells and used to perform real-time *in vitro* PLD assays was also used to label HeLa cells. The ultimate goal of the project to create a live *in vivo* PLD assay using the BODIPY labelled PtdCho and Cherry-PLD was ultimately achieved in the HeLa cell line. Analysis of co-localisation between the novel lipid and Cherry-PLD provided an insight into the interaction between PLD1 and its substrate in live cells.

5.2: Characterisation of GFP, Cherry-PLD and Rac1 in HeLa cells

5.2.1: Transient transfections using eGFP-PLD and the effect of EGF stimulation of HeLa cells

PLD localisation and response to EGF stimulation was characterised in HeLa cells by comparing localisation between the enhanced green fluorescent protein (eGFP) and Cherry-labelled PLD1b or PLD2a with and without EGF stimulation. PLD2a expression was consistent and therefore used in subsequent experiments as a control for PLD1-dependent EGF response (see Fig. 5.1, panels e, f – Shen *et al*., 2001). Although PLD2 does not appear to have a role in the endocytosis of EGFR, co-expression of PLD2 and EGFR has identified a pathway by which PLD2 can be regulated in HeLa cells (Watanabe and Kanaho, 2000).

HeLa cells were fixed following transfection as fixing enabled clearer more distinct protein expression. HeLa cells transiently transfected with eGFP alone, exhibited diffuse green fluorescence uniformly expressed throughout the cytosol, nucleus and nucleoplasm. Expression of eGFP alone was routinely included in subsequent experiments as a control (see Fig. 5.1, panels a, b). After stimulation with EGF (20 nM EGF for 10 minutes at 37^{o}C and 5% CO_2), eGFP largely maintained its diffuse cytosolic and nuclear expression although there appeared to be a small increase in eGFP in the plasma membrane. The modest change in overall localisation of eGFP in cells stimulated by EGF could be a result of the shape change associated with stimulation rather than a primary response to stimulation. HeLa cells, transiently transfected with eGFP-PLD1b displayed punctate fluorescence consistent with endosomes, trans-Golgi or other structures in the perinuclear region (Toda *et al*., 1999; Hughes and Parker, 2001; Hiroyama and Exton, 2005b). Upon EGF stimulation, eGFP-PLD1b was clearly expressed at the plasma membrane (see Fig. 5.1 panels c, d) although this was not confirmed using FM4-64 as the cells were fixed. Although PLD1b appeared primarily on the plasma membrane (see arrows Fig. 5.1, panel d), there was also a change in the localisation of the punctiform structures within the cells. The punctate structures appeared to accumulate to a defined intracellular region (see circles Fig. 5.1, panel d) indicating that there may be a dual effect of EGF stimulation on PLD1 localisation. Quantification of the amount of

PLD1b migrating to the plasma membrane compared to that maintained within the cell was not possible. PLD1 localisation to calveolin-enriched membrane (CEM) is integral to both its activation and phosphorylation in EGF-stimulated cells (Han *et al*., 2002b). Stimulation of HeLa cells using EGF moved PLD1 to the plasma membrane where the EGFRs are endocytosed. Recent data suggests PtdOH plays an important role in the endocytosis of EGFRs, although the mechanism by which PtdOH acts and is regulated is as yet unknown (C.S. Lee *et al*., 2009). PLD1 expression and localisation has been identified at the perinuclear site, the trans-Golgi apparatus, late endosomes, multivesicular endosomes and seldom in early endosomes (Hiroyama and Exton, 2005b). The discrepancy between PLD1 localisation may be attributed to the use of different cell lines and the variety of molecular markers chosen (Hiroyama and Exton, 2005b).

Localisation of eGFP-PLD2a in transiently transfected HeLa cells was unlike PLD1b, indicating a difference in localisation, which has been characterised elsewhere (Slaaby *et al*., 1998). eGFP-PLD2a exhibited diffuse cytosolic expression which was not membranous and excluded the nucleus (see Fig. 5.1, panels e, f). No change in the localisation of eGFP-PLD2a was observed upon EGF stimulation. Although eGFP-PLD2a expressed consistently in the cytosol, two phenotypes of expression were apparent. The most common of these was diffuse (see Fig. 5.1, panels e, f) and the second of which was punctate but mostly located throughout the cytosol (see Fig. 5.1, panels g, h). Punctate localisation of eGFP-PLD2a occurred in approximately 30% of transfections and within the population of these transfected cells at a frequency of approximately 40-50%. Cytosolic localisation of PLD2 similar to that displayed in the HeLa cell line was also seen in the Chinese Hamster Ovary-T (CHO-T) cell line (Emoto *et al*., 2000). Although plasma membrane localisation of PLD2 has been seen in numerous cell lines including HeLa cells, PLD2a was unaltered in cells stimulated by EGF under the transient transfection conditions used. The confocal settings used to detect green fluorescence were kept consistent (excitation using the argon laser at 488 nm and emission bandwidth 500 nm-608 nm) between constructs and experiments. The unaltered cytosolic expression of eGFP-PLD2a could therefore be considered an additional control for punctiform localisation of PLD1b and its response to EGF stimulation.

Figure 5.1: The effect of EGF on eGFP-PLD localisation in HeLa cells. HeLa cells grown on coverslips were transiently transfected with 3 µg of eGFP (panels **a**, **b**), eGFP-PLD1b (panels **c**, **d**) or eGFP-PLD2a (panels **e**, **f**, **g**, **h**) DNA for 24 hours. Cells were stimulated with EGF (panels b, d, f, h – 20 nM, for 10 minutes at 37^{o}C), fixed in 4% paraformaldehyde and mounted on glass slides. Green fluorescence was detected by confocal microscopy (SP5) by excitation at 488 nm and emission band width between 500 nm-608 nm using an argon laser (20%). A scale bar calibrated to 25 µm is shown in each panel. The data presented are representative images for 1 experiment repeated at least 3 times.

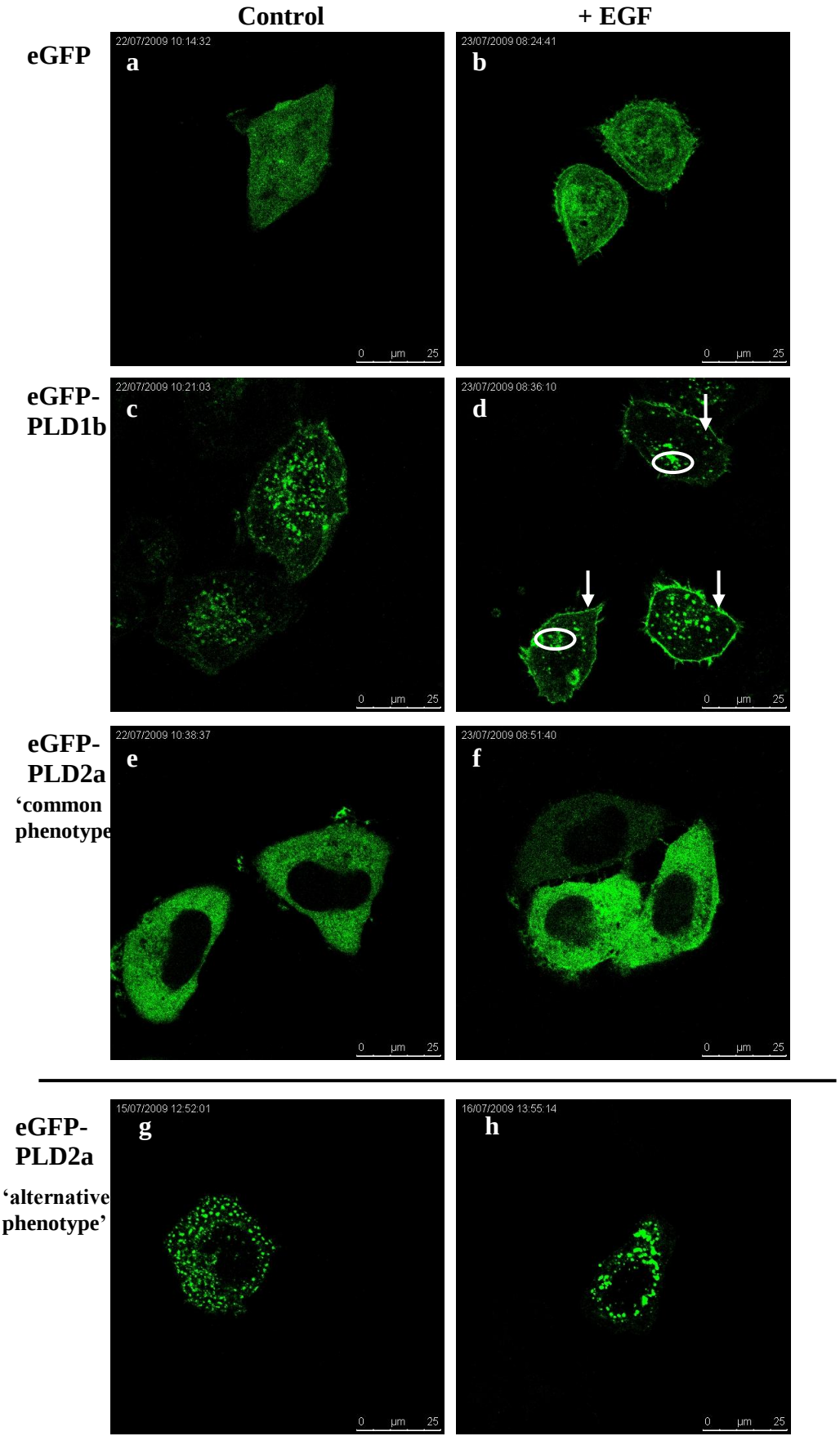
Control
+ EGF
eGFP
22/07/2009 10:14:32
a
23/07/2009 08:24:41
b
eGFP-PLD1b
22/07/2009 10:21:03
c
23/07/2009 08:36:10
d
eGFP-PLD2a
'common phenotype
22/07/2009 10:38:37
e
23/07/2009 08:51:40
f
eGFP-PLD2a
'alternative phenotype'
15/07/2009 12:52:01
g
16/07/2009 13:55:14
h
0 µm 25

5.2.2: Localisation of a PLD Chimera in HeLa cells

A PLD2a/PLD1b chimera was created by Dr Matthew Hodgkin (Coventry, UK) by fusing the first 283 N-terminal amino acid residues of PLD2a to the last 851 C-terminal amino acid residues of PLD1b. The strategy used to make this construct relied on locating an aspartate residue within PLD2a to enable blunt-end cloning at a side generated by the EcoRV restriction enzyme. The N-terminal region of PLD2a was subject to PCR using a forward primer from the ATG at the start of PLD2a and reverse primer starting at aspartate (D) residue 283. The PCR product was cloned directly into pcDNA3.1(-)-GFP restricted with EcoRV generating pcDNA3.1(-)-GFP-PLD2a(N1-283). The C-terminal region of PLD1b was subject to PCR using a forward primer from tyrosine residue 186 and reverse primer to the C-terminal sequence that included the stop codon. The PCR product was cloned directly into pcDNA3.1(-)-GFP-PLD2aN and restricted with EcoRV. The construct was sequenced and analysed using the SMART web-based bioinformatics tool which demonstrated the presence of one N-terminal PX- and one PH-domain (Schultz *et al*., 1998) as well as 2 PLD domains. In effect, the chimera was the N-terminus and PX domain of PLD2a fused to the PH domain and catalytic half of PLD1b. Transiently transfected HeLa cells consistently expressed PLD1b and PLD2a in the same manner enabling comparison with the expression of the Chimera. This data would indicate whether there was a region within these domains which influenced where PLD localised within the transiently transfected cells and whether this localisation was affected by EGF stimulation.

Localisation of eGFP alone, eGFP-PLD1b, -PLD2a and -Chimera were assessed in resting and EGF-stimulated HeLa cells (see Fig. 5.2). The eGFP tag alone displayed nuclear and cytoplasmic localisation in non-stimulation cells (see Fig. 5.2, panel a). Upon EGF stimulation, eGFP was largely retained in the cytoplasm and nucleus (see Fig. 5.2, panel b). eGFP-PLD1b localised predominantly in cytoplasmic punctiform structures and on the plasma membrane in resting cells (see Fig. 5.2, panel c). Plasma membrane localisation of PLD1b in resting cells varied in intensity from cell to cell. Following EGF-stimulation, eGFP-PLD1b was expressed at the plasma membrane (see arrows Fig. 5.2, panel d) and the punctiform structures aggregated

within the cell (see circles Fig. 5.2, panel d). eGFP-PLD2a was expressed in the cytoplasm but not the nucleus in resting and EGF-stimulated cells (see Fig. 5.2, panels e, f) and did not alter in response to EGF stimulation (see Section 5.2.1). The expression of eGFP-Chimera in resting cells was diffuse and found in both the cytoplasm and the nucleus, unlike both PLD1b or PLD2a (see Fig. 5.2, panel g). The localisation of eGFP-Chimera does not alter upon EGF stimulation (see Fig. 5.2, panel h). The expression pattern of eGFP-Chimera within the nucleus (nucleoplasmic expression) was distinct from that of eGFP. In particular, the Chimera appeared within the nuclear matrix but excluded the (presumed) nucleolus and smaller nuclear bodies. The nuclear localisation of the Chimera construct was unlikely to be a result of the cloning methodology as both PLD1b and PLD2a expression was characteristic and distinct from the nucleus.

Figure 5.2: The effect of EGF on eGFP-PLD and -Chimera localisation in HeLa cells. HeLa cells grown on coverslips were transiently transfected with 3 µg of eGFP (panels **a**, **b**), eGFP-PLD1b (panels **c**, **d**) or eGFP-PLD2a (panels **e**, **f**) and eGFP-Chimera (panels **g**, **h**) DNA for 24 hours. Cells were stimulated with EGF (panels **b**, **d**, **f**, **h** – 20 nM, for 10 minutes at 37^{o}C), fixed in 4% paraformaldehyde and mounted on glass slides. Green fluorescence was detected by confocal microscopy (SP5) by excitation at 488 nm and emission band width between 500 nm-608 nm using an argon laser (20%). A scale calibrated to 25 µm is shown in each panel. The data presented are representative images for 1 experiment repeated at least 3 times.

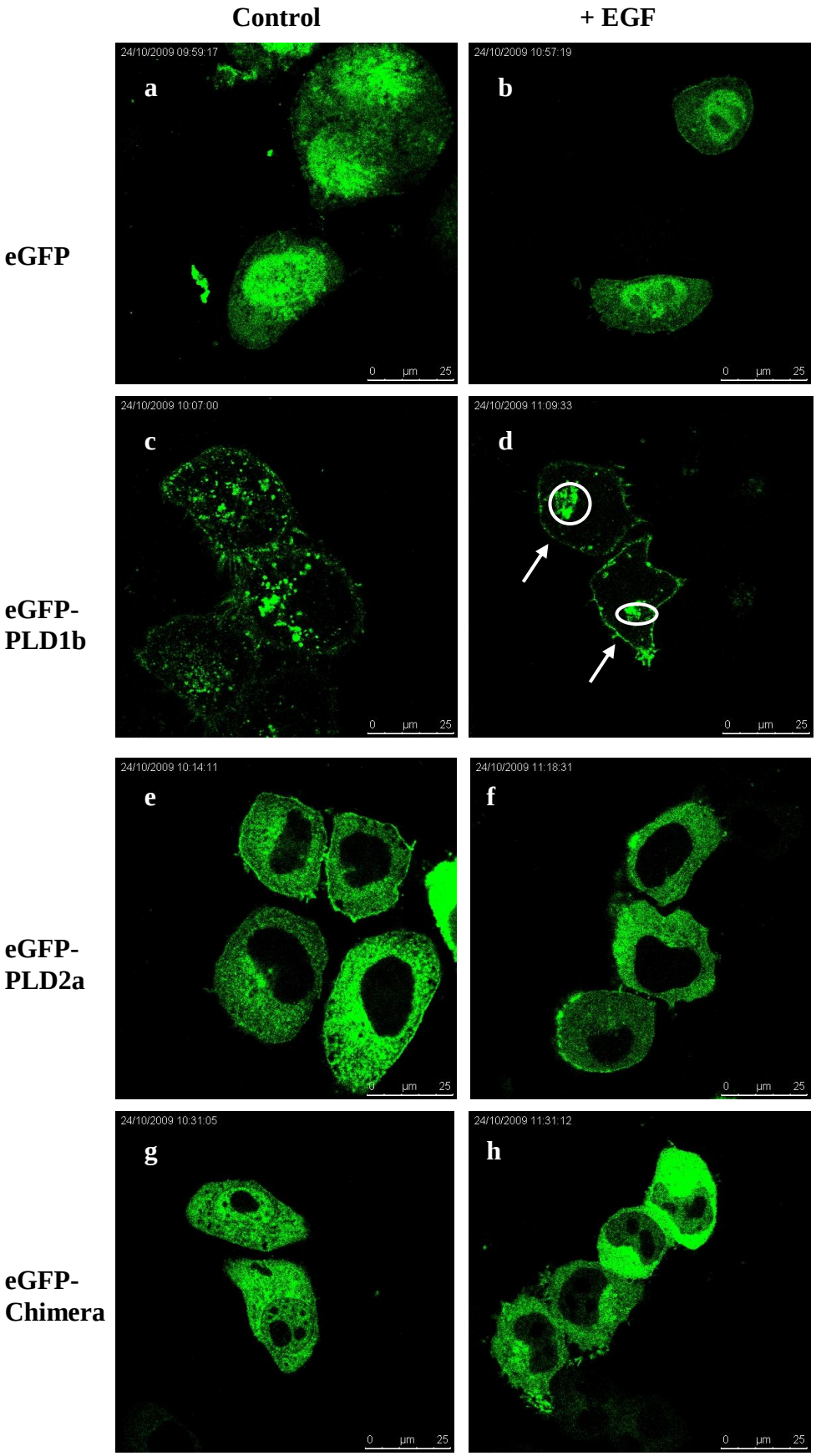
Control
+ EGF
eGFP
eGFP-PLD1b
eGFP-PLD2a
eGFP-Chimera
24/10/2009 09:59:17
a
24/10/2009 10:57:19
b
24/10/2009 10:07:00
c
24/10/2009 11:09:33
d
24/10/2009 10:14:11
e
24/10/2009 11:18:31
f
24/10/2009 10:31:05
g
24/10/2009 11:31:12
h
0 µm 25

5.2.3: The effect of EGF on HeLa cells co-expressing Cherry-PLD and eGFP-Chimera

Red fluorescent versions of PLD1b and PLD2a were generated in the pcDNA3.1(-) plasmid. This process involved generating pcDNA3.1(-)-Cherry then fusing the PLD open reading frames (ORFs) to the C-terminus via a minimal linker sequence to better facilitate ligation. This approach provided a similar plasmid organisation to that of eGFP-labelled PLDs. The predecessor of the Cherry label was the less efficient monomeric red fluorescent protein (mRFP) which had a low yield of fluorescence and exhibited considerable toxicity when expressed in the RBL-2H3 cell line. As the use of the eGFP tag was characterised previously (Wright *et al*., 2008), it provided an appropriate control against which the new Cherry tag could be compared. HeLa cells were transiently transfected with Cherry-labelled PLD1b or 2a in the same way as their eGFP labelled counterparts. HeLa cells were stimulated 24 hours post-transfection with EGF (20 nM for 10 minutes at 37^{o}C) and fixed with 4% paraformaldehyde. Fixing the cells produced clearer more defined localisation of the proteins.

HeLa cells co-transfected using Cherry-PLD and eGFP-Chimera highlighted the differences in expression patterns between these constructs (see Fig. 5.3, panels a-c). In unstimulated cells, Cherry-PLD1b was consistently punctate and localised to the cytoplasm; whereas Chimera expression was both nuclear and cytoplasmic (see Fig. 5.3, panel d). In response to EGF stimulation Cherry-PLD1b was also expressed at the plasma membrane (see arrows, Fig. 5.3, panel d), and aggregated to a region in the cytoplasm (see circles Fig. 5.3, panel d) as seen with eGFP-PLD. The Chimera may have exited the nucleus following EGF stimulation but largely maintained both cytoplasmic and nuclear localisation, and there is no similarity in PLD1b and Chimera expression.

However, in cells which express Cherry-PLD1b in the nucleus there is co-localisation between PLD1b and the Chimera in the nucleus but excluding the nucleoli (see Fig. 5.3, panel g). This may indicate that the N-terminus of PLD1b controls its localisation and that PLD1b contains a nuclear localisation sequence (Nakai *et al*., 1999). The PLD1b, PLD2a, and Chimera sequences were analysed

using a variety of software algorithms that can identify nuclear localisation signals (NLS). Although PSORT II, ROSTLAB and NLStradamus software were used for this analysis (see Table 5.1), only PSORT II identified a potential NLS in PLD1b and the Chimera but not PLD2a (Nakai and Horton, 1999; Cokol *et al*., 2000; Nguyen Ba *et al*., 2009). All the algorithms identified the NLS in SV40 large T proteins. The NLS identified in hPLD1b and the Chimera was composed of four residues: lysine, proline, arginine and lysine (KPRK) residues. Although POSTLAB II is a useful tool for identifying NLS, its predictions about where proteins should localise were not always accurate. This program predicted that hPLD1b expression would be cytoplasmic, but instead hPLD1b was clearly expressed in vesicles of the secretory system (see Table 5.2).

HeLa cells co-transfected using Cherry-PLD2a and eGFP-Chimera localised to the cytoplasm and not the nucleus. Although the two constructs consistently localised to the cytoplasm (see Fig. 5.4, panels a-c), there was no co-localisation within the nuclear region, which only expressed eGFP-Chimera. Both the Chimera and Cherry-PLD2a did not alter their localisation following EGF stimulation (see Fig. 5.4, panels d-f). This indicates that the N-terminus of PLD1b may be responsible for EGFR endocytotsis upon EGF stimulation and that diffuse cytoplasmic expression is encoded by the N-terminus of PLD2a, hence its retention by the Chimera construct.

The eGFP-Chimera and Cherry-PLD constructs are close in excitation/emission spectra. To minimise cross-channel fluorescence detection, samples were scanned sequentially (which scans each channel individually) using confocal microscopy. Excitation/emission settings for both fluorophores were restricted and kept consistent throughout all experiments.

Table 5.1: Identifying NLS in hPLD1b, hPLD2a, Chimera and SV40 T sequences using various database searching programs. The sequences of hPLD1b, hPLD2a, Chimera and SV40 T were analysed using the following software:

1) PSORTII (Nakai and Horton, 1999; ROSTLAB http://psort.ims.u-tokyo.ac.jp/),
2) NLStradamus (Nguyen Ba *et al*., 2009; http://www.bar.utoronto.ca/~anguyenba/) and
3) ROSTLAB (Cokol *et al*., 2000; http://rostlab.org/old_before2008/services/predict/NLS)

	PSORT II Sequence/position	**POSTLAB Sequence/position**	**NLStradamus Sequence/position**
hPLD1b	KPRK $_{553}$	None	None
hPLD2a	None	None	None
Chimera	KPRK 651	None	None
SV40 T	PPKKKRK $_{125}$ PKKRYWL $_{417}$	PPKKKRK$_{125}$	KKKRK

Table 5.2: Analysing hPLD1b, hPLD2a, Chimera and SV40 T sequences using POSTLAB II software. The sequences for hPLD1b, hPLD2a, Chimera and SV40 T were analysed using the PSORT II, (Nakai and Horton, 1999; http://psort.ims.u-tokyo.ac.jp/). The database search then suggested the most likely localisation of these sequences (expressed in percentage) in various organelles.

	hPLD1b	**hPLD2a**	**Chimera**	**SV40 T**
Cytoplasmic	56.5%	22.2%	60.9%	52.2%
Cytoskeletal				4.3%
Endoplasmic reticulum		44.4%		
Golgi		11.1%	34.8%	
Mitochondrial	4.3%	11.1%		8.7%
Nuclear	34.8%	11.1%		34.8%
Vesicles of secretory system	4.3%		4.3%	

Figure 5.3: The effect of EGF on co-localisation between eGFP-Chimera and Cherry-PLD1b in HeLa cells. HeLa cells were grown on coverslips and transiently co-transfected with 3 µg eGFP-Chimera (panels **b**, **e**) DNA, and 3 µg Cherry-PLD1b (panels **a**, **d**) DNA for 24 hours. Cells were stimulated with EGF (panels **d-i**– 20 nM EGF, 10 minutes at 37^{o}C), fixed in 4% paraformaldehyde and mounted onto glass slides. Fluorescence was detected using sequential scanning confocal microscopy (SP5) in which parameters were narrowed for emission band width. Green fluorescence was detected with excitation at 488 nm using the argon laser (20%) with emission band width between 500 nm-565 nm. Red fluorescence was detected using the DPSS 561 laser and excited at 561 nm with an emission band width between 607 nm-790 nm. A scale calibrated to 25 µm is shown in each panel. The data presented are representative images for 1 experiment repeated twice.

Control

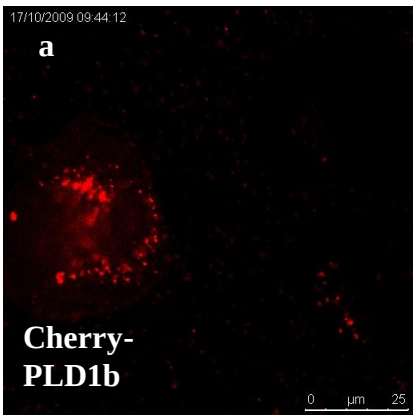

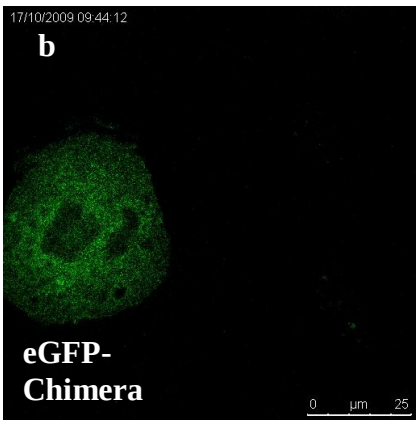

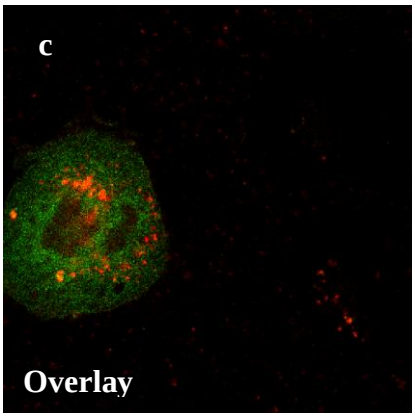

+ EGF stimulation

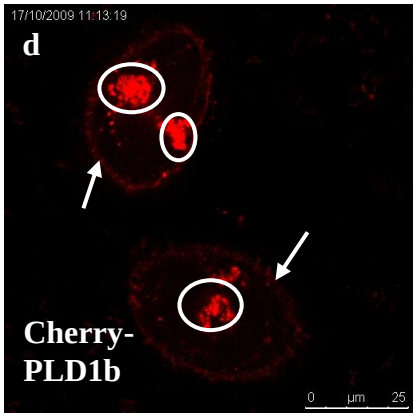

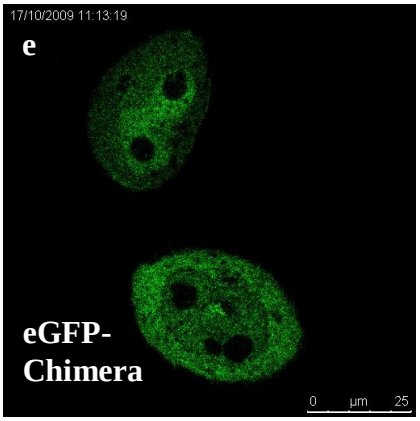

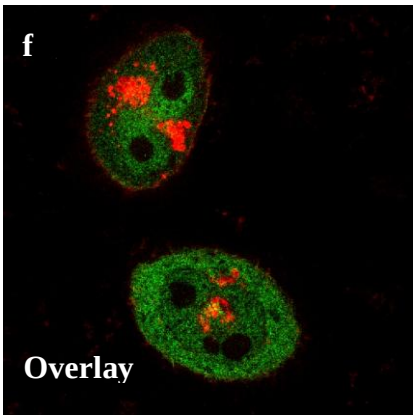

+ EGF stimulation

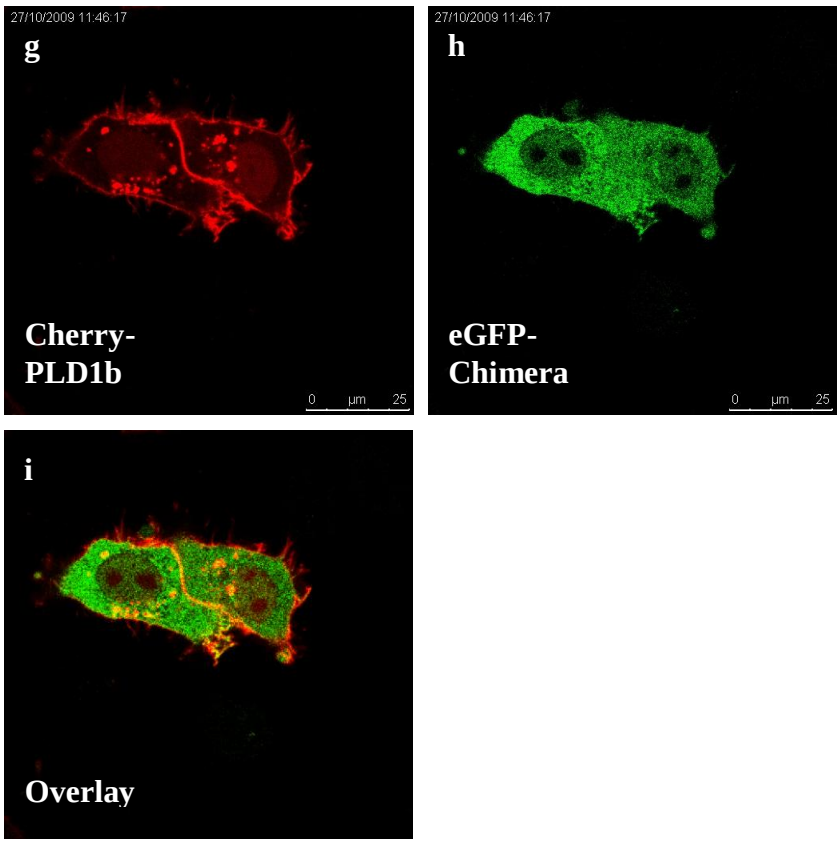

Figure 5.4: The effect of EGF on co-localisation between eGFP-Chimera and Cherry-PLD2a in HeLa cells. HeLa cells were grown on coverslips and transiently co-transfected with 3 µg eGFP-Chimera (panels **b**, **e**) DNA, and 3 µg Cherry-PLD2a (panels **a**, **d**) DNA for 24 hours. Cells were stimulated with EGF (panels **d**-**f** – 20 nM EGF, 10 minutes at 37^{o}C), fixed in 4% paraformaldehyde and mounted onto glass slides. Fluorescence was detected using sequential scanning confocal microscopy (SP5) where parameters were narrowed as detailed in Figure 6.3. A scale calibrated to 25 µm is shown in each panel. The data presented are representative images for 1 experiment repeated twice.

Control

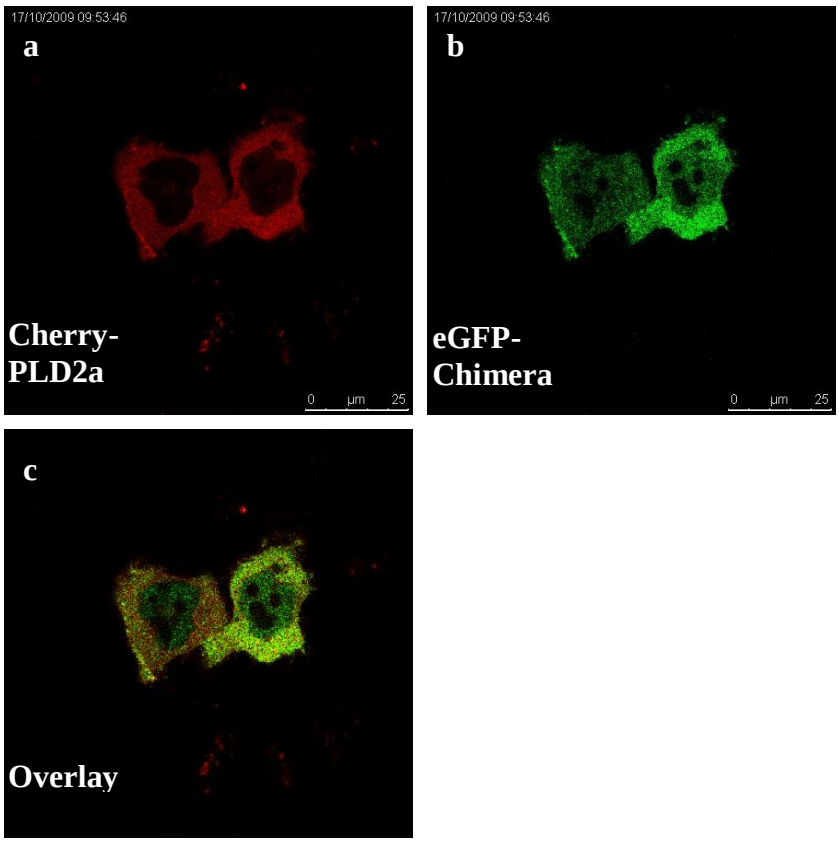

+ EGF stimulation

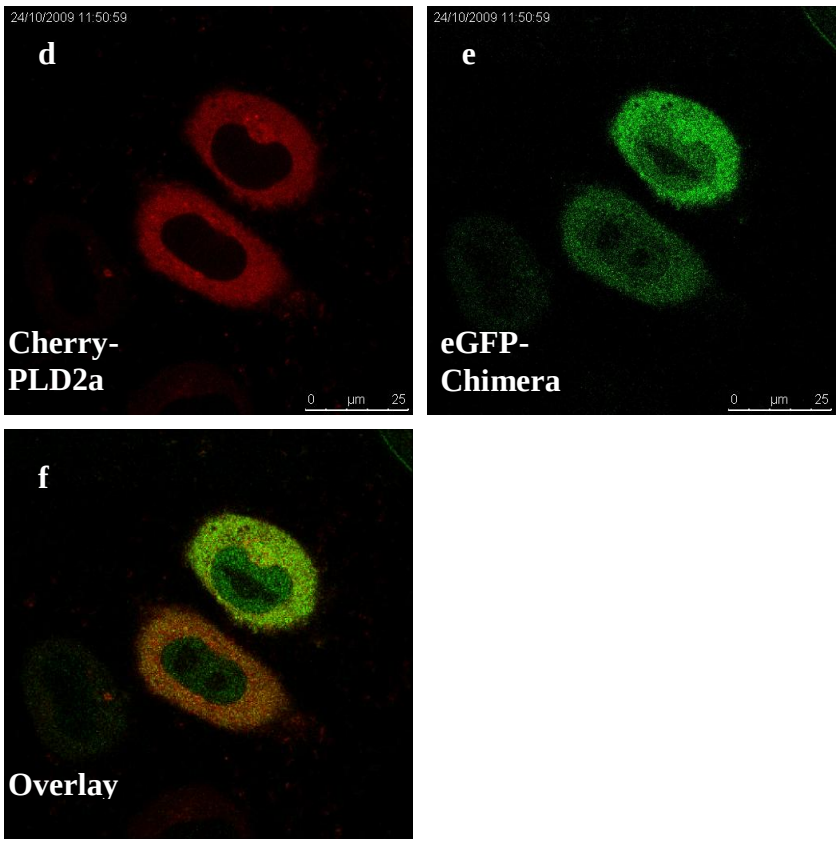

5.2.4: Transient transfections using Cherry-PLD and the effect of EGF stimulation on HeLa cells

The expression of Cherry-labelled PLD in transiently transfected HeLa cells was observed with and without EGF stimulation (see Fig. 5.5). Expression of Cherry alone was diffuse, present in the cytosol and nuclear compartment, and unaffected by EGF stimulation (see Fig. 5.5, panels a, b). Cherry-PLD1b exhibited punctate localisation similar to its eGFP-labelled counterpart, being concentrated in perinuclear structures which possibly represented lysosomes or endosomes (Toda *et al*., 1999; Hughes and Parker, 2001; Hiroyama and Exton, 2005b) and on the plasma membrane (see Fig. 5.5, panels c, d). EGF stimulation resulted in clear translocation of Cherry-PLD1b from the cytoplasmic punctiform structures to the plasma membrane (see arrows, Fig. 5.5, panel d), although a small pool maintained punctiform structures and appeared to concentrate at an intracellular site (see circles, Fig. 5.5, panel d). Over-expression of Cherry-PLD2a displayed 2 phenotypes of expression similar to that seen in eGFP-labelled PLD2a. Cherry-PLD2a is expressed in the cytosol of HeLa cells (see Fig. 5.5, panels e, f) and excludes the nuclear compartment. As with the eGFP-PLD2a, Cherry-PLD2a exhibited a second punctate localisation which occurs with less frequency (see Fig. 5.5, panels g, h). Punctate PLD2a localisation occurred in approximately 10% of transfections with a frequency of 20% amongst transfected cells. Cherry-PLD2a localisation remained unaltered upon EGF stimulation (see Fig. 5.5, panels f, h). The localisation of PLD2 has been observed on the plasma membrane (Han *et al*., 2002b), however the cytoslic expression seen consistently in both eGFP- and Cherry-labelled PLD2a has also been documented (Emoto *et al*., 2000). Establishing that the expression of Cherry-PLD2a remains unaltered upon EGF stimulation and is distinct from Cherry-PLD1b localisation facilitates its use as an important control.

Figure 5.5: The effect of EGF on Cherry-PLD localisation in HeLa cells. HeLa cells grown on coverslips were transiently transfected with 3 µg Cherry (panels **a**, **b**), Cherry-PLD1b (panels **c**, **d**) or Cherry-PLD2a (panels **e**, **f**, **g**, **h**) DNA for 24 hours. Cells were stimulated with EGF (panels **b**, **d**, **f**, **h** – 20 nM, for 10 minutes at 37^{o}C), fixed in 4% paraformaldehyde and mounted on glass slides. Red fluorescence was detected by confocal microscopy (SP5) by excitation at 561 nm and emission band width between 610 nm-790 nm using the DPSS 561 laser. A scale calibrated to 25 µm is shown in each panel. The data presented are representative images for 1 experiment repeated at least 3 times.

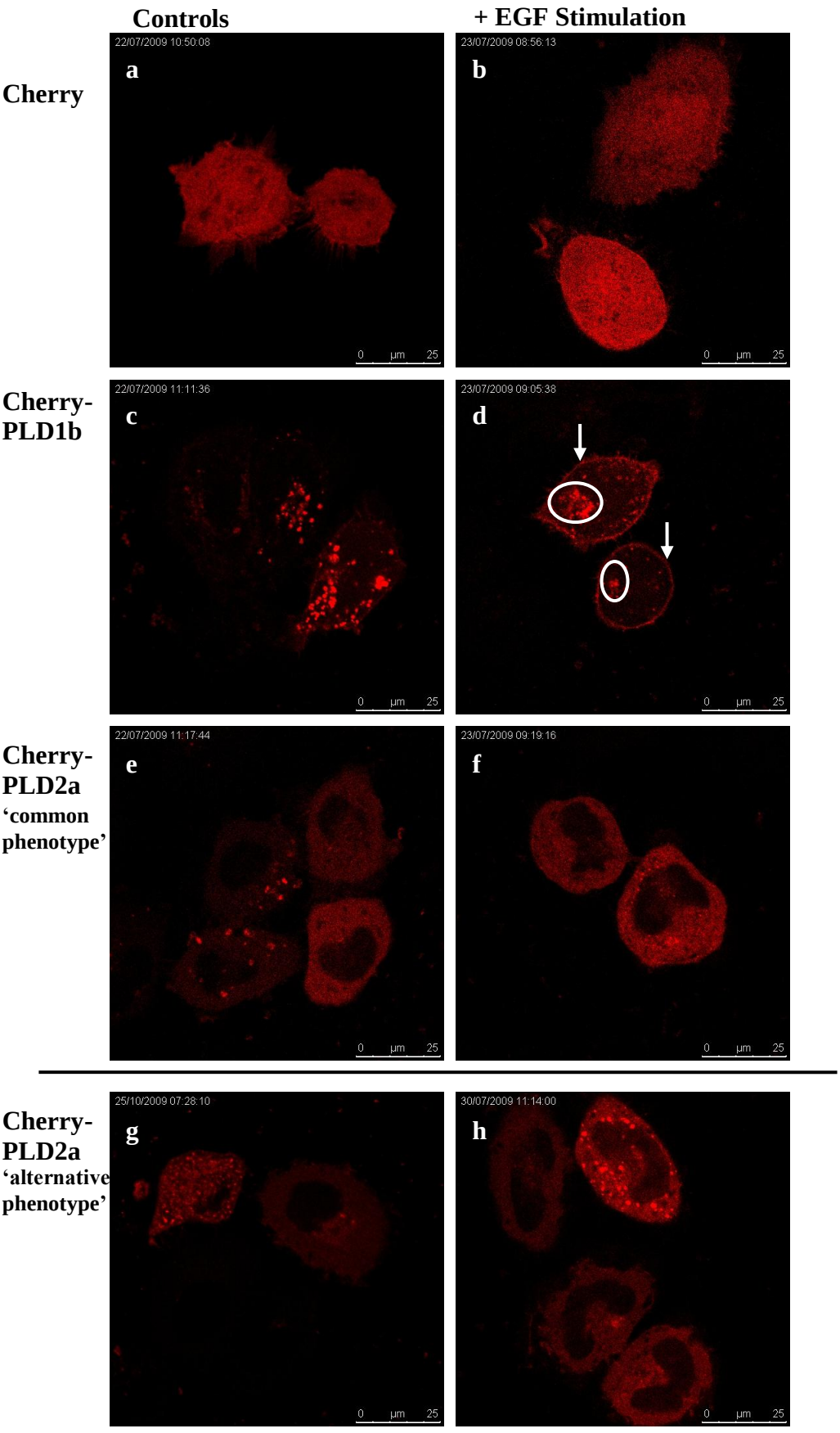
Controls
+ EGF Stimulation
Cherry
Cherry-PLD1b
Cherry-PLD2a 'common phenotype'
Cherry-PLD2a 'alternative phenotype'
22/07/2009 10:50:08
a
23/07/2009 08:56:13
b
22/07/2009 11:11:36
c
23/07/2009 09:05:38
d
22/07/2009 11:17:44
e
23/07/2009 09:19:16
f
25/10/2009 07:28:10
g
30/07/2009 11:14:00
h
0 µm 25

Western blotting was used to demonstrate that the full length Cherry-PLD1b and Cherry-PLD2a proteins were being expressed in transiently transfected HeLa cells. The detection of fluorescence (see Fig. 5.5) indicates that the N-termini of both PLD1b and PLD2a is intact. Western blotting using rabbit polyclonal antibodies raised to PLD1b (see Fig. 5.6, lanes 1-4) and PLD2a (see Fig. 5.6, lanes 5-8) indicate that both proteins were expressed to their full-length (150kDa and 136kDa respectively). The signal for PLD2a was significantly stronger than PLD1b, probably due to variation in the affinity of the different antibodies. A doublet was detected in the PLD2a samples, possibly due to post-translational modification (see Fig. 5.6, lanes 7 and 8 - Manifava *et al*., 1999 Xie *et al*., 2001 Sugars *et al*., 2002).

Figure 5.6: Western blotting analysis of Cherry-PLD1b or PLD2a harvested from transiently transfected HeLa cells. HeLa cells were grown in 6-well plates overnight and transiently transfected with 3 µg of Cherry-PLD1b (lanes **1**,**2**,**5**,**6**) or Cherry-PLD2a (lanes **3**,**4**,**7**,**8**) DNA for 24 hours. The cells were then washed with 1 ml PBS and 3 wells were scrapped into a total of 50 µl x2 NuPAGE Sample Reducing Buffer to produce usable protein lysates. Samples were collected in duplicate and analysed using gel electrophoresis and immunoblotting. Samples analysed in lanes **1-4** were probed with a polyclonal anti-rabbit PLD1b antibody overnight, whilst samples in lanes 5-8 were probed with a polyclonal anti-rabbit PLD2a antibody overnight. The blots were then probed with anti-rabbit HRP secondary antibody and developed for 3 minutes in ECL. Cherry-PLD1b (lanes **1**,**2**,**5**,**6**) and Cherry-PLD2a (lanes 3,4,7,8) lysates were analysed as shown below.

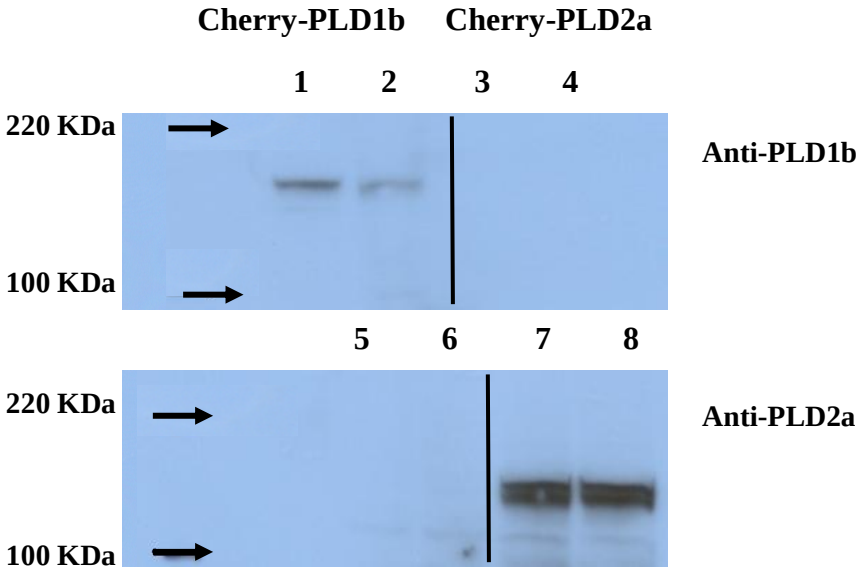

5.2.5: Co-localisation between Cherry- and eGFP-labelled PLD isoforms in HeLa cells and the effect of EGF stimulation

Transiently transfected HeLa cells expressing Cherry-PLD and eGFP-PLD display similar phenotypes (see Fig. 5.1 and 5.5). HeLa cells transiently co-transfected using the Cherry-PLD1b (see Fig. 5.7, panels a, d) and eGFP-PLD1b (see Fig. 5.7, panels b, e) constructs exhibited some co-localisation. Both PLD1b constructs showed the characteristic punctiform and (partial) plasma membrane localisations (see Fig. 5.7, panels a-c). eGFP-PLD1b and Cherry-PLD1b were expressed at the plasma membrane (see arrows, Fig. 5.7, panel f) in response to EGF stimulation, resulting in extensive co-localisation (see Fig. 5.7, panels d-f). The characteristic pool of PLD1b which concentrates within the cell (see circles Fig. 5.7, f) also displayed strong co-localisation between eGFP-PLD1b and Cherry-PLD1b. Co-transfected cells were imaged using sequential scanning confocal microscopy with the separate fluorescence channels overlayed. Excitation/emission parameters for both fluorphores were maintained throughout co-localisation analysis. Although co-localisation was evident, the GFP fluorescence yield was much higher than for Cherry constructs.

HeLa cells were also transiently co-transfected with Cherry-PLD2a (see Fig. 5.8, panels a, d) and eGFP-PLD2a (see Fig. 5.8, panels b, e) both of which displayed the same characteristic diffuse cytoplasmic expression (excluding the nucleus – see Fig. 5.8, panel c). PLD2a expression remained unaffected by EGF stimulation (see Fig. 5.8, panels d-f) and co-localisation between eGFP- and Cherry-PLD2a was retained. Although localisation between the 2 constructs was evident, the levels of expression, fluorescence yield and transfection efficiency varied and so overlays appeared more green than yellow.

Figure 5.7: The effect of EGF on the localisation of eGFP-PLD1b and Cherry-PLD1b in co-transfected HeLa cells. HeLa cells were grown on coverslips and transiently co-transfected with 3 µg eGFP-PLD1b (panels **b**, **e**) DNA, and 3 µg Cherry-PLD1b (panels **a**, **d**) DNA for 24 hours. Cells were stimulated with EGF (panels **d-f** – 20 nM EGF, 10 minutes at 37^{o}C), fixed in 4% paraformaldehyde and mounted onto glass slides. Fluorescence was detected using sequential scanning confocal microscopy (SP5) where parameters were narrowed for emission band width. Green fluorescence was detected by confocal microscopy (SP5) with excitation at 488 nm and emission band width between 500 nm-565 nm using an argon laser (20%). Red fluorescence was detected using the DPSS 561 laser and excited at 561 nm with an emission band width between 607 nm-790 nm. A scale calibrated to 25 µm is shown in each panel. The data presented are representative images for 1 experiment repeated twice.

Control

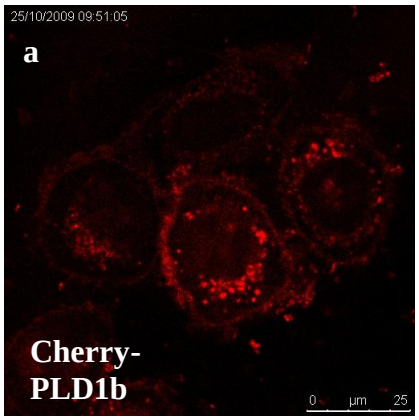

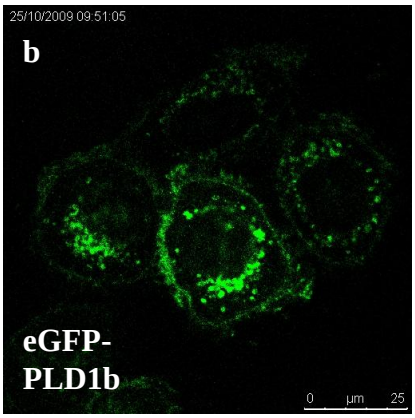

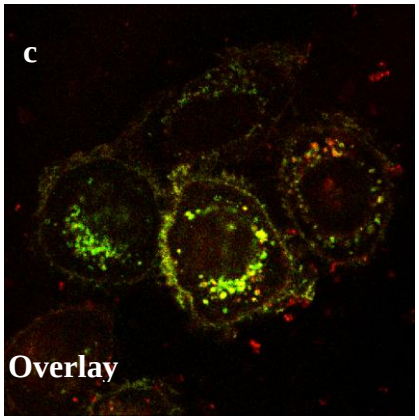

+ EGF stimulation

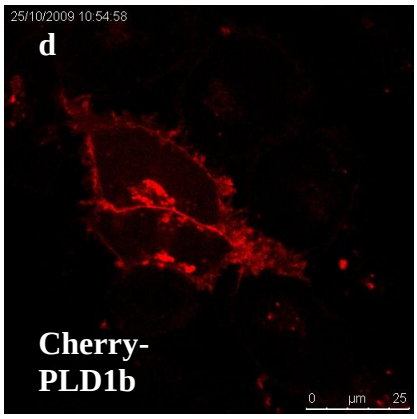

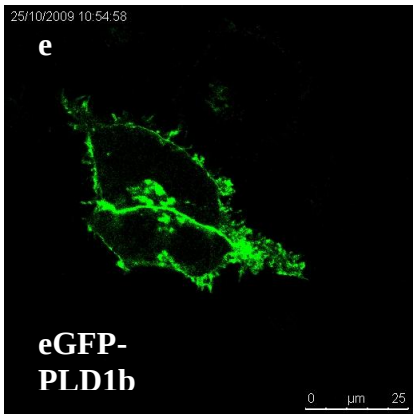

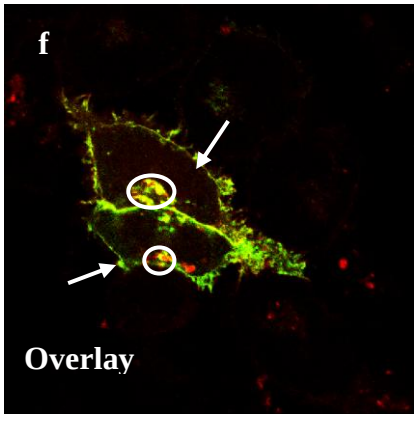

Figure 5.8: The effect of EGF on the localisation of eGFP-PLD2a and Cherry-PLD2a in co-transfected HeLa cells. HeLa cells were grown on coverslips and transiently co-transfected with 3 µg eGFP-PLD2a (panels **b**, **e**) DNA, and 3 µg Cherry-PLD2a (panels **a**, **d**) DNA for 24 hours. Cells were stimulated with EGF (panels **d-f** – 20 nM EGF, 10 minutes at 37^{o}C), fixed in 4% paraformaldehyde and mounted onto glass slides. Fluorescence was detected using sequential scanning confocal microscopy (SP5) where parameters were narrowed as detailed in Figure 6.7. A scale calibrated to 25 µm is shown in each panel. The data presented are representative images for 1 experiment repeated twice.

Control

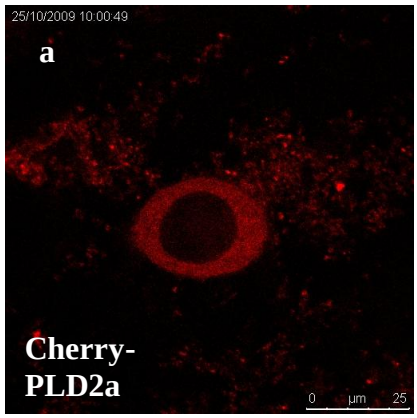

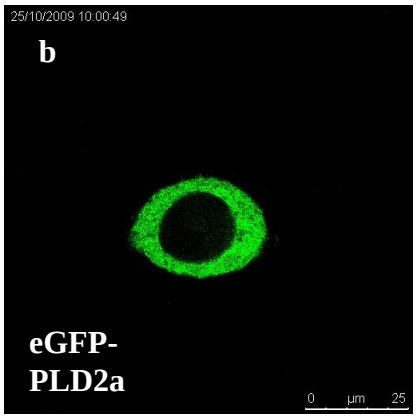

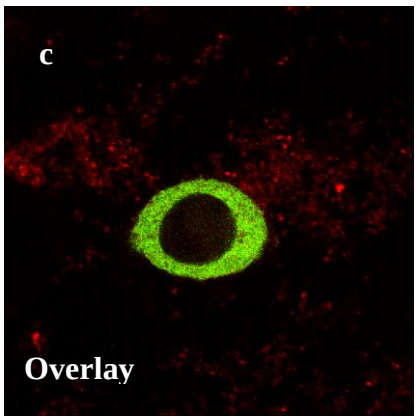

+ EGF stimulation

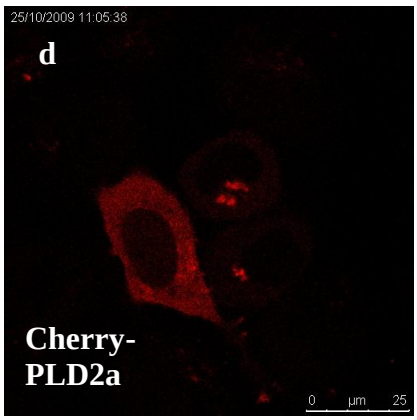

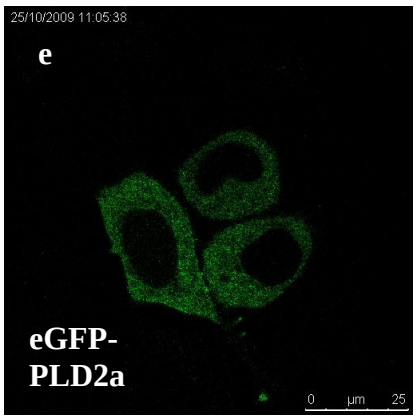

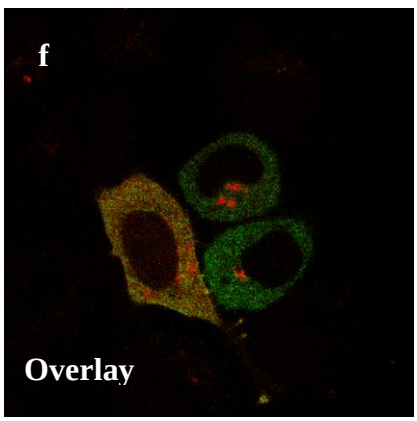

HeLa cells transiently co-transfected with Cherry-PLD1b (see Fig. 5.9, panels a, d) and eGFP-PLD2a (see Fig. 5.9, panels b, e) did not alter the localisation of either PLD isoform (see Fig. 5.1 and 5.5). This consistently distinct localisation suggests that their functions and activators are discrete within the cell system and that dimerisation between the 2 is unlikely. PLD1b localises primarily to punctiform structures within the cytoplasm in resting cells and so some co-localisation occurred between PLD1b and PLD2a within the cytoplasm (see Fig. 5.9, panel c). Upon EGF stimulation, PLD1b was expressed at the plasma membrane (see Fig. 5.9, panel d) as expected, whilst PLD2a expression remained diffuse and unaltered (see Fig. 5.9, panel e). Cytoplasmic co-localisation between the 2 isoforms was retained (see Fig. 5.9, panel f); however there was also weak expression of PLD1b in the nucleus of stimulated cells whilst PLD2a expression was absent. The over-expression of both PLD isoforms may have contributed to the expression of PLD1b in the nucleus of the co-transfected HeLa cells as endogenous PLD expression is normally relatively low. To confirm that the localisation of PLD2a and PLD1b were not affected by co-transfection in HeLa cells, a similar experiment using Cherry-PLD2a and eGFP-PLD1b was completed.

Transiently co-transfected HeLa cells expressing Cherry-PLD2a maintained the characteristic diffuse expression (see Fig. 5.10, panels a, d). eGFP-PLD1b localised in punctiform structures within the cytoplasm (see Fig. 5.10, panel b) in resting cells. Although the expression of Cherry-PLD2a remained unaffected by EGF stimulation (see Fig. 5.10, panel d), eGFP-PLD1b was expressed at the plasma membrane (see arrows, Fig. 5.10, panel f). The aggregated pool of PLD1b within the cytoplasm upon EGF stimulation was also noted (see circles Fig. 5.10, panel f). This confirmed that localisation of PLD1b and PLD2a was unaffected by labelling with either the eGFP or Cherry fluorescent tags.

Figure 5.9: The effect of EGF on the localisation of eGFP-PLD2a and Cherry-PLD1b in co-transfected HeLa cells. HeLa cells were grown on coverslips and transiently co-transfected with 3 µg eGFP-PLD2a (panels **b**, **e**) DNA, and 3 µg Cherry-PLD1b (panels **a**, **d**) DNA for 24 hours. Cells were stimulated with EGF (panels **d-f** – 20 nM EGF, 10 minutes at 37^{o}C), fixed in 4% paraformaldehyde and mounted onto glass slides. Fluorescence was detected using sequential scanning confocal microscopy (SP5) where parameters were narrowed as detailed in Figure 6.7. A scale calibrated to 25 µm is shown in each panel. The data presented are representative images for 1 experiment repeated twice.

Control

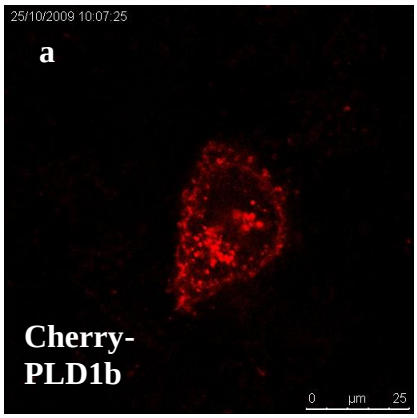

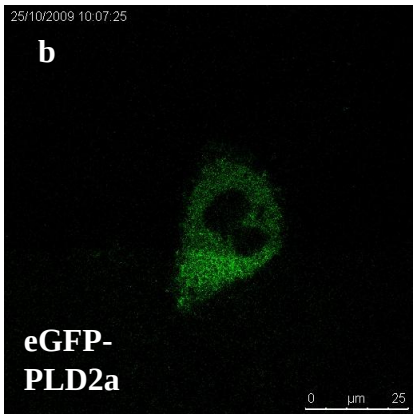

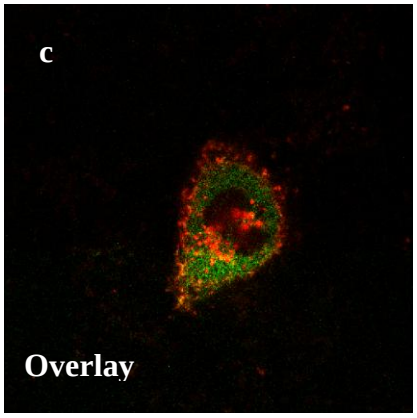

+ EGF stimulation

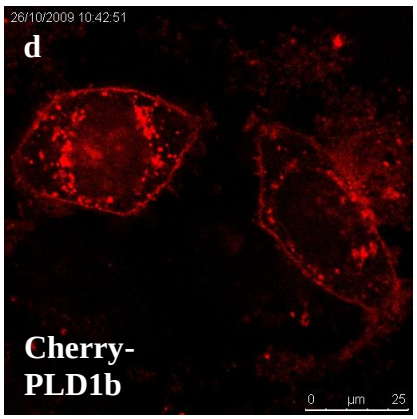

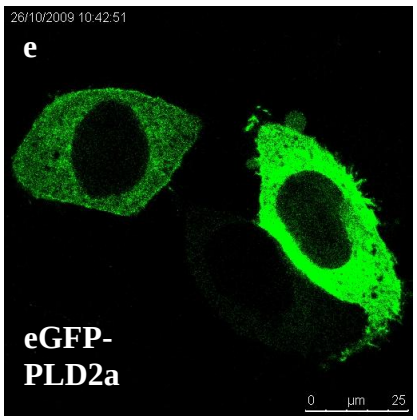

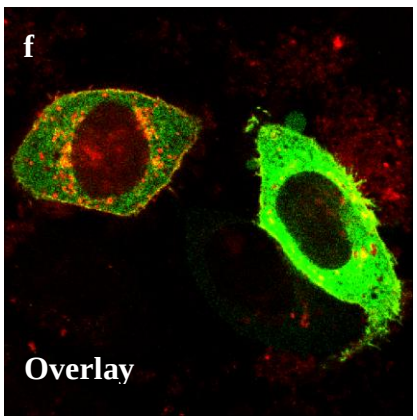

Figure 5.10: The effect of EGF on the localisation of eGFP-PLD1b and Cherry-PLD2a in co-transfected HeLa cells. HeLa cells were grown on coverslips and were transiently co-transfected with 3 µg eGFP-PLD1b (panels **b**, **e**) DNA, and 3 µg Cherry-PLD2a (panels **a**, **d**) DNA for 24 hours. Cells were stimulated with EGF (panels **d-f** – 20 nM EGF, 10 minutes at 37^{o}C), fixed in 4% paraformaldehyde and mounted onto glass slides. Fluorescence was detected using sequential scanning confocal microscopy (SP5) where parameters were narrowed as detailed in Figure 6.7. A scale calibrated to 25 µm is shown in each panel. The data presented are representative images for 1 experiment repeated twice.

Control

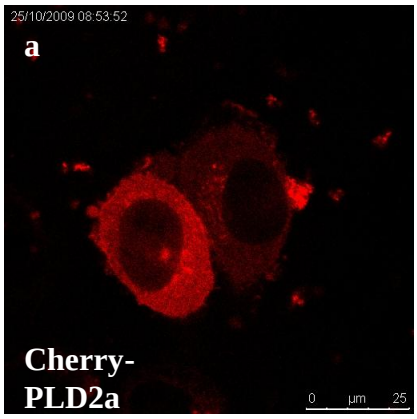

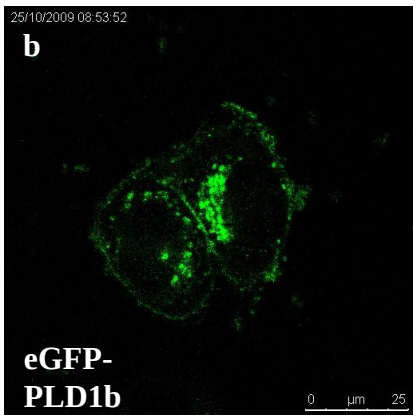

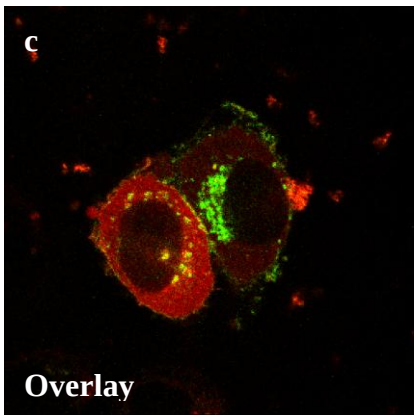

+ EGF stimulation

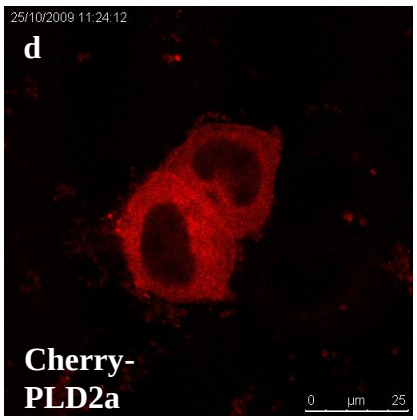

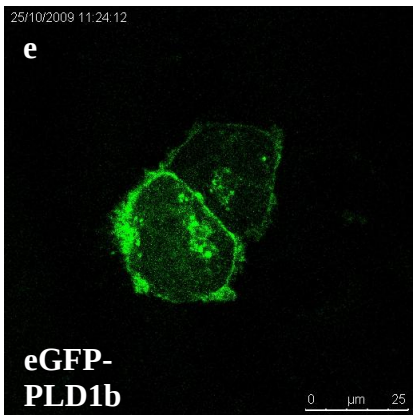

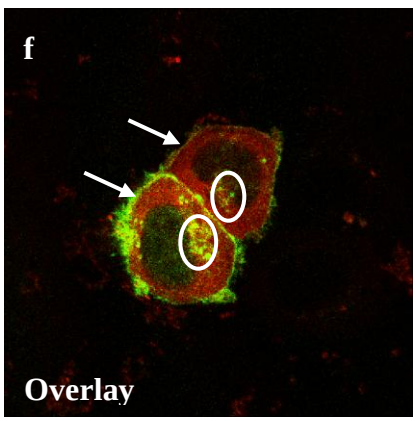

5.2.6: Transiently transfected HeLa cells expressing eGFP-Rac1 and their response to EGF stimulation

Characterisation of Cherry-PLD provided the opportunity to observe PLD localisation with the PLD1 activator, Rac1. Although the localisation of PLD1 with another small G-protein activator Arf-6, has been characterised in a similar manner (Hiroyama and Exton, 2005b), PLD1 co-expression with Rac1 in HeLa cells has yet to be demonstrated. eGFP-Rac1 wild type (wt) and its mutants were characterised in transiently transfected HeLa cells before co-expressing with Cherry-PLD constructs.

In HeLa cells, eGFP-Rac1 (wt) exhibited prominent membranous localisation as well as being expressed in punctiform structures within the cytosol (see Fig. 5.11, panels a, b). In response to EGF stimulation, eGFP-Rac1 (wt) appeared to be expressed more prominently at the plasma membrane, particularly at cell junctions. A dominant negative mutant of Rac1 (T17N) in which threonine (T) 17 was substituted for an asparagine (N) residue displayed similar localisation to Rac1 (wt). Rac1 (T17N) showed punctate and membrane localisation prior to EGF stimulation and localisation on the plasma membrane and associated processes generated after EGF stimulation. In Swiss 3T3 cells, the dominant negative Rac1 (T17N) mutant inhibited the stimulation of cells to EGF (Ridley *et al*., 1992).

Expression of a constitutively active GTP-bound eGFP-Rac1 in which glutamine (Q) 61 was substituted with leucine (L) (eGFP-Rac1 (Q61L)) resulted in a dramatic shape change, with transfected cells displaying membrane ruffling and large vacuole formation within the cell structure (see Fig. 5.11, panels e, f, g, h). Stimulation of Rac1 (Q61L) transfected cells with EGF did not alter the localisation or affect the cell morphology seen prior to stimulation (see Fig. 5.11, panels f, h). The most commonly observed morphology of cells expressing Rac1 (Q61L) showed membrane ruffling, changes in cell shape and increased size (see Fig. 5.11, panels e, f). There was a second morphology seen in Rac1 (Q61L) expressing HeLa cells which appeared in approximately 30% of transfected cells and is notably brighter (see Fig. 5.11, panels g, h). The less frequent morphology was characterised by numerous intracellular vacuoles located within the cytosol appearing to form one large structure (see arrows Fig. 5.11, panels g, h).

Figure 5.11: The effect of EGF on eGFP-Rac1 (wt and mutants) localisation in HeLa cells. HeLa cells were grown on coverslips and transiently transfected with 3 µg eGFP-Rac (wt – panels **a**, **b**), eGFP-Rac (T17N – panels **c**, **d**) and eGFP-Rac (Q61L – panels **e**, **f**, **g**, **h**) DNA for 24 hours. HeLa cells were stimulated with EGF (panels **b**, **d**, **f**, **h** – 20 nM EGF, 10 minutes at 37^{o}C), fixed in 4% paraformaldehyde and mounted onto glass slides. Green fluorescence was detected by confocal microscopy (SP5) with excitation at 488 nm and emission band width between 500 nm-608 nm using an argon laser (20%). A scale calibrated to 25 µm is shown in each panel. The data presented are representative images for 1 experiment repeated at least 3 times.

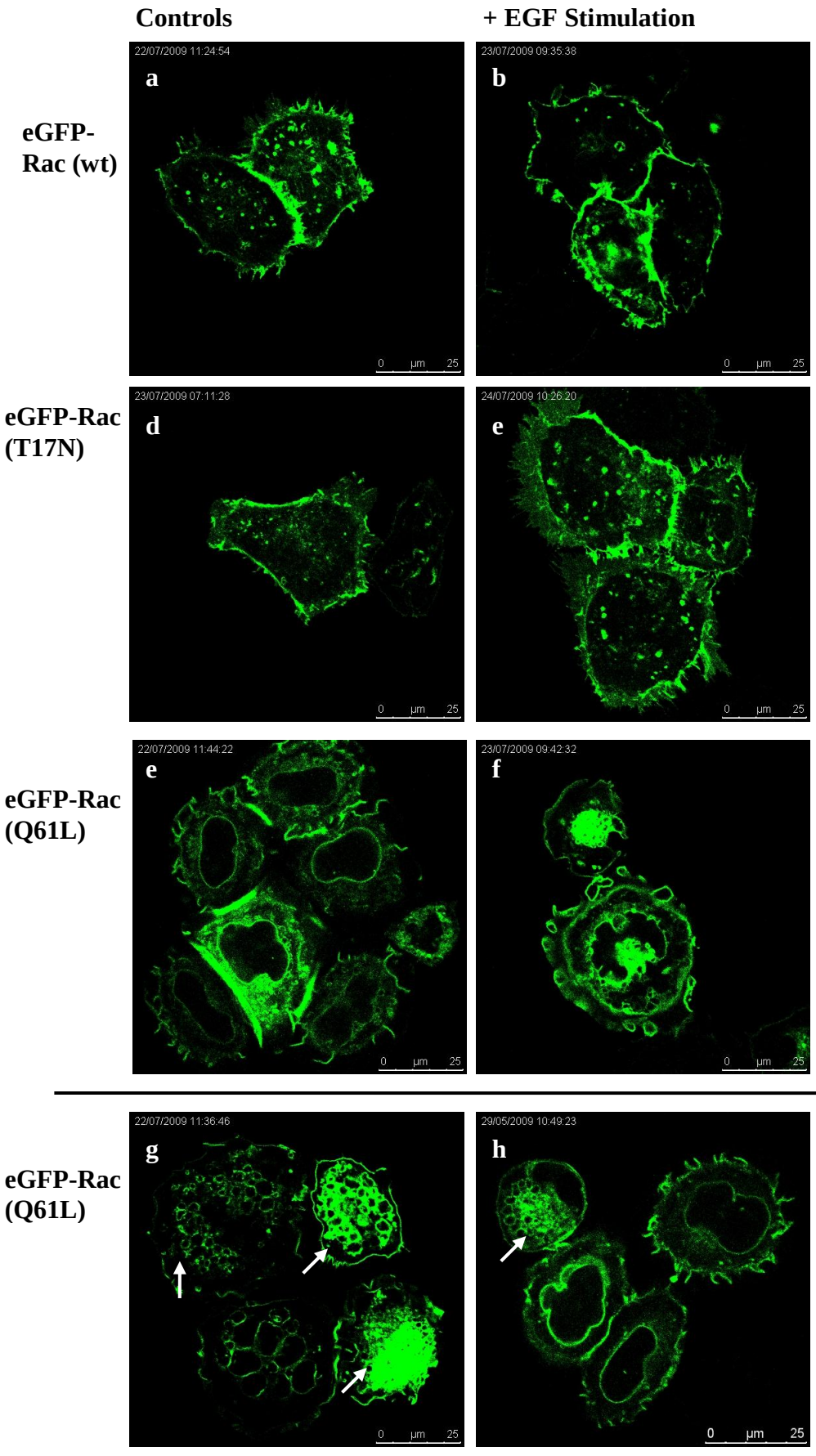
Controls
+ EGF Stimulation
eGFP-Rac (wt)
eGFP-Rac (T17N)
eGFP-Rac (Q61L)
eGFP-Rac (Q61L)
22/07/2009 11:24:54
a
23/07/2009 09:35:38
b
23/07/2009 07:11:28
d
24/07/2009 10:26:20
e
22/07/2009 11:44:22
e
23/07/2009 09:42:32
f
22/07/2009 11:36:46
g
29/05/2009 10:49:23
h
0 µm 25

5.2.7: Characterising Cherry-PLD1b and eGFP-Rac1 co-localisation in HeLa cells with EGF stimulation

Figure 5.12 shows HeLa cells co-transfected with Cherry-PLD1b and eGFP-Rac1 (wt) and the change in localisation in response to EGF stimulation. Cherry-PLD1b and eGFP-Rac1 (wt) did not co-localise in unstimulated HeLa cells. PLD1b was concentrated predominantly in punctiform structures within the cell and Rac1 was on the membrane and also present in punctiform structures, which were distinct from and did not co-localise with PLD1b (see Fig. 5.12, panels a-c). Results indicate that transient transfections of HeLa cells with DNA constructs did not result in artificial punctate localisation simply because of plasmid over-expression.

EGF stimulation caused Cherry-PLD1b expression at the plasma membrane which co-localised with Rac1 (wt) – (Fig. 5.12, panels d, f). However, there was a smaller pool of PLD1b which concentrated within the cell and did not co-localise with Rac1 (see circles Fig. 5.12, panels d, f). These phenotypes are independent of possible interactions and are possibly only relevant to one another following EGF stimulation. eGFP-Rac1 mutants Q61L and T17N were also co-transfected with Cherry-PLD1b (see Fig. 5.13 and 5.14). Co-expression of Cherry-PLD1b and eGFP-Rac1 (Q61L) showed localisation of Cherry-PLD1b was severely affected by Rac1 (Q61L – see Fig. 5.13, panels a-c). Upon EGF stimulation, PLD1b was not expressed at the plasma membrane and was not localised in punctiform structures (see Fig. 5.13, panels d-f). Instead, PLD1b co-localised partly with the small vacuoles caused by Rac1 (Q61L – see arrows Fig. 5.13, panel f).

Unstimulated HeLa cells co-transfected with eGFP-Rac1 (T17N) and Cherry-PLD1b showed no co-localisation between the 2 constructs (see Fig. 5.14, panels a-d). PLD1b and Rac1 (T17N) were predominantly expressed in distinct punctiform structures within the cells that did not co-localise. Rac1 (T17N) also localised to the plasma membrane prior to EGF stimulation. Upon EGF stimulation, PLD1b was expressed at the plasma membrane and co-localised with Rac1 (T17N – see Fig. 5.14, panels e-h). A proportion of PLD1b remained in punctiform structures within the cytosol aggregating towards a confined region (see arrow Fig. 5.14, panel h).

Expression of Rac1 (T17N) in punctiform structures within the cell reduced substantially upon EGF stimulation.

Figure 5.12: The effect of EGF on localisation of eGFP-Rac1 (wt) and Cherry-PLD1b in co-transfected HeLa cells. HeLa cells were grown on coverslips and transiently co-transfected with 3 µg eGFP-Rac1 (wt – panels **b**, **e**) DNA, and 3 µg Cherry-PLD1b (panels **a**, **d**) DNA for 24 hours. Cells were stimulated with EGF (panels **d-f** – 20 nM EGF, 10 minutes at 37^{o}C), fixed in 4% paraformaldehyde and mounted onto glass slides. Fluorescence was detected using sequential scanning confocal microscopy (SP5) where parameters were narrowed for emission band width. Green fluorescence was detected by confocal microscopy (SP5) with excitation at 488 nm and emission band width between 500 nm-565 nm using an argon laser (20%). Red fluorescence was detected using the DPSS 561 laser and excited at 561 nm with an emission band width between 607 nm-790 nm. A scale calibrated to 25 µm is shown in each panel. The data presented are representative images for 1 experiment repeated at least 3 times.

Control

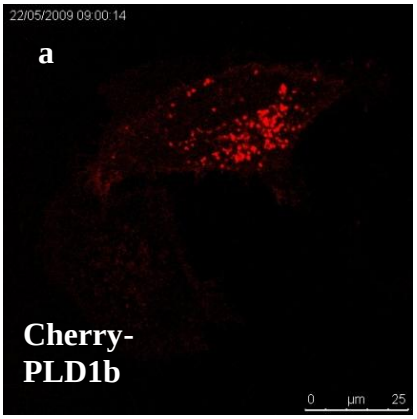

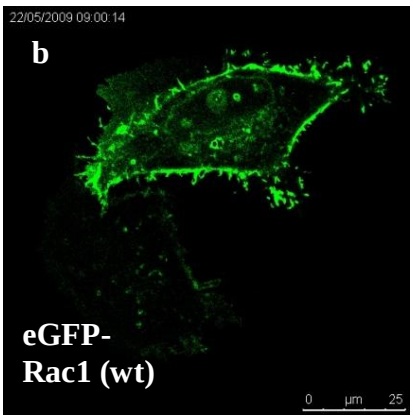

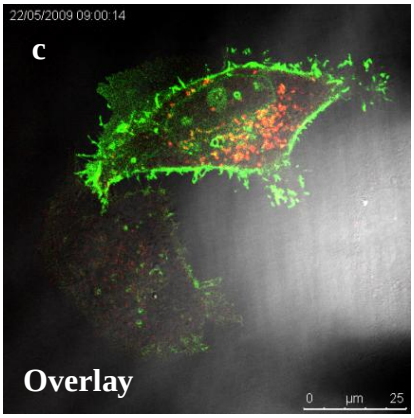

+ EGF stimulation

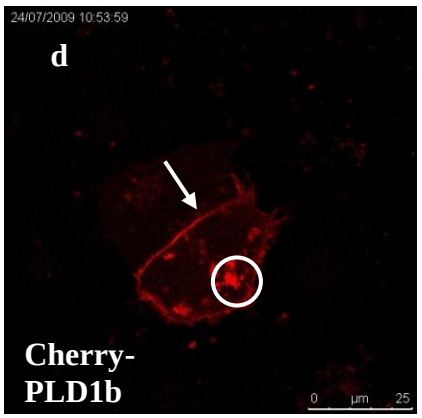

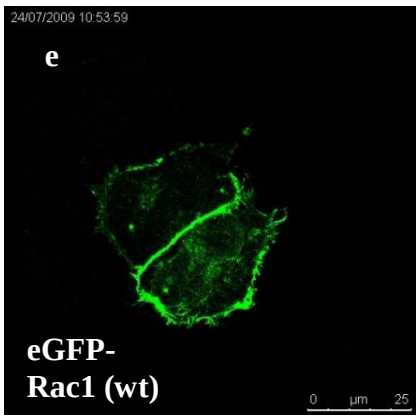

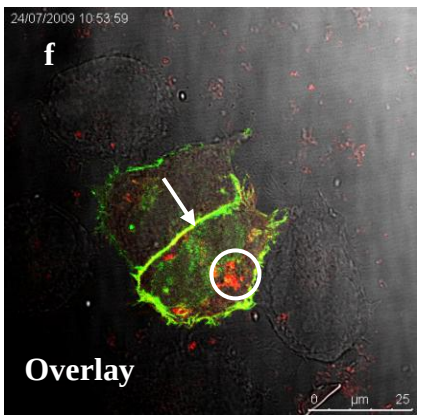

Figure 5.13: The effect of EGF on localisation of eGFP-Rac1 (Q61L) and Cherry-PLD1b in co-transfected HeLa cells. HeLa cells were grown on coverslips and transiently co-transfected with 3 µg eGFP-Rac1 (Q61L– panels **b**, **e**) DNA, and 3 µg Cherry-PLD1b (panels **a**, **d**) DNA for 24 hours. Cells were stimulated with EGF (panels **d**, **e**, **f** – 20 nM EGF, 10 minutes at 37^{o}C) then fixed in 4% paraformaldehyde and mounted onto glass slides. Fluorescence was detected using sequential scanning confocal microscopy (SP5) where parameters were narrowed as detailed in Figure 6.12. Briefly green fluorescence was detected with the argon laser (20%) excited at 488 nm with an emission band width of 500 nm-565 nm. Red fluorescence was detected with the DPSS 561 laser at 561 nm with an emission band width of 607 nm-790 nm. A scale calibrated to 25 µm is shown in each panel. The data presented are representative images for 1 experiment repeated at least 3 times.

Control

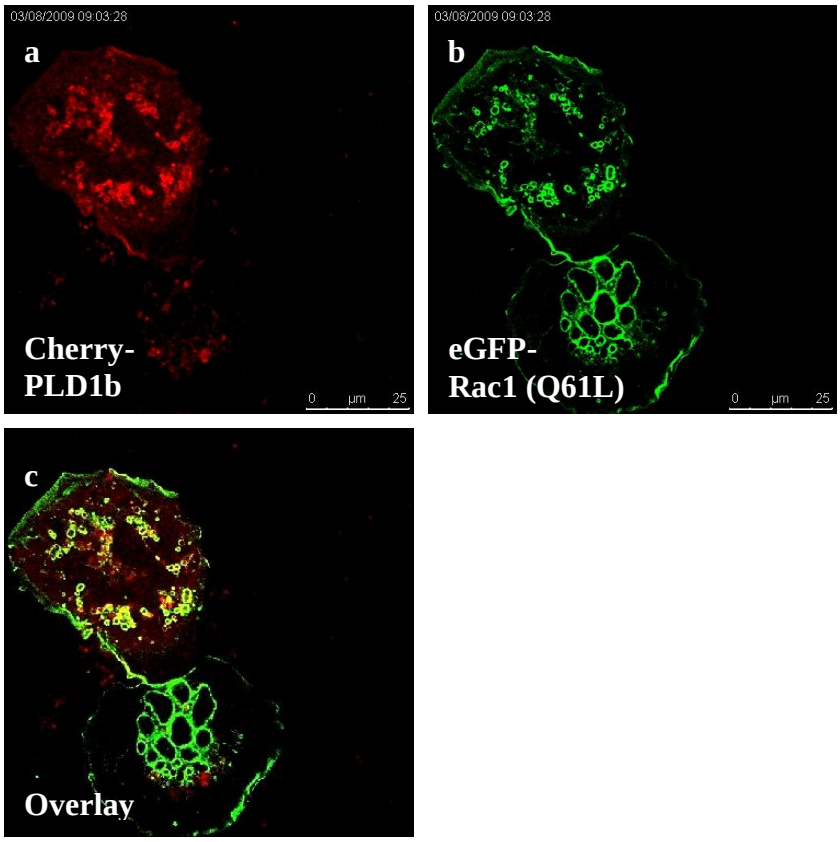

+ EGF stimulation

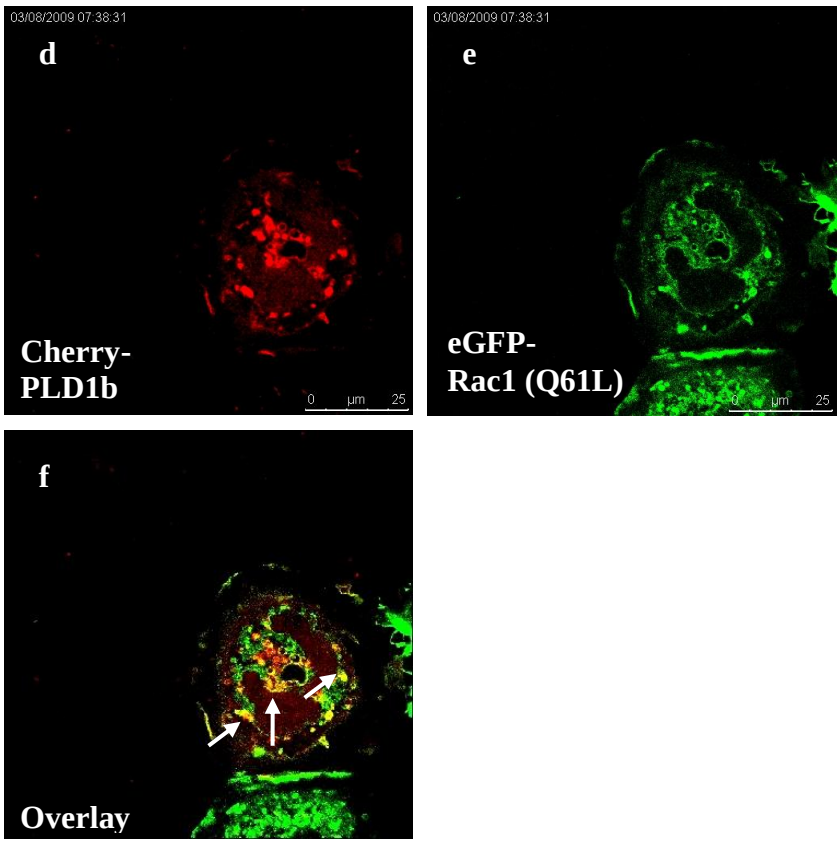

Figure 5.14: The effect of EGF on localisation of eGFP-Rac1 (T17N) and Cherry-PLD1b in co-transfected HeLa cells. HeLa cells were grown on coverslips and transiently co-transfected with 3 µg eGFP-Rac1 (T17N – panels **b**, **f**) DNA, and 3 µg Cherry-PLD1b (panels **a**, **e**) DNA for 24 hours. Cells were stimulated with EGF (panels **e-h** – 20 nM EGF, 10 minutes at 37^{o}C) then fixed in 4% paraformaldehyde and mounted onto glass slides. Fluorescence was detected using sequential scanning confocal microscopy (SP5) where parameters were narrowed as detailed in Figure 6.12. A scale calibrated to 25 µm is shown in each panel. The data presented are representative images for 1 experiment repeated at least 3 times.

Control

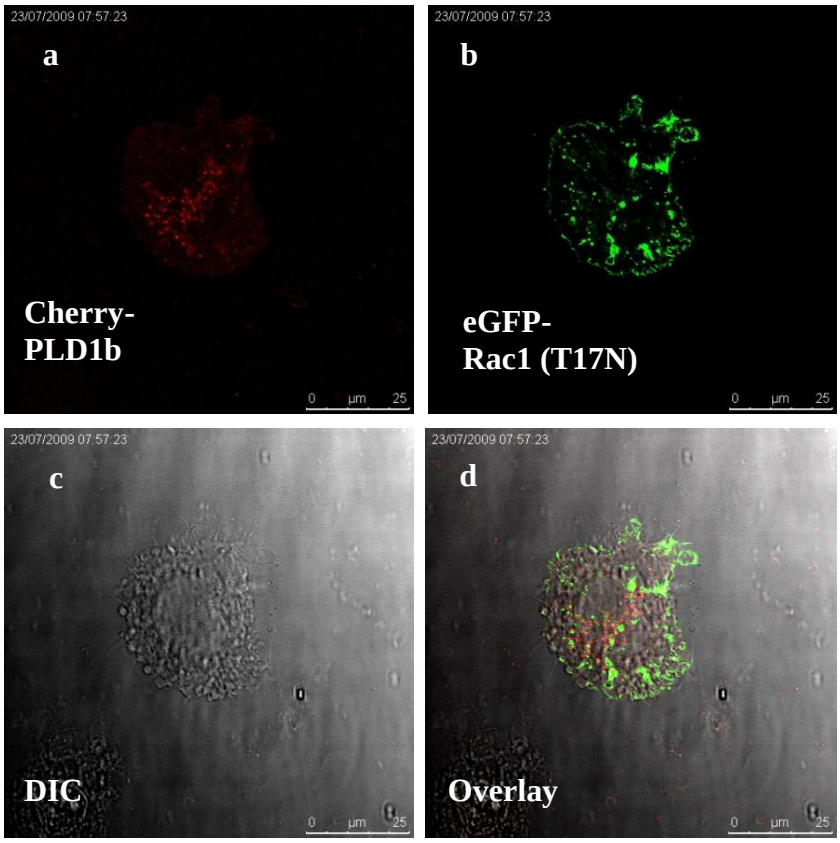

+ EGF stimulation

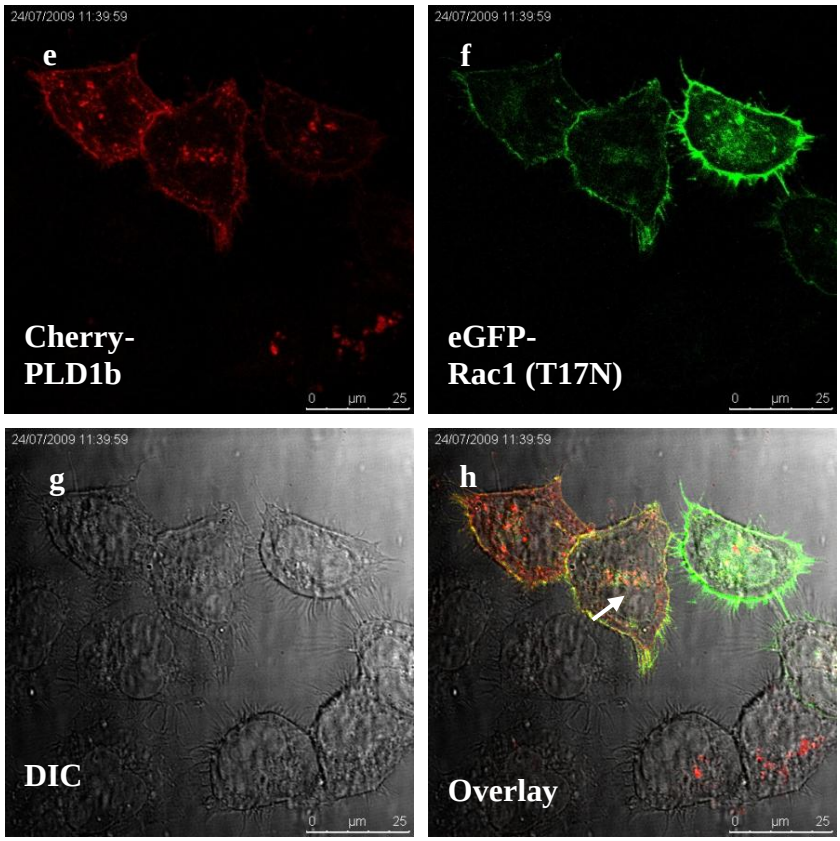

5.2.8: Characterising Cherry-PLD2a and eGFP-Rac1 co-localisation in HeLa cells with EGF stimulation

Cherry-PLD2a localisation was reproducible and distinct to that of Cherry-PLD1b localisation in HeLa cells. HeLa cells co-transfected using Cherry-PLD2a and eGFP-Rac1 could therefore be used as a control to compare with Cherry-PLD1b and eGFP-Rac1 co-transfections. HeLa cells transiently transfected with Cherry-PLD2a and eGFP-Rac1 (wt) were imaged using the same confocal parameters as previous co-localisation experiments (see Fig. 5.15). Cherry-PLD2a was diffusely expressed in the cytosol but not the nucleus (see Fig. 5.15, panels a, e) in both unstimulated and EGF-stimulated cells. eGFP-Rac1 (wt) localised to the plasma membrane and the nucleus (see Fig. 5.15, panel b). eGFP-Rac1 (wt) expression in the nucleus of HeLa cells was more commonly seen as a result of double transfections when compared to the phenotype of single transfections. EGF stimulation did not alter PLD2a which retained its diffuse cytosolic expression whilst Rac1 aggregated to the plasma membrane (see Fig. 5.15, panels e-h). EGF stimulation did not induce co-localisation between PLD2a and Rac1 (wt).

Cherry-PLD2a co-transfected with Rac1 mutants also provided controls for the small degree of co-localisation seen using the Cherry-PLD1b construct. Cherry-PLD2a retained its characteristic diffuse expression (see Fig. 5.16, panel a) despite the dramatic change in cell morphology induced by over-expression of Rac1 (Q61L – see Fig. 5.15, panel b). EGF stimulation did not alter the expression of PLD2a or Rac1 (Q61L) and did not cause co-localisation between the 2 constructs (see Fig. 5.15, panels e-h). Cherry-PLD2a and Rac1 (T17N) did not co-localise in transiently transfected HeLa cells (see Fig. 5.17, panels a-d). Rac1 (T17N) localised to the plasma membrane and in punctiform structures within the cytoplasm (see Fig. 5.17, panel b) whilst Cherry-PLD2a retained its characteristic diffuse cytoplasmic expression (see Fig. 5.17, panel a). Cherry-PLD2a expression did not change after EGF stimulation (see Fig. 5.17, panel e) but Rac1 (T17N) was expressed primarily on the plasma membrane (see Fig. 5.17, panel f). Although there appeared to be some co-localisation between the Rac1 (T17N) cytoplasmic structures and PLD2a (see Fig. 5.17, panel h), this was probably due to uniform expression of PLD2a

throughout the cytoplasm. Expression and morphology of all constructs was reproducible between experiments (see Figs. 5.5, 5.11, 5.12-14 and 5.15-17).

Figure 5.15: The effect of EGF on localisation of eGFP-Rac1 (wt) and Cherry-PLD2a in co-transfected HeLa cells. HeLa cells were grown on coverslips and transiently co-transfected with 3 µg eGFP-Rac1 (wt – panels **b**, **f**) DNA, and 3 µg Cherry-PLD2a (panels **a**, **e**) DNA for 24 hours. Cells were stimulated with EGF (panels **e**-**h** – 20 nM EGF, 10 minutes at 37^{o}C), fixed in 4% paraformaldehyde and mounted onto glass slides. Confocal microscopy (SP5) was used to image co-transfected HeLa cells using sequential scanning. The parameters used for sequential scanning were detailed in Figure 6.12. Briefly green fluorescence was detected with the argon laser (20%) excited at 488 nm with an emission band width of 500 nm-565 nm. Red fluorescence was detected with the DPSS 561 laser at 561 nm with an emission band width of 607 nm-790 nm. A scale calibrated to 25 µm is shown in each panel. The data presented are representative images for 1 experiment of at least 3.

Control

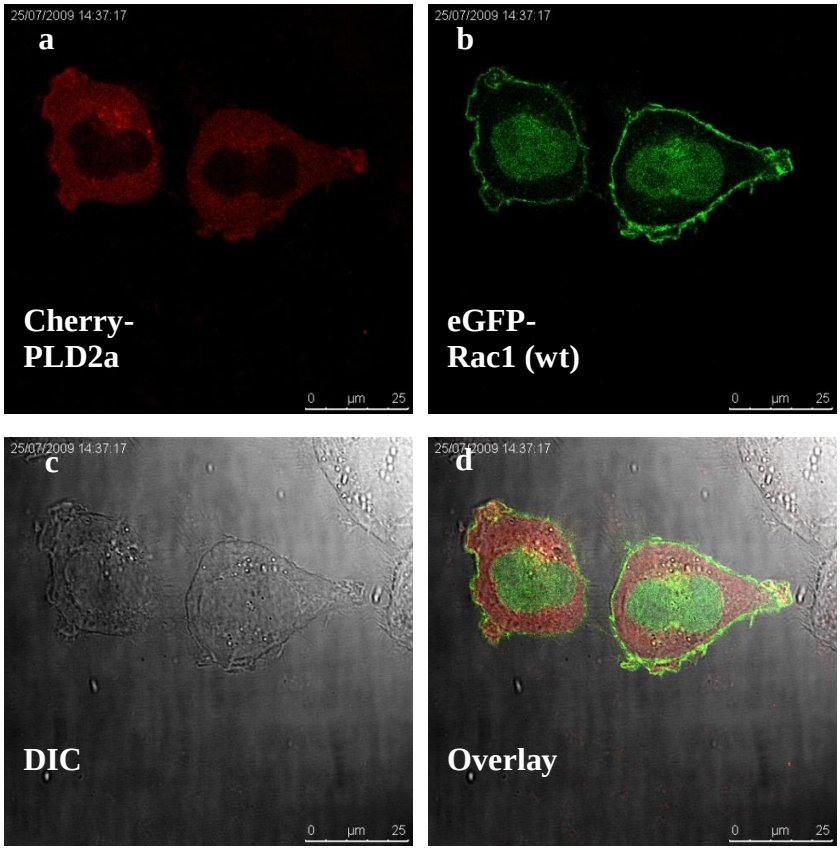

+ EGF stimulation

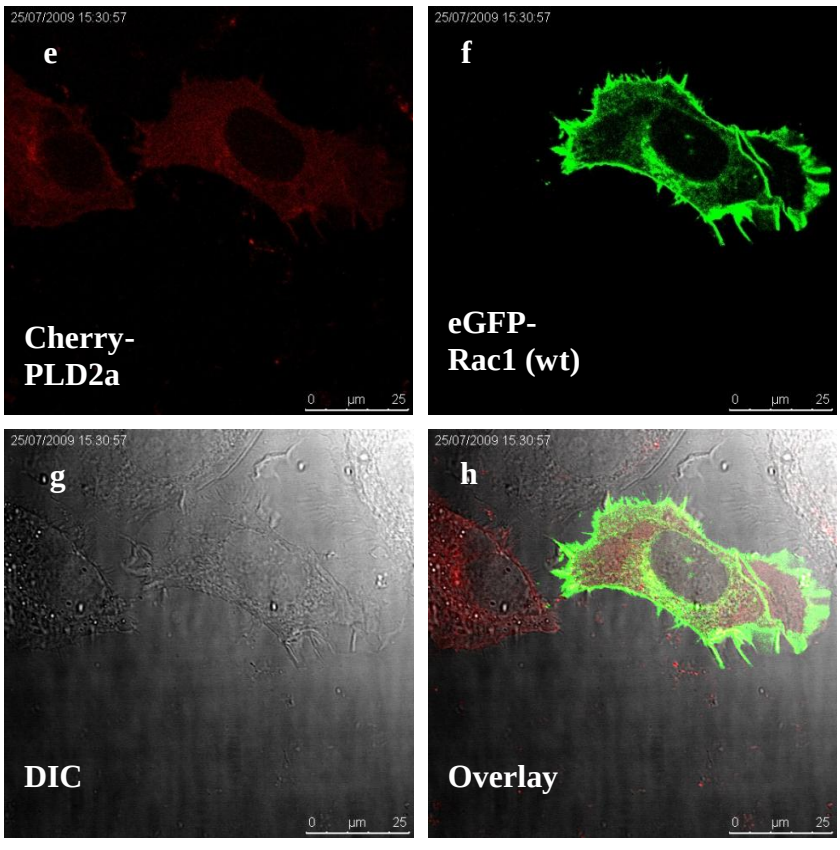

Figure 5.16: The effect of EGF on localisation of eGFP-Rac1 (Q61L) and Cherry-PLD2a in co-transfected HeLa cells. HeLa cells were grown on coverslips and transiently co-transfected with 3 µg eGFP-Rac1 (Q61L – panels **b**, **f**) DNA, and 3 µg Cherry-PLD1b (panels **a**, **e**) DNA for 24 hours. Cells were stimulated with EGF (panels **e-h** – 20 nM EGF, 10 minutes at 37^{o}C) then fixed in 4% paraformaldehyde and mounted onto glass slides. Fluorescence was detected using sequential scanning confocal microscopy (SP5) where parameters were narrowed as detailed in Figure 6.12. A scale calibrated to 25 µm is shown in each panel. The data presented are representative images for 1 experiment with at least an n=3.

Control

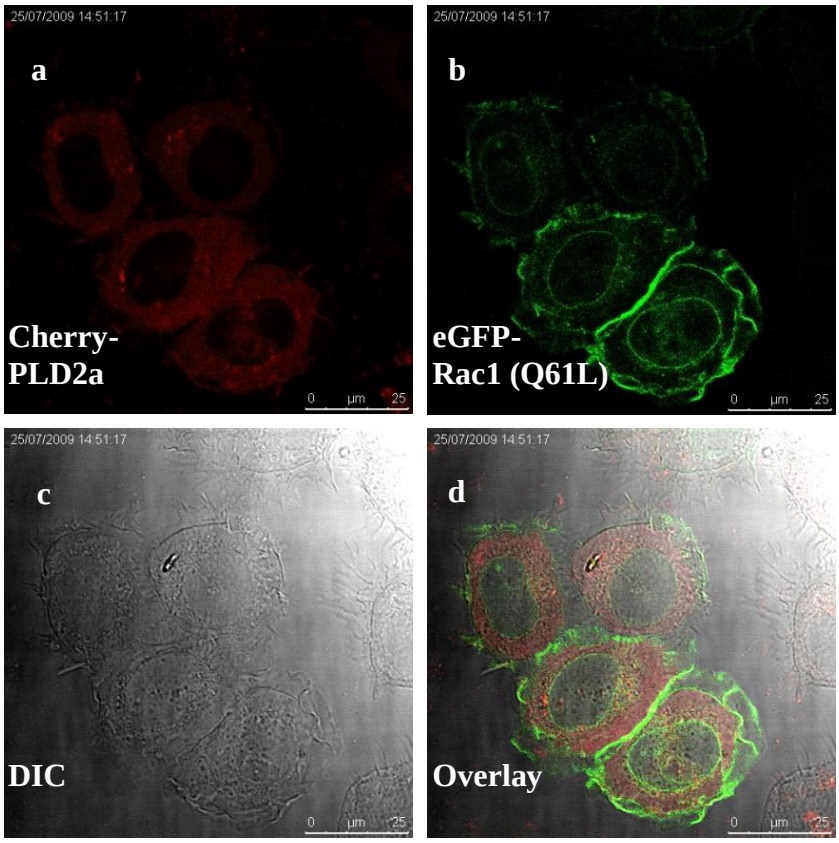

+ EGF stimulation

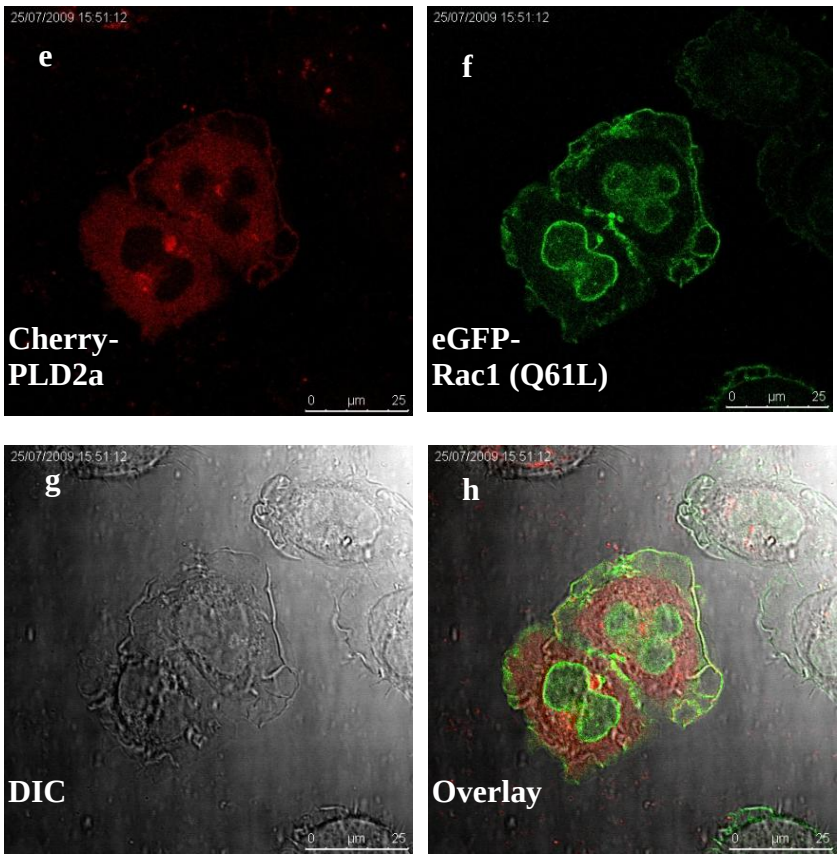

Figure 5.17: The effect of EGF on localisation of eGFP-Rac1 (T17N) and Cherry-PLD2a in co-transfected HeLa cells. HeLa cells were grown on coverslips and transiently co-transfected with 3 µg eGFP-Rac1 (T17N – panels **b**, **f**) DNA, and 3 µg Cherry-PLD1b (panels **a**, **e**) DNA for 24 hours. Cells were stimulated with EGF (panels **e-h** – 20 nM EGF, 10 minutes at 37^{o}C) then fixed in 4% paraformaldehyde and mounted onto glass slides. Fluorescence was detected using sequential scanning confocal microscopy (SP5) where parameters were narrowed as detailed in Figure 6.12. A scale calibrated to 25 µm is shown in each panel. The data presented are representative images for 1 experiment with at least an n=3.

Control

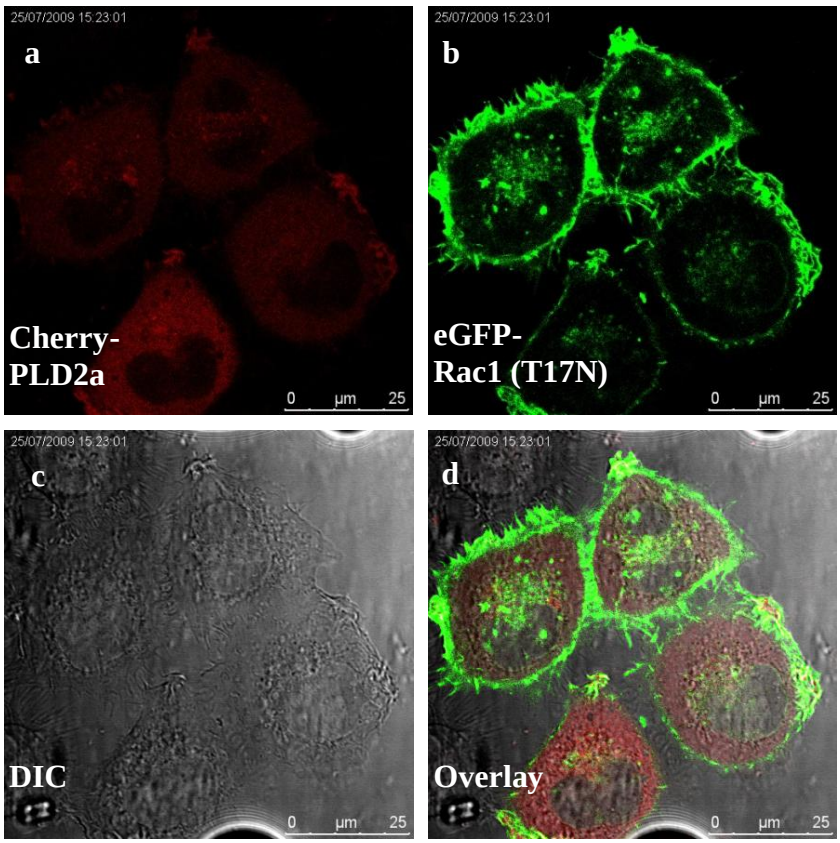

+ EGF stimulation

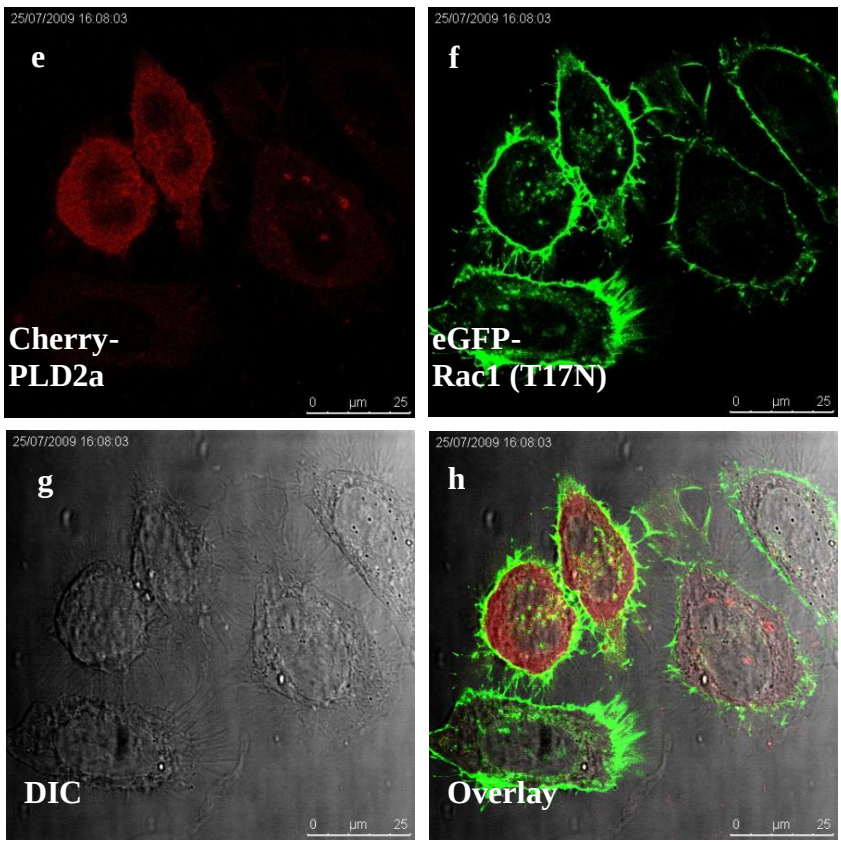

5.3: Characterising Cherry-PLD and the novel substrate in HeLa cells in real-time

5.3.1: The localisation of the novel fluorescent PtdCho and LysoTracker Red in the HeLa cell line

Although HeLa cells were more readily transfected than RBL-2H3 cells, their staining with the novel fPtdCho was untested. HeLa cells treated with the fluorescent lipid for 2 hours exhibited punctiform staining throughout the cytoplasm with marked exclusion of the nucleus (see Fig. 5.18, panels a-c). In RBL-2H3 cells, the lysosomal marker LysoTracker Red exhibited similar staining to that of the fluorescent lipid *in vivo* with up to 50% co-localisation. In HeLa cells, LysoTracker Red also localised in cytoplasmic punctiform structures. However, these structures are more densely concentrated in their distribution and were located in the outer region of cells which is also distinct from the nucleus (see Fig. 5.18, panels d-f). As the labelling of HeLa cells by fPtdCho and LysoTracker Red were notably different co-staining experiments were not performed.

Figure 5.18: Staining of HeLa cells with LysoTracker Red or the novel fluorescent PtdCho. HeLa cells grown in glass bottomed fluorodishes (approx. 50% confluencey) overnight were stained with 1 µg fPtdCho for 2 hrs in HBSS + 1 mM Ca^{2+}. The fluorescent lipid stained 100% of cells and localised to punctiform structures which were localised in the cytoplasm (see panels **a-c**) excluding the nucleus. Live confocal microscopy on a heated stage (37^{o}C) was used to detect fluorescence. Green fluorescent was excited by the 488 nm argon laser with an emission bandwidth of 500 nm-608 nm. HeLa cells were also stained using LysoTracker Red (100 nM) for 1 minute in HBSS + Ca^{2+} and then washed twice prior to live confocal imaging (see panels **d-f**). LysoTracker Red was excited using the HeNe 594 nm laser with an emission bandwidth of 658 nm-794 nm. A scale calibrated to 25 µm is shown in each panel. The data presented are representative images for 1 experiment with at least an n=3 for the novel fluorescent lipid and n=2 at least for LysoTracker Red.

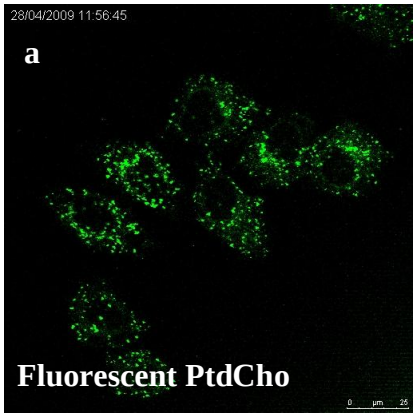
28/04/2009 11:56:45
a
Fluorescent PtdCho

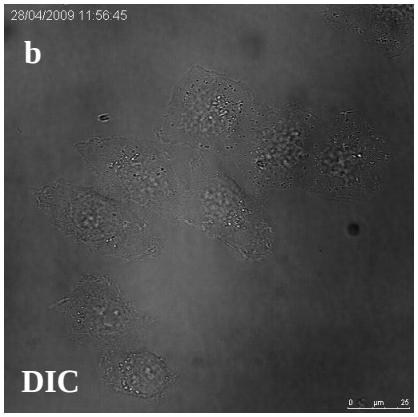
28/04/2009 11:56:45
b
DIC

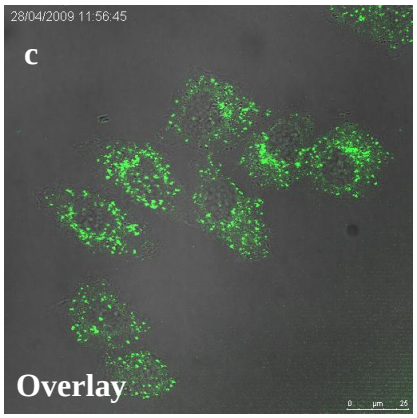
28/04/2009 11:56:45
c
Overlay

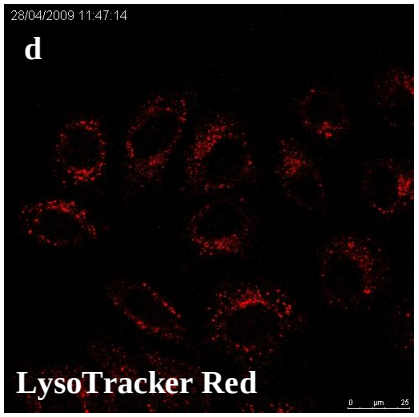
28/04/2009 11:47:14
d
LysoTracker Red

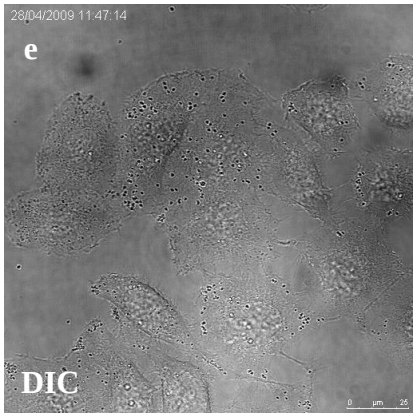
28/04/2009 11:47:14
e
DIC

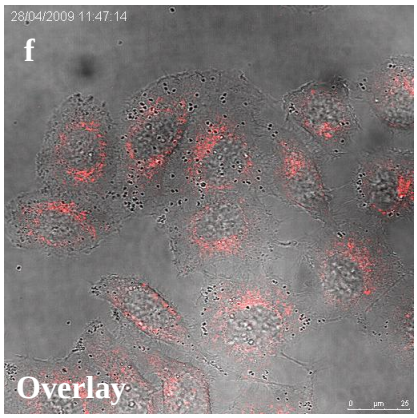
28/04/2009 11:47:14
f
Overlay

5.3.2: Novel fluorescent PdtCho treatment of living HeLa cells and the effect on EGF

Characterising the localisation and movement of the novel fPtdCho in living HeLa cells, provided an opportunity to compare the localisation to that of Cherry-PLD1b (see Section 5.3.3). HeLa cells were quiesced for 2 hours prior to labelling with 0.5 µg fPtdCho in HBSS + Ca^{2+} for 3 hours at 37^{o}C/5% CO_2. Still images were taken of the live labelled cells prior to stimulation with 20 nM EGF. Localisation of the fPtdCho was consistently in punctiform structures located in the cytoplasm of unstimulated HeLa cells (see Fig. 5.19, panels a-c) and upon EGF stimulation, the fluorescent PtdCho was not expressed at the plasma membrane, but assembled to a confined intracellular site (see arrows Fig 5.19, panel f) whilst remaining in punctiform structures despite notable cell shape change(see Fig. 5.19, panels d-f).

Real-time imaging of HeLa cells labelled with fPtdCho supported data indicating an aggregation of fPtdCho in the cell cytoplasm after EGF stimulation (see Fig. 5.19). Still images from the 15 minutes of recording fPtdCho-labelled, EGF-stimulated HeLa cells showed the same concentration of punctiform structures (see Fig. 5.20a for still images and 5.20b for the recording). Movement of the punctiform structures was recorded over 15 minutes, where 1 frame was recorded every 10 seconds. Real-time recordings such as Fig. 5.20b have been accelerated to show 15 minutes of imaging in 18 seconds.

Figure 5.19: The effect of EGF stimulation on HeLa cells labelled with the novel fluorescent PtdCho. HeLa cells were grown in glass bottomed fluorodishes (approx. 50% confluencey) overnight. Cells were labelled for 3-4 hours using 0.5 µg fPtdCho in HBSS + 1 mM Ca^{2+} and imaged live at 37^{o}C by confocal microscopy. Labelled HeLa cells quiesced for 5 hours and imaged prior to stimulation (panels **a**-**c**). Cells were then stimulated with 20 nM EGF and imaged immediately (panels **d**-**f**). Real-time imaging was recorded over 15 minutes (1 frame/10 seconds) using the argon laser at 488 nm with an emission band width of 500 nm-608 nm. A scale calibrated to 25 µm is shown in each panel. The data presented are representative images for 1 experiment of at least 2.

Controls

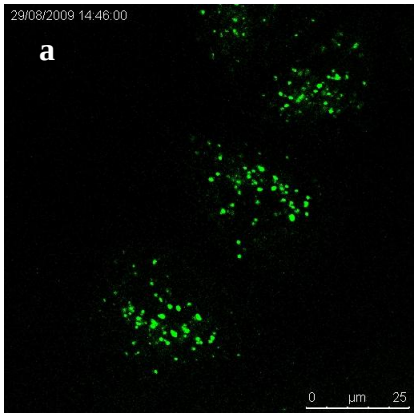

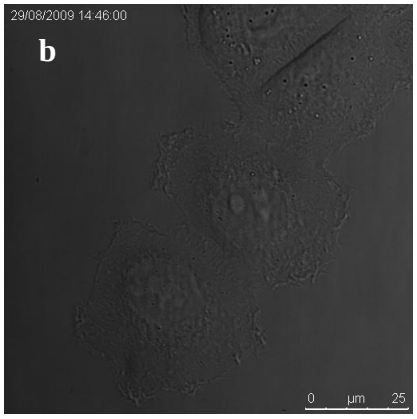

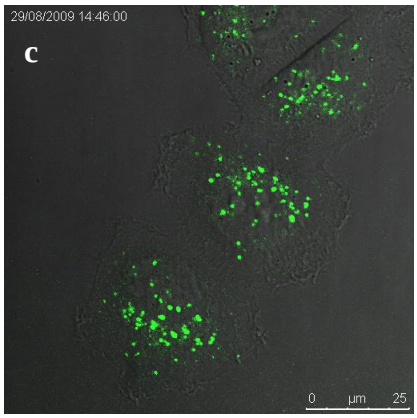

+ EGF Stimulation

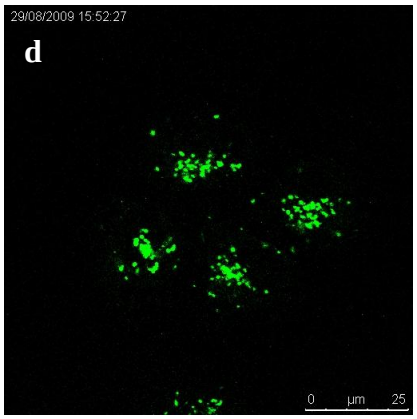

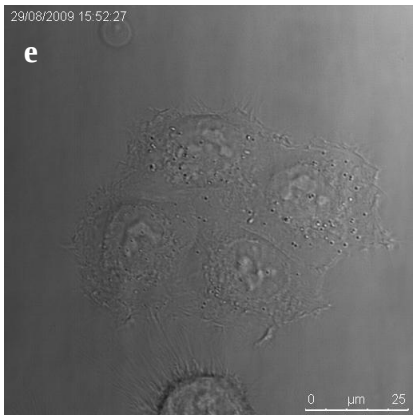

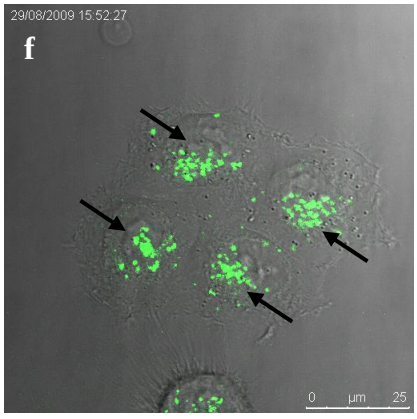

Figure 5.20a: Live imaging of fluorescent PtdCho labelled HeLa cells stimulated by EGF. HeLa cells were grown in glass bottomed fluorodishes overnight and quiesced for 2 hours. Cells were then labelled with 0.5 µg fPtdCho for 3 hours in HBSS + 1 mM Ca^{2+}, EGF stimulated on a heated stage (37^{o}C) and imaged over 15 minutes using confocal microscopy. Real-time recording was over 15 minutes (1 frame/10 seconds) using the argon laser at 488 nm with an emission band width of 500 nm-608 nm. A scale calibrated to 25 µm is shown in each panel. The data presented are representative images for 1 experiment of at least 2. Still images of the real-time recording are represented in Fig. 5.20 whilst the full length film is shown in Fig. 5.20**b**.

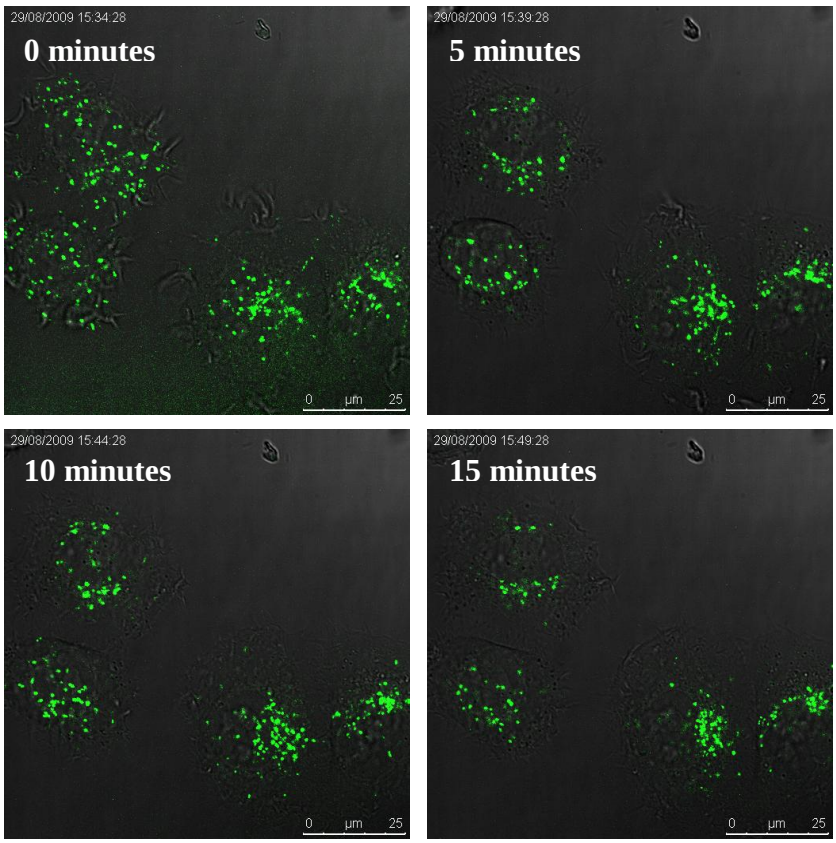

5.3.3: Characterising Cherry-PLD1b in live transiently transfected HeLa cells and the response to EGF stimulation

Although movement of PLD1b to the plasma membrane of HeLa cells has been documented in fixed cells, migration has never previously been recorded in real-time. HeLa cells transiently transfected with Cherry-PLD1b were incubated in a buffered salt solution prior to live confocal imaging in glass bottomed fluorodishes (on a heated stage at 37^{o}C). The movement of Cherry-PLD1b was first recorded in resting cells (see Fig 5.21a and Fig. 5.21b showing recording). The movement of Cherry-PLD1b containing structures was recorded over 15 minutes where 1 frame was recorded every 10 seconds. Real-time recordings such as Fig. 5.21b have been accelerated to show 15 minutes of imaging in 18 seconds. Characterising the movement and localisation of Cherry-PLD1b in real-time facilitated a comparison with the localisation of its fluorescent substrate.

Figure 5.21a: Live recording of Cherry-PLD1b movement in resting HeLa cells. HeLa cells grown in glass bottomed fluorodishes (approx. 50% confluencey) were transiently transfected using 3 µg of Cherry-PLD1b DNA for 24 hours. Cells were then washed and incubated in 1 ml HBSS + 1 mM Ca^{2+} ready for confocal imaging. Real-time imaging was recorded over 15 minutes (1 frame/10 seconds) using the DPSS 561 laser at 561 nm with an emission band width of 607 nm-790 nm. A scale calibrated to 25 µm is shown in each panel. The data presented are representative images for 1 experiment of 2. Still images of the real-time recording are represented in Fig. 6.21 whilst the recording is shown in Fig. 5.21**b**.

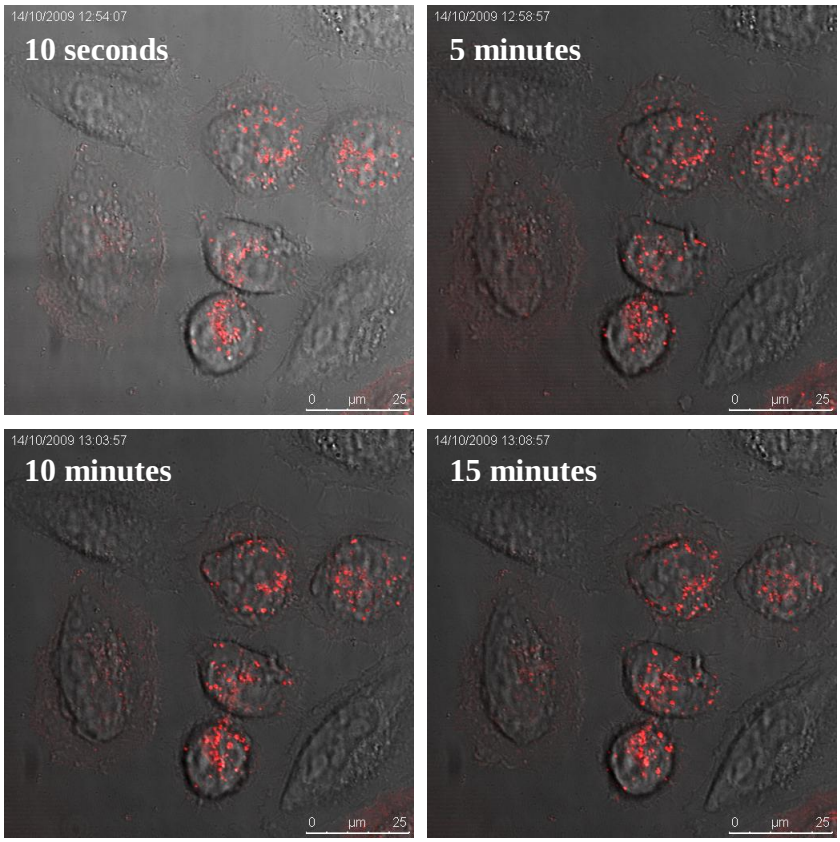

Cherry-PLD1b moved throughout resting cells and did not aggregate to a particular intracellular region. HeLa cells were stimulated with EGF and immediately live imaged. The effects of EGF were seen within only 5 minutes of recording (see Fig. 5.5). Transiently transfected HeLa cells expressing Cherry-PLD1b and stimulated with 20 nM EGF were recorded over 15 minutes (see Fig. 5.22a for still images and Fig. 5.22b for the recording). The real-time recording shows the PLD1b vesicles migrating primarily to the plasma membrane. Although there was a directional movement towards the plasma membrane (see black arrow Fig 5.22a), the vesicles also concentrated to a region in the cell cytoplasm (see white arrow Fig. 5.22a). Although there was movement towards the plasma membrane (see black arrow Fig. 5.22a), there was a lack of definition when compared against fixed (i.e. dehydrated) samples (see Fig. 5.5).

Figure 5.22a: Live recording of Cherry-PLD1b movement in EGF stimulated HeLa cells. HeLa cells grown in glass bottomed fluorodishes (approx. 50% confluencey) were transiently transfected using 3 µg of Cherry-PLD1b DNA for 24 hours. Cells were then washed and incubated in 1 ml HBSS + 1 mM Ca^{2+} ready for confocal imaging. HeLa cells were stimulated with 20 nM EGF immediately prior to imaging. Real-time recording was over 15 minutes (1 frame/10 seconds) using the DPSS 561 laser at 561 nm with an emission band width of 607 nm-790 nm. The nucleus is outlined in black in the 15 minutes frame. A scale calibrated to 25 µm is shown in each panel. The data presented are representative images for 1 experiment of at least 2. Still images of the real-time recording are represented in Fig. 5.22 whilst the full length film is shown in Fig. 5.22**b**.

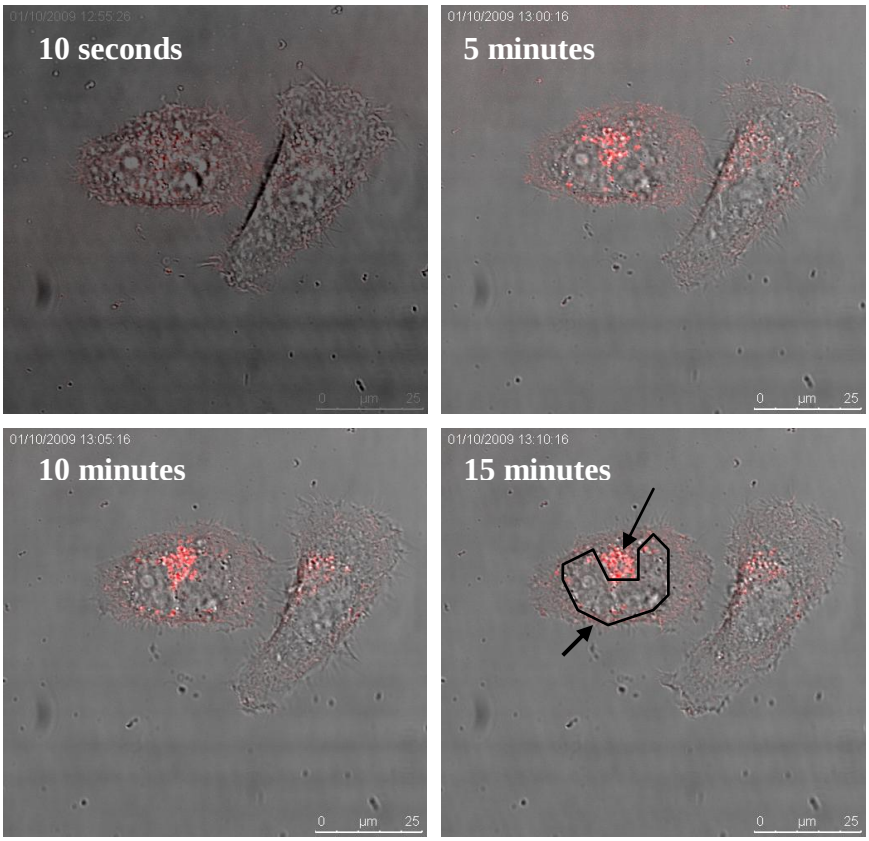

5.3.4: The effect of Cytochalasin D on fluorescent PtdCho localisation and response to EGF in HeLa cells

Cytochalasin D (CD) was used to determine the role of the cytoskeleton in the localisation and movement of fPtdCho in resting and EGF stimulation HeLa cells. HeLa cells were labelled with the novel fluorescent lipid prior to treatment with 1 µM CD (see Fig. 5.23, panels a-c – see Section 5.3.5). CD-treated cells were then imaged in real-time following EGF stimulation. Cells treated with 1 µM CD exhibited blebbing and formation of numerous processes, indicating possible stress. The cells maintained their ability to respond to EGF stimulation and demonstrated the same aggregation of the punctiform structures when compared with the controls (see Fig. 5.23, panels d-f).

Figure 5.23: The effect of CD on fluorescent PtdCho localisation and response to EGF stimulation in HeLa cells. HeLa cells grown in glass bottomed fluorodishes were quiesced for 1 hour and then labelled with 0.5 µg fPtdCho for 3 hours in HBSS + 1 mM Ca^{2+} and imaged (panels **a**-**c**). HeLa cells were then treated with 1 µM CD for 1 hour 37^{o}C/5% CO_2 and imaged again (panels **d**-**f**). Confocal microscopy was used to image the cells using the argon laser at 488 nm with an emission bandwidth of 500 nm-608 nm. A scale calibrated to 25 µm is shown in each panel. The data presented are representative images for 1 experiment of 2.

Controls

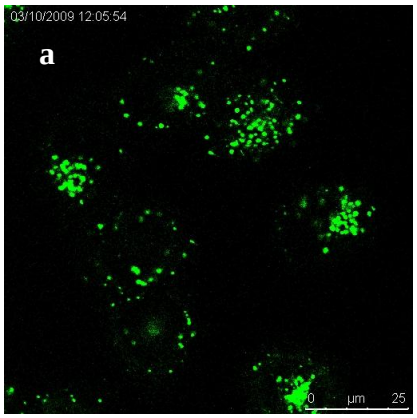

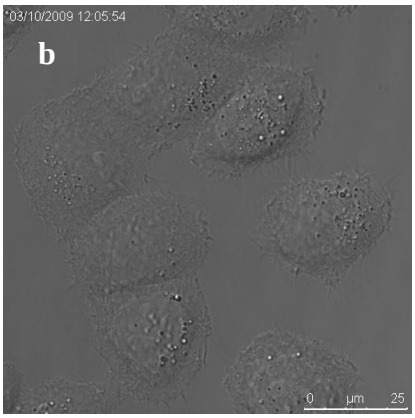

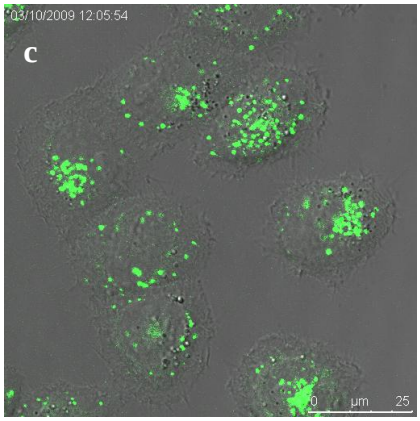

+ Cytochalasin D

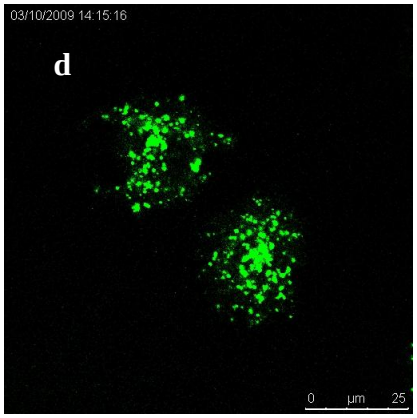

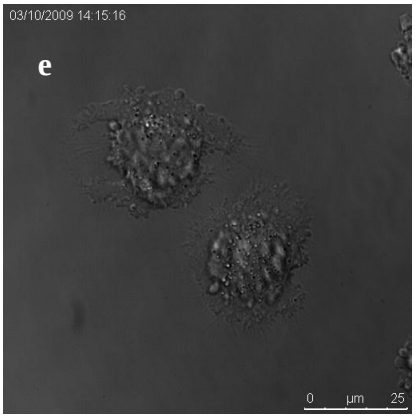

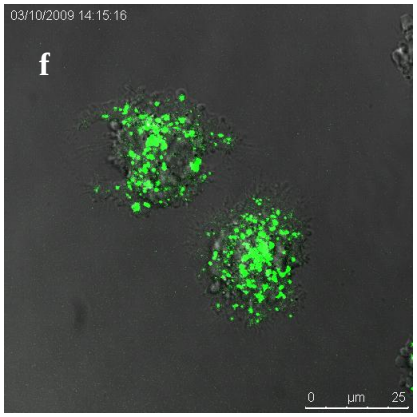

Real-time imaging of cells prior to CD treatment (see Fig. 5.24a, panels a, b) and following CD treatment with EGF stimulation (see Fig. 5.24a, panels c, d) were also recorded. The fPtdCho moved both within and between focal planes prior to CD treatment (see Fig. 5.24b for real-time recording). The response of fPtdCho labelled cells treated with 1 µM CD and stimulated with 20 nM EGF was also recorded immediately following EGF stimulation. The punctiform structures containing fPtdCho concentrated within the cytoplasm (see arrows Fig. 5.24a, panel d). The migration of fPtdCho suggests that CD did not render the cells unable to respond to EGF stimulation (see Fig. 5.24c for real-time recording). Real-time imaging was recorded over 15 minutes (1 frame/10 seconds) and condensed into 18 seconds in Figs 5.24b and 5.24c.

Figure 5.24a: The effect of CD on fluorescent PtdCho localisation and response to EGF stimulation. HeLa cells grown in glass bottomed fluorodishes were quiesced for 1 hour and labelled with 0.5 µg fPtdCho for 3 hours in HBSS + 1 mM Ca^{2+}. Cells were imaged in real-time prior to CD treatment (panels a, b) – the corresponding recording is Fig. 5.24**b**. HeLa cells were then treated with 1 µM CD for 1 hour 37°C/5% CO_2 and imaged immediately after EGF stimulation (panels c, d) – the corresponding recording is Fig. 5.24**c.** Real-time recording was over 15 minutes (1 frame/10 seconds) using the argon laser at 488 nm with an emission band width of 500 nm-608 nm. A scale calibrated to 25 µm is shown in each panel. The data presented are representative images for 1 experiment of 2.

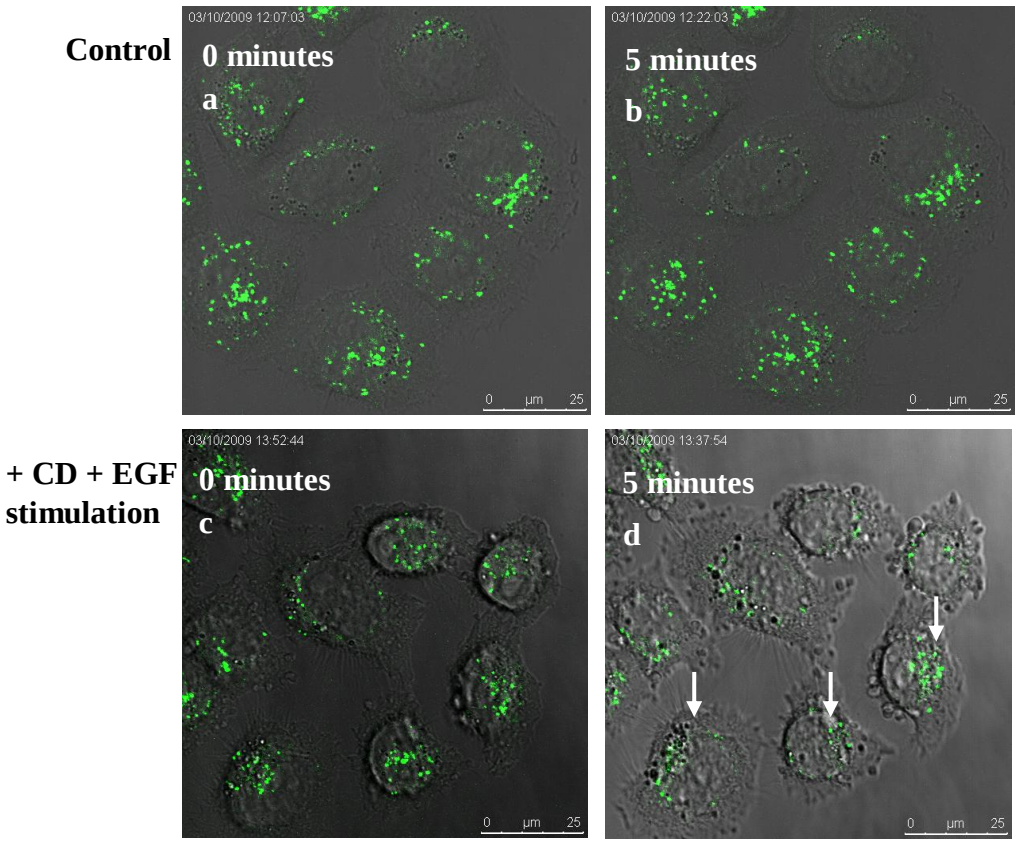

5.3.5: The effects of Cytochalasin D on Cherry-PLD1b localisation and response to EGF in HeLa cells

The movement of fPtdCho was unaffected by cytochalasin D (CD) treatment, but the cytoskeleton was a potential framework by which Cherry-PLD1b could move out around the cell (see Section 5.3.3). HeLa cells transiently transfected with Cherry-PLD1b were treated with 1 μM CD 24 hours post-transfection and imaged live following EGF stimulation (see Fig. 5.25).

Cells treated with CD exhibited signs of stress and activation in the form of membrane blebbing and multiple processes, although this did not affect their ability to respond to EGF. Living cells imaged prior to CD treatment (see Fig. 5.25, panel a) showed the punctate cytoplasmic localisation of PLD1b. The localisation of Cherry-PLD1b did not change upon CD treatment (see Fig. 5.25, panel b), however approximately 5% of cells exhibited an altered localisation pattern (see Fig. 5.25, panel d). The less common phenotype was not punctate and instead appeared to be aggregated along intracellular structures which could be identified by further investigation with molecular markers. Cells treated with CD maintained their ability to respond to EGF stimulation (see Fig. 5.25, panel c). Cells responded with PLD1b expression at the plasma membrane and also localising in a pool within the cell (see arrow Fig. 5.25, panel c).

Figure 5.25: The effect of CD on Cherry-PLD1b localisation and response to EGF stimulation. HeLa cells grown in glass bottomed fluorodishes (approx. 50% confluencey) were transiently transfected using 3 µg of Cherry-PLD1b DNA for 24 hours. Transfected cells were quiesced for 4 hours in no additions DMEM, then washed and incubated in 1 ml HBSS + 1 mM Ca^{2+} prior to CD or EGF treatment (panel **a**). Cells were washed once and treated with 1 µM CD for 1 hour in HBSS + Ca^{2+} at 37^{o}C/5% CO_2 (panels **b**, **d**). Following CD treatment cells were stimulated with 20 nM EGF for 15 minutes prior to imaging (panel **c**). Confocal microscopy was used to image the transfected cells using the DPSS 561 laser at 561 nm with an emission bandwidth of 607 nm-790 nm. A scale calibrated to 25 µm is shown in each panel. The data presented are representative images for 1 experiment of 2.

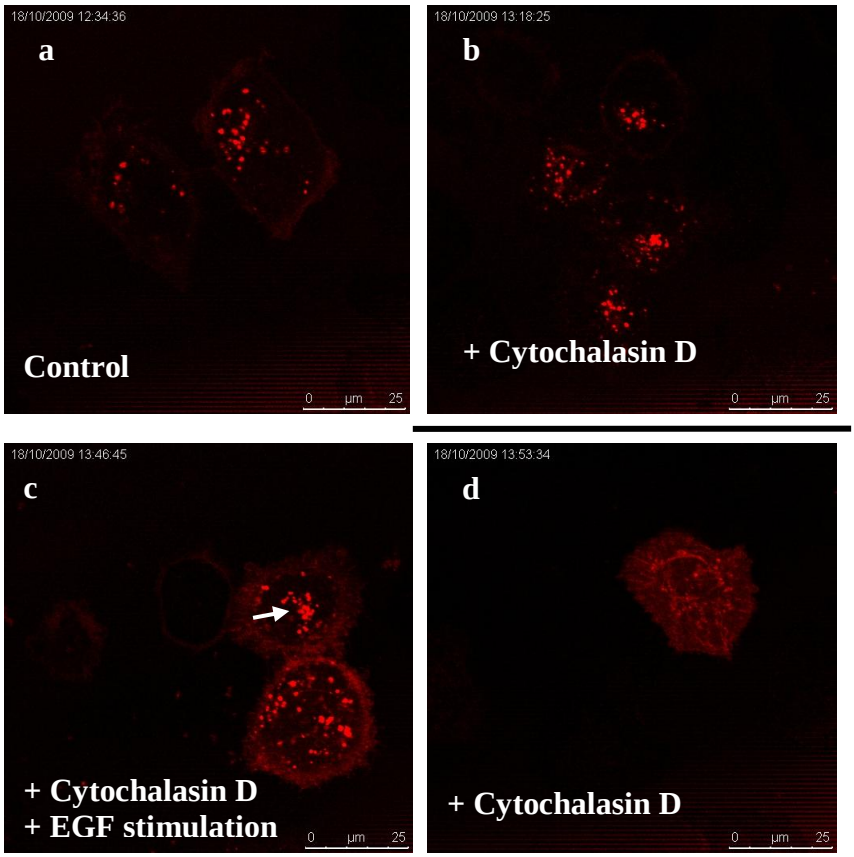

5.3.6: Co-localisation between LysoTracker Red and eGFP-PLD in living cells

PLD1 localisation varies in different cell lines but often localises to lysosomes (Toda *et al*., 1999). As HeLa cells were easily stained with the lysosomal marker LysoTracker Red, cells were transiently transfected with eGFP-PLD1b or -PLD2a for 24 hours and labelled with 100 nM LysoTracker Red. eGFP-PLD2a was used as a control in the analysis of co-localisation between eGFP-PLD and LysoTracker Red because of its diffuse cytosolic expression.

Image J was used to analyse the co-localisation between transiently transfected HeLa cells overexpressing eGFP-PLD (green) and the lysosomal marker LysoTracker Red (red). To reduce fluorescence bleed-through, the emission bandwidths of the photo multiplier tubes (PMTs) were narrowed as detailed above. Background fluorescence was minimised to limit non-fluorescent pixels from influencing co-localisation results. Image J was used to isolate individual cells in each field and identify the degree of co-localisation using a Pearson's correlation coefficient (Pearson's R). Pearson's R expresses the relationship between 2 variables, in this case 2 fluorophores and their relationship mapped using a gradient of +1 to -1. The closer the values are to the slope, the more likely they are to be dependent upon one another.

Separate experiments were used to compare the differences in co-localisation between eGFP-PLD and LysoTracker red (data not shown). Co-localisation is not substantial in cells overexpressing eGFP-PLD1b and stained with LysoTracker Red; the mean Pearson's R is 0.33 (n=1) and 0.26 (n=2) in 2 separate experiments (data not shown).

5.3.7: Co-localisation between fluorescent PtdCho and Cherry-PLD in living cells

As the HeLa cells were readily stained with the novel fluorescent lipid, a key aim was to stain cells transiently transfected with Cherry-PLD. Information about the stability of the lipid in Swiss 3T3 cells and RBL-2H3 cells was used to overcome experimental constraints. HeLa cells seeded in fluorodishes were exposed to 0.5 µg of fPtdCho in 1 ml HBSS + Ca^{2+} for 3 hours prior to transfection. The stability of the fPtdCho stain within the cells enabled an assessment of the localisation between Cherry-PLD and its fluorescent substrate (see Fig. 5.26).

Prior to confocal microscopy, cells were washed with HBSS + Ca^{2+}, incubated in a final volume of 1 ml and imaged live at 37^{o}C. Living HeLa cells overexpressing Cherry-PLD1b displayed co-localisation with the green fluorescent substrate (see Fig. 5.26, panels a-c). The reliability of the results was augmented via direct comparison between PLD1b and PLD2a co-localisation with fPtdCho can be made using the same settings (see Fig. 5.26, panels d-f). Co-localisation between Cherry-PLD2a and the fluorescent lipid was analysed using Image J.

Figure 5.26: Co-localisation between Cherry-PLD and the novel fluorescent PtdCho in HeLa cells. HeLa cells were grown in fluorodishes overnight and labelled with 0.5 µg of fPtdCho in 1 ml HBSS + Ca^{2+} for 3 hours. Cells were transiently transfected with 3 µg Cherry-PLD1b (panels **a**-**c**) or Cherry-PLD2a (panel **d**-**f**) DNA for 24 hours. Cells were then imaged live using sequential scanning confocal microscopy (SP5) on a heated stage at 37^{o}C. Green fluorescence was excitation at 488 nm with an emission band width between 496 nm-593 nm using an argon laser (20%). Red fluorescence was detected using the DPSS 561 laser and excited at 561 nm with an emission band width between 607 nm-790 nm. A scale calibrated to 25 µm is shown in each panel. The data presented are representative images for 1 experiment of at least 3.

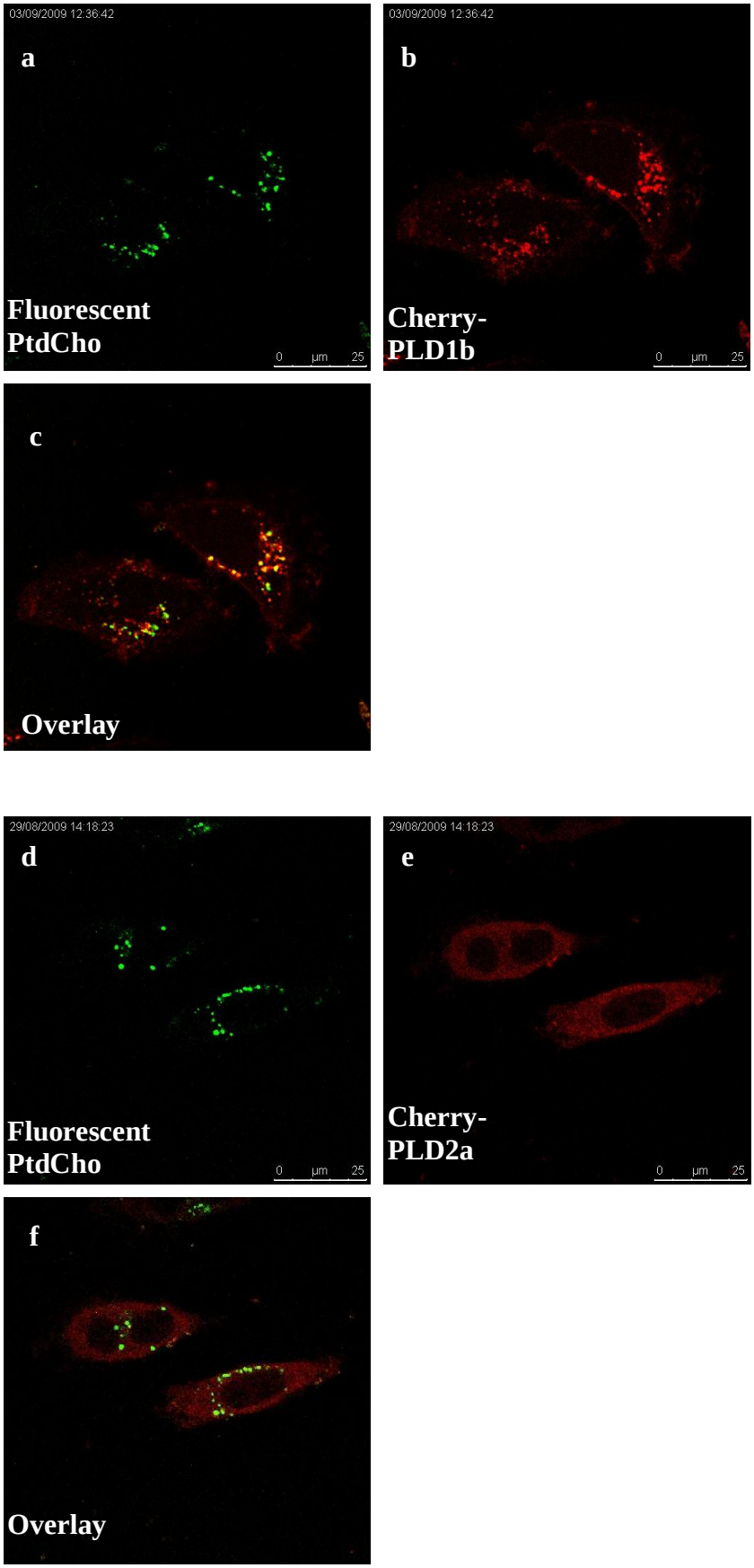
03/09/2009 12:36:42
a
Fluorescent PtdCho
0 µm 25
03/09/2009 12:36:42
b
Cherry-PLD1b
0 µm 25
c
Overlay
29/08/2009 14:18:23
d
Fluorescent PtdCho
0 µm 25
29/08/2009 14:18:23
e
Cherry-PLD2a
0 µm 25
f
Overlay

Image J was used to analyse the co-localisation between transiently transfected HeLa cells overexpressing Cherry-PLD (red) and the novel fluorescent lipid (green). Transiently transfected HeLa cells were first labelled with the fluorescent lipid and transfected using either Cherry-PLD1b or Cherry-PLD2a for 24 hours prior to imaging live using confocal microscopy. To reduce the identification of co-localisation due to fluorescence bleed-through, the detection parameters of the photo multiplier tubes (PMTs) were narrowed. Image J was then used to analyse co-localisation as previously described (see Section 5.3.1).

The relationship between Cherry-PLD1b and fPtdCho in 2 experiments showed substantial co-localisation with an average Pearson's R of 0.81 and 0.84 (n=1 and n=2 respectively – data not shown). The first experiment compared 15 cells from 8 fields whereas the second experiment compared 22 cells from 12 fields. Analysis using an unpaired 2-tailed t-test revealed that there was no significant difference between the means of these data sets.

The spatial proximity with which Cherry-PLD1b and its fluorescent substrate co-localise was investigated using fluorescence recovery after photobleaching (FRAP) – Förster (or fluorescence) resonance energy transfer (FRET) confocal microscopy. The BODIPY label of fPtdCho (donor) was detected using the FRAP AB setting on the (SP5) confocal microscope and excited using the argon laser (488 nm), with an emission bandwidth between 495 nm-570 nm. The acceptor parameters were set in the Cherry spectrum using the DPSS 561 laser (561 nm) with an emission bandwidth between 622 nm-790 nm. The same settings were used to photobleach selected areas of co-localisation (see Fig. 5.27, panel b). The proximity of PLD1b to its fluorescent substrate was determined by photobleaching the Cherry-PLD1b and then detecting changes in donor fluorescence (FRAP). If the substrate and lipase were in close proximity, the photobleaching of Cherry-PLD1b would result in increased novel fPtdCho fluorescence. This technique of FRET by FRAP identifies energy transfer between Cherry-PLD1b and fPtdCho, indicating whether the 2 are within 10 nm. To maximise the accuracy of FRAP, small areas of co-localisation were chosen for photobleaching.

Each experiment was analysed using 3 parameters, namely the increase of the donor, decrease of the acceptor and the efficiency, all of which were expressed as a percentage. The mean percentages of each parameter in 3 separate experiments were compared (see Fig. 5.27, panel a). The mean increase in donor fluorescence ranged from 12-30% whilst the acceptor photobleaching ranged from 56-69% decrease and efficiency (defined as the efficiency of energy transfer from donor to acceptor following bleaching) ranged from 10-19%. A sample of the FRAP data accumulated over the 3 experiments provides an indication of the energy transfer once Cherry-PLD1b was photobleached (see Table 5.3). Although there were technical difficulties associated with FRAP analysis (detailed later) data was reproducible and a close association between lipase and substrate was established.

Table 5.3: Sample data of FRET analysis using FRAP detecting co-localisation between Cherry-PLD1b (acceptor) and its fluorescent substrate (donor). Confocal microscopy was used to complete FRET-FRAP analysis between Cherry-PLD1b (acceptor) and the fluorescently labelled PtdCho (donor). The FRAP AB confocal software was used to set sequential scanning parameters using the argon laser (488 nm) and DPSS 561 laser (561 nm). The BODIPY (donor) fluorescent tag was excited by the argon laser and the emission bandwidth was between 495 nm-579 nm. The Cherry-PLD1b (acceptor) fluorescent tag was excited by 561 nm with an emission bandwidth between 622 nm-790 nm. The acceptor was photobleached and then the efficiency and donor fluorescence was recorded.

Experiment Number	Donor Pre Bleaching	Donor Post Bleaching	Acceptor Pre Bleaching	Acceptor Post Bleaching	Efficiency (%)
1	27.67	53.17	40.59	8.77	50.74
2	56.34	64.75	103.28	24.32	12.98
3	57.87	139.76	50.87	19.14	58.59
3	141.98	186.68	213.42	52.9	23.95
3	78.64	90.85	131.71	9.52	13.45

Although FRET-FRAP analysis was performed on numerous 'vesicles' which appeared to exhibit co-localisation, few exhibited a large increase in donor fluorescence and approximately 70% showed a decline in donor fluorescence post-photobleaching. Limitations to these FRAP experiments included the movement of vesicles out of the region isolated as they were mobile within the cell, movement of the cell, and transfection/labelling efficiency. Weakly transfected cells could not be photobleached as effectively as cells expressing a high yield of fluorescence. Technical difficulties associated with the SP5 confocal microscope upon FRAP analysis of vesicles typically 1 µm in diameter also affected the number of data points that could be collected. Although the data reflected these limitations, approximately 30% of data points from each experiment showed the efficiency and donor fluorescence increase required.

Although these experimental limitations hindered the amount of data collected, the experiments (see Fig. 5.27, panel a) compiled 6, 12 and 16 data points for experiments n=1, 2 and 3 respectively. An example of FRET-FRAP analysis (see Fig. 5.27, panel b) shows where regions of suspected co-localisation were isolated

and photobleached before the donor fluorescence was re-recorded. The intensity of the fPtdCho labelling of the cells was also integral to FRET-FRAP analysis as high laser strength could bleach a weakly labelled cell, thus ultimately affecting the data.

Figure 5.27: FRET-FRAP analysis of co-localisation between Cherry-PLD and fluorescent PtdCho. HeLa cells were grown in fluorodishes overnight and labelled with 0.5 µg of fPtdCho in 1 ml HBSS + Ca^{2+} for 3 hours. Cells were transfected with 3 µg Cherry-PLD1b DNA for 24 hours, then sequentially scanned using live confocal microscopy (SP5) on a heated stage at 37^{o}C using the FRAP AB Leica software (see panel **b**, **1**-**3**). Green fluorescence was excitation at 488 nm with an emission band width between 496 nm-593 nm using an argon laser (20%). Red fluorescence was detected using the DPSS 561 laser and excited at 561 nm with an emission band width between 607 nm-790 nm. Regions of co-localisation were isolated (panel **b**, **1**) and bleached using the DBPSS 561 laser (panel **b**, **2**). Fluorescence readings were then taken after bleaching (panel **b**, **3**). Collated results for acceptor and donor fluorescence and efficiency for 3 separate experiments are compared (panel **a**).

a

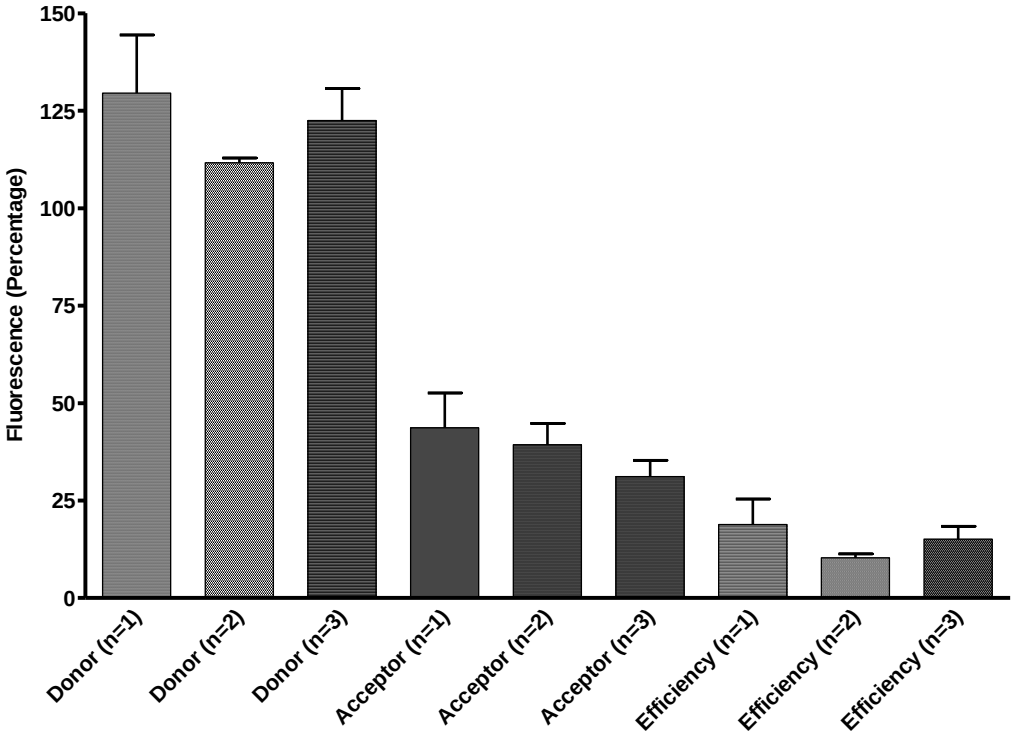
Fluorescence (Percentage)
150
125
100
75
50
25
0
Donor (n=1)
Donor (n=2)
Donor (n=3)
Acceptor (n=1)
Acceptor (n=2)
Acceptor (n=3)
Efficiency (n=1)
Efficiency (n=2)
Efficiency (n=3)

b

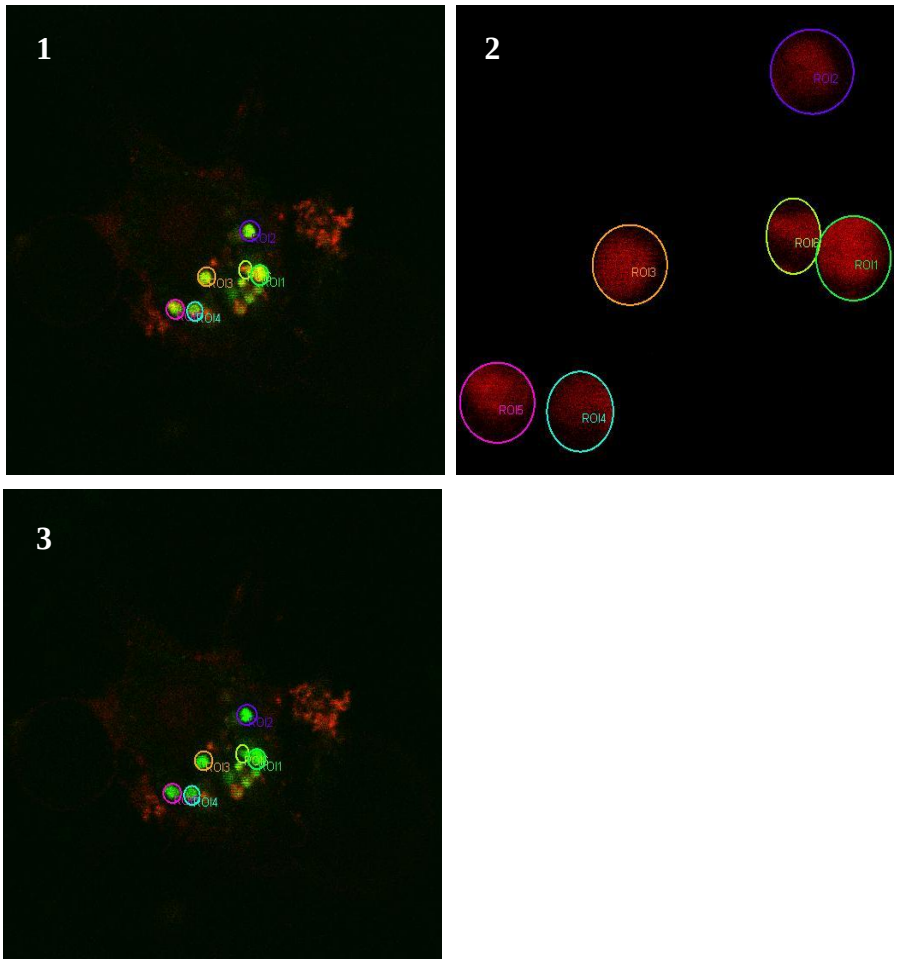
1
2
3
ROI2
ROI3
ROI1
ROI4
ROI5

5.4 Discussion

5.4.1: Transient expression of Cherry- or eGFP-PLD in HeLa cells and the effect of EGF stimulation

The HeLa cell line was robust and readily transfected with either Cherry- or eGFP-PLD. The localisation and response to EGF stimulation of PLD1b and PLD2a was unaffected by either of the fluorescent labels. PLD1b localised to punctiform structures within the HeLa cell cytoplasm, perhaps multivesicular endosomes, late endosomes, the trans-Golgi apparatus or early endosomes (Hiroyama and Exton, 2005b). In response to EGF stimulation, phosphorylated PLD1b migrated to the plasma membrane and has been previously documented to co-localise with EGFR and calveolin-1 (Han *et al*., 2002b). PLD1b also appeared to concentrate at a distinct region within the cytoplasm of the cells following EGF stimulation. PLD2a often displayed diffuse cytosolic expression and marked sparing of the nucleus. In many cell lines, including HeLa cells, PLD2a localises to the plasma membrane (Hiroyama and Exton, 2005b). However, cytosolic localisation of PLD2 similar to that shown in HeLa cells (see Fig. 6.1) has also been documented in CHO-T cells (Emoto *et al*., 2000). PLD2 expression and localisation remained unaltered following EGF stimulation. Previous work in the HEK-293 cells indicated that PLD2 is constitutively associated with EGFR and is therefore unaffected by EGF stimulation (Slaaby *et al*., 1998).

5.4.2: Co-expression of Cherry- and eGFP-PLD in HeLa cells and the effect of EGF stimulation

Both expression and EGF stimulation of PLD were unaffected by the Cherry or eGFP fluorescent protein labels. Co-transfection experiments between Cherry-PLD and eGFP-PLD constructs indicated co-localisation between the same PLD isoforms. Although there is co-localisation, this cannot be used to infer formation of homodimers (between HKD motifs of 1 PLD) or heterodimers (between HKD motifs of 2 PLDs). Cherry-PLD1b and eGFP-PLD1b co-localised in cytoplasmic punctiform structures in unstimulated cells and was also expressed at the plasma membrane upon EGF stimulation. Cherry-PLD2a and eGFP-PLD2a exhibited the

same diffuse expression and did not respond to EGF stimulation. Co-localisation between PLD1b and PLD2a was observed in the cytoplasm, however the expression pattern was different with PLD1b displaying punctate localisation and PLD2a diffuse cytosolic expression.

Members of the PLD superfamily have conserved HKD motifs which reportedly dimerise to form the active site (Stuckey and Dixon, 1999). Although the HKD motifs are known to dimerise, whether this happens intramolecularly or intermolecularly is still controversial. The bacterial endonuclease Nuc, a member of the PLD superfamily containing only one HKD motif crystallises as a dimer (Stuckey and Dixon, 1999). However, most members of the PLD superfamily contain two HKD motifs and the mechanism by which the active site is formed is not well understood. Recent studies using the two mammalian PLD isoforms PLD1 and PLD2, proposed that rPLD1 and rPLD2 have the potential to exist in homodimers but also form heterodimers (Kam and Exton, 2002). Further experiments co-immunopreciptating Cherry- and eGFP-PLD would provide more information about the association between overexpressed PLD isoforms in HeLa cells.

5.4.3: Co-expression of Cherry-PLD with eGFP-Chimera and the effect of EGF stimulation in HeLa cells

The eGFP-Chimera construct was characterised by its diffuse cytoplasmic and nuclear expression which excluded the nucleoli or nuclear bodies. The Chimera, like PLD2a, did not respond to EGF stimulation. Preliminary data suggests that the terminal 851 residues of PLD1b may contain a nuclear localisation signal (NLS). There are a variety of NLS motifs, however a monopartite motif (KPRK) was identified in both hPLD1b and the Chimera. A monopartite motif is characterised by a cluster of basic residues (e.g. arginine or lysine) followed by a helix-disrupting residue (e.g. proline – Cokol *et al*., 2000). PLD1b localises to the nucleus (although infrequently) and so the C-terminal NLS of PLD1b may be responsible for the nuclear localisation of the Chimera construct. Although these results are at an early stage, further experiments mutating the identified NLS region may confirm that PLD1b has an encrypted NLS motif. Furthermore, data presented here suggests that

the first 283 base pairs of the PLD2a N-terminus are responsible for the diffuse expression of PLD2a and the lack of responsivity to EGF.

5.4.4: Co-localisation of Cherry-PLD with Rac1 and the effect of EGF stimulation in HeLa cells

Cherry-PLD1b and eGFP-Rac1 (wt) did not co-localise in resting HeLa cells, although both localised to distinct punctiform structures within the cytoplasm. However, upon EGF stimulation, there was co-localisation between eGFP-Rac1 (wt) and Cherry-PLD1b on the plasma membrane, as expected. Rac1 (wt) overexpression was characterised by its punctiform localisation and multiple processes of transfected cells. Previous studies have suggested that Rac1 (wt) has a role in cytoskeletal rearrangement and the formation of lamellipodia (Ridley et al., 1992; Machesky and Hall, 1997; Hiroyama and Exton, 2005a), although the signalling pathway(s) involved are still elusive. Cherry-PLD2a did not co-localise with eGFP-Rac1 (wt) in HeLa cells and co-transfection did not affect PLD2a expression following EGF stimulation.

Cherry-PLD1b and eGFP-Rac1 (T17N) did not co-localise in unstimulated HeLa cells. Co-localisation between PLD1b and Rac1 (T17N) occurred on the plasma membrane following EGF stimulation. The migration of PLD1b to the plasma membrane indicated that the dominant negative mutant does not affect EGF stimulation. Other studies found that overexpressing dominant negative or Rac1 (wt) did not affect the ability to activate PLD using PMA stimulation in HeLa cells (Hiroyama and Exton, 2005a). Cherry-PLD2a co-transfected with eGFP-Rac1 (T17N) did not alter in its diffuse cytosolic expression and nor co-localise with Rac1 (T17N). Rac1 (T17N) did not affect the lack of PLD2a response to EGF stimulation.

The co-tranfection of Cherry-PLD1b with constitutively active Rac1 (Q61L) resulted in a significant change in cell shape and localisation of PLD1b. Rac1 is thought to be involved in membrane ruffling and cytoskeletal rearrangement (Ridley et al., 1992; Machesky and Hall, 1997; Hiroyama and Exton, 2005a), although previous studies overexpressing constitutively active Rac1 in HeLa cells did not exhibit such a dramatic change in cell morphology (Hiroyama and Exton, 2005a). Experiments

using constitutively active Arf6, another known PLD1 activator, have also shown altered localisation similar to that seen using Rac1 (Q61L) (Hiroyama and Exton, 2005b). The two small G-proteins are both PLD1 activators and Rac1 is probably involved downstream of Arf6 to induce membrane ruffling (Hiroyama and Exton, 2005a). Although the cell morphology was dramatically changed by Rac1 (Q61L), expression of PLD2a was unaffected as was the inability to respond to EGF stimulation.

5.4.5: Characterising the novel fluorescent PtdCho and Cherry-PLD1b in HeLa cells using live confocal microscopy

The novel fluorescent PtdCho (fPtdCho) localised in motile punctiform structures in the cytoplasm of HeLa cells. Upon EGF stimulation, the fPtdCho would concentrate in one place within the cell. The fPtdCho localised with the lysosomal marker LysoTracker Red in RBL-2H3 cells but not in HeLa cells. In an attempt to inhibit the movement of the novel fPtdCho, labelled cells were treated with cytochalasin D (CD) which caps actin filaments and competitively inhibits capping proteins that stabilise the cytoskeleton (Wakatsuki *et al*., 2000). The net effect is that CD destabilises the cytoskeleton. CD treatment of HeLa cells labelled with the novel fPtdCho did not alter its localisation nor affect its ability to migrate upon EGF stimulation. This indicates that the movement exhibited by the novel fPtdCho is not linked to the cytoskeleton. Similarly, CD treatment of Cherry-PLD1b expressing HeLa cells does not affect the localisation of PLD1b. CD also has no impact on the ability of PLD1b expression at the plasma membrane upon EGF stimulation.

The aim of this project was to establish a live *in vivo* PLD assay which was achieved using HeLa cells expressing Cherry-PLD and labelled with the novel fluorescent lipid. Co-localisation between Cherry-PLD1b or -PLD2a and the fPtdCho was first analysed using Image J. Using the Image J Colocalisation Finder plugin, co-localisation between Cherry-PLD1b and its fluorescent substrate was calculated to be up to 84%. Despite technical difficulties, FRET-FRAP analysis of fPtdCho and Cherry-PLD1b showed a close association between the lipase and substrate, finally validating this live *in vivo* PLD assay.

Chapter 6: General Discussion

6.1: Real-time *in vitro* assay

The kinetics of phospholipase D (PLD)-mediated phosphatidylcholine (PtdCho) hydrolysis have previously been studied using radio-chemical end-point assays (Ohguchi *et al*., 1997; Hodgkin *et al*., 1999; Henage *et al*., 2006). Although these studies contributed to our current understanding of PLD activity and its response to various activators, none were capable of characterising PLD activation in real-time. Monitoring the activity of GST-hPLD1 in real-time using a fluorescent *in vitro* assay identified the existence of a lag period (of up to 20 minutes) before GST-hPLD1 activity increased in response to small G-protein activators. This lag period was consistent between assays and may indicate that the dynamics between lipase, substrate, activators and other co-factors (such as Mg^{2+} and Ca^{2+}) are more complex than previously identified. This lag period may indicate that there is no change (i.e. increase) in basal GST-hPLD1 activity until a multi-component complex (proteins and lipid) is formed.

PLD1 activation by small G-proteins such as Rac1 and Arf1, have been well characterised using end-point assays and the fluorescent real-time data presented here corroborates previous observations (Henage *et al*., 2006). Although both methods established that PLD1 activity increases notably upon small G-protein activation, none identified how small G-proteins interact with PLD to dramatically change its PtdCho hydrolysing ability. Small G-proteins are known to cycle between two conformational states, an active GTP-bound state and an inactive GDP-bound state. Cycling between GTP- and GDP-bound states is controlled in cells by many regulators such as GTPase activating proteins (GAPs), guanine nucleotide exchange factors (GEFs) and GDP dissociation inhibitors (GDIs – Hakoshima *et al*., 2003; Dai *et al*., 2008). Furthermore, small G-protein structure is dependent upon GTP/GDP cycling (Hakoshima *et al*., 2003). Small G-protein activation of PLD1 may also impact on the structure of the lipase, possibly altering PLD1 from a weakly active to a more active conformation. The novel fluorescent PtdCho (fPtdCho) could be used to characterise the coupled molecular relationship between G-proteins and their

effectors (in this case GST-hPLD1). As there is now a real-time model to measure fluorescent PtdCho hydrolysis, the assay could be modified to quantify GTP hydrolysis or possibly G-protein loading status in relation to effector output which, in this case, could be PLD1-catalysed fPtdCho hydrolysis. The fluorescent assay would require further development, possibly using a labelled GTP construct. The hydrolysis of fPtdCho could therefore be quantified with increase in green fluorescence whilst a decrease in another (e.g. red fluorescence) could be used to identify GTP hydrolysis in real-time. Elucidating the molecular interaction between GST-hPLD1 and its small G-protein activators would indicate whether small G-proteins are amplifiers of PLD1 activity or merely transducers. *In vitro* interactions between small G-proteins and the non-hydrolysable GTP analogue GTPγS indicate that cycling between GTP/GDP bound states may have little influence on GST-hPLD1 activation. It is therefore possible that binding of the small G-protein activators to the lipase alone changes the conformation of PLD and encourages substrate binding. Further experiments using GTP instead of GTPγS *in vitro* might clarify the role of small G-proteins in GST-hPLD1 activation.

6.2: Lipid versus LysoTracker Red localisation in RBL-2H3 cells

Both the novel fluorescent PtdCho (fPtdCho) and lysosomal marker LysoTracker Red label localise in a punctate manner within the RBL-2H3 mast cell line with approximately 50% co-localisation. However, stimulation (e.g. antigenic, PMA or A23187) of these cells has different effects on the two labels, with the lipid remaining punctate but the LysoTracker Red rapidly fading (and becoming more diffuse).

PMA is a non-hydrolysable DAG mimetic used to activate Ca^{2+}-dependent PKCα, a known PLD1 activator (Takai *et al*., 1979; Castagna *et al*., 1982). PMA stimulation of RBL-2H3 cells causes dramatic change in cell morphology resulting in membrane ruffling, blebbing, and the retraction of cellular processes. During these rapid changes in cell morphology, the novel fPtdCho maintained its punctiform labelling of intracellular structures. Similarly the lysosomal marker LysoTracker Red maintained punctate labelling in PMA-stimulated RBL-2H3 cells, although some marker was lost over a 15 minute period. PMA, calcium ionophore A23187 and

antigenic stimulation of RBL-2H3 cells were all quantified using a previously validated β-hexosaminidase assay. Although PMA stimulation of RBL-2H3 cells resulted in dramatic cell membrane ruffling, β-hexosaminidase was not secreted. Previous studies have also recorded the absence of β-hexosaminidase secretion in response to PMA-stimulation of RBL-2H3 cells (Brown *et al*., 1998).

Stimulation of RBL-2H3 cells using the calcium ionophore A23187 resulted in similar morphological changes to those previously seen in response to PMA stimulation. However, A23187 (0.1 μM) resulted in approximately 50% β-hexosaminidase secretion compared with approximately 15% secreted in response to PMA. The calcium ionophore is an established inducer of β-hexosaminidase secretion in RBL-2H3 cells (Mitsutake *et al*., 2004). A23187 stimulation of RBL-2H3 cells did not alter the characteristic labelling of the novel fluorescent lipid. However, in response to A23187 stimulation, LysoTracker Red labelling of RBL-2H3 cells disappeared rapidly, i.e. within 5 minutes of real-time confocal recording. Similarly, LysoTracker Red labelling of RBL-2H3 cells was notably reduced following antigenic stimulation of cells, whereas fPtdCho-labelling appeared unaffected. This suggests that, although the lipid and lysosomal marker appear to label common structures (50%), the two labels behave differently in RBL-2H3 cells in response to stimulation.

PtdCho is a substantial component of the plasma membrane (Taylor *et al*., 2007), however none of the cell lines treated with the novel PtdCho exhibited labelling of the plasma membrane. The plasma membrane was not labelled possibly because the fluorescent PtdCho was exogenously added and was not compatible with plasma membrane-labelling. Our hypothesis is that the novel lipid may have labelled vesicle membranes and hence fluorescence appeared punctiform. The acidotropic and soluble lysosomal marker possibly labels vesicular contents and the two markers may therefore label different regions of the same organelle. Loss of LysoTracker Red labelling (e.g. in response to A23187 treatment) could be attributed to the secretion of secretory granule contents, including the red marker, but fPtdCho staining could be maintained if it is in the granule membrane. Previous studies have shown that, although secretory granules are acidic, the lysosomal membrane is ruptured upon degranulation and the pH is no longer maintained (Dragonetti *et al*., 2000). It is

therefore also possible that LysoTracker Red, an acidotropic molecular marker, undergoes loss of fluorescence as a result of the change in vesicle pH associated with secretion.

Analysis of mastoparan (MP) analogue treatment of RBL-2H3 cells indicated that two pools of secretory vesicles were responsible for the exocytosis of different secretory markers. These appear to be regulated by different molecular mechanisms (Farquhar *et al*., 2002). Peptide-induced stimulation of PLD resulted in exocytosis of β-hexosaminidase but not 5-hydroxytryptamine (5-HT – Farquhar *et al*., 2002). LysoTracker Red was more likely to label both pools of vesicles as this molecular marker labels all acidic organelles, including secretory vesicles. It is therefore plausible that the novel fluorescent lipid may label only one of the pools of secretory vesicles. This distinction between the two pools would correspond to data indicating only 50% co-localisation between the lysosomal marker and novel lipid in RBL-2H3 cells. The novel lipid may therefore only label vesicles responsible for PLD-dependent β-hexosaminidase secretion as treatment with primary alcohol demonstrates that the integrity of vesicle labelling is dependent on basal PLD activity (see Fig. 3.36).

Functional inhibition of PLD and the accumulation of Ptd-alcohol have previously demonstrated a role for PLD in intracellular processes as well as providing a convenient PLD assay *in vivo* (Wakelam *et al*., 1995; Frohman *et al*., 1999). RBL-2H3 cells treated with butan-1-ol (0.3%) rapidly lost the characteristic punctate localisation of the novel fPtdCho. Importantly, treatment with butan-2-ol (0.3%) did not change the intracellular labelling by the novel fPtdCho. Furthermore, levels of primary alcohol used to inhibit basal PLD activity are consistent with those optimised in previous studies (Brown *et al*., 1998). The dramatic effect of butan-1-ol treatment on PtdCho-labelled cells strongly suggests that basal PLD-catalysed PtdCho turnover and generation of PtdOH is required for the punctate localisation and integrity of fluorescent PtdCho in RBL-2H3 cells.

Basal PLD activity (as determined using Ptd-alcohol accumulation) is generally regarded low relative to PLD activity measured after PMA or agonist stimulation (Gruchalla *et al*., 1990; Edwards and Murray, 1995). However, as measurement of

Ptd-alcohol accumulation has been used comparatively, the role of low basal PLD activity has not been extensively investigated (Colley *et al*., 1997; Slaaby *et al*., 1998; Kim *et al*., 1999; O'Luanaigh *et al*., 2002).

Mammalian PLD2 over-expression has indicated a high level of constitutive activity relative to PLD1 activity (Colley *et al*., 1997; Slaaby *et al*., 1998; Kim *et al*., 1999). The turnover of PtdOH generated *in vivo* by basal PLD2 activity is possibly a requirement for the integrity of vesicle membranes and ultimately punctate localisation of the novel fPtdCho. Antigenic stimulation of RBL-2H3 cells in the context of IgE resulted in membrane ruffling and β-hexosaminidase secretion, and PLD2 is reportedly responsible for membrane ruffling during both antigenic and PMA stimulation of RBL-2H3 cells (O'Luanaigh *et al*., 2002; Sarri *et al*., 2003). RBL-2H3 cells labelled with fPtdCho, treated with butan-1-ol and antigenically stimulated using IgE did not display obvious membrane ruffling. PLD-dependent membrane ruffling in response to antigenic stimulation could therefore be functionally inhibited using primary alcohol (O'Luanaigh *et al*., 2002). Functional inhibition of PLD2 with butan-1-ol would also inhibit PtdOH turnover changing native membrane constitution and potentially resulting in the loss of punctate fPtdCho-labelling.

Analysis of human PLD1b and PLD2a in epithelial, endothelial and fibroblast cell lines indicated that both PLD isoforms utilise a structurally similar PtdCho pool *in vivo* and generate an identical PtdOH product enriched in mono- and di-unsaturated fatty acids (Pettitt *et al*., 2001). Although PLD2 has higher basal activity than PLD1, transient expression of GFP-PLD2 in RBL-2H3 cells localised this protein to the plasma membrane (Sarri *et al*., 2003). RBL-2H3 cells transiently expressing eGFP-PLD1b showed co-localisation between the lipase and markers for secretory granules and lysosomes (Brown *et al*., 1998). The fPtdCho has 50% localisation with the lysosomal marker LysoTracker Red, which corresponds to previously characterised PLD1 expression in RBL-2H3 cells. This indicates that low basal PLD1 activity (and consequent PtdOH production) could be responsible for maintaining vesicle membrane integrity, thus providing some explanation for punctate PtdCho-labelling.

The structure of PtdCho may also contribute to function and intracellular localisation and contribute to punctiform fPtdCho-labelling seen in RBL-2H3 cells. PtdCho constitutes approximately 30-50% of total mammalian cell phospholipid content and is a cylindrical lipid (Hodgkin *et al*., 1998; van Meer and Sprong, 2004). PLD catalysed hydrolysis of PtdCho produces mono-unsaturated PtdOH, which is a cone shaped lipid (Hodgkin *et al*., 1998). A patch of cone shaped lipids within a monolayer should adopt a negative curvature as the lipid heads are able to pack more closely together than their tail (van Meer and Sprong, 2004). Furthermore, cone shaped lipids (such as PtdOH) contribute to membrane fusion and fission, whereas cylindrical lipids (such as PtdCho) resist bending and fusion (Chernomordik and Kozlov, 2003; Koojiman *et al*., 2003; van Meer and Sprong, 2004). The curved cone shape of PtdOH generated by PLD-mediated catalysis may therefore be required for the stability and integrity of the novel fluorescent lipid in punctiform structures.

PtdOH is also an established second messenger and mediates a variety of cellular processes ranging from targeting effectors responsible for promoting cell growth to translational control (Fang *et al*., 2003; Stahelin *et al*., 2005). Inhibition of PLD-catalysed generation of PtdOH creates deficiencies in a range of processes, including actin stress fibre formation, vesicle fusion and secretion. PLD-catalysed production of mono- or di-unsaturated PtdOH is thought to raise intracellular levels of PtdOH (possibly above a threshold), triggering their roles as cell signalling molecules (Pettitt *et al*., 2001). As PtdOH is a signalling molecule, the integrity of fPtdCho-labelling of RBL-2H3 cells may depend on that activity on one of its range of effectors.

PtdOH produced by PLD-mediated hydrolysis of PtdCho is an activator of phosphatidylinositol 4-phosphate 5-kinase (PtdIns 4-P 5-kinase), which is in turn responsible for production of phosphatidylinositol 4,5-bisphosphate (PtdIns(4,5)P_2 – Mortiz *et al*., 1992). Although PtdIns(4,5)P_2 is a known activator of both PLD1 and PLD2, it comprises only a small part of the lipid environment and is therefore unlikely to contribute greatly to membrane integrity. PtdOH is also an effector of another lipid kinase, sphingosine kinase-1, which phosphorylates sphingosine to produce sphingosine 1-phosphate (Stahelin *et al*., 2005). Sphingosine 1-phosphate is known as a bioactive lipid which promotes cell growth and inhibits programmed cell

death (Stahelin *et al*., 2005). Furthermore, sphingosine 1-phosphate generation increases in immune cells (such as monocytes and marcophages) upon receptor cross-linking and PLD activation (Melendez and Allen, 2002; Stace and Ktistakis, 2006). As PtdOH is an activator of sphingosine 1-kinase and PLD activation correlates with levels of sphingosine 1-phosphate, the levels of this lipid may also aid maintenance of punctate fPtdCho labelling.

The Raf-1 kinase is an important component of the MAP signalling cascade (as it is a MAP kinase kinase kinase) and binding PtdOH may facilitate translocation to the plasma membrane (Ghosh *et al*., 1996; Hodgkin *et al*., 1998; Anderson *et al*., 2002). The translocation of Raf-1 to the plasma membrane in Madin-Derby canine kidney (MDCK) cells was PLD-dependent as translocation was inhibited following treatment with primary alcohol (Ghosh *et al*., 1996; Hodgkin *et al*., 1998). Treatment of RBL-2H3 cells with butan-1-ol also potentially inhibited Raf-1 with downstream implications on the MAP kinase signalling cascade, which may also have influenced labelling with the novel PtdCho. PtdOH is also an effector of protein kinase Cε (PKCε), a novel PKC with an N-terminal C2 domain (Corbalán-Garcia *et al*, 2003). PLD-generated PtdOH is an essential activator of PKCε (through its C2 domain) and both PtdOH and PLC-generated diacylglycerol (DAG) regulate plasma membrane localisation in RBL-2H3 cells (Jose Lopez-Andreo *et al*., 2003). Although the events downstream of PKCε are not well characterised, PKCε is another possible effector of PLD-generated PtdOH, which could impact on labelling of the novel PtdCho in RBL-2H3 cells. Finally, the mammalian target of rapamycin (mTOR) is another known PtdOH target *in vivo* (Fang *et al*., 2003). PLD-generated PtdOH possibly activates mTOR which then goes on to phosphorylate downstream targets involved in translational control (Fang *et al*., 2003; Stace and Ktistakis, 2006).

Of the five PtdOH targets identified above (phosphatidylinositol 4,5-bisphosphate, sphingosine 1-phosphate, Raf-1, protein kinase Cε and the mammalian target for rapamycin) there is little evidence to suggest that sphingosine 1-phosphate production as a novel extracellular signal has an impact on intracellular vesicle integrity and/or movement. Similarly, Raf-1 is involved in regulating mitogenic signalling via activation of the MAP kinase cascade, although there is little evidence to support its role in maintaining intracellular vesicles. Whilst PKCε is involved in a

number of important processes by regulating factors and phosphorylating or interacting with a multitude of substrates (including the cytoskeleton), there is little direct evidence of its role in maintenance vesicles (Das *et al*., 2009). Similarly, mTOR is involved in translational control by phosphorylating downstream targets (such as those responsible for the recruitment of ribosomes to mRNA – Fang *et al*., 2003; Stace and Ktistakis, 2006) and so membrane integrity is unlikely to be dependent on the mTOR-PtdOH interaction. The production of PtdIns(4,5)P_2 from PtdIns(4)P is known to play a significant role in signalling and may have a function in vesicle organisation and integrity (Hammond *et al*., 2009). A recent report suggests a role for PtdIns(4)P in regulating the Golgi apparatus and highlights the possibility that there are distinct pools of PtdIns(4)P and PtdIns(4,5)P_2 in the Golgi apparatus and plasma membrane (Hammond *et al*., 2009). Regulation of the conversion of PtdIns(4)P to PtdIns(4,5)P_2 via PLD may therefore have a distinct role to play in regulating Golgi-plasma membrane vesicular traffic.

6.3: The association between Cherry-PLD1b and its novel substrate in HeLa cells

Transiently expressed Cherry-labelled PLD1b showed co-localisation with a hydrophobic fluorescently dequenched PtdCho analogue (fPtdCho) in resting HeLa cells. The degree of proximity of lipase and substrate could be inferred from experiments using Förster (or fluorescence) resonance energy transfer (FRET) detected via fluorescence recovery after photobleaching (FRAP). FRET refers to a dipole-dipole interaction between two suitable fluorophores (i.e. a donor and acceptor) that can occur when fluorophores are within approximately 10 nm of each other (Festy *et al*., 2007). The suitability of FRET for the fluorophores is dependent on the donor's fluorescence emission spectrum overlapping with the acceptor's absorption spectrum when the two are in the correct orientation. In this case, the wide emission spectrum of the fPtdCho BODIPY group ensures it is a suitable donor for the Cherry label of PLD1b to act as an acceptor (Festy *et al*., 2007). Experiments using FRET technology increased the resolution of images showing co-localisation between substrate and lipase beyond that achieved by methods offering only co-localisation or simply overlaying of pixels. The spatiotemporal interaction of fPtdCho and Cherry-PLD1b was analysed using FRET by FRAP. Acceptor

fluorescence (Cherry-PLD1b) was bleached and the levels of donor (fPtdCho) fluorescence recovery measured using confocal software. Our preliminary FRET efficiency and mean photobleaching (i.e. of the donor) were comparable with other studies using similar techniques to analyse dynamic intracellular protein-protein interactions (Gu *et al*., 2004; van Munster *et al*., 2005). FRET-FRAP technology enabled the visualisation and analysis of proximity between lipase and substrate in living cells. This work lays the foundations for further work to isolate the sites and orientation of interactions between substrate and lipase *in vivo*.

Analysis of the novel fPtdCho and Cherry-PLD1b *in vivo* provided valuable insight into their spatiotemporal interactions. Although the novel lipid was useful in preliminary characterisation of interactions between Cherry-PLD1b and a PtdCho analogue in living cells, fPtdCho may not be suitable for further development of a live *in vivo* PLD assay. When the novel fPtdCho is hydrolysed by PLD *in vivo*, its fluorescent BODIPY label attached to the soluble choline head group is cleaved from the lipid, however we were unable to detect an increase in fluorescence. A number of factors may have contributed to our inability to detect changes in fluorescence of the novel fluorescent PtdCho in living cells. First, the high basal fluorescence of the intact lipid, which is derived from incomplete quenching, makes determining subsequent changes in fluorescence difficult. This is compounded by the fact that vesicles can move in and out of the focal plane. In addition, our *in vitro* data shows that extensive metabolism of microgram quantities of the lipid by purified recombinant PLD only results in doubling of fluorescence. Thus the signal-to-noise ratio for the lipid in terms of it being intact or metabolised to a fluorescent choline is sub-optimal. Finally, it is plausible that the lipid, when added to cells, cannot be metabolised, although *in vitro* data presented here suggests that it is a suitable PLD substrate. Detectable increases in fluorescence may be achieved by attaching the fluorophore label to the lipid end of PtdCho and quenching groups to the soluble choline headgroup. However, this new substrate would have to be re-established as a PLD substrate *in vitro*. Furthermore, the fluorescent PtdOH produced by PLD-mediated hydrolysis of this new PtdCho substrate could be as metabolically labile as native PtdOH. The rapid dephosphorylation of PtdOH to DAG by PtdOH phosphatase would make it difficult to detect increases in fluorescence and ensure that the fluorescence being detected is in fact PtdOH and not DAG. Although

obstacles would need to be overcome using a new PLD substrate analogue, the foundations of a real-time *in vivo* PLD assay have been established using FRET by FRAP technology.

6.4: Identifying the intracellular clusters formed by PLD1b and its novel substrate

Whilst PLD1 co-localises with calveolin-1 and the EGF receptor (EGFR) on the plasma membrane in response to EGF (Han *et al*., 2002), our data suggests that there is also a secondary phenotype. Our data confirms that Cherry-PLD1b translocates to the plasma membrane but also clusters in a distinct intracellular region within the cytoplasm of HeLa cells following EGF stimulation. The cellular response is consistent and reliable, although previous studies have not characterised this cytoplasmic aggregation of PLD1b upon stimulation.

PLD activity is necessary for the endocytosis of EGFR which can be functionally inhibited using primary alcohol (Shen *et al*., 2001). Treatment of cells using primary alcohol also inhibited the budding of nascent vesicles from the *trans*-Golgi network (TGN), suggesting a dependence on PLD-generated PtdOH (Chen *et al*., 1997). Endocytosed EGFR is eventually targeted for degradation after EGF stimulation; however in fibroblasts over-expressing EGFR there is a lag period of up to 4 hours between receptor endocytosis and degradation (Shen *et al*., 2001). The early endosomes which are responsible for EGFR endocytosis cycle between the plasma membrane and TGN (Gu *et al*., 2001). Cherry-PLD1b may co-localise with EGFR on the plasma membrane and with the intracellular membranes of the TGN or early endosomes as there is evidence of cycling between these structures. Arf1, a known PLD1 activator, also localises to the TGN where it could stimulate the PLD-mediated PtdOH required for budding of nascent secretory vesicles shown in endocrine cells (Chen *et al*., 1997). Importantly, over-expression of wildtype PLD accelerated EGF-induced EGFR endocytosis whereas the catalytically inactive PLD delayed endocytosis (Shen *et al*., 2001).

The complete contribution of endocytic trafficking to EGFR physiology remains unclear. However, the small molecular weight (25kDa) GTP binding protein Rab5 is

a possible candidate for the regulation of EGFR trafficking (Dinneen and Ceresa, 2004). Rab5 localises to the cytoplasmic side of the plasma membrane and the early endosomes (Chavrier *et al*., 1990). Rab5 is geranylgeranylated on the carboxyl terminus which facilitates its association with the plasma membrane (Sanford *et al*., 1995; Dinneen and Ceresa, 2004). Over-expression of dominant negative Rab5 delays EGFR degradation in response to EGF stimulation, suggesting that Rab5 may mediate EGFR endocytic trafficking distal from the plasma membrane and is a regulator of vesicle fusion (Dinneen and Ceresa, 2004). EGFR is known to cycle between early endosomes and the plasma membrane and so the characteristic change in intracellular Cherry-PLD1b expression in response to EGF stimulation is possibly co-localisation with the EGFR.

Section 6.5: Future work and experimental strategies

In RBL-2H3 cells, PLD-generated PtdOH was identified as essential to maintenance of the integrity of punctate fPtdCho-labelling. This project was unable to confirm which PLD isoform was essential for basal PtdOH generation in RBL-2H3 cells. Depleting endogenous PLD expression using PLD1 or PLD2 small interfering RNA (siRNA – Lehman *et al*., 2006)) would identify the isoform required for PtdOH turnover which is essential for punctate fPtdCho-labelling of RBL-2H3 cells. RBL-2H3 cells transiently expressing dominant negative PLD1b or PLD2a mutants would also identify which PLD isoform is responsible to the punctate labelling of fPtdCho labelled RBL-2H3 cells. The levels of protein expression associated with both siRNA knockdown and over-expression of PLD1 or PLD2 could be quantified using established Western blotting techniques.

Localisation between Cherry-PLD1b and Rac1 in EGF stimulated HeLa cells has been characterised in fixed cells. Mutagenesis of the N-terminal PLD1b region which interacts with Rho family members (McDermott *et al*., 2004) may alter the co-localisation in response to ligand stimulation. In addition, co-localisation between Cherry-PLD1b and eGFP-Rac1 in EGF stimulated HeLa cells would be supported by live analysis of co-localisation using FRAP by FRET analysis.

HeLa cells labelled with the novel fluorescent PtdCho (fPtdCho) and stimulated with EGF showed the same intracellular clustering as Cherry-PLD1b. Localisation has been established between the novel fluorescent PtdCho (fPtdCho) and Cherry-PLD1b in resting HeLa cells. Further experiments using FRET by FRAP technology would establish if there is co-localisation between Cherry-PLD1b and clustering of fPtdCho in response to EGF stimulation. In addition, HeLa cells transiently expressing Cherry-labelled galactosyltransferase could identify if there is co-localisation between the novel fPtdCho and the TGN in response to EGF-stimulation (Roth and Berger, 1982; Liopis *et al*., 1998). Antibody markers (such as TGN38 or TGN46) could also be used to further investigate possible localisation between Cherry-PLD1b and TGN upon EGF stimulation in fixed cells (Nokes *et al*., 2008). Alternatively, transient co-expression of Cherry-PLD1b with an eGFP labelled *trans*-Golgi cisternae marker, such as the type II membrane anchored protein galactosyltransferase, could be used to detect co-localisation in response to ligand stimulation (Roth and Berger, 1982; Liopis *et al*., 1998). Intracellular clustering of both Cherry-PLD1b and fPtdCho in EGF-stimulated HeLa cells may correspond to the endosome. Similarly, FRET by FRAP technology could identify potential localisation between PLD1b or fPtdCho with early endosome markers, such as early endosome-associated antigen 1 (EEA1 – Mu *et al*., 1995), labelled with either green or cherry fluorescent protein.

Localisation between Cherry-PLD1b and the novel fPtdCho substrate has been characterised utilising FRET by FRAP confocal microscopy. Further confirmation of the region of PLD1b which is associated with the substrate *in vivo* could be characterised by mutagenesis of key residues. Modification of the HKD motif associated with PLD1b catalytic activity may impact on the co-localisation observed between lipase and substrate in resting HeLa cells. Although this project has established the foundations of a real-time *in vivo* PLD assay, further experiments are required to accomplish a truly quantitative assay.

References

Abousalham, A., Liossis, C., O'Brien, L. and Brindley, D.N. (1996). Cell-permeable ceramides prevent the activation of phospholipase D by ADP-ribosylation factor and RhoA. *J. Biol. Chem*. **272,** 1069-1075.

Ahn, B.H., Kim, S.Y., Kim, E.H., Choi, K.S., Kwon, T.K., Lee, Y.H., Chang, J.S., Kim, M.S., Jo, Y.H. and Min, D.S. (2003). Transmodulation between phospholipase D and c-Src enhances cell proliferation. *Mol. Cell. Biol*. **23,** 3103–3115.

Ahn, B.H., Rhim, H., Kim, S.Y., Sung, Y.M., Lee, M.Y., Choi, J.Y., Wolozin, B., Chang, J.S., Lee, Y.H., Kwon, T.K., Chung, K.C., Yoon, S.H., Hahn, S.J., Kim, M.S., Jo, Y.H. and Min, D.S. (2002). alpha-Synuclein interacts with phospholipase D isozymes and inhibits pervanadate-induced phospholipase D activation in human embryonic kidney-293 cells. *J. Biol. Chem*. **277,** 12334-12342.

Allersma, M.W., Bittner, M.A., Axelrod, D. and Holz, R.W. (2006). Motion matters: Secretory granule motion adjacent to the plasma membrane and exocytosis. *Mol. Biol. Cell*. **17,** 242-2438.

Anderson, R.G.W. and Orci, L. (1988). A view of acidic intracellular compartments. *J. Cell Biol*. **106,** 539-543.

Andresen, B.T., Rizzo, M.A., Shome, K. and Romero, G. (2002). The role of phosphatidic acid in the regulation of the Ras/MEK/Erk signaling cascade. *FEBS Lett*. **531,** 65-68.

Antonescu, C.N., Danuser, G. and Schmid, S.L. (2010). Phosphatidic acid plays a regulatory role in clathrin-mediated endocytosis. *Mol. Biol. Cell*. **21,** 2944-1952.

Arneson, L.S., Kunz, J., Anderson, R.A. and Traub, L.M. (1999). Coupled inositide phosphorylation and phospholipase D activation initiates clathrin-coat assembly on lysosomes. *J. Biol. Chem*. **274,** 17794-17805.

Arora, N., Williamson, L.C., Leppla, S.H. and Halpern, J.L. (1994). Cytotoxic effects of chimeric protein consisting of tetanus toxin light chain and anthrax toxin lethal factor in non-neuronal cells. *J. Biol. Chem*. **269,** 26165-26171.

Aspenström, P., Fransson, A. and Saras, J. (2004). Rho GTPases have diverse effects on the organization of the actin filament system. *Biochem. J*. **377**, 327-337.

Assunção Guimarães, C. and Linden, R. (2004). Programmed cell deaths. Apoptosis and alternative deathstyles. *Eur. J. Biochem*. **271,** 1638-1650.

Avila-Flores, A., Santos, T., Rincón, E. and Mérida, I. (2005). Modulation of the mammalian target of rapamycin pathway by diacylglycerol kinase-produced phosphatidic acid. **J. Biol. Chem**. **280,** 10091-10099.

Ayscough, K.R., Stryker, J., Pokala, N., Sanders, M., Crews, P. and Drubin, D.G. (1997). High rates of actin filament turnover in budding yeast and roles for actin establishment and maintenance of cell polarity revealed using the actin inhibitor latrunculin-A. *J. Cell Biol*. **137,** 399-416.

Bae, C.D., Min, D.S., Fleming, I.N. and Exton, J.H. (1998). Determination of interaction sites on the small G protein RhoA for phospholipase D. *J. Biol. Chem*. **273,** 11596-11604.

Bae, Y.S., Kim, Y., Kim, J.H., Lee, T.G., Kim, Y., Suh, P.G. and Ryu, S.H. (2000). Independent functioning of cytosolic phospholipase A_2 and phospholipase D1 in Trp-Lys-Tyr-Met-Val-D-Met-induced superoxide generation in human monocytes. *J. Immunol*. **164,** 4089-4096.

Bai, X. and Jiang, Y. (2010). Key factors in mTOR regulation. *Cell. Mol. Life Sci*. **67,** 239-253.

Baillie, G.S., Huston, E., Scotland, G., Hodgkin, M., Gall, I., Peden, A.H., MacKenzie, C., Houslay, E.S., Currie, R., Pettitt, T.R., Walmsley, A.R., Wakelam, M.J., Warwicker, J. and Houslay, M.D. (2002). TAPAS-1, a novel microdomain within the unique N-terminal region of the PDE4A1 cAMP-specific phosphodiesterase that allows rapid, Ca^{2+}-triggered membrane association with selectivity for interaction with phosphatidic acid. *J. Biol. Chem*. **277,** 28298-28309.

Baird, G.S., Zacharias, D.A. and Tsien, R.Y. (2000). Biochemistry, mutagenesis, and oligomerization of DsRed, a red fluorescent protein from coral. *Proc. Natl. Acad. Sci. U.S.A*. **97,** 11984-11989.

Balboa, M.A. and Insel, P.A. (1995). Nuclear phospholipase D in Madin-Darby canine kidney cells. Guanosine 5′-O-(thiotriphosphate)-stimulated activation is mediated by RhoA and is downstream of protein kinase C. *J. Biol. Chem*. **270,** 29843–29847.

Baram, D., Linial, M., Mekori, Y.A. and Sagi-Eisenberg, R. (1998). Cutting edge: Ca^{2+}-dependent exocytosis in mast cells is stimulated by the Ca^{2+} sensor, synaptotagmin I. *J. Immun*. **161,** 5120-5123.

Baram, D., Adachi, R., Medalia, O., Tuvim, M., Dickey, B.F., Mekori, Y.A. and Sagi-Eisenberg, R. (1999). Synaptotagmin II negatively regulates Ca^{2+}-triggered exocytosis of lysosomes in mast cells. *J. Exp. Med*. **189,** 1649-1657.

Beavo, J.A. and Brunton, L.L. (2002). Cyclic nucleotide research - still expanding after half a century. *Nat. Rev. Mol. Cell Biol*. **3,** 710-718.

Betz, W.J., Mao, F. and Smith, C.B. (1996). Imaging exocytosis and endocytosis. *Curr. Biol*. **6,** 365-371.

Bevis, B.J. and Glick, B.S. (2002). Rapidly maturing variants of *Discosoma* red fluorescent protein (DsRed). *Nat. Biotechnol*. **20,** 83-87.

Bhattacharya, M., Babwah, A.V. Godin, C., Anborgh, P.H., Dale, L.B., Poulter, M.O., and Ferguson, S.S.G. (2004). Ral and phospholipase D2-dependent pathway for constitutive metabotropic glutamate receptor endocytosis. *AJOB Neurosci*. **24**, 8752– 8761.

Birnie, G.D. (1988). The HL60 cell line: a model system for studying human myeloid cell differentiation. *Br. J. Cancer Suppl*. **9,** 41-45.

Blott., E.J. and Griffiths, M.G. (2002). Secretory lysosomes. *Nat. Rev. Mol. Cell Biol*. **3,** 122-131.

Boman, A.L. and Kahn, R.A. (1995). Arf proteins: the membrane traffic police? *Trends Biochem. Sci*. **20,** 147-150.

Bonser, R.W., Thompson, N.T., Randall, R.W., Tateson, J.E., Spacey, G.D., Hodson, H.F. and Garland., L.G. (1991). Demethoxyviridin and wortmannin block phospholipase C and D activation in the human neutrophil. *Br. J. Pharmacol*. **103,** 1237-1241.

Bos, J.L., Rehmann, H. and Wittinghofer, A. (2007). GEFs and GAPs: Critical elements in the control of small G proteins. *Cell*. **129,** 865-877.

Bosch, R.R., Smeets, R.L.L., Sleutels, F., Patel, A.M.P., van Emst-de Vries, S.E., Joep, J., De Pont, H.H.M. and Willems, P.H. (1999). Concerted action of cytosolic Ca^{2+} and protein kinase C in receptor-mediated phospholipase D activation in Chinese hamster ovary cells expressing the cholecystokinin-A receptor. *Biochem. J*. **337,** 263–268.

Brown, E.J., Albers, M.W., Shin, T.B., Ichikawa, K., Keith, C.T., Lane, W.S. and Schreiber, S.L. (1994). A mammalian protein targeted by G1-arresting rapamycin-receptor complex. *Nature*. **369,** 756-758.

Brown, H.A., Gutowski, S., Moomaw, C.R., Slaughter, C. and Sternweis, P.C. (1993). ADP-ribosylation factor, a small GTP-dependent regulatory protein, stimulates phospholipase D activity. *Cell*. **75,** 1137-1144.

Brown, H.A., Gutowski, S., Kahn, R.A. and Sternweis, P.C. (1995). Partial purification and characterization of Arf-sensitive phospholipase D from porcine brain. *J. Biol. Chem*. **270,** 14935-14943.

Brown, F.D., Thompson, N., Saqib, K.M., Clark, J.M., Powner, D., Thompson, N.T., Solari. R. and Wakelam M.J.O. (1998). Phospholipase D1 localises to secretory granules and lysosomes and is plasma-membrane translocated on cellular stimulation. *Curr. Biol*. **8,** 835-838.

Burchfield, J.G., Lopez, J.A., Mele, K., Vallotton, P. and Hughes, W.E. (2010). Exocytotic vesicle behaviour assessed by total internal reflection fluorescence microscopy. *Traffic*. **11,** 429-439.

Burgoyne., R.D. and Morgan, A. (2003). Secretory granule exocytosis. *Physiol Rev*. **83,** 581-632.

Cai, H., Erhardt, P., Szeberényi, J., Diaz-Meco, M.T., Johansen, T., Moscat, J. and Cooper, G.M. (1992). Hydrolysis of phosphatidylcholine is stimulated by Ras proteins during mitogenic signal transduction. *Mol. Cell Biol*. **12,** 5329-5335.

Cai, S. and Exton, J.H. (2001). Determination of interaction sites of phospholipase D1 for RhoA. *Biochem. J*. **355,** 779-785.

Caloca, M.J., Zugaza, J.L. and Bustelo, X.R. (2008). Mechanistic analysis of the amplification and diversification events induced by Vav proteins in B-lymphocytes. *J. Biol. Chem*. **283,** 36454-36464.

Campbell, R.E., Tour, O., Palmer, A.E., Steinbach, P.A., Baird, G.S., Zacharias, D.A. and Tsien, R.Y. (2002). A monomeric red fluorescent protein. *Proc. Natl. Acad. Sci. U.S.A*. **99,** 7877-7882.

Carpenter, G. and Cohen, S. (1990). Epidermal growth factor. *J. Biol. Chem*. **265,** 7709-7712.

Castagna, M., Takai, Y., Kaibuchi, K., Sano, K., Kikkawa, U. and Nishizuka, Y. (1982). Direct activation of calcium-activated, phospholipid-dependent protein kinase by tumor-promoting phorbol esters. *J. Biol. Chem*. **13,** 7847-7851.

Chardin, P., Paris, S., Antonny, B., Robineau, S., Béraud-Dufour, S., Jackson, C.L., and Chabre, M. (1996). A human exchange factor for ARF contains Sec7- and pleckstrin-homology domains. *Nature*. **384,** 481-484.

Chae, Y.C., Kim, J.H., Kim, K.L., Kim, H.W., Lee, H.Y., Heo, W.D., Meyer, T., Suh, P.G. and Ryu, S.H. (2008). Phospholipase D activity regulates integrin-mediated cell spreading and migration by inducing GTP-Rac translocation to the plasma membrane. *Mol. Biol. Cell*. **19,** 3111–3123.

Chae, Y.C., Lee, S., Lee, H.Y., Heo, K., Kim, J.H., Kim. J.H., Suh, P.G. and Ryo, S.H. (2005). Inhibition of muscarinic receptor-linked phospholipase D activation by association with tubulin. *J. Biol. Chem*. **280,** 3723-3730.

Chahdi, A., Choi, W.S., Kim, Y.M., Fraundorfer, P.F. and Beaven, M.A. (2001). Serine/threonine protein kinases synergistically regulate phospholipase D1 and 2 and secretion in RBL-2H3 mast cells. *Mol. Immunol*. **38,** 1269-1276.

Chalifa, C., Möhn, H. and Liscovitch, M. (1990). A neutral phospholipase D activity from rat brain synaptic plasma membranes. Identification and partial characterization. *J. Biol. Chem*. **265,** 17512-17519.

Chang, Y.C., Nalbant, P., Birkenfeld., J., Change., Z.F. and Bokoch, G.M. (2008). GEF-H1 couples nocodazole-induced microtubule disassembly to cell contractility via RhoA. *Mol. Biol. Cell*. **19,** 2147-2153.

Chapman, E.R. (2002). Synaptotagmin: a Ca^{2+} sensor that triggers exocytosis?. *Nat. Rev. Mol. Cell Biol*. **3,** 498-508.

Chavrier, P., Parton, R.G., Hauri, H.P., Simons, K. and Zerial, M. (1990). Localization of low molecular weight GTP binding proteins to exocytic and endocytic compartments. *Cell*. **62,** 317-329.

Chen, J,, Zheng, X.F., Brown, E.J. and Schreiber, S.L. (1995). Identification of an 11-kDa FKBP12-rapamycin-binding domain within the 289-kDa FKBP12-rapamycin-associated protein and characterization of a critical serine residue. *Proc. Natl. Acad. Sci. U.S.A*. **92,** 4947-4951.

Chen, J.S. and Exton, J.H. (2005). Sites of phospholipase D2 phosphorylated by PKCα. *Biochem. Biophys. Res. Commun*. **333,** 1322-1326.

Chen, Y.G., Siddhanta, A., Austin, C.D. Hammond, S.M., Sung, T.C., Frohman, M.A., Morris, A.J. and Shields, D. (1997). Phospholipase D stimulates release of nascent secretory vesicles from the trans-Golgi network. *J. Cell Biol*. **138,** 495–504.

Chernomordi, L.V. and Kozlov, M.M. (2003). Protein-lipid interplay in fusion and fission of biological membranes. *Annu. Rev. Biochem*. **72,** 175-207.

Cho. C.H., Lee. C.S., Chang, M., Jang, I.H., Kim, S.J., Hwang, I., Ryu, S.H., Lee, C.O. and Koh, G.Y. (2004). Localization of VEGFR-2 and PLD2 in endothelial caveolae is involved in VEGF-induced phosphorylation of MEK and ERK. *Am. J. Physiol. Heart Circ. Physiol*. **286,** H1881-8.

Chung, J.K., Sekiya, F., Kang, H.S., Lee, C., Han, J.S., Kim, S.R., Bae, Y.S., Morris, A.J. and Rhee, S.G. (1997). Synaptojanin inhibition of phospholipase D activity by hydrolysis of phosphatidylinositol 4,5-bisphosphate. *J. Biol. Chem*. **272,** 15980-15985.

Cockcroft, S., Way, G., O'Luanaigh, N., Pardo, R., Sarri, E. and Fensome, A. (2001). Signalling role for ARF and phospholipase D in mast cell exocytosis stimulated by crosslinking of the high affinity FcεR1 receptor. *Mol. Immunol*. **38,** 1277–1282.

Cohen, L.A., Honda, A., Varnai, P., Brown, F.D., Balla, T. and Donaldson, D.G. (2007). Active Arf6 recruits ARNO/cytohesin GEFs to the PM by binding their PH domains. *Mol. Biol. Cell*. **18,** 2244–2253.

Cokol, M., Nair, R. and Rost, B. (2000). Finding nuclear localization signals. *EMBO Rep*. **1,** 411-415.

Colley, W.C., Sung, T.C., Roll, R., Jenco, J., Hammond, S.M., Altshuller, Y., Bar-Sagi, D., Morris, A.J. and Frohman, M.A. (1997). Phospholipase D2, a distinct phospholipase D isoform with novel regulatory properties that provokes cytoskeletal reorganization. *Curr. Biol*. **7,** 191-201.

Cook, S.J. and Wakelam, M.J.O. (1992). Epidermal growth factor increases sn-1,2-diacylglycerol levels and activates phospholipase D-catalysed phosphatidylcholine

breakdown in Swiss 3T3 cells in the absence of inositol-lipid hydrolysis. *Biochem. J*. **285,** 247-253.

Corbalán-Garcia, S., Sánchez-Carrillo, S., García-García, J. and Gómez-Fernández, J.C. (2003). Characterization of the membrane binding mode of the C2 domain of PKC epsilon. *Biochemistry*. **42,** 11661-11668.

Cross, M.J., Hodgkin, M.N., Plumb, J.A., Brunton, V.G., Stewart, A., MacAully, G., Hill, R., Kerr, D.J., Workman, P. and Wakelam, M.J.O. (1997). Inhibition of phospholipid signalling and proliferation of Swiss 3T3 cells by the wortmannin analogue demethoxyviridin. *Biochim. Biophys. Acta*. **1362,** 29-38.

Cross, M.J., Roberts, S., Ridley, A.J., Hodgkin, M.N., Stewart, A., Claesson-Welsh, L. and Wakelam, M.J. (1996). Stimulation of actin stress fibre formation mediated by activation of phospholipase D. *Curr. Biol*. **6,** 588-597.

Cross, M.J., Stewart, A., Hodgkin, M.N., Kerr, D.J. and Wakelam, M.J.O. (1995). Wortmannin and its structural analogue demethoxyviridin inhibit stimulated phospholipase A_2 activity in Swiss 3T3 Cells. Wortmannin is not a specific inhibitor of phosphtidylinositol 3-kinase. *J. Biol. Chem*. **270,** 25352-25355.

Dai, Y., Dudek, N.L., Patel, T.B. and Muma, N.A. (2008). Transglutaminase-catalyzed transamidation: A novel mechanism for Rac1 activation by 5-hydroxytryptamine$_{2A}$ receptor stimulation. *J. Pharmacol. Exp. Ther*. **326,** 153–162.

Das, J., Pany, S., Rahman, G.M. and Slater, S.J. (2009). PKCε has an alcohol-binding site in its second cysteine-rich regulatory domain. *Biochem. J*. **421,** 405–413.

Dascher, C. and Balch, W.E. (1994). Dominant inhibitory mutants of ARF1 block endoplasmic reticulum to Golgi transport and trigger disassembly of the Golgi apparatus. *J. Biol. Chem*. **269,** 1437-1448.

Davies, D.R., Interthal, H., Champoux, J.J. and Hol, W.G.J. (2002). Insights into substrate binding and catalytic mechanism of human tyrosyl-DNA phosphodiesterase (Tdp1) from vanadate and tungstate-inhibited structures. *J.Mol.Biol*. **324,** 917-932.

Degterev, A., Boyce, M. and Yuan, J. (2003). A decade of caspases. *Oncogene*. **22,** 8543-8567.

Derrien, V., Couillault, C., Franco, M., Martineau, S., Montcourrier, P., Houlgatte, R. and Chavrier, P. (2002). A conserved C-terminal domain of EFA6-family ARF6-guanine nucleotide exchange factors induces lengthening of microvilli-like membrane protrusions. *J. Cell Sci*. **115,** 2867-2879.

DiNitto, J.P. and Lambright, D.G. (2006). Membrane and juxtamembrane targeting by PH and PTB domains. *Biochim. Biophys. Acta*. **1761,** 850-867.

Dinneen, J.L. and Ceresa, B.P. (2004). Expression of dominant negative rab5 in HeLa cells regulates endocytic trafficking distal from the plasma membrane. *Exp. Cell Res*. **294,** 509– 522.

Divecha, N., Roefs, M., Halstead, J.R., D'Andrea, S., Fernandez-Borga, M., Oomen, L., Saqib, K.M., Wakelam, M.J. and D'Santos, C. (2000). Interaction of the type Ialpha PIPkinase with phospholipase D: a role for the local generation of phosphatidylinositol 4, 5-bisphosphate in the regulation of PLD2 activity. *EMBO J*. **19,** 5440-5449.

Donaldson, J.G. (2009). Phospholipase D in endocytosis and endosomal recycling pathways. *Biochim. Biophys. Acta*. **1791,** 845-849.

Donaldson, J.G., Finazzi, D. and Klausner, R.D. (1992). Brefeldin A inhibits Golgi membrane-catalysed exchange of guanine nucleotide onto ARF protein. *Nature*. **360,** 350-352.

Donaldson, J.G. and Honda, A. (2005). Localization and function of Arf family GTPases. *Biochem. Soc, Trans*. **33,** 639-642.

Dowhan, W. and Bogdanov, M. (2002). Functional roles of lipids in membranes. In *Biochemistry of Lipids, Lipoproteins and Membranes*, 4th edn, pp. 1-35. Edited by Vanve, D.E. and Vance, J.E. London: Elsevier.

Dragonetti1, A., Baldassarre, M., Castino, R., Démoz, M., Luini, A., Buccione, R. and Isidoro, C. (2000). The lysosomal protease cathepsin D is efficiently sorted to and secreted from regulated secretory compartments in the rat basophilic/mast cell line RBL. *J. Cell Sci*. **113,** 3289-3298.

Du, G., Altshuller, Y.M., Kim, Y., Han, J.M., Ryu, S.H., Morris, A.J. and Frohman, M.A. (2000). Dual requirement for Rho and protein kinase C in direct activation of phospholipase D1 Through G protein-coupled receptor signaling. *Mol. Biol. Cell*. **11,** 4359–4368.

Du, G., Altshuller, Y.M., Vitale, N., Huang, P., Chasserot-Golaz, S., Morris, A.J., Bader, M.F. and Frohman, M.A. (2003). Regulation of phospholipase D1 subcellular cycling through coordination of multiple membrane association motifs. *J. Cell Biol*. *J. Cell Biol*. **162,** 305-315.

Du, G., Huang, P., Liang, B.T. and Frohman, M.A. (2004). Phospholipase D2 localizes to the plasma membrane and regulates angiotensin II receptor endocytosis. *Mol. Biol. Cell*. **15,** 1024–1030.

Edwards, Y.S. and Murray, A.W. (1995). Accumulation of phosphatidylalcohol in cultured cells: use of subcellular fractionation to investigate phospholipase D activity during signal transduction. *Biochem. J*. **308,** 473-480.

El Bawab, S., Macovschi, O., Sette, C., Conti, M., Lagarde, M., Nemoz, G. and Prigent, A.F. (1997). Selective stimulation of a cAMP-specific phosphodiesterase (PDE4A5) isoform by phosphatidic acid molecular species endogenously formed in rat thymocytes. *Eur. J. Biochem*. **247,** 1151-1157.

Eldar, H., Ben-Av, P., Schmidt, U.S., Livneh, E. and Liscovitch, M. (1993). Up-regulation of phospholipase D activity induced by over-expression of protein kinase

C-alpha. Studies in intact Swiss/3T3 cells and in detergent-solubilized membranes in vitro. *J. Biol. Chem*. **268,** 12560-12564.

Ella, K.M., Meier, G.P., Bradshaw, C.D., Huffman, K.M., Spivey, E.C. and Meier, K.E. (1994). A fluorescent assay for agonist-activated phospholipase D in mammalian cell extracts. *Anal. Chem*. **218,** 136-142.
Elmore, S. (2007). Apoptosis: A Review of Programmed Cell Death. *Toxicol. Pathol*. **35,** 495-516.

Emoto, M., Klarlund, J.K., Waters, S.B., Hu, V., Buxton, J.M., Chawla, A. and Czech, M.P. (2000). A role for phospholipase D in GLUT4 glucose transporter translocation. *J. Biol. Chem*. **275,** 7144–7151.

English, D., Cui, Y. and Siddiqui, R.A. (1996). Messenger functions of phosphatidic acid. *Chem. Phys. Lipids*. **80,** 117-132.

Exton, J.H. (1997). New developments in phospholipase D. *J. Biol. Chem*. **272,** 15579-15582.

Exton, J.H. (1999). Regulation of phospholipase D. *Biochim. Biophys. Acta*. **1439,** 121-133.

Exton, J.H. (2002). Regulation of phospholipase D. *FEBS Lett*. **531,** 58-61.

Fang, Y., Park, I.H., Wu, A.L., Du, G., Huang, P., Frohman, M.A., Walker, S.J., Brown, H.A. and Chen, J. (2003). PLD1 Regulated mTOR signaling and mediates Cdc42 activation of S6K1. *Curr. Biol*. **13,** 2037-2044.

Fang, Y., Vilella-Bach, M., Bachmann, R., Flanigan, A. and Chen, J. (2001). Phosphatidic acid-mediated mitogenic activation of mTOR signaling. *Science*. **294,** 1942-1945.

Faraudo, J. and Travesset, A. (2007). Phosphatidic acid domains in membranes: Effect of divalent counterions. *Biophys. J*. **92,** 2806-2818.

Farquhar, M., Soomets, U., Bates, R.L., Martin, A., Landel, Ü. and Howl., J. (2002). Novel mastroparan analogs induce differential secretion from mast cells. *Chem. Biol*. **9,** 63-70.

Farquhar, M.J., Powner, D.J., Levine, B.A., Wright, M.H., Ladds, G. and Hodgkin, M.N. (2007). Interaction of PLD1b with actin in antigen-stimulated mast cells. *Cell Signal*. **19,** 349-358.

Fedeli, C., Carrea, G. and Monti, D. (2006). On the effects of site-specific mutations on activity and expression of the *Streptomyces* PMF phospholipase D. *J. Mol. Catal. B Enzym*. **41,** 1-7.

Feng, L., Manabe, K., Shope, J.C., Widmer, S., DeWald, D.B. and Prestwich, G.D. (2002). A real-time fluorogenic phospholipase A_2 assay for biochemical and cellular activity measurements. *Chem. Biol*. **9,** 795-803.

Feng, X., Becker, K.P., Stribling, S.D., Peters, K.G. and Hannun, Y.A. (2000). Regulation of receptor-mediated protein kinase C membrane trafficking by autophosphorylation. *J. Biol. Chem*. **275,** 17024-17034.

Festy, F., Ameer-Beg, S.M., Ngab, T. and Suhling, K. (2007). Imaging proteins in vivo using fluorescence lifetime microscopy. *Mol. BioSyst*. **3,** 381–391.

Fisher, G.J., Henderson, P.A., Voorhees, J.J. and Baldassare, J.J. (1991). Epidermal growth factor-induced hydrolysis of phosphatidylcholine by phospholipase D and phospholipase C in human dermal fibroblasts. *J. Cell. Physiol*. **146,** 309-17.

Fisher-Parton, S., Parton, R.M., Hickey, P.C., Dijksterhuis, J., Atkinson, H.A. and Read, N.D. (2000). Confocal microscopy of FM4-64 as a tool for analysing endocytosis and vesicle trafficking in living fungal hyphae. *J. Microsc*. **198,** 246-259.

Fleming, I.N., Elliott, C.M., Collard, J.G. and Exton, J.H. (1997). Lysophosphatidic acid induces threonine phosphorylation of Tiam1 in Swiss 3T3 fibroblasts via activation of protein kinase C. *J. Biol. Chem*. **272,** 33105-33110.

Franco, M., Peters, P.J., Boretto, J., van Donselaar, E., Neri, A., D'Souza-Schorey, C. and Chavrier, P. (1999). EFA6, a sec7 domain-containing exchange factor for ARF6, coordinates membrane recycling and actin cytoskeleton organization. *EMBO J*. **18,** 1480–1491.

Freyberg, Z., Bourgoin, S. and Shields, D. (2002). Phospholipase D2 is localized to the rims of the Golgi apparatus in mammalian cells. *Mol. Biol. Cell*. **13,** 3930-3942.

Freyberg, Z., Sweeney, D., Siddhanta, A., Bourgoin, S., Frohman, M. and Shields, D. (2001). Intracellular localization of phospholipase D1 in mammalian cells. *Mol. Biol. Cell*. **12,** 943-955.

Frohman, M.A. and Morris, A.J. (1999). Phospholipase D structure and regulation. *Chem. Phys. Lipids*. **98,** 127-140.

Frohman, M.A., Sung, T.S. and Morris, A.J. (1999). Mammalian phospholipase D structure and regulation. *Biochim. Biophys. Acta*. **1439,** 175-186.

Fukami, K., Sawada, N., Endo, T. and Takenawa, T. (1996). Identification of a phosphatidylinositol 4,5-bisphosphate-binding site in chicken skeletal muscle alpha-actinin. *J. Biol. Chem*. **271,** 2646-2650.

Fukami, K. and Takenawa, T. (1992). Phosphatidic acid that accumulates in platelet-derived growth factor-stimulated Balb/c 3T3 cells is a potential mitogenic signal. *J. Biol. Chem*. **267,** 10988-10993.

Funaba, M., Ikeda, T. and Abe, M. (2003). Degranulation in RBL-2H3 cells: regulation by calmodulin pathway. *Cell Biol. Int*. **27,** 879-885.

Ganley, I.G. Walker, S.J., Manifava, M., Li, D., Brown, A. and Ktistakis, N.T. (2001). Interaction of phospholipase D1 with a casein-kinase-2-like serine kinase. *Biochem. J*. **354,** 369-378.

Gemeinhardt, A., Alfalah, M., Gück, T., Naim, H.Y. and Fuhrmann, H. (2009). The influence of linoleic and linolenic acid on the activity and intracellular localisation of phospholipase D in COS-1 cells. *Biol. Chem*. **390,** 253-258.

Ghosh, S., Moore, S., Bell, R.M. and Dush, M. (2003). Functional analysis of a phosphatidic acid binding domain in human Raf-1 kinase: mutations in the phosphatidate binding domain lead to tail and trunk abnormalities in developing zebrafish embryos. *J. Biol. Chem*. **278,** 45690-45696.

Ghosh, S., Strum, J.C., Sciorra, V.A., Daniel, L. and Bell, R.M. (1996). Raf-1 kinase possesses distinct binding domains for phosphatidylserine and phosphatidic acid. Phosphatidic acid regulates the translocation of Raf-1 in 12-O-tetradecanoylphorbol-13-acetate-stimulated Madin-Darby canine kidney cells. *J. Biol. Chem*. **271,** 8472-8480.

Ghosh, S., Xie, W.Q., Quest, A.F., Mabrouk, G.M., Strum, J.C. and Bell, R.M. (1994). The cysteine-rich region of raf-1 kinase contains zinc, translocates to liposomes, and is adjacent to a segment that binds GTP-ras. *J. Biol. Chem*. **269,** 10000-10007.

Goldberg, J. (1998). Structural basis for activation of ARF GTPase: Mechanisms of guanine nucleotide exchange and GTP–Myristoyl Switching. *Cell*. **95,** 237–248.

Grange, M., Picq, M., Prigent, A.F., Lagarde, M. and Nemoz, G. (1998). Regulation of PDE-4 cAMP phosphodiesterases by phosphatidic acid. *Cell Biochem. Biophys*. **29,** 1-17.

Grange, M., Sette, C., Cuomo, M., Conti, M., Lagarde, M., Prigent, A.F. and Némoz, G. (2000). The cAMP-specific phosphodiesterase PDE4D3 is regulated by phosphatidic acid binding. Consequences for cAMP signaling pathway and characterization of a phosphatidic acid binding site. *J. Biol. Chem*. **275,** 33379-33387.

Griffiths, G.M. (1996). Secretory lysosomes – a special mechanism of regulated secretion in haemopoietic cells. *Trends Cell Biol*. **6,** 329-332.

Gruchalla, R.S., Dinh, T.T. and Kennerly, D.A. (1990). An indirect pathway of receptor-mediated 1,2-diacylglycerol formation in mast cells. I. IgE receptor-mediated activation of phospholipase D. *J. Immunol*. **144,** 2334-2342.

Gu, F., Crump, C.M. and Thomas, G. (2001). Trans-Golgi network sorting. *Cell. Mol. Life Sci*. **58,** 1067–1084.

Gu, Y., Di, W.L., Kelsell, D.P. and Zicha, D. (2004). Quantitative fluorescence resonance energy transfer (FRET) measurement with acceptor photobleaching and spectral unmixing. *J. Microsc*. **215,** 162-173.

Guillemain, I. and Exton, J.H. (1997). Effects of brefeldin A on phosphatidylcholine phospholipase D and inositolphospholipid metabolism in HL-60 cells. *Eur. J. Biochem*. **249,** 812-819.

Gupta, M.L. Jr., Bode, C.J., Georg, G.I. and Himes, R.H. (2003). Understanding tubulin-Taxol interactions: mutations that impart Taxol binding to yeast tubulin. *Proc. Natl. Acad. Sci. U.S.A*. **100,** 6394-6397.

Ha, K.S. and Exton, J.H. (1993). Activation of actin polymerization by phosphatidic acid derived from phosphatidylcholine in IIC9 fibroblasts. *J. Cell Biol*. **123,** 1789-1796.

Hakoshima, T., Shimizu, T. and Maesaki, R. (2003). Structural basis of the Rho GTPase signaling. *J. Biochem*. **134,** 327-331.

Hammond, G.R.V., Schiavo, G. and Irvine, R.F. (2009). Immunocytochemical techniques reveal multiple, distinct cellular pools of PtdIns4P and PtdIns(4,5)P_2. *Biochem J*. **422,** 23–35.

Hammond, S.M., Altshuller, Y.M., Sung, T.C., Rudge, S.A., Rose, K., Engebrecht, J., Morris, A.J. and Frohman, M.A. (1995). Human ADP-ribosylation factor-activated phosphatidylcholine-specific phospholipase D defines a new and highly conserved gene family. *J. Biol. Chem*. **270,** 29640-29643.

Hammond, S.M., Jenco, J.M., Nakashima, S., Cadwallader, K., Gu, Q.M., Cooks, S., Nozawa, Y., Prestwich, G.D., Frohman, M.A. and Morris, A.J. (1997). Characterization of two alternatively spliced forms of phospholipase D1: Activation of the purified enzymes by phosphatidylinositol 4,5-bisphosphate, ADP-ribosylation factor, and Rho family monomeric GTP-binding proteins and protein kinase C-α. *J. Biol. Chem*. **272,** 3860-3868.

Han, J.M., Kim, J.H., Lee, B.D., Lee, S.D., Kim, Y., Jung, Y.W., Lee, S., Cho, W., Ohba, M., Kuroki, T., Suh, P.G. and Ryu, S.H. (2002a). Phosphorylation-dependent regulation of phospholipase D2 by protein kinase C delta in rat pheochromocytoma PC12 cells. *J. Biol. Chem*. **277,** 8290-8297.

Han, J.M., Kim, Y., Lee, J.S. Lee, C.S., Lee, B.D., Ohba, M., Kuroki, T., Suh, P.G. and Ryu, S.H. (2002b). Localization of phospholipase D1 to caveolin-enriched membrane via palmitoylation: Implications for epidermal growth factor signaling. *Mol. Biol. Cell*. **13,** 3976–3988.

Harel, M., Schalk, I., Ehret-Sabatier, L., Bouet, F., Goeldner, M., Hirth, C., Axelsen, P.H., Silman, I. and Sussman, J.L. (1993). Quaternary ligand binding to aromatic residues in the active-site gorge of acetylcholinesterase. *Proc. Natl. Acad. Sci. U.S.A*. **90,** 9031–9035.

Haucke, V. (2005). Phosphoinositide regulation of clathrin-mediated endocytosis. *Biochem. Soc. Trans*. **33,** 1285-1289.

Haucke, V. and De Camilli, P. (1999). AP-2 recruitment to synaptotagmin stimulated by tyrosine-based endocytic motifs. *Science*. **285,** 1268-1271.

Hay, N. and Sonenberg, N. (2004). Upstream and downstream of mTOR. *Genes Dev*. **18,** 1926-1945.

Henage, L.G., Exton, J.H. and Brown, H.A. (2006). Kinetic analysis of a mammalian phospholipase D: allosteric modulation by monomeric GTPases, protein kinase C, and polyphosphoinositides. *J Biol Chem*. **281,** 3408-3417.

Herbert, J.M., Augereau, J.M., Gleye, J. and Maffrand, J.P. (1990). Chelerythrine is a potent and specific inhibitor of protein kinase C. *Biochem. Biophys. Res. Commun*. **172,** 993-999.

Hibi, T., Hirashima, N. and Nakanishi. (2000). Rat basophilic leukaemia cells express syntaxin-3 and VAMP-7 in granule membranes. *Biochem. Biophys. Res. Commun*. **271,** 36-41.

Hinchliffe, K.A., Ciruela, A. and Irvine, R.F. (1998). PIPkins1, their substrates and their products: new functions for old enzymes. *Biochim. Biophys. Acta*. **1436,** 87-104.

Hiroyama, M. and Exton, J.H. (2005a). Studies of the roles of ADP-ribosylation factors and phospholipase D in phorbol ester-induced membrane ruffling. *J. Cell. Physiol*. **202,** 608–622.

Hiroyama, M. and Exton, J.H. (2005b). Localization and regulation of phospholipase D2 by ARF6. *J. Cell. Biochem*. **95,** 149–164.

Hodgkin, M.N., Clark, J.M., Rose, S., Saqib, K. and Wakelam, M.J.O. (1999). Characterization of the regulation of phospholipase D activity in the detergent-insoluble fraction of HL60 cells by protein kinase C and small G-proteins. *Biochem. J*. **339,** 87-93.

Hodgkin, M.N., Masson, M.R., Powner, D., Saqib., K.M., Ponting, C.P. and Wakelam, M.J.O. (2000). Phospholipase D regulation and localisation is dependent upon a phosphatidylinositol 4, 5-bisphosphate-specific PH domain. *Curr. Biol*. **10,** 43-46.

Hodgkin, M.N., Pettitt, T.R., Martin, A., Michell, R.H., Pemberton, A.J. and Wakelam, M.J. (1998). Diacylglycerols and phosphatidates: which molecular species are intracellular messengers? *Trends Biochem. Sci*. **23,** 200-204.

Höer, A., Cetindag, C. and Oberdisse, E. (2000). Influence of phosphtidylinositol 4,5-bisphosphate on human phospholipase D1 wild-type and deletion mutants: is there evidence for an interaction of phosphatidylinositol 4,5-bisphosphate with the putative pleckstrin homology domain? *Biochim. Biophys. Acta*. **1481,** 189-201.

Holbrook, P.G., Geetha, V., Beaven, M.A. and Munson, P.J. (1999). Recognizing the pleckstrin homology domain fold in mammalian phospholipase D using hidden Markov models. *FEBS Lett*. **448,** 269-272.

Holz, R.W., Hlubek, M.D., Sorensen, S.D., Fisher, S.K., Balla, T., Ozaki, S., Prestwich, G.D., Stuenkel, E.L. and Bittner, M.A. (2000). A pleckstrin homology domain specific for phosphatidylinositol 4, 5-bisphosphate (PtdIns-4,5-P_2) and fused to green fluorescent protein identifies plasma membrane PtdIns-4,5-P2 as being important in exocytosis. *J. Biol. Chem*. **275,** 17878-17885.

Honda, A., Nogami, M., Yokozeki, T., Yamazaki, M., Nakamura, H., Watanabe, H., Kawamoto, K., Nakayama, K., Morris, A.J., Frohman, M.A. and Kanaho, Y. (1999). Phosphatidylinositol 4-phosphate 5-kinase alpha is a downstream effector of the small G protein ARF6 in membrane ruffle formation. *Cell*. **99,** 521-532.

Hong, S., Horiuchi, H. and Ohta, A. (2003). Molecular cloning of a phospholipase D gene from *Aspergillus nidulans* and characterization of its deletion mutants. *FEMS Microbiol. Lett*. **224,** 231-237.

Howl, J., Jones, S., and Farquhar, M. (2003). Intracellular delivery of bioactive peptides to RBL-2H3 cells induces β-hexosaminidase secretion and phospholipase D activation. *ChemBioChem*. **4,** 1312-1316.

Houslay, M.D. and Adams, D.R. (2003). PDE4 cAMP phosphodiesterases: modular enzymes that orchestrate signalling cross-talk, desensitization and compartmentalization. *Biochem. J*. **370,** 1–18.

Howell, T.W., Cockcroft, S. and Gomperts, B.D. (1987). Essential synergy between Ca^{2+} and guanine nucleotides in exocytotic secretion from permeabilized rat mast cells. *J. Cell Biol*. **105,** 191–197.

Hu, T. and Exton, J.H. (2003). Mechanisms of regulation of phospholipase D1 by protein kinase C alpha. *J. Biol. Chem*. **278,** 2348-2355.

Hube, B., Hess, D., Baker, C.A., Schaller, M., Schäfer, A. and Dolan, J.W. (2001). The role and relevance of phospholipase D1 during growth and dimorphism of *Candida albicans*. *Microbiology*. **147,** 879-889.

Hughes, W.E., Larijani, B. and Parker, P.J. (2002). Detecting protein-phospholipid interactions: Epidermal growth factor-induced activation of phospholipase D1b in situ. *J. Biol. Chem*. **277,** 22974-22979.

Hughes, W.E. and Parker, P.J. (2001). Endosomal localization of phospholipase D1a and 1b is defined by the C-termini of the proteins, and is independent of activity. *Biochem. J*. **356,** 727-736.

Hurtubise, R.J. (1975). Fluorescence quenching of phenolic antioxidants and selective determination of propyl gallate. *Anal. Chem*. **47,** 2457-2458.

Huston, E., Gall, I., Houslay, T.M. and Houslay, M.D. (2006). Helix-1 of the cAMP-specific phosphodiesterase PDE4A1 regulates its phospholipase-D-dependent redistribution in response to release of Ca^{2+}. *J. Cell Sci*. **119,** 3799-3810.

Ishihara, H., Asano, T., Tsukuda, K., Katagiri, H., Inukai, K., Anai, M., Kikuchi, M., Yazaki, Y., Miyazaki, J.I. and Oka, Y. (1993). Pancreatic beta cell line MIN6 exhibits characteristics of glucose metabolism and glucose-stimulated insulin secretion similar to those of normal islets. *Diabetologia*. **36,** 1139-1145.

IUPAC-IUBMB. (1982). Introduction, definitions, order of reaction and rate constants. *Eur. J. Biochem*. **128,** 281–291.

Jacobs, R.L., Devlin, C., Tabas, I. and Vance, D.E. (2004). Targeted deletion of hepatic CTP:phosphocholine cytidylyltransferase alpha in mice decreases plasma high density and very low density lipoproteins. *J. Biol. Chem*. **279,** 47402-47410.

Jaffe, A.B. and Hall, A. (2005). Rho GTPases: biochemistry and biology. *Annu. Rev. Cell Dev. Biol*. **21,** 247-269.

Jenco, J.M., Rawlingson, A., Daniels, B. and Morris, A.J. (1998). Regulation of phospholipase D2: selective inhibition of mammalian phospholipase D isoenzymes by alpha- and beta-synucleins. *Biochemistry*. **37,** 4901-4909.

Jones, D.H., Bax, B., Fensome, A. and Cockcroft, S. (1999). ADP ribosylation factor 1 mutants identify a phospholipase D effector region and reveal that phospholipase D participates in lysosomal secretion but is not sufficient for recruitment of coatomer I. *Biochem. J*. **341,** 185–192.

Jones, D.R., Sanjuan, M.A. and Merida, I. (2000). Type Ialpha phosphatidylinositol 4-phosphate 5-kinase is a putative target for increased intracellular phosphatidic acid. *FEBS Lett*. **476,** 160–165.

Jordan, M.A. and Wilson, L. (2004). Microtubules as a target for anticancer drugs. *Nat. Rev. Cancer*. **4,** 253-265.

Jose Lopez-Andreo, M., Gomez-Fernandez, J.C. and Corbalan-Garcia, S. (2003). The simultaneous production of phosphatidic acid and diacylglycerol is essential for the translocation of protein kinase Cepsilon to the plasma membrane in RBL-2H3 cells. *Mol. Biol. Cell*. **14,** 4885-4895.

Jurgen, R. and Berger, E.B. (1982). Immunocytochemical localization of galactosyltransferase in HeLa cells: codistribution with thiamine pyrophosphatase in trans-Golgi cisternae. *J. Cell Biol*. **93,** 223–229.

Kam, Y. and Exton, J.H. (2002). Dimerization of phospholipase D isozymes. *Biochem. Biophys. Res. Commun*. **290,** 375–380.

Katayama, K., Kodaki, T., Nagamachi, Y. and Yamashita, S. (1998). Cloning, differential regulation and tissue distribution of alternatively spliced isoforms of

ADP-ribosylation-factor-dependent phospholipase D from rat liver. *Biochem. J*. **329,** 647-652.

Kaur, J. and Cutler, D.F. (2002). P-selectin targeting to secretory lysosomes of RBL-2H3 cells. *J. Biol. Chem*. **277,** 10498-10505.

Kawabe, K., Kodaki, T., Katayama, K., Okamura, S., Mori, M. and Yamashita, S. (1998). Identification of lipid inhibitor of mammalian phospholipase D. *J. Biochem*. **123,** 870-875.

Kim, J.H., Kim, J.H., Ohba, M., Suh, P.G. and Ryu, S.H. (2005). Novel functions of the phospholipase D2-phox homology domain in protein kinase Cζ activation. *Mol. Cell. Biol*. **25,** 3194-3208.

Kim, J.H., Kim, H.W., Jeon, H., Suh, P.G. and Ryu, S.H. (2006). Phospholipase D1 regulates cell migration in a lipase activity-independent manner. *J. Biol. Chem*. **281,** 15747–15756.

Kim, J.H., Kim, Y., Lee, S.D., Lopez, I., Arnold, R.S., Lambeth, J.D., Suh, P.G. and Ryu. S.H. (1999). Selective activation of phospholipase D2 by unsaturated fatty acid. *FEBS Lett*. **454,** 42-46.

Kim, Y., Han, J.M., Han, B.R., Lee, K.A., Kim, J.H., Lee, B.D., Jang, I.H., Suh, P.G. and Ryu, S.H. (2000). Phospholipase D1 is phosphorylated and activated by protein kinase C in caveolin-enriched microdomains within the plasma membrane. *J. Biol. Chem*. **275,** 13621-13627.

Kinkaid, A.R. and Wilton, D.C. (1995). Enhanced hydrolysis of phosphatidylcholine by human group II non-pancreatic secreted phospholipase A2 as a result of interfacial activation by specific anions. Potential role of cholesterol sulphate. *Biochem. J*. **308,** 507–512.

Klarlund, J.K., Guilherme, A., Holik, J.J., Virbasius, J.V., Chawla, A. and Czech, M.P. (1997). Signaling by phosphoinositide-3,4,5-trisphosphate through proteins containing pleckstrin and Sec7 homology domains. *Science*. **275,** 1927-1930.

Klausner, R.D., Donaldson, J.G., and Lippincott-Schwartz. J. (1992). Brefeldin A: insights into the control of membrane traffic and organelle structure. *J. Cell Biol*. **116,** 1071-1080.

Koch, T., Brandenburg, L. O., Liang, Y., Schulz, S., Beyer, A., Schroder, H., and Hollt, V. (2004). Phospholipase D2 modulates agonist-induced mu-opioid receptor desensitization and resensitization. *J. Neurochem*. **88,** 680-688.

Koojiman, E.E., Chupin, V., de Kruijff, B. and Burger, K.N.J. (2003). Modulation of membrane curvature of phosphatidic acid and lysophosphatidic acid. *Traffic*. **4,** 162-174.

Kremer, W., Steiner, G., Sophie, B.D. and Kalbitzer, H.R. (2004). Conformational states of the small G protein Arf-1 in complex with the guanine nucleotide exchange factor ARNO-Sec7. *J. Biol. Chem*. **279,** 17004–17012.

Ktistakis, N.T., Brown, H.A., Waters, M.G., Sternweis, P.C. and Roth, M.G. (1996). Evidence that phospholipase D mediates ADP ribosylation factor- dependent formation of Golgi coated vesicles. *J. Cell Biol*. **134,** 295–306.

Kulms, D. and Schwarz, T. (2000). Molecular mechanisms of UV-induced apoptosis. *Photodermatol. Photoimmunol. Photomed*. **16,** 195-201.

Kupferberg, J.P., Yokoyama, S. and Kezdy, F.J. (1981). The kinetics of the phospholipase A_2-catalyzed hydrolysis of egg phosphatidylcholine in unilamellar vesicles. Product inhibition and its relief by serum albumin. *J. Biol. Chem*. **256,** 6274-6281.

Kurz, T. Kemken, D., Mier, K., Weber, I. and Richardt, G. (2004). Human cardiac phospholipase D activity is tightly controlled by phosphatidylinositol 4,5-bisphosphate. *J. Mol. Cell. Cardiol*. **36,** 225-232.

Kuwahara, T., Koyama, A., Koyama, S., Yoshina, S., Ren, C.H., Kato, T., Mitani, S. and Iwatsubo, T. (2008). A systematic RNAi screen reveals involvement of endocytic pathway in neuronal dysfunction in alpha-synuclein transgenic *C. elegans*. *Hum. Mol. Genet*. **17,** 2997-3009.

Lagace, T.A. and Ridgway, N.D. (2005). The rate-limiting enzyme in phosphatidylcholine synthesis regulates proliferation of the nucleoplasmic reticulum. *Mol. Biol. Cell*. **16,** 1120–1130.

Lang, T., Wacker, I., Wunderlich, I., Rohrbach, A., Giese, G., Soldati, T. and Almers, W. (2000). Role of actin cortex in the subplasmalemmal transport of secretory granules in PC-12 cells. *Biophys. J*. **78,** 2863-2877.

Larrodera, P., Cornet, M.E., Diaz-Meco, M.T., Lopez-Barahona, M., Diaz-Laviada, I., Guddal, P.H., Johansen, T. and Moscat, J. (1990). Phospholipase C-mediated hydrolysis of phosphatidlycholine is an important step in PDGF-stimulated DNA synthesis. *Cell*. **61,** 1113-1120.

Laulagnier, K., Vincent-Schneider, H., Hamdi, S., Subra, C., Lankar, D. and Record M. (2005). Characterization of exosome subpopulations from RBL-2H3 cells using fluorescent lipid. *Blood Cells Mol. Dis*. **35,** 116-121.

Lawrence, J.T.R. and Birnbaum, M.J. (2003). ADP-ribosylation factor 6 regulates insulin secretion through plasma membrane phoshatidylinositol 4,5-bisphosphate. *Proc. Natl. Acad. Sci. U.S.A*. **100,** 13320-13325.

Lee, C., Kang, H.S., Chung, J.K., Sekiya, F., Kim, J.R., Han, J.S., Kim, S.R., Bae, Y.S., Morris, A.J. and Rhee, S.G. (1997). Inhibition of phospholipase D by clathrin assembly protein 3 (AP3). *J. Biol. Chem*. **272,** 15986-1599.

Lee, C., Kim, S.R., Chung, J.K., Frohman, M.A., Kilimann, M.W. and Rhee, S.G. (2000). Inhibition of phospholipase D by amphiphysins. *J. Biol. Chem*. **275**, 18751-18758.

Lee, C.S., Kim, K.L., Jang, J.H., Choi, Y.S., Sug, P.G. and Ryu, S.H. (2009). Review: The roles of phospholipase D in EGFR signalling. *Biochim. Biophys. Acta*. 1**791,** 862-868.

Lee, C.S., Kim, I.S., Park, J.B., Lee, M.N., Lee, H.Y., Suh, P.G. and Ryu, S.H. (2006). The phox homology domain of phospholipase D activates dynamin GTPase activity and accelerates EGFR endocytosis. *Nat. Cell Biol*. **8,** 477-484.

Lee, J.S., Kim, J.H., Jang, I.H., Kim, H.S., Han, J.M., Kazlauskas, A., Yagisawa, H., Suh, P.G. and Ryu, S.H. (2005). Phosphatidylinositol (3,4,5)-trisphosphate specifically interacts with the phox homology domain of phospholipase D1 and stimulates its activity. *J. Cell Sci*. **118,** 4405-4413.

Lee, J.S., Kim, I.S., Kim, J.H., Cho, W., Suh, P.G. and Ryo, S.H. (2009). Determination of EGFR endocytosis kinetic by auto-regulatory association of PLD1 with μ2. *PLoS One*. **4,** e7090.

Lee, S., Park, J.B., Kim, J.H., Kim, Y., Kim, J.H., Shin, K.J., Lee, J.S., Ha, S.H., Suh, P.G. and Ryu, S.H. (2001). Actin directly interacts with phospholipase D, inhibiting its activity. *J. Biol. Chem*. **276,** 28252-28260.

Lee, Y.H., Kim, H.S., Pai, J.K., Ryu, S.H. and Suh, P.G. (1994). Activation of phospholipase D induced by platelet-derived growth factor is dependent upon the level of phospholipase C-gamma 1. *J. Biol. Chem*. **269,** 26842–26847.

Lehman, N., Ledford, B., Di Fulvio, M., Frondorf, K., McPhail, L.C. and Gomez-Cambronero, J. (2007). Phospholipase D2-derived phosphatidic acid binds to and activates ribosomal p70 S6 kinase independently of mTOR. *FASEB J*. **21,** 1075-1087.

Leiros, I., Secundo, F., Zambonelli, C., Servi, S. and Hough, E. (2000). The first crystal structure of a phospholipase D. *Structure*. **8,** 655-667.

Lemmon, M.A. (2008). Membrane recognition by phospholipid-binding domains. *Nat. Rev. Mol. Cell Biol*. **9,** 99-111.

Li, H.S., Shome, K., Rojas, R., Rizzo, M.A., Vasudevan, C., Fluharty, E., Santy, L.C., Casanova, J.E. and Romero, G. (2003). The guanine nucleotide exchange factor ARNO mediates the activation of ARF and phospholipase D by insulin. *BMC Cell Biol*. **11,** 4:13.

Li, Z. and Vance, D.E. (2008). Phosphatidylcholine and choline homeostasis. *J. Lipid Res*. **49,** 1187-1194.

Liopis, J., McCaffery, J.M., Miyawaki, A., Farquhar, M.G. and Tsien, R.Y. (1998). Measurement of cytosolic, mitochondrial, and Golgi pH in single living cells with green fluorescent proteins. *Proc. Natl. Acad. Sci. U S A*. **95,** 6803-6808.

Liscovitch, M., Chalifa, V., Pertile, P., Chen, C.S. and Cantley, L.C. (1994). Novel function of phosphatidylinositol 4,5-bisphosphate as a cofactor for brain membrane phospholipase D. *J. Biol. Chem*. **269,** 21403-21406.

Liscovitch, M., Czarny, M., Fiucci, G. and Tang, X. (2000). Review: Phospholipase D: molecular and cell biology of a novel gene family. *Biochem. J*. **345**, 401-415.

Lister, M.D., Glaser, K.B., Ulevitch, R.J. and Dennis, E.A. (1989). Inhibition studies on the membrane-associated phospholipase A_2 in vitro and prostaglandin E2 production in vivo of the macrophage-like P388D1 cell. Effects of manoalide, 7,7-dimethyl-5,8-eicosadienoic acid, and p-bromophenacyl bromide. *J. Biol. Chem*. **264,** 8520-8528.

Lopez, I., Arnold, R.S. and Lambeth, J.D. (1998). Cloning and initial characterization of a human phospholipase D2 (hPLD2). ADP-ribosylation factor regulates hPLD2. *J. Biol. Chem*. **273,** 12846-12852.

Lukowski, S., Lecomte, M.C., Mira, J.P., Marin, P., Gautero, H., Russo-Marie, F. and Geny, B. (1996). Inhibition of phospholipase D activity by fodrin. An active role for the cytoskeleton. *J. Biol. Chem*. **271,** 24164-24171.

Lukowski, S., Mira, J.P., Zachowski, A. and Geny, B. (1998). Fodrin inhibits phospholipases A_2, C, and D by decreasing polyphosphoinositide cell content. *Biochem. Biophys. Res. Commun*. **248,** 278-284.

Luckasen, J.R., White, J.G. and Kersey, J.H. (1974). Mitogenic properties of a calcium ionophore, A23187. *Proc. Natl. Acad. Sci. U.S.A*. **71,** 5088-90.

Lykidis, A., Jackson, P. and Jackowski, S. (2001). Lipid activation of CTP:phosphocholine cytidylyltransferase α: characterization and identification of a second activation domain. *Biochemistry*. **40,** 494-503.

Lynch, K.L. and Martin, T.F. (2007). Synaptotagmins I and IX function redundantly in regulated exocytosis but not endocytosis in PC12 cells. *J. Cell Sci*. **120,** 617-627.

Machesky, L.M. and Hall, A. (1997). Role of actin polymerization and adhesion to extracellular matrix in Rac- and Rho-induced cytoskeletal reorganization. *J. Cell Biol*. **138,** 913–926.

Madesh, M. and Balasubramanian, K.A. (1997). Metal ion stimulation of phospholipase D-like activity of isolated rat intestinal mitochondria. *Lipids*. **32,** 471-479.

Manganiello, V. (2002). Short-term regulation of PDE4 activity. *Br. J. Pharmacol*. **136,** 339–340.

Manifava, M., Sugars, J. and Ktistakis, N.T. (1999). Modification of catalytically active phospholipase D1 with fatty acid in vivo. *J. Biol. Chem*. **274,** 1072-1077.

Mansfeld, J. and Ulbrich-Hofmann, R. (2009). Modulation of phospholipase D activity in vitro. *Biochim. Biophys. Acta*. **1791,** 913-926.

Marcil, J., Harbour, D., Naccache, P.H. and Bourgoin, S. (1997). Human phospholipase D1 can be tyrosine-phosphorylated in HL-60 granulocytes. *J. Biol. Chem*. **272,** 20660-20664.

Martin A, Brown FD, Hodgkin MN, Bradwell AJ, Cook SJ, Hart M, Wakelam MJ. (1996). Activation of phospholipase D and phosphatidylinositol 4-phosphate 5-kinase in HL60 membranes is mediated by endogenous Arf but not Rho. *J. Biol. Chem*. **271,** 17397-17403.

Mason, C.S., Springer, C.J., Cooper, R.G., Superti-Furga, G., Marshall, C.J. and Marais, R. (1999). Serine and tyrosine phosphorylations cooperate in Raf-1, but not B-Raf activation. *EMBO J*. **18,** 2137-2148.

Massenburg, D., Han, J.S., Liyanage, M., Patton, W.A., Rhee, S.G., Moss, J. and Vaughan, M. (1994). Activation of rat brain phospholipase D by ADP-ribosylation factors 1, 5, and 6: Separation of ADP-ribosylation factor-dependent and oleate-dependent enzymes. *Proc. Natl. Acad. Sci. U.S.A*. **91,** 11718-11722.

Mayr, J.A., Kohlwein, S.D. and Paltauf, F. (1996). Identification of a novel, Ca^{2+}-dependent phospholipase D with preference for phosphatidylserine and phosphatidylethanolamine in *Saccharornyces cerevisiae*. *FEBS Lett*. **393,** 236-240.

McDermott, M., Wakelam, M.J. and Morris, A.J. (2004). Phospholipase D. *Biochem. Cell Biol*. **82,** 225-253.

Meacci, E., Tsai, S.C., Adamik, R., Moss, J. and Vaughan, M. (1997). Cytohesin-1, a cytosolic guanine nucleotide-exchange protein for ADP-ribosylation factor. *Proc. Natl. Acad. Sci. U.S.A*. **94,** 1745-1748.

Mebarek, S., Komati, H., Naro, F., Zeiller, C., Alvisi, M., Lagarde, M., Prigent, A.F. and Némoz, G. (2007). Inhibition of de novo ceramide synthesis upregulates phospholipase D and enhances myogenic differentiation. *J. Cell Sci*. **120,** 407-416.

Mehta, S., Maglio, J., Kobayashi, M.S., Sipple, A.M. and Horwitz, J. (2003). Activation of phospholipase D is not mediated by direct phosphorylation on tyrosine residues. *Biochim. Biophys. Acta*. **1631,** 246-254.

Meier, K.E., Gibbs, T.C., Knoepp, S.M. and Ella, K.M. (1999). Expression of phospholipase D isoforms in mammalian cells. *Biochim. Biophys. Acta*. **1439,** 199-213.

Melendez, A.J. and Allen, J.M. (2002). Phospholipase D and immune receptor signalling. *Semin. Immunol*. **14,** 49-55.

Millar, C.A., Jess, T.J., Saqib, K.M., Wakelam, M.J. and Gould, G.W. (1999). 3T3-L1 adipocytes express two isoforms of phospholipase D in distinct subcellular compartments. *Biochem. Biophys. Res. Commun*. **254,** 734-738.

Min, D.S. and Exton, J.H. (1998a). Phospholipase D is associated in a phorbol ester-dependent manner with protein kinase C-α and with a 220-kDa protein which is phosphorylated on serine and threonine. *Biochem. Biophys. Res. Commun*. **248,** 533–537.

Min, D.S., Kim, E.G. and Exton, J.H. (1998b). Involvement of tyrosine phosphorylation and protein kinase C in the activation of phospholipase D by H_2O_2 in Swiss 3T3 fibroblasts. *J. Biol. Chem*. **273,** 29986-29994.

Min, D.S., Park, S.K. and Exton, J.H. Characterization of a rat brain phospholipase D isozyme. *J. Biol. Chem*. (1998). **273,** 7044-7051.

Mitsutake, S., Kim, T.J., Inagaki, Y., Kato, M., Yamashita, T. and Igarashi, Y. (2004). Ceramide kinase is a mediator of calcium-dependent degranulation in mast cells. *J. Biol. Chem*. **279,** 17570-17577.

Miyazaki, J., Araki, K., Yamato, E., Ikegami, H., Asano, T., Shibasaki, Y., Oka, Y. and Yamamura, K. (1990). Establishment of a pancreatic beta cell line that retains glucose-inducible insulin secretion: special reference to expression of glucose transporter isoforms. *Endocrinology*. **127,** 126-132.

Moritz, A., De Graan, P.N., Gispen, W.H. and Wirtz, K.W. (1992). Phosphatidic acid is a specific activator of phosphatidylinositol-4-phosphate kinase. *J. Biol. Chem*. **267,** 7207-7210.

Mortensen, K. and Larsson, L.I. (2003). Effects of Cytochalasin D on the actin cytoskeleton: association of neoformed actin aggregates with proteins involved in signalling and endocytosis. *Cell. Mol. Life Sci*. **60,** 1007-1012.

Moss, J. and Vaughan, M. (1998). Molecules in the ARF orbit. *J. Biol. Chem*. **273,** 21431-21434.

Mu, F.T., Callaghan, J.M., Steele-Mortimer, O., Stenmark, H., Parton, R.G., Campbell, P.L., McCluskey, J., Yeo, J.P., Tock, E.P. and Toh, B.H. (1995). EEA1, an early endosome-associated protein. EEA1 is a conserved alpha-helical peripheral membrane protein flanked by cysteine "fingers" and contains a calmodulin-binding IQ motif. *J. Biol. Chem*. **270,** 13503-13511.

Müller-Taubenberger, A., Vos, M.J., Böttger, A., Lasi, M., Lai, F.P., Fischer, M. and Rottner, K. (2006). Monomeric red fluorescent protein variants used for imaging studies in different species. *Eur. J. Cell Biol*. **85,**1119-1129.

Murthy, K.S. and Makhlouf, G.M. (1998). Differential regulation of phospholipase A_2 (PLA_2)-dependent Ca^{2+} signaling in smooth muscle by cAMP- and cGMP-dependent protein kinases. Inhibitory phosphorylation of PLA2 by cyclic nucleotide-dependent protein kinases. *J. Biol. Chem*. **273,** 34519-34526.

Nakai, K. and Horton, P. (1999). PSORT: a program for detecting sorting signals in proteins and predicting their subcellular localization. *Trends Biochem. Sci*. **24,** 34-36.

Nakamura, M., Nakashima, S., Katagiri, Y. and Nozawa, Y. (1997). Effect of wortmannin and 2-(4-morpholinyl)-8-phenyl-4H-1-benzopyran-4-one (LY294002) on N-formyl-methionyl-leucyl-phenylalanine-induced phospholipase D activation in differentiated HL60 cells: possible involvement of phosphatidylinositol 3-kinase in phospholipase D activation. *Biochem. Pharmacol*. **53,** 1929-1936.

Nakamura, Y., Nakashima, S., Ojio, K., Banno, Y., Miyata, H. and Nozawa, Y. (1996). Ceramide inhibits IgE-mediated activation of phospholipase D, but not of phospholipase C, in rat basophilic leukemia (RBL-2H3) cells. *J. Immunol*. **156,** 256-262.

Natarajan, V., Scribner, W.M. and Vepa, S. (1997). Phosphatase inhibitors potentiate 4-hydroxynonenal-induced phospholipase D activation in vascular endothelial cells. *Am. J. Respir. Cell Mol. Biol*. **17,** 251-259.

Némoz, G., Sette, C. and Conti, M. (1997). Selective activation of rolipram-sensitive, cAMP-specific phosphodiesterase isoforms by phosphatidic acid. *Mol. Pharmacol*. **51,** 242-249.

Neumann-Giesen, C., Fernow, I., Amaddii, M. and Tikkanen, R. (2007). Role of EGF-induced tyrosine phosphorylation of reggie-1/flotillin-2 in cell spreading and signalling to the actin cytoskeleton. *J. Cell Sci*. **120,** 395-406.

Nguyen Ba, A.N., Pogoutse, A., Provart, N. and Moses, A.M. (2009). NLStradamus: a simple Hidden Markov Model for nuclear localization signal prediction. *BMC Bioinformatics*. **10,** 202.

Nokes, R.L., Fields, I.C., Collins, R.N. and Fölsch, H. (2008). Rab13 regulates membrane trafficking between TGN and recycling endosomes in polarized epithelial cells. *J. Cell Biol*. **182,** 845–853.

Offterdinger, M., Georget, V., Girod, A. and Bastiaens, P.I. (2004). Imaging phosphorylation dynamics of the epidermal growth factor receptor. *J. Biol. Chem*. **279,** 36972-36981.

Ohguchi, K., Nakashima, S., Tan, Z., Banno, Y., Dohi, S. and Nozawa, Y. (1997). Increased activity of small GTP-binding protein-dependent phospholipase D during differentiation in human promyelocytic leukemic HL60 cells. *J. Biol. Chem*. **272,** 1990–1996.

Oka, T., Sato, K., Hori, M., Ozaki, H. and Karaki, H. (2002). FcεRI cross-linking-induced actin assembly mediates calcium signalling in RBL-2H3 mast cells. *Br. J. Pharmacol*. **136,** 837-846.

Okamoto, T., Schlegel, A., Scherer, P.E. and Lisanti, M.P. (1998). Caveolins, a family of scaffolding proteins for organizing "preassembled signaling complexes" at the plasma membrane. *J. Biol. Chem*. **273,** 5419-5422.

Okamura, S. and Yamashita, S. (1994). Purification and characterization of phosphatidylcholine phospholipase D from pig lung. *J. Biol. Chem*. **269,** 31207-31213.

Olson, S.C., Bowman, E.P. and Lambeth, J.D. (1991). Phospholipase D activation in a cell-free system from human neutrophils by phorbol 12-myristate 13-acetate and guanosine 5'-O-(3-thiotriphosphate). Activation is calcium dependent and requires protein factors in both the plasma membrane and cytosol. *J. Biol. Chem*. **266,** 17236-17242.

O'Luanaigh, N., Pardo, R., Fensome, A., Allen-Baume, V., Jones, D., Holt, M.R. and Cockcroft S. (2002). Continual production of phosphatidic acid by phospholipase D is essential for antigen-stimulated membrane ruffling in cultured mast cells. *Mol. Biol. Cell*. **13,** 3730-3746.

Oxford, G. and Theodorescu, D. (2003). Ras superfamily monomeric G proteins in carcinoma cell motility. *Cancer Lett*. **189,** 117-128.

Padrón, D., Tall, R.D. and Roth, M.G. (2006). Phospholipase D2 is required for efficient endocytic recycling of transferrin receptors. *Mol. Biol. Cell*. **17,** 598-606.

Pai, J.K., Dobek, E.A. and Bishop, W.R. (1991). Endothelin-1 activates phospholipase D and thymidine incorporation in fibroblasts overexpressing protein kinase C beta 1. *Cell Regul*. **2,** 897–903.

Park, J.B., Lee, C.S., Lee, H.Y., Kim, I.S., Lee, B.D., Jang, I.H., Jung, Y.W., Oh, Y.S., Han, M.Y., Jensen, O.N., Roepstorff, P., Suh, P.G. and Ryu, S.H. (2004). Regulation of phospholipase D2 by GTP-dependent interaction with dynamin. *Adv. Enzyme Regul*. **44,** 249-264.

Park, J.B., Kim, J.H., Kim, Y., Ha, S.H., Yoo, J.S., Du, G., Frohman, M.A., Suh, P.G. and Ryu, S.H. (2000). Cardiac phospholipase D2 localizes to sarcolemmal membranes and is inhibited by alpha-actinin in an ADP-ribosylation factor-reversible manner. *J. Biol. Chem*. **275,** 21295-21301.

Park, S.K., Min, D.S. and Exton, J.H. (1998). Definition of the protein kinase C interaction site of phospholipase D. *Biochem. Biophys. Res. Commun*. **244,** 364-367.

Paumet, F., Le Mao, J., Martin, S., Galli, T., David, B., Blank, U. and Roa, M. (2000). Soluble NSF attachment protein receptors (SNAREs) in RBL-2H3 mast cells: Functional role of syntaxin 4 in exocytosis and identification of a vesicle-associated membrane protein 8-containing secretory compartment. *J. Immunol*. **164,** 5850-5857.

Payton, J.E., Perrin, R.J., Woods, W.S. and George, J.M. (2004). Structural determinants of PLD2 inhibition by alpha-synuclein. *J. Mol. Biol*. **337,** 1001-1009.

Pendleton, A. and Koffer, A. (2001). Effects of Latrunculin reveal requirements for the actin cytoskeleton during secretion from mast cells. *Cell Motil. Cytoskeleton*. **48,** 37-51.

Pettitt, T.R., McDermott, M., Saqib, K.M., Shimwell, N. and Wakelam, M.J. (2001). Phospholipase D1b and D2a generate structurally identical phosphatidic acid species in mammalian cells. *Biochem. J*. **360,** 707-715.

Ponting, C.P. (1996). Novel domains in NADPH oxidase subunits, sorting nexins, and PtdIns 3-kinases: binding partners of SH3 domains? *Protein Sci*. **5,** 2353–2357.

Ponting, C.P. and Kerr, I.D. (1996). A novel family of phospholipase D homologues that includes phospholipid synthases and putative endonucleases: identification of duplicated repeats and potential active site residues. *Protein Sci*. **5,** 914-922.

Powner, D.J., Hodgkin, M.N. and Wakelam, M.J.O. (2002). Antigen-stimulated activation of phospholipase D1b by Rac1, ARF6, and PKCα in RBL-2H3 Cells. *Mol. Cell Biol*. **13,** 1252-1262.

Pritchard, P.H. and Vance, D.E. (1981). Choline metabolism and phosphatidylcholine biosynthesis in cultured rat hepatocytes. *Biochem. J*. **196,** 261–267.

Provost, J.J., Fudge, J., Israelit, S., Siddiqi, A.R. and Exton, J.H. (1996). Tissue-specific distribution and subcellular distribution of phospholipase D in rat: evidence for distinct RhoA- and ADP-ribosylation factor (ARF)-regulated isoenzymes. *Biochem. J*. **319,** 285–291.

Puri, N. and Roche, P.A. (2008). Mast cells possess distinct secretory granule subsets whose exocytosis is regulated by different SNARE isoforms. *Proc. Natl. Acad. Sci. U.S.A.* **105,** 2580-2585.

Redina, O.E. and Frohman, M.A. (1998). Genomic analysis of murine phospholipase D1 and comparison to phospholipase D2 reveals an unusual difference in gene size. *Gene*. **222,** 53-60.

Reed, P.W. and Lardy, H.A. (1972). A23187: A divalent cation ionophore. *J. Biol. Chem*. **247,** 6970-6977.

Reinhold, S.L., Prescott, S.M., Zimmerman, G.A. and McIntyre, T.M. (1990). Activation of human neutrophil phospholipase D by three separable mechanisms. *FASED J*. **4,** 208-214.

Ridley, A.J., Paterson, H.F., Johnston, C.L., Diekmann, D. and Hall, A. (1992). The small GTP-binding protein rat regulates growth factor-induced membrane ruffling. *Cell*. **70,** 401-410.

Rivera, J. and Olivera, A. (2008). A current understanding of FcεRI-dependent mast cell activation. *Curr. Allergy Asthma Rep*. **8,** 14-20.

Rizzo, M. and Romero, G. (2002). Pharmacological importance of phospholipase D and phosphatidic acid in the regulation of the mitogen-activated protein kinase cascade. *Pharmacol. Ther*. **94,** 35-50.

Rizzo, M.A., Shome, K., Vasudevan, C., Stolz, D.B., Sung, T.C., Frohman, M.A., Watkins, S.C. and Romero, G. (1999). Phospholipase D and its product, phosphatidic acid, mediate agonist-dependent raf-1 translocation to the plasma membrane and the activation of the mitogen-activated protein kinase pathway. *J. Biol. Chem*. **274** 1131-1139.

Rizzo, M.A., Shome, K., Watkins, S.C. and Romero, G. (2000). The recruitment of Raf-1 to membranes is mediated by direct interaction with phosphatidic acid and is independent of association with Ras. *J. Biol. Chem*. **275,** 23911-23918.

Rose, T.M. and Prestwich. G.D. (2006). Synthesis and evaluation of fluorogenic substrates for phospholipase D and phospholipase C. *Org. Lett*. **8,** 2575–2578.

Roth, J. and Berger, E.G. (1982). Immunocytochemical localization of galactosyltransferase in HeLa cells: codistribution with thiamine pyrophosphatase in trans-Golgi cisternae. *J. Cell Biol*. **93,** 223–229.

Roth, M.G. (1999). Lipid regulators of membrane traffic through the Golgi complex. *Trends Cell Biol*. **9,** 174-179.

Rümenapp, U., Geiszt, M., Wahn, F., Schmidt, M. and Jakobs, K.H. (1995). Evidence for ADP-ribosylation-factor-mediated activation of phospholipase D by m3 muscarinic acetylcholine receptor. *Eur. J. Biochem*. **234,** 240-244.

Rümenapp, U., Schmidt, M., Wahn, F., Tapp, E., Grannass, A. and Jakobs, K.H. (1997). Characteristics of protein-kinase-C- and ADP-ribosylation-factor-stimulated phospholipase D activities in human embryonic kidney cells. *Eur. J. Biochem*. **248,** 407-414.

Rydzewska, G. and Morisset, J. (1995). Activation of pancreatic acinar cell phospholipase D by epidermal, insulin-like, and basic fibroblast growth factors involves tyrosine kinase. *Pancreas*. **10,** 59-65.

Saito, K., Kuga-Uetake, Y. and Saito, M. (2004). Acidic vesicles in living hyphae of an arbuscular mycorrhizal fungus, *Gigaspora margarita*. *Plant Soil*. **261,** 231-237.

Saito, M. and Kanfer, J. (1973). Solubilization and properties of a membrane-bound enzyme from rat brain catalyzing a base-exchange reaction. *Biochem. Biophys. Res. Commun*. **3,** 391-398.

Sanford, J.C., Pan, Y. and Wessling-Resnick, M. (1995). Properties of Rab5 N-terminal domain dictate prenylation of C-terminal cysteines. *Mol. Biol. Cell*. **6,** 71-85.

Sarri, E., Pardo, R., Fensome-Green, A. and Cockcroft, S. (2003). Endogenous phospholipase D2 localizes to the plasma membrane of RBL-2H3 mast cells and can be distinguished from ADP ribosylation factor-stimulated phospholipase D1 activity by its specific sensitivity to oleic acid. *Biochem. J.* **369,** 319-329.

Schimmöller, F., Simon, I. and Pfeffer, S.R. (1998). Rab GTPases, directors of vesicle docking. *J. Biol. Chem*. **273,** 22161-22164.

Schmidt, M., Voss, M., Weernink, P.A., Wetzel, J., Amano, M., Kaibuchi, K. and Jakobs, K.H. (1999). A role for rho-kinase in rho-controlled phospholipase D stimulation by the m3 muscarinic acetylcholine receptor. *J. Biol. Chem*. **274,** 14648-14654.

Sciorra, V.A., Rudge, S.A., Prestwich, G.D., Frohman, M.A., Engebrecht, J. and Morris, A.J. (1999). Identification of a phosphoinositide binding motif that mediates activation of mammalian and yeast phospholipase D isoenzymes. *EMBO J*. **18,** 5911-5921.

Sciorra, V.A., Rudge, S.A., Wang, J., McLaughlin, S., Engebrecht, J. and Morris, A.J. (2002). Dual role for phosphoinositides in regulation of yeast and mammalian phospholipase D enzymes. *J. Cell Biol*. **159,** 1039-1049.

Schultz, J., Milpetz, F., Bork, P. and Ponting, C.P. (1998). SMART, a simple modular architecture research tool: Identification of signaling domains. *Proc. Natl. Acad. Sci. USA*. **95,** 5857–5864.

Scott, S.A., Selvy, P.E., Buck, J.R., Cho, H.P., Criswell, T.L., Thomas, A.L., Armstrong, M.D., Arteaga, C.L., Lindsley, C.W. and Brown, H.A. (2009). Design of isoform-selective phospholipase D inhibitors that modulate cancer cell invasiveness. *Nat. Chem. Biol*. **5,** 108-117.

Seet, L.F. and Hong, W. (2006). The phox (PX) domain proteins and membrane traffic. *Biochim. Biophys. Acta*. **1761,** 878-896.

Shaner, N.C., Campbell, R.E., Steinbach, P.A., Giepmans, B.N.G., Palmer, A.E. and Tsien, R.Y. (2004). Improved monomeric red, orange and yellow fluorescent proteins derived from *Discosoma sp.* Red fluorescent protein. *Nat. Biotechol*. **22,** 1567-1572.

Shaner, N.C., Steinbach, P.A. and Tsien R. (2005). A guide to choosing fluorescent proteins. *Nat. Methods*. **2,** 905-909.

Shen, Y., Xu, L. and Foster, D.A. (2001). Role for phospholipase D in receptor-mediated endocytosis. *Mol. Cell. Biol*. **21,** 595-602.

Shields, D.J., Lehner, R., Agellon, L.B. and Vance, D.E. (2003). Membrane topography of human phosphatidylethanolamine N-methyltransferase. *J. Biol. Chem*. **278,** 2956-2962.

Siddhanta, A., Backer, J.M. and Shields, D. (2000). Inhibition of phosphatidic acid synthesis alters the structure of the Golgi apparatus and inhibits secretion in endocrine cells. *J. Biol. Chem*. **275,** 12023-12031.

Siddiqi, A.R., Smith, J.L., Ross, A.H., Qiu, R.G., Symons, M. and Exton, J.H. (1995). Regulation of phospholipase D in HL60 cells. Evidence for a cytosolic phospholipase D. *J. Biol. Chem*. **270,** 8466-8473.

Siddiqi, A.R., Srajer, G.E. and Leslie, C.C. (2000). Regulation of human PLD1 and PLD2 by calcium and protein kinase C. *Biochim. Biophys. Acta.* **1497,** 103-114.

Singer, W.D., Brown, H.A., Jiang, X. and Sternweis, P.C. (1996). Regulation of phospholipase D by protein kinase C is synergistic with ADP-ribosylation factor and independent of protein kinase activity. *J. Biol. Chem*. **271,** 4504-4510.

Singh, I.N., Stromberg, L.M., Bourgoin, S.G., Sciorra, V.A., Morris, A.J. and Brindley, D.N. (2001). Ceramide inhibition of mammalian phospholipase D1 and D2 activities is antagonized by phosphatidylinositol 4,5-bisphosphate. *Biochemistry*. **40,** 11227-11233.

Sjöblom, B., Salmazo, A. and Djinović-Carugo, K. (2008). Alpha-actinin structure and regulation. *Cell. Mol. Life Sci*. **65,** 2688-2701.

Skippen, A., Jones, D.H., Morgan, C.P., Li, M. and Cockcroft, S. (2002). Mechanism of ADP ribosylation factor-stimulated phosphatidylinositol 4,5-bisphosphate synthesis in HL60 cells. *J. Biol. Chem*. **277,** 5823-5831.

Slaaby, R., Du, G., Altshuller, Y.M., Frohman, M.A. and Seedorf, K. (2000). Insulin-induced phospholipase D1 and phospholipase D2 activity in human embryonic kidney-293 cells mediated by the phospholipase C gamma and protein kinase C alpha signalling cascade. *Biochem. J*. **351,** 613–619.

Slaaby, R., Jensen, T., Hansen, H.S., Frohman, M.A. and Seedorf, K. (1998). PLD2 complexes with the EGF receptor and undergoes tyrosine phosphorylation at a single site upon agonist stimulation. *J. Biol. Chem*. **273,** 33722–33727.

Smrcka, A.V., Hepler, J.R., Brown, K.O. and Sternweis, P.C. (1991). Regulation of polyphosphoinositide-specific phospholipase C activity by purified Gq. *Science*. **251,** 804-807.

Snyder, M.D. and Pierce, S.K. (2006). A mutation in Epstein-Barr virus LMP2A reveals a role for phospholipase D in B-Cell antigen receptor trafficking. *Traffic*. **7,** 993-1006.

Sprong, H., van der Sluijs, P. and van Meer, G. (2001). How proteins move lipids and lipids move proteins. *Nat. Rev. Mol. Cell Biol*. **2,** 504-513.

Stace, C.L. and Ktistakis, N.T. (2006). Phosphatidic acid- and phosphatidylserine-binding proteins. *Biochim. Biophys. Acta*. **176,** 913-926.

Stahelin, R.V., Hwang, J.H., Kim, J.H., Park, Z.Y., Johnson, K.R., Obeid, L.M. and Cho, W. (2005). The mechanism of membrane targeting of human sphingosine kinase 1. *J. Biol. Chem*. **280,** 43030-43038.

Stahelin, R.V., Ananthanarayanan, B., Blatner, N.R., Singh, S., Bruzik, K.S., Murray, D. and Cho, W. (2004). Mechanism of membrane binding of the phospholipase D1 PX domain. *J. Biol. Chem*. **279,** 54918-54926.

Stanacev, N.Z. and Stuhne-Sekalec, L. (1970). On the mechanism of enzymatic phosphatidylation. Biosynthesis of cardiolipin catalyzed by phospholipase D. *Biochim. Biophys. Acta*. **210,** 350-352.

Steed, P.M., Clark, K.L., Boyar, W.C. and Lasala, D.J. (1998). Characterization of human PLD2 and the analysis of PLD isoform splice variants. *FASEB J*. **12,** 1309-1317.

Stinchcombe, J.C. and Griffiths, G.M. (2001). Normal and abnormal secretion by haemopoietic cells. *Immunology*. **103,** 10-16.

Stuckey, J.A. and Dixon, J.E. (1999). Crystal structure of a phospholipase D family member. *Nat. Struct. Biol*. **6,** 278-284.

Stutchfield, J. and Cockcroft, S. (1993). Correlation between secretion and phospholipase D activation in differentiated HL60 cells. *Biochem. J*. **93,** 649-655.

Su, W., Yeku, O., Olepu, S., Genna, A., Park, J.S., Ren, H., Du, G., Gelb, M.H., Morris, A.J. and Frohman, M.A. (2009). 5-fluoro-2-indolyl des-chlorohalopemide (FIPI), a phospholipase D pharmacological inhibitor that alters cell spreading and inhibits chemotaxis. *Mol. Pharmacol*. **75,** 437-446.

Sugars, J.M., Cellek, S., Manifava, M., Coadwell, J. and Ktistakis, N.T. (1999). Fatty acylation of phospholipase D1 on cysteine residues 240 and 241 determines localization on intracellular membranes. *J. Biol. Chem*. **274,** 30023-30027.

Sugars, J.M., Cellek, S., Manifava, M., Coadwell, J. and Ktistakis, N.T. (2002). Hierarchy of membrane-targeting signals of phospholipase D1 involving lipid modification of a pleckstrin homology domain. *J. Biol. Chem*. **277,** 29152-29161.

Sung, T.C., Altshuller, Y.M., Morris, A.J. and Frohman, M.A. (1999a). Molecular analysis of mammalian phospholipase D2. *J. Biol. Chem*. **274,** 494-502.

Sung, T.C., Roper, R.L., Zhang, Y., Rudge, S.A., Temel, R., Hammond, S.M., Morris, A.J., Moss, B., Engebrecht, J. and Frohman, M.A. (1997). Mutagenesis of phospholipase D defines a superfamily including a trans-Golgi viral protein required for poxvirus pathogenicity. *EMBO J*. **16,** 4519–4530.

Sung, T.C., Zhang, Y., Morris, A.J. and Frohman. (1999b). Structural analysis of human phospholipase D. *J. Biol. Chem*. **274,** 3659-3666.

Takai, Y., Kishimoto, A., Kikkawa, U., Mori, T. and Nishizuka, Y. (1979). Unsaturated diacylclycerol as a possible messenger for the activation of calcium-activated, phospholipid-dependent protein kinase system. *Biochem. Biophys. Res. Commun*. **91,** 1218-1224.

Taylor, L.A., Arends, J., Hodina, A.K., Unger, C. and Massing, U. (2007). Plasma lyso-phosphatidylcholine concentration is decreased in cancer patients with weight loss and activated inflammatory status. *Lipids Health Dis*. **6,** 17.

Teraki, Y. and Shiohara, T. (1999). Apoptosis and the skin. *Eur. J. Bermatol*. **9,** 413-425.

Thomas, C., Fricke, I., Scrima, A., Berken, A. and Wittinghofer, A. (2007). Structural evidence for a common intermediate in small G protein-GEF reactions. *Mol. Cell*. **25,** 141-149.

Toda, K., Nogami, M., Murakami, K., Kanaho, Y. and Nakayama, K. (1999). Colocalization of phospholipase D1 and GTP-binding-defective mutant of ADP-ribosylation factor 6 to endosomes and lysosomes. *FEBS J*. **442,** 221-225.

Toru, H., Ra, C., Nonoyama, S., Suzuki, K., Yata, J.I. and Nakahata, T. (1996). Induction of the high-affinity IgE receptor (FcεRI) on human mast cells by IL-4. *Int. Immunol*. **8,** 1367-1373.

Uesugi, Y., Arima, J., Iwabuchi, M. and Hatanaka, T. (2007). Sensor of phospholipids in Streptomyces phospholipase D. *FEBS J*. **274,** 2672-2681.

Uesugi, Y. and Hatanaka, T. (2009). Phospholipase D mechanism using *Streptomyces* PLD. *Biochim. Biophys. Acta*.**1791,** 962-969.

Uesugi, Y., Mori, K., Arima, J., Iwabuchi, M. and Hatanaka, T. (2005). Recognition of phospholipids in Streptomyces phospholipase D. *J. Biol. Chem*. **280,** 26143-26151.

Ullrich, A., Coussens, L., Hayflick, J.S., Dull, T.J., Gray, A., Tam, A.W., Lee, J., Yarden, Y., Libermann, T.A., Schlessinger, J., Downward, J., Mayes, E.L.V., Whittle, N., Waterfield, M.D. and Seeburg, P.H. (1984). Human epidermal growth factor receptor cDNA sequence and aberrant expression of the amplified gene in A431 epidermoid carcinoma cells. *Nature*. **309,** 418-425.

Ushiro, H. and Cohen, S. (1980). Identification of phosphotyrosine as a product of epidermal growth factor-activated protein kinase in A-431 cell membranes. *J. Biol. Chem*. **255,** 8363-8365.

Van Meer, G. and Sprong, H. (2004). Membrane lipids and vesicular traffic. *Curr. Opin. Cell Biol*. **16,** 373-378.

Van Munster, E.B., Kremers, G.J., Adjobo-Hermans, M.J. and Gadella, T.W. Jr. (2005). Fluorescence resonance energy transfer (FRET) measurement by gradual acceptor photobleaching. *J. Microsc*. **218,** 253-62.

Vance, D.E. and Ridgway, N.D. (1988). The methylation of phosphatidylethanolamine. *Prog. Lipid Res*. **27,** 61-79.

Vance, D.E. and Vance, J.E. (2008). Phospholipid biosynthesis in eukaryotes. In *Biochemistry of Lipids, Lipoproteins and Membranes,* 5th edn, pp. 214-243. Edited by Vance, D.E. and Vance, J.E. London: Elsevier.

Venable, M.E., Bielawska, A. and Obeid, L.M. (1996). Ceramide inhibits phospholipase D in a cell-free system. *J. Biol. Chem*. **271,** 24800-24805.

Viparelli, F., Doti, N., Sandomenico, A., Marasco, D., Dathan, N.A., Miele, C., Beguinot, F., Monti, S.M. and Ruvo, M. (2008). Expression and purification of the D4 region of PLD1 and characterization of its interaction with PED-PEA15. *Protein Expr. Purif*. **59,** 302–308.

Vitale, N., Chasserot-Golaz, S., Bailly, Y., Morinaga, N., Frohman, M.A. and Bader, M.F. (2002). Calcium-regulated exocytosis of dense-core vesicles requires the activation of ADP-ribosylation factor (ARF)6 by ARF nucleotide binding site opener at the plasma membrane. *J. Cell Biol*. **159,** 79-89.

Voss, M., Weernink, P.A., Haupenthal, S., Möller, U., Cool, R.H., Bauer, B., Camonis, J.H., Jakobs, K.H. and Schmidt, M. (1999). Phospholipase D stimulation by receptor tyrosine kinases mediated by protein kinase C and a Ras/Ral signaling cascade. *J. Biol. Chem*. **274,** 34691-34698.

Waksman, M., Tang, X., Eli, Y., Gerst, J.E. and Liscovitch, M. (1997). Identification of a novel Ca^{2+}-dependent, phosphatidylethanolamine hydrolyzing phospholipase D in yeast bearing a disruption in PLD1. *J. Biol. Chem*. **272,** 36–39.

Wakatsuki, T., Schwab, B., Thompson, N.C. and Elson, E.L. (2001). Effects of cytochalasin D and lactrunculin B on mechanical properties of cells. *J. Cell Sci*. **114,** 1025-1036.

Walker, S.J. and Brown, H.A. (2002). Specificity of Rho insert-mediated activation of phospholipase D1. *J. Biol. Chem*. **277,** 26260-26267.

Walker, S.J., Wu, W.J., Cerione, R.A. and Brown, H.A. (2000). Activation of phospholipase D1 by Cdc42 requires the Rho insert region. *J. Biol. Chem*. **275,** 15665-15668

Wang, C. and Wang, X. (2001). The novel phospholipase D of *Arabidopsis* that is activated by oleic acid and associated with the plasma membrane. *Plant Physiol*. **127,** 1102-1112.

Wang, X., Wang, C., Sang, Y., Qin, C. and Welti, R. (2002). Networking of phospholipases in plant signal transduction. *Physiol. Plant*. **115,** 331-335.

Watanabe, H. and Kanaho, Y. (2000). Rapid report: inhibition of phosphatidylinositol 4,5-bisphosphate-stimulated phospholipase D2 activity by Ser/Thr phosphorylation. *Biochim. Biophys. Acta*. **1495,** 121-124.

Wantanabe, K. (1936). Biochemical studies on carbohydrates: XXII. On animal β-N-monoacetylglucosaminidase. Preliminary report. *J. Biochem*. **24,** 297-303.

Way, G., O'Luanaigh, N. and Cockcroft, S. (2000). Activation of exocytosis by cross-linking of the IgE receptor is dependent on ADP-ribosylation factor 1-regulated phospholipase D in RBL-2H3 mast cells: evidence that the mechanism of activation is via regulation of phosphatidylinositol 4,5-bisphosphate synthesis. *Biochem. J*. **346,** 63-70.

Wendeler, M. and Sandhoff, K. (2009). Hexosaminidase assays. *Glycoconj. J*. **26,** 945-952.

West, M.A., Bright, N.A. and Robinson, M.S. (1997). The role of ADP-ribosylation factor and phospholipase D in adaptor recruitment. *J. Cell Biol*. **138,** 1239–1254.

Wright, M.H., Farquhar, M.J., Aletrari, M.O., Ladds, G. and Hodgkin, M.N. (2008). Identification of caspase 3 motifs and critical aspartate residues in human phospholipase D1b and phospholipase D2a. *Biochem. Biophys. Res. Commun*. **369,** 478–484.

Wu, Y., Matsui, H. and Tomizawa, K. (2009). Amphiphysin I and regulation of synaptic vesicle endocytosis. *Acta. Med. Okayama*. **63,** 305-323.

Xie, Z., Ho, W.T. and Exton, J.H. (2000). Association of the N- and C-terminal domains of phospholipase D. Contribution of the conserved HKD motifs to the interaction and the requirement of the association for Ser/Thr phosphorylation of the enzyme. *J. Biol. Chem*. **275,** 24962-24969.

Xie, Z., Ho, W.T. and Exton, J.H. (2001). Requirements and effects of palmitoylation of rat PLD1. *J. Biol. Chem*. **276,** 9383-9391.

Xie, M., Smith, J.L., Ding, Z., Zhang, D. and Cornell, R.B. (2004). Membrane binding modulates the quaternary structure of CTP:phosphocholine cytidylyltransferase. *J. Biol. Chem*. **279,** 28817-28825.

Xie, Z., Ho, W.T. and Exton, J.H. (1998). Association of N- and C-terminal domains of phospholipase D is required for catalytic activity. *J. Biol. Chem*. **273,** 34679-34682.

Xu, L., Frankel, P., Jackson, D., Rotunda, T., Boshans, R.L., D'Souza-Schorey, C. and Foster, D.A. (2003). Elevated phospholipase D activity in H-Ras- but not K-Ras-transformed cells by the synergistic action of RalA and ARF6. *Mol. Cell. Biol*. **23,** 645-654.

Xu, L., Shen, Y., Joseph, T., Bryant, A., Luo, J.Q., Frankel, P., Rotunda, T. and Foster, D.A. (2000). Mitogenic phospholipase D activity is restricted to caveolin-enriched membrane microdomains. *Biochem. Biophys. Res. Commun*. **273,** 77-83.

Xu, Y., Colletier, J.P., Weik, M., Jiang, H., Moult, J., Silman, I. and Sussman, J.L. (2008). Flexibility of aromatic residues in the active-site gorge of acetylcholinesterase: X-ray versus molecular dynamics. *Biophys. J*. **95,** 2500–2511.

Xu, Y., Seet, L.F., Hanson, B. and Hong, W. (2001). The phox homology (PX) domain, a new player in phosphoinositide signalling. *Biochem. J*. **360,** 513–530.

Yamazaki, M., Zhang, Y., Watanabe, H., Yokozeki, T., Ohno, S., Kaibuchi, K., Shibata, H., Mukai, H., Ono, Y., Frohman, M.A. and Kanaho, Y. (1999). Interaction of the small G protein RhoA with the C terminus of human phospholipase D1. *J. Biol. Chem*. **274,** 6035-6038.

Yang, H. and Roberts, M.F. (2003). Phosphohydrolase and transphosphatidylation reactions of two *Streptomyces* phospholipase D enzymes: Covalent versus noncovalent catalysis. *Protein Sci*. **12,** 2087–2098.

Yang, S.F., Freer, S. and Benson, A.A. (1967). Transphosphatidylation by phospholiase D. *J. Biol. Chem*. **242,** 477-484.

Yeo, E.J. KazlauskasS, A. and Exton, J.H. (1994). Activation of phospholipase C-gamma is necessary for stimulation of phospholipase D by platelet-derived growth factor. *J. Biol. Chem.* **269,** 27823-27826.

Zhao, C., Du, G., Skowronek, K., Frohman, M.A. and Bar-Sagi, D. (2007). Phospholipase D2-generated phosphatidic acid couples EGFR stimulation to Ras activation by Sos. *Nat. Cell Biol*. **6,** 706-712.

Appendices

Appendix I: Primer names, sequences and orientations used for cloning

Primer Name	Primer Sequence	Forward or Reverse
1491	5' - TA GAA GGC ACA GTC GAG G - 3'	Reverse primer for the plasmid pcDNA3.1(-)
T7	5' - AAT ACG ACT CAC TAT AG - 3'	Forward primer upstream of multiple cloning site of pcDNA3.1(-)
PLD1b Xho Reverse	5' - TCT GTT GTG GCA TGA TAG - 3'	Reverse primer for the sequence between XhoI and PvulI of PLD1b
Forward Xho PLD2	5' - TGG CTG GTG GTG AAG GAC T - 3'	Forward primer from the XhoI site of PLD2
ApaI PLD2	5' - ACT TCC TCT ACA TTG AGA - 3'	Forward primer from the ApaI site of PLD2 (3036)
Inside Xho PLD2	5' - ATG TAC AGC AGG AAG GAG T - 3'	Reverse primer beginning in the XhoI restriction site of PLD2a
XmnR PLD2	5' - TCC GCC CAT CTG AGC AGC TAA T - 3'	Reverse primer for XmnI of PLD2 (3040)
dsRed Sequencing	5' - TAC ACC GTG GTG GAG CAG TA - 3'	Forward primer used to sequence monomeric dsRed after insertion into pcDNA3.1(-) plasmid
PLD2a Inside XhoI Reverse	5' - TGT ACA GCA GGA AGG AGT CCT - 3'	Reverse primer beginning inside the XhoI restriction site of PLD2a
PLD1b YLTK F	5' - TAC TTG ACA AAG ATA CTA A -3'	Forward primer covering the YLTK sequence of PLD1b
EcoRV Forward	5' - TAT CGG TCC CTT TCT TAT CC - 3'	Forward primer upstream of the EcoRV (3760) restriction site of PLD1b
295PheS Forward	5' - TGG AAT CCG AAT TGA TAA - 3'	Forward primer covering Phe (295) of PLD1b
MHD542A-S Forward	5' - TTC AAA ACT GAA AGG AAT AGG A -3'	Forward primer for sequence between HindIII (3078) and Pst (3616)
ERV-PLD1b-F	5' - CAA ACA ACA GCC CAT GAG TT - 3'	Forward primer starting prior to EcoRV site of PLD1b (815)
dsRed sequencing R	5' - TGG TAT GGC TGA TTA TGA TCA - 3'	Reverse primer of monomeric dsRed used for sequencing after insertion into pcDNA3.1(-)
Pst Reverse	5' - AGC GCT GGA TGA AGT GA -3'	Reverse primer of PLD1b downstream of Pst1 (3616)
PLD1b (start) F	5' - ATG TCA CTG AAA	Forward primer starting at

	AAC GAG CCA - 3'	ATG of PLD1b
PLD1b Reverse	5' - TTA AGT CCA AAC CTC CAT GGG CA - 3'	Reverse primer of PLD1b
PLD2a (start) F	5' - ATG ACG CGC ACC CCT GAG A - 3'	Forward primer starting at ATG of PLD2a
PLD2a Reverse	5' - CTA TGT CCA CAC TTC TAG GGG GAT - 3'	Reverse primer which binds to the PLD2a stop codon
Move dsRed F XbaI	5' - GGG TCT AGA ATG GAC AAC ACC GAG GAC GTC A - 3'	Forward primer used to clone monomeric dsRed into pcDNA3.1(-) and insert an XbaI restriction site at the N-terminus
Move dsRed R	5' - TAC CGT CGA CTG CAG AAT TCG A - 3'	Reverse primer used to insert monomeric dsRed into pcDNA3.1(-)
XmnI PLD2a	5' - ACT TCC TCT ACA TTG AGA - 3'	Forward primer which binds to XmnI (3640) of PLD2a
PLD1b Inside Xho I	5' - AGG CTC CTC TCT GAC GTT - 3'	Reverse primer to detect the correct orientation of XhoI (2152)
Cherry Forward	5' - GGG GTC AAT GGT GAG CAA GGG CGA GGA - 3'	Forward primer used to insert the Cherry sequence into pcDNA3.1(-)
Cherry Reverse	5' - ATC CTT GTA CAG CTC GTC CAT - 3'	Reverse primer used to insert the Cherry sequence into pcDNA3.1(-)

Appendix II: Cherry-PLD1b DNA sequence

ATGGTGAGCAAGGGCGAGGAGGATAACATGGCCATCATCAAGGAGTTCATGCGCTTCAAGGTGCACATGGAGGGCTCCGTGAACGGCCACGAGTTCGAGATCGAGGGCGAGGGCGAGGGCCG
CCCCTACGAGGGCACCCAGACCGCCAAGCTGAAGGTGACCAAGGGTGGCCCCCTGCCCTTCGCCTGGGACATCCTGTCCCCTCAGTTCATGTACGGCTCCAAGGCCTACGTGAAGCACCCCG
CCGACATCCCCGACTACTTGAAGCTGTCCTTCCCCGAGGGCTTCAAGTGGGAGCGCGTGATGAACTTCGAGGACGGCGGCGTGGTGACCGTGACCCAGGACTCCTCCCTGCAGGACGGCGAG
TTCATCTACAAGGTGAAGCTGCGCGGCACCAACTTCCCCTCCGACGGCCCCGTAATGCAGAAGAAGACCATGGGCTGGGAGGCCTCCTCCGAGCGGATGTACCCCGAGGACGGCGCCCTGAA
GGGCGAGATCAAGCAGAGGCTGAAGCTGAAGGACGGCGGCCACTACGACGCTGAGGTCAAGACCACCTACAAGGCCAAGAAGCCCGTGCAGCTGCCCGGCGCCTACAACGTCAACATCAAGT
TGGACATCACCTCCCACAACGAGGACTACACCATCGTGGAACAGTACGAACGCGCCGAGGGCCGCCACTCCACCGGCGGCATGGACGAGCTGTACAAGgatATGTCACTGAAAAACGAGCCA
CGGGTAAATACCTCTGCACTGCAGAAAATTGCTGCTGACATGAGTAATATCATAGAAAATCTGGACACGCGGGAACTCCACTTTGAGGGAGAGGAGGTAGACTACGACGTGTCTCCCAGCGA
TCCCAAGATACAAGAAGTGTATATCCCTTTCTCTGCTATTTATAACACTCAAGGATTTAAGGAGCCTAATATACAGACGTATCTCTCCGGCTGTCCAATAAAAGCACAAGTTCTGGAAGTGG
AACGCTTCACATCTACAACAAGGGTACCAAGTATTAATCTTTACACTATTGAATTAACACATGGGGAATTTAAATGGCAAGTTAAGAGGAAATTCAAGCATTTTCAAGAATTTCACAGAGAG
CTGCTCAAGTACAAAGCCTTTATCCGCATCCCCATTCCCACTAGAAGACACACGTTTAGGAGGCAAAACGTCAGAGAGGAGCCTCGAGAGATGCCCAGTTTGCCCCGTTCATCTGAAAACAT
GATAAGAGAAGAACAATTCCTTGGTAGAAGAAAACAACTGGAAGATTACTTGACAAAGATACTAAAAATGCCCATGTATAGAAACTATCATGCCACAACAGAGTTTCTTGATATAAGCCAGC
TGTCTTTCATCCATGATTTGGGACCAAAGGGCATAGAAGGTATGATAATGAAAAGATCTGGAGGACACAGAATACCAGGCTTGAATTGCTGTGGTCAGGGAAGAGCCTGCTACAGATGGTCA
AAAAGATGGTTAATAGTGAAAGATTCCTTTTTATTGTATATGAAACCAGACAGCGGTGCCATTGCCTTCGTCCTGCTGGTAGACAAAGAATTCAAAATTAAGGTGGGGAAGAAGGAGACAGA
AACGAAATATGGAATCCGAATTGATAATCTTTCAAGGACACTTATTTTAAAATGCAACAGCTATAGACATGCTCGGTGGTGGGGAGGGGCTATAGAAGAATTCATCCAGAAACATGGCACCA
ACTTTCTCAAAGATCATCGATTTGGGTCATATGCTGCTATCCAAGAGAATGCTTTAGCTAAATGGTATGTTAATGCCAAAGGATATTTTGAAGATGTGGCAAATGCAATGGAAGAGGCAAAT
GAAGAGATTTTTATCACAGACTGGTGGCTGAGTCCAGAAATCTTCCTGAAACGCCCAGTGGTTGAGGGAAATCGTTGGAGGTTGGACTGCATTCTTAAACGAAAAGCACAACAAGGAGTGAG
GATCTTCATAATGCTCTACAAAGAGGTGGAACTCGCTCTTGGCATCAATAGTGAATACACCAAGAGGACTTTGATGCGTCTACATCCCAACATAAAGGTGATGAGACACCCGGATCATGTGT
CATCCACCGTCTATTTGTGGGCTCACCATGAGAAGCTTGTCATCATTGACCAATCGGTGGCCTTTGTGGGAGGGATTGACCTGGCCTATGGAAGGTGGGACGACAATGAGCACAGACTCACA
GACGTGGGCAGTGTGAAGCGGGTCACTTCAGGACCGTCTCTGGGTTCCCTCCCACCTGCCGCAATGGAGTCTATGGAATCCTTAAGACTCAAAGATAAAAATGAGCCTGTTCAAAACCTACC
CATCCAGAAGAGTATTGATGATGTGGATTCAAAACTGAAAGGAATAGGAAAGCCAAGAAAGTTCTCCAAATTTAGTCTCTACAAGCAGCTCCACAGGCACCACCTGCACGACGCAGATAGCA
TCAGCAGCATTGACAGCACCTCCAATACCGGGTCCATCCGTAGTTTACAGACAGGTGTGGGAGAGCTGCATGGGGAAACCAGATTCTGGCATGGAAAGGACTACTGCAATTTCGTCTTCAAA
GACTGGGTTCAACTTGATAAACCTTTTGCTGATTTCATTGACAGGTACTCCACGCCCCGGATGCCCTGGCATGACATTGCCTCTGCAGTCCACGGGAAGGCGGCTCGTGATGTGGCACGTCA
CTTCATCCAGCGCTGGAACTTCACAAAAATTATGAAATCAAAATATCGGTCCCTTTCTTATCCTTTTCTGCTTCCAAAGTCTCAAACAACAGCCCATGAGTTGAGATATCAAGTGCCTGGGT
CTGTCCATGCTAACGTACAGTTGCTCCGCTCTGCTGCTGATTGGTCTGCTGGTATAAAGTACCATGAAGAGTCCATCCACGCCGCTTACGTCCATGTGATAGAGAACAGCAGGCACTATATC
TATATCGAAAACCAGTTTTTCATAAGCTGTGCTGATGACAAAGTTGTGTTCAACAAGATAGGCGATGCCATTGCCCAGAGGATCCTGAAAGCTCACAGGGAAAACCAGAAATACCGGGTATA
TGTCGTGATACCACTTCTGCCAGGGTTCGAAGGAGACATTTCAACCGGCGGAGGAAATGCTCTACAGGCAATCATGCACTTCAACTACAGAACCATGTGCAGAGGAGAAAATTCCATCCTTG
GACAGTTAAAAGCAGAGCTTGGTAATCAGTGGATAAATTACATATCATTCTGTGGTCTTAGAACACATGCAGAGCTCGAAGGAAACCTAGTAACTGAGCTTATCTATGTCCACAGCAAGTTG
TTAATTGCTGATGATAACACTGTTATTATTGGCTCTGCCAACATAAATGACCGCAGCATGCTGGGAAAGCGTGACAGTGAAATGGCTGTCATTGTGCAAGATACAGAGACTGTTCCTTCAGT
AATGGATGGAAAAGAGTACCAAGCTGGCCGGTTTGCCCGAGGACTTCGGCTACAGTGCTTTAGGGTTGTCCTTGGCTATCTTGATGACCCAAGTGAGGACATTCAGGATCCAGTGAGTGACA
AATTCTTCAAGGAGGTGTGGGTTTCAACAGCAGCTCGAAATGCTACAATTTATGACAAGGTTTTCCGGTGCCTTCCCAATGATGAAGTACACAATTTAATTCAGCTGAGAGACTTTATAAAC
AAGCCCGTATTAGCTAAGGAAGATCCCATTCGAGCTGAGGAGGAACTGAAGAAGATCCGTGGATTTTTGGTGCAATTCCCCTTTTATTTCTTGTCTGAAGAAAGCCTACTGCCTTCTGTTGG
GACCAAAGAGGCCGTCGTGCCCATGGAGGTTTGGACTTAA

Appendix III: Cherry-PLD1b protein sequence

MVSKGEEDNMAIIKEFMRFKVHMEGSVNGHEFEIEGEGEGEGR
PYEGTQTAKLKVTKGGPLPFAWDILSPQFMYGSKAYVKHPA
DIPDYLKLSFPEGFKWERVMNFEDGGVVTVTQDSSLQDGEF
IYKVKLRGTNFPPSDGPVMQKKTMGWEASSERMYPEDGALKG
EIKQRLKLKDGGHYDAEVKTTYKAKPVQLPGAYNVNIKLD
ITSHNEDYTIVEQYERAEGRHSTGGMDELYKDMSLKNEPRV
NTSALQKIAADMSNIIEENLDTRELHFEGEEVDYDVSPSDPK
IQEVYIPFSAIYNTQGFKEPNIQTYLSGCPIKAQVLEVERF
TSTTRVPSINLYTIELTHGEFKWQVKRKFKHFQEFHRELLK
YKAFIRIPIPTRRHTFRRQNVREEPRESSENMIRE
EQFLGRRKQLEDYLTKILKMPMYRNYHATTEFLDISQLSFI
HDLGPKGIEMIMKRSGGHRIPGLNCCGQGRACYRWSKRWL
IVKDSFLLYMKPDSGAIAFVLLVDKEFKIKVGKKETETKYG
IRIDNLSRTLIKCNSYRHARWWGGAIEEFIQKHGTNFLKD
HRFGSYAAIQENALAKWYVNAKGYFEDVANAMEEANEEIFI
TDWWLSPEIFLKRPVVEGNRWRLDCILKRKAQQGVRIFIML
YKEVELALGINSEYTKRTLMRLHPNIKVMRHPDHVSSSTVYL
WAHHEKLVIIDQSVAFVGGIDLAYGRWDDNEHRLTDVGSVK
RVTSGPSLGSLPPAAMESMESLRLKDKNEPVQNLPIQKSIDD
DVDSKLKGIGKPRKFSKFSLYKQLHRHHLHDASDSISSSIDST
SNTGSIRSLQTGVGELHGEFTRFWHGKDYCNFVFKDWVQLDK
PFADFIDRYSTPRMPWHDIASAVHGKAARDVARHFIQRWNF
TKIMKSKYRSLSYPFLLPNDEVHNLIQLRDFINKPVLAKEDV
LRSAADWSAGIKYHVIEENSRHYIYIYIENQFFIS
CADDKVVFNKIGDAIAQRILKAHRENQKYRVYVVIPLLPG
FEGDISTGGGNALQAIMHFNYRTMCRGENSILGQLKAELGN
QWINYISFCGLRTHAELEGNLVTELIYVHSKLLIADDNTVI
IGSANININDRSMLGKRDSEMAVIVQDTETVPSVMDGKEYQAG
RFARGLRLQCFRVVLGYLDDPSEDIQDPVSDKFFKEVWVS
AARNATIYDKVFRCLPNDEVHNLIQLRDFIKPVLAKEDP
RAEEELKKIRGFLVQFPFYFLSEESLLPSVGTKEAVVPM
WT

Appendix IV: Cherry-PLD1b plasmid map

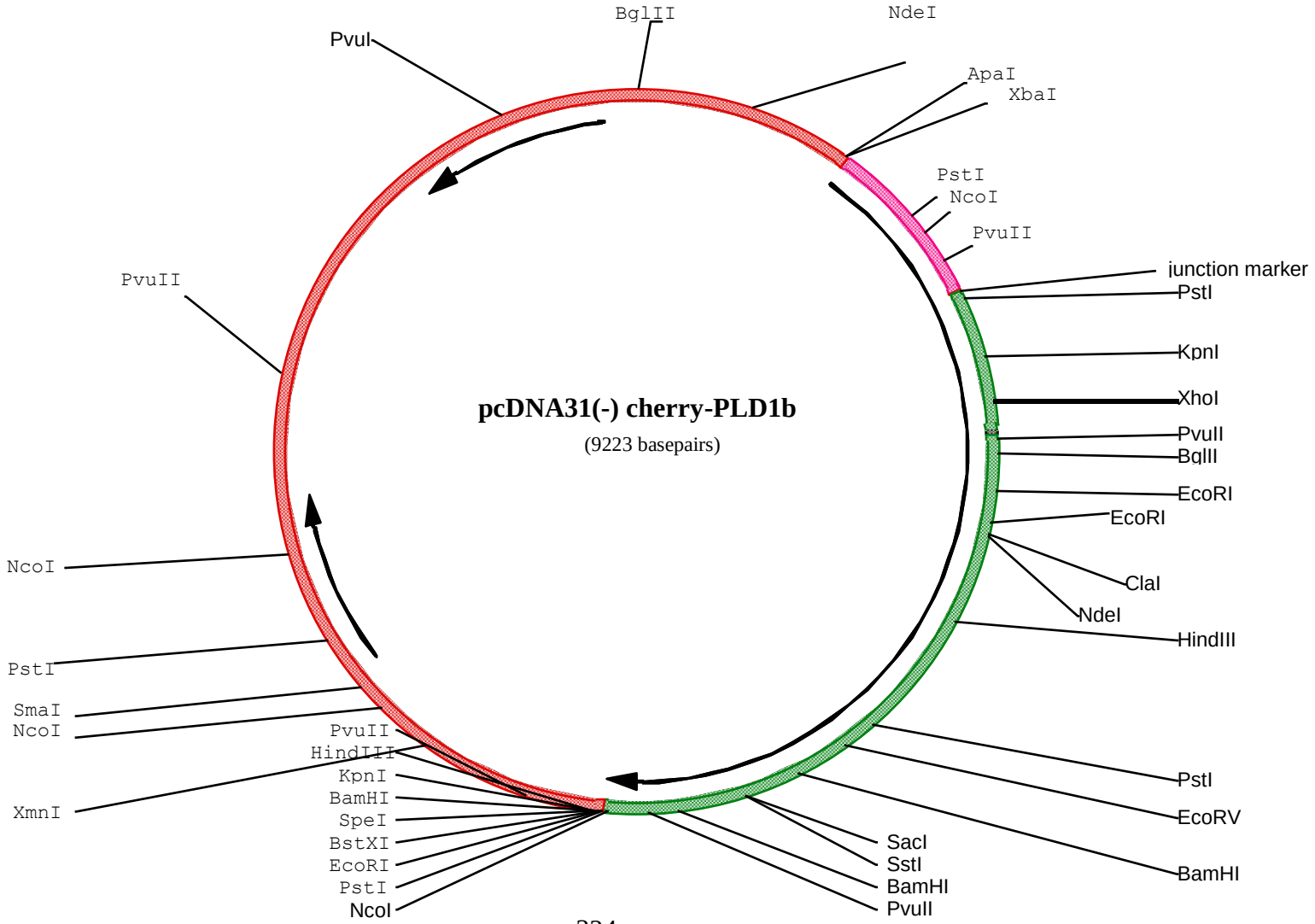

Appendix V: Cherry-PLD2a DNA sequence

ATGGTGAGCAAGGGCGAGGAGGATAACATGGCCATCATCAAGGAGTTCATGCGCTTCAAGGTGCACATGGAGGGCTCCGTGAACGGCCACGAGTTCGAGATCGAGGGCGAGGGCGAGGGCCG
CCCCTACGAGGGCACCCAGACCGCCAAGCTGAAGGTGACCAAGGGTGGCCCCCTGCCCTTCGCCTGGGACATCCTGTCCCCTCAGTTCATGTACGGCTCCAAGGCCTACGTGAAGCACCCCG
CCGACATCCCCGACTACTTGAAGCTGTCCTTCCCCGAGGGCTTCAAGTGGGAGCGCGTGATGAACTTCGAGGACGGCGGCGTGGTGACCGTGACCCAGGACTCCTCCCTGCAGGACGGCGAG
TTCATCTACAAGGTGAAGCTGCGCGGCACCAACTTCCCCTCCGACGGCCCCGTAATGCAGAAGAAGACCATGGGCTGGGAGGCCTCCTCCGAGCGGATGTACCCCGAGGACGGCGCCCTGAA
GGGCGAGATCAAGCAGAGGCTGAAGCTGAAGGACGGCGGCCACTACGACGCTGAGGTCAAGACCACCTACAAGGCCAAGAAGCCCGTGCAGCTGCCCGGCGCCTACAACGTCAACATCAAGT
TGGACATCACCTCCCACAACGAGGACTACACCATCGTGGAACAGTACGAACGCGCCGAGGGCCGCCACTCCACCGGCGGCATGGACGAGCTGTACAAGgatATGACGGCGACCCCTGAGAGC
CTCTTCCCCACTGGGGACGAACTGGACTCCAGCCAGCTCCAGATGGAGTCCGATGAGGTGGACACCCTGAAGGAGGGAGAGGACCCAGCCGACCGGATGCACCCGTTTCTGGCCATCTATGA
GCTTCAGTCTCTGAAAGTGCACCCCTTGGTGTTCGCACCTGGGGTCCCTGTCACAGCCCAGGTGGTGGGCACCGAAAGATATACCAGCGGATCCAAGGTGGGAACCTGCACTCTGTATTCTG
TCCGCTTGACTCACGGCGACTTTTCCTGGACAACCAAGAAGAAATACCGTCATTTTCAGGAGCTGCATCGGGACCTCCTGAGACACAAAGTCTTGATGAGTCTGCTCCCTCTGGCTCGTTTT
GCCGTTGCCTATTCTCCAGCCCGAGATGCAGGCAACAGAGAGATGCCCTCTCTACCCCGGGCAGGTCCTGAGGGCTCCACCAGACATGCAGCCAGCAAACAGAAATACCTGGAGAATTACCT
CAACCGTCTCTTGACCATGTCTTTCTATCGCAACTACCATGCCATGACAGAGTTCCTGGAAGTCAGTCAGCTGTCCTTTATCCCGGACTTGGGCCGCAAAGGACTGGAGGGGATGATCCGGA
AGCGCTCAGGTGGCCACCGTGTTCCTGGCCTCACCTGCTGTGGCCGAGACCAAGTTTGTTATCGCTGGTCCAAGAGGTGGCTGGTGGTGAAGGACTCCTTCCTGCTGTACATGTGCCTCGAG
ACAGGTGCCATCTCATTTGTTCAGCTCTTTGACCCTGGCTTTGAGGTGCGAGTGGGGAAAAGGAGCACGGAGGCACGGCACGGCGTGCGGATCGATACCTCCCACAGGTCCTTGATTCTCAA
GTGCAGCAGCTACCGGCAGGCACGGTGGTGGGCCCAAGAGATCACTGAGCTGGCACAGGGCCCAGGCAGAGACTTCCTACAGCTGCACCGGCATGACAGCTACGCCCCACCCCGGCCTGGGA
CCTTGGCCCGGTGGTTTGTGAATGGGGCAGGTTACTTTGCTGCTGTGGCAGATGCCATCCTTCGAGCTCAAGAGGAGATTTTCATCACAGACTGGTGGTTGAGTCCTGAGGTTTACCTGAAG
CGTCCGGCCCATTCAGATGACTGGAGACTGGACATTATGCTCAAGAGGAAGGCGGAGGAGGGTGTCCGTGTGTCTATTCTGCTGTTTAAAGAAGTGGAATTGGCCTTGGGCATCAACAGTGG
CTATAGCAAGAGGGCGCTGATGCTGCTGCACCCCAACATAAAGGTGATGCGTCACCCAGACCAAGTGACGTTGTGGGCCCATCATGAGAAGCTCCTGGTGGTGGACCAAGTGGTAGCATTCC
TGGGGGGACTGGACCTTGCCTATGGCCGCTGGGATGACCTGCACTACCGACTGACTGACCTTGGAGACTCCTCTGAATCAGCTGCCTCCCAGCCTCCCACCCCGCGCCCAGACTCACCAGCC
ACCCCAGACCTCTCTCACAACCAATTCTTCTGGCTGGGCAAGGACTACAGCAATCTTATCACCAAGGACTGGGTGCAGCTGGACCGGCCTTTCGAAGATTTCATTGACAGGGAGACGACCCC
TCGGATGCCATGGCGGGACGTTGGGGTGGTCGTCCATGGCCTACCGGCCCGGGACCTTGCCCGGCACTTCATCCAGCGCTGGAACTTCATCAAGACCACCAAGGCCAAGTACAAGACTCCCA
CATACCCCTACCTGCTTCCCAAGTCTACCAGCACGGCCAATCAGCTCCCCTTCACACTTCCAGGAGGGCAGTGCACCACCGTACAGGTCTTGCGATCAGTGGACCGCTGGTCAGCAGGGACT
CTGGAGAACTCTATCCTCAATGCCTACCTGCACACCATCAGGGAGAGCCAGCACTTCCTCTACATTGAGAATCAGTTCTTCATTAGCTGCTCAGATGGGCGGACGGTTCTGAACAAGGTGGG
CGATGAGATTGTGGACAGAATCCGGAAGGCCCACAAACAGGGGTGGTGTTACCGAGTCTACGTGCTTTTGCCCTTACTCCCTGGCTTCGAGGGTGACATCTCCACGGGCGGTGGCAACTCCA
TCCAGGCCATTCTGCACTTTACTTACAGGACCCTGTGTCGTGGGGAGTATTCAATCCTGCATCGCCTTAAAGCAGCCATGGGGACAGCATGGCGGGACTATATTTCCATCTGCGGGCTTCGT
ACACACGGAGAGCTGGGCGGGCACCCCGTCTCGGAGCTCATCTACATCCACAGCAAGGTGCTCATCGCAGATGACCGGACAGTCATCATTGGTTCTGCAAACATCAATGACCGGAGCTTGCT
GGGGAAGCGGGACAGTGAGCTGGCCGTGCTAATCGAGGACACAGAGACGGAACCATCCCTCATGAATGGGGCAGAGTATCAGGCGGGCAGGTTTGCCTTGAGTCTGCGGAAGCACTGCTTCA
GTGTGATTCTTGGAGCAAATACCCGGCCAGACTTGGATCTCCGAGACCCCATCTGTGATGACTTCTTCCAGTTGTGGCAAGACATGGCTGAGAGCAACGCCAATATCTATGAGCAGATCTTC
CGCTGCCTGCCATCCAATGCCACGCGTTCCCTGCGGACTCTCCGGGAGTACGTGGCCGTGGAGCCCTTGGCCACGGTCAGTCCCCCCTTGGCTCGGTCTGAGCTCACCCAGGTCCAGGGCCA
CCTGGTCCACTTCCCCCTCAAGTTCCTAGAGGATGAGTCTTTGCTGCCCCCGCTGGGTAGCAAGGAGGGCATGATCCCCCTAGAAGTGTGGACATAG

Appendix VI: Cherry-PLD2a protein sequence

M V S K G E E D N M A I I K E F M R F K V H M E G S V N G H E F E I E G E G E G R
P Y E G T Q T A K L K V T K G G P L P F A W D I L S P Q F M Y G S K A Y V K H P A
D I P D Y L K L S F P E G F K W E R V M N F E D G G V V T V T Q D S S L Q D G E F
I Y K V K L R G T N F P S D G P V M Q K K T M G W E A S S E R M Y P E D G A L K G
E I K Q R L K L K D G G H Y D A E V K T T Y K A K K P V Q L P G A Y N V N I K L D
I T S H N E D Y T I V E Q Y E R A E G R H S T G G M D E L Y K D M T A T P E S L F
P T G D E L D S S Q L Q M E S D E V D T L K E G E D P A D R M H P F L A I Y E L Q
S L K V H P L V F A P G V P V T A Q V V G T E R Y T S G S K V G T C T L Y S V R L
T H G D F S W T T K K K Y R H F Q E L H R D L L R H K V L M S L L P L A R F A V A
Y S P A R D A G N R E M P S L P R A G P E G S T R H A A S K Q K Y L E N Y L N R L
L T M S F Y R N Y H A M T E F L E V S Q L S F I P D L G R K G L E G M I R K R S G
G H R V P G L T C C G R D Q V C Y R W S K R W L V V K D S F L L Y M C L E T G A I
S F V Q L F D P G F E V R V G K R S T E A R H G V R I D T S H R S L I L K C S S Y
R Q A R W W A Q E I T E L A Q G P G R D F L Q L H R H D S Y A P P R P G T L A R W
F V N G A G Y F A A V A D A I L R A Q E E I F I T D W W L S P E V Y L K R P A H S
D D W R L D I M L K R K A E E G V R V S I L L F K E V E L A L G I N S G Y S K R A
L M L L H P N I K V M R H P D Q V T L W A H H E K L L V V D Q V V A F L G G L D L
A Y G R W D D L H Y R L T D L G D S S E S A A S Q P P T P R P D S P A T P D L S H
N Q F F W L G K D Y S N L I T K D W V Q L D R P F E D F I D R E T T P R M P W R D
V G V V V H G L P A R D L A R H F I Q R W N F I K T T K A K Y K T P T Y P Y L L P
K S T S T A N Q L P F T L P G G Q C T T V Q V L R S V D R W S A G T L E N S I L N
A Y L H T I R E S Q H F L Y I E N Q F F I S C S D G R T V L N K V G D E I V D R I
R K A H K Q G W C Y R V Y V L L P L L P G F E G D I S T G G G N S I Q A I L H F T
Y R T L C R G E Y S I L H R L K A A M G T A W R D Y I S I C G L R T H G E L G G H
P V S E L I Y I H S K V L I A D D R T V I I G S A N I N D R S L L G K R D S E L A
V L I E D T E T E P S L M N G A E Y Q A G R F A L S L R K H C F S V I L G A N T R
P D L D L R D P I C D D F F Q L W Q D M A E S N A N I Y E Q I F R C L P S N A T R
S L R T L R E Y V A V E P L A T V S P P L A R S E L T Q V Q G H L V H F P L K F L
E D E S L L P P L G S K E G M I P L E V W T

Appendix VII: Cherry-PLD1b plasmid map